



Terms and Conditions of Use of Digitised Theses from Trinity College Library Dublin

Copyright statement

All material supplied by Trinity College Library is protected by copyright (under the Copyright and Related Rights Act, 2000 as amended) and other relevant Intellectual Property Rights. By accessing and using a Digitised Thesis from Trinity College Library you acknowledge that all Intellectual Property Rights in any Works supplied are the sole and exclusive property of the copyright and/or other IPR holder. Specific copyright holders may not be explicitly identified. Use of materials from other sources within a thesis should not be construed as a claim over them.

A non-exclusive, non-transferable licence is hereby granted to those using or reproducing, in whole or in part, the material for valid purposes, providing the copyright owners are acknowledged using the normal conventions. Where specific permission to use material is required, this is identified and such permission must be sought from the copyright holder or agency cited.

Liability statement

By using a Digitised Thesis, I accept that Trinity College Dublin bears no legal responsibility for the accuracy, legality or comprehensiveness of materials contained within the thesis, and that Trinity College Dublin accepts no liability for indirect, consequential, or incidental, damages or losses arising from use of the thesis for whatever reason. Information located in a thesis may be subject to specific use constraints, details of which may not be explicitly described. It is the responsibility of potential and actual users to be aware of such constraints and to abide by them. By making use of material from a digitised thesis, you accept these copyright and disclaimer provisions. Where it is brought to the attention of Trinity College Library that there may be a breach of copyright or other restraint, it is the policy to withdraw or take down access to a thesis while the issue is being resolved.

Access Agreement

By using a Digitised Thesis from Trinity College Library you are bound by the following Terms & Conditions. Please read them carefully.

I have read and I understand the following statement: All material supplied via a Digitised Thesis from Trinity College Library is protected by copyright and other intellectual property rights, and duplication or sale of all or part of any of a thesis is not permitted, except that material may be duplicated by you for your research use or for educational purposes in electronic or print form providing the copyright owners are acknowledged using the normal conventions. You must obtain permission for any other use. Electronic or print copies may not be offered, whether for sale or otherwise to anyone. This copy has been supplied on the understanding that it is copyright material and that no quotation from the thesis may be published without proper acknowledgement.

Investigations of the potential of crystalline excipients to prevent the process-induced amorphisation of active pharmaceutical ingredients

Presented by

Vincent Curtin, B.Sc. (Pharm.), PG Dip. Stat., M.P.S.I.

being a thesis submitted for the degree of
Doctor of Philosophy in Pharmaceutics

at the

University of Dublin, Trinity College

under the direction and supervision of

Professor Anne Marie Healy, B.Sc. (Pharm.), Ph.D., M.P.S.I., F.T.C.D.

and

Lidia Tajber, B.Sc. (Pharm.), Ph.D., M.P.S.I

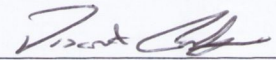
and

**Professor Owen I. Corrigan,
B.Sc. (Pharm.) (N.U.I.), M.A., Ph.D. (N.U.I.), F.P.S.I., F.T.C.D.**

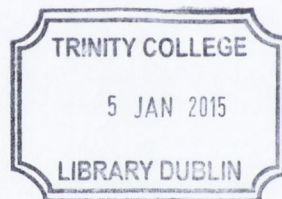
September 2013

DECLARATION

This thesis is submitted by the undersigned to the University of Dublin, Trinity College, for examination for the degree of Doctor of Philosophy. This thesis has not been submitted as an exercise for a degree at any other university. It is entirely the work of the undersigned author, except where duly acknowledged. This manuscript was completely written by the undersigned author, with the aid of editorial advice from Prof. Anne Marie Healy and Dr. Lidia Tajber and Professor O.I. Corrigan. It is agreed that the library may lend or copy this thesis upon request.



Vincent Curtin



Thesis 10811

TABLE OF CONTENTS

Acknowledgements	i
Presentations and publications associated with this work	ii
Summary	iv

INTRODUCTION

Origin and scope	1
Chapter 1 Introduction	
1.1 Polymorphism	4
1.1.1 Pseudo-polymorphism	5
1.2 Amorphous state	5
1.2.1 Polyamorphism/pseudo-polyamorphism	7
1.2.2 Glass transition temperature	9
1.3 Solid dispersions	12
1.4 Stability of the amorphous state	13
1.4.1 Crystallisation from the amorphous state	13
1.4.2 Plasticisation	15
1.4.3 Structural interactions	16
1.5 Vapour sorption properties of crystalline and amorphous solids	18
1.6 Drug-excipient solubility	21
1.7 Milling	23
1.7.1 Co-milling	26
1.8 Dry mixing	28
1.9 Solid state amorphisation	28

1.10	Spray drying	30
------	--------------	----

EXPERIMENTAL

Chapter 2 Materials and Methods

2.1	Materials	33
2.2	Methods	34
2.2.1	Milling	34
2.2.1.1	Sulfadimidine and sulfadimidine:excipient composites	34
2.2.1.2	Salbutamol sulphate and salbutamol sulphate:excipient composites	34
2.2.1.3	Budesonide and budesonide:glutaric acid composites	35
2.2.2	Dry mixing	35
2.2.3	Spray drying	36
2.2.4	Freeze drying	36
2.2.5	Melt quench	37
2.2.6	Physical mixtures	37
2.2.7	Thermal analysis	37
2.2.7.1	Differential scanning calorimetry (DSC)	37
2.2.7.2	Modulated temperature differential scanning calorimetry (MTDSC)	38
2.2.7.2.1	Quantification of amorphous content by MTDSC	38
2.2.7.3	High performance differential scanning calorimetry (HyperDSC)	39
2.2.7.4	Thermal annealing and heating rate experiments	39
2.2.7.5	Thermogravimetric analysis (TGA)	40
2.2.8	Powder X-Ray Diffraction (pXRD)	41
2.2.8.1	Quantification of amorphous content by pXRD	41

2.2.9	Scanning electron microscopy (SEM)	42
2.2.10	Infrared spectroscopy	43
2.2.10.1	Fourier Transform Infra-Red Spectroscopy (FTIR)	43
2.2.10.2	Near Infrared Spectroscopy (NIR)	43
2.2.10.2.1	Quantification of amorphous content by NIR	44
2.2.11	Dynamic vapour sorption (DVS)	44
2.2.11.1	Quantification of amorphous content by DVS	45
2.2.12	Surface area by BET	45
2.2.13	High Performance Liquid Chromatography (HPLC)	46
2.2.14	Solubility studies	47
2.2.14.1	Solubility determination of excipients in sulfadimidine by thermal analysis	47
2.2.14.2	Solubility determination of excipients in salbutamol sulphate by thermal analysis	47
2.2.14.3	Hildebrand solubility parameter	48
2.2.15	Statistical analysis	48

RESULTS AND DISCUSSION

Chapter 3 Characterisation and quantification of amorphous content in mechanically activated and spray dried active pharmaceutical ingredients.

3.1	Introduction	49
3.2	Sulfadimidine	50
3.2.1	PXRD and thermal analysis of unprocessed, milled and spray dried sulfadimidine	50
3.2.2	FTIR analysis	52
3.2.3	SEM	53

3.2.4	Quantification of amorphous content in milled sulfadimidine	55
3.2.4.1	Vapour sorption analysis and amorphous content quantification by DVS	55
3.2.4.2	Amorphous content quantification by pXRD	60
3.2.4.3	Amorphous content quantification by MTDSC	60
3.2.4.4	Amorphous content quantification by NIR	60
3.2.4.5	Comparative analysis of amorphous content quantification by different methods for sulfadimidine milled at room temperature	61
3.2.5	Sulfadimidine milled at 4°C	63
3.3	Salbutamol sulphate	66
3.3.1	PXRD and thermal analysis of unprocessed, milled, dry mixed and spray dried salbutamol sulphate	66
3.3.2	Vapour sorption analysis	68
3.3.3	SEM analysis	72
3.4	Budesonide	73
3.4.1	PXRD and thermal analysis of unprocessed, milled and spray dried budesonide	73
3.4.2	SEM	75
3.4.3	Vapour sorption analysis	76
3.5	Conclusion	78

Chapter 4 Investigation of the capacity of low glass transition temperature excipients to minimise amorphisation of API on co-milling

4.1	Introduction	81
4.2	Sulfadimidine co-milled with glutaric acid	82
4.2.1	Glutaric acid	82

4.2.2	PXRD and thermal analysis of sulfadimidine:glutaric acid co-milled composites	85
4.2.3	Quantification of amorphous content	88
4.2.3.1	DVS	88
4.2.3.2	NIR	91
4.2.4	Physical mixture of milled sulfadimidine and milled glutaric acid	91
4.3	Adipic acid	94
4.4	Succinic acid	95
4.5	Malic acid	96
4.6	Glass transition temperatures and solubility parameters of sulfadimidine and the dicarboxylic acids	98
4.7	Sulfadimidine co-milled with adipic acid, succinic acid and malic acid	100
4.8	Comparison of API crystallinity on co-milling with a series of dicarboxylic acids	102
4.9	Physical mixtures of milled sulfadimidine with milled adipic acid, succinic acid and malic acid	104
4.10	Characterisation by FTIR	107
4.11	Co-milling milled sulfadimidine with excipient	109
4.12	Solubility determination of glutaric acid and adipic acid in amorphous sulfadimidine by thermal analysis	110
4.13	Budesonide co-milled with glutaric acid	113
4.14	Conclusion	117

Chapter 5 Reducing mechanical activation-induced amorphisation of salbutamol sulphate by co-processing with selected carboxylic acids

5.1	Introduction	118
5.2	Solubility determination of glutaric acid, adipic acid and pimelic acid in amorphous milled salbutamol sulphate	119
5.3	Salbutamol sulphate co-milled with glutaric acid	120
5.3.1	Physical mixture of milled salbutamol sulphate and milled glutaric acid	124
5.4	Pimelic acid	125
5.5	Salbutamol sulphate co-milled with adipic acid and pimelic acid	128
5.5.1	Physical mixtures of milled salbutamol sulphate with milled adipic acid and with milled pimelic acid	130
5.6	Salbutamol sulphate co-mixed with the dicarboxylic acids	132
5.7	Linking API crystallinity on co-milling to composite Tg lowering effect of excipient	137
5.8	Conclusion	139

Chapter 6 Co-milling and co-spray drying of sulfadimidine:polyol and sulfadimidine:diacid composites

6.1	Introduction	141
6.2	Sulfadimidine and mannitol co-milled composites	142
6.2.1	Mannitol	142
6.2.2	Solubility determination of mannitol in amorphous sulfadimidine	144
6.2.2.1	Hildebrand solubility parameter	144
6.2.3	PXRD and thermal analysis of sulfadimidine:mannitol co-milled composites	145

6.2.4	Physical mixture of milled sulfadimidine and milled mannitol	147
6.2.5	Quantification of amorphous content	149
6.2.6	FTIR analysis	150
6.3	Sulfadimidine and xylitol co-milled composites	153
6.4	Sulfadimidine and mannitol co-spray dried composites	154
6.4.1	PXRD and thermal analysis	154
6.4.1.1	Endothermic event	157
6.4.1.1.1	Thermal annealing and heating rate studies	158
6.4.1.1.2	Thermal cycling	160
6.4.1.2	Exothermic event	161
6.4.1.3	Polymorphic transformation	162
6.4.2	DVS analysis	163
6.4.3	Physical mixture of spray dried sulfadimidine and spray dried mannitol	164
6.5	Glutaric acid and sulfadimidine:glutaric acid spray dried systems	165
6.5.1	Physical stability	167
6.5.2	SEM analysis	170
6.6	Sulfadimidine:adipic acid and sulfadimidine:succinic acid co-spray dried systems	173
6.7	DVS analysis of sulfadimidine:diacid co-spray dried composites	175
6.8	Conclusion	177
Chapter 7	General Discussion	
7.1	Introduction	179
7.2	Amorphisation of API on processing	179
7.2.1	Inter-comparison of the amorphous state of drugs produced	

	by different processes	182
7.3	Quantifying amorphous content in single and multi-component systems	185
7.4	Mitigating API amorphisation on co-processing with low Tg excipients	188
7.5	Comparison of co-spray dried composites and composites produced by mechanical activation	192
7.6	Main findings	196
7.7	Suggestions for future work	198
	References	199
	Appendices	
	Appendix I	226
	Appendix II	229
	Appendix III	230
	Appendix IV	233

ACKNOWLEDGEMENTS

I would like to thank my supervisors Prof. Anne Marie Healy, Dr. Lidia Tajber and Prof. Owen Corrigan for their guidance and support during the course of my research. I am very grateful to Prof. Healy for allowing me to be part of her research group, and for being my tutor and mentor since first arriving in Trinity in 2004.

I wish to thank the Solid State Pharmaceutical Cluster and Science Foundation Ireland for their support and for the opportunity to present my research at international conferences in Asia, Europe and the US. Many thanks to Dr. Yun Hu and the research group in NUIG for their collaborative work.

I am grateful to the academic, secretarial and technical staff in the School of Pharmacy and Pharmaceutical Sciences for their assistance and support. Many thanks to my fellow postgrads (Christine, Johanna, Joanne, Maria, Janani, Stephany, Bo, Cathal, Cliff, Clare and all the gang (too many to mention) in chemistry) and postdocs (Fred and KP) who had such a positive influence in every sense and made the lab an enjoyable place to be! Thanks to Vincent Caron and Evelyn for introducing me to the exciting world of milling. I am grateful to Youness for the enthusiasm and impact he had for the short time he was here. A special word to my Italian friend, Stefano Bianconi, for the banter, the Mozzarella, the copious amounts of ‘genius’ that was had and for the many interesting scientific discussions that went late into the night! Thanks to my parents and to Denis, Pat and Karen for being there whenever I needed them.

DEDICATED TO MY PARENTS

PRESENTATIONS AND PUBLICATIONS ASSOCIATED WITH THIS THESIS

Oral presentations

‘Transformation of crystalline sulfadimidine and mannitol upon milling and co-milling’ presented at CGOM9, Nanyang University, Singapore, 2010. [V Curtin, V Caron, L Tajber, OI Corrigan, AM Healy].

‘Solid state characterisation of sulfadimidine and mannitol upon milling and co-milling’ presented at APSGB, University of Nottingham, 2010. [V Curtin, V Caron, L Tajber, OI Corrigan, AM Healy]. (*Oral presentation award*)

Poster presentations

‘The impact of co-milling sulfadimidine with low glass transition temperature excipients as a strategy for preventing process induced amorphisation’ presented at UKICRS, Queens University Belfast, 2011. [V Curtin, V Caron, L Tajber, OI Corrigan, AM Healy].

‘Use of glutaric acid excipient to minimise amorphisation of salbutamol sulphate and sulfadimidine upon co-milling’ presented at All-Ireland Schools of Pharmacy Research Seminar, University College Cork, 2012. [V Curtin, S Corcoran, Y Hu, P McArdle, A Erxleben, V Caron, L Tajber, OI Corrigan, AM Healy].

‘The capability of glutaric acid excipient to preserve the crystallinity of sulfadimidine and salbutamol sulphate upon co-milling’ presented at PBP World Meeting, Istanbul. [V Curtin, S Corcoran, Y Hu, P McArdle, A Erxleben, V Caron, L Tajber, OI Corrigan, AM Healy].

‘Investigation of the capability of crystalline dicarboxylic acids to minimise amorphisation of sulfadimidine on co-milling’ presented at AAPS Annual Meeting,

Chicago, 2012. [V Curtin, Y Amharar, Y Hu, P McArdle, A Erxleben, V Caron, L Tajber, OI Corrigan, AM Healy].

‘Mitigating amorphisation in mechanically activated salbutamol sulphate’ presented at All-Ireland Schools of Pharmacy Research Seminar, University of Ulster, Coleraine, 2013. [V Curtin, Y Amharar, S Corcoran, L Tajber, OI Corrigan, AM Healy].

Publications

‘Investigation of the capacity of low glass transition temperature excipients to minimise amorphisation of sulfadimidine on co-milling’, *Mol. Pharm.* 2013, 10 (1), 386-396. [V Curtin, Y Amharar, Y Hu, A Erxleben, P McArdle, V Caron, L Tajber, OI Corrigan, AM Healy].

‘Reducing mechanical activation-induced amorphisation of salbutamol sulphate by co-processing with selected carboxylic acids’ *Int. J. Pharm.* 2013, 456 (2), 508-516. [V Curtin, Y Amharar, KH Gallagher, S Corcoran, L Tajber, OI Corrigan, AM Healy].

SUMMARY

The focus of this thesis was to evaluate the impact of mechanical activation (milling and dry mixing) and spray drying on the crystallinity of selected active pharmaceutical ingredients (APIs) and to explore the feasibility of co-processing these drugs with low glass transition temperature (T_g) excipients as a strategy for preventing process induced amorphisation. Co-milling investigations were initially performed on sulfadimidine and salbutamol sulphate. Based on the data obtained for these two APIs, further analysis was conducted on budesonide to see if results could be generalised to other compounds. Co-spray drying experiments were performed with sulfadimidine as API. The excipients chosen were dicarboxylic acids (glutaric, adipic, succinic, pimelic and malic acid) and sugar alcohols (mannitol and xylitol). The selection of excipients was based on their low T_g values. Physicochemical characterisation of the systems was carried out by thermal analysis, powder X-Ray diffraction, infrared and near infrared spectroscopy and scanning electron microscopy. Vapour sorption properties and amorphous content quantification calculations were determined by dynamic vapour sorption (DVS).

All three APIs were amorphised when spray dried alone. Milling budesonide for 12 hours and salbutamol sulphate for 2 hours resulted in complete crystalline to amorphous transformations in both drugs. Moreover dry mixing salbutamol sulphate with glass beads for 8 hours resulted in complete amorphisation of the API. Sulfadimidine was predominantly amorphous ($76 \pm 3\%$ as quantified by DVS) when subjected to 10 hours of milling. Amorphous systems for each API had different thermal and vapour sorption properties according to whether the drug was exposed to milling or spray drying.

No amorphous content was detected on co-milling sulfadimidine with 50% w/w glutaric acid, and amorphous content of the API was reduced by almost 30%, relative to the API milled alone, on co-milling with 50% w/w adipic acid. In contrast, amorphisation of

sulfadimidine was promoted on co-milling with 50% w/w succinic acid and the API was completely amorphised on co-milling with 50% w/w malic acid.

The solubility of glutaric acid and adipic acid in amorphous sulfadimidine was estimated by thermal methods to be 34% and 20%, respectively. Maximum crystallinity of API on co-milling was reached at excipient concentrations comparable to the solubility of the excipient in the API. Moreover, the closer the Hildebrand solubility parameter of the excipient to sulfadimidine, the greater was the inhibition of API amorphisation on co-milling. The Hildebrand solubility parameter for another API, budesonide, was calculated to be $25.9 \text{ MPa}^{1/2}$ which was also very close to the value of glutaric acid ($25.8 \text{ MPa}^{1/2}$). Co-milling budesonide with 50% w/w glutaric acid eliminated amorphisation of the API.

Amorphisation of salbutamol sulphate was eliminated on co-milling with 50% w/w glutaric acid, and was more than halved, relative to the API milled alone, on co-milling with 50% w/w adipic acid and pimelic acid, respectively. Co-mixing with each excipient also resulted in a decrease in salbutamol sulphate amorphicity, although the extent of reduction was considerably less compared to the co-milling experiments. No further reduction in API amorphisation was achieved on co-mixing with 50% w/w excipient, compared to concentrations corresponding to the solubility of each excipient in the amorphous API ($\text{Sol}_{\text{Glutaric}} = 35\%$, $\text{Sol}_{\text{Adipic}} = 21\%$, $\text{Sol}_{\text{pimelic}} = 22\%$). In contrast to co-mixing, co-milling salbutamol sulphate at excipient weight fractions above their respective solubilities in the amorphous drug resulted in further reductions in API amorphisation attributed to the generation of a molecular dispersion of amorphous API, supersaturated with excipient, resulting in a more pronounced composite Tg lowering effect.

The Tg of mannitol was evaluated to be 13°C but the excipient solubility in amorphous sulfadimidine was determined to be only 4%. API amorphisation was promoted on co-milling with mannitol and the enhanced physical stability of the amorphous phase on co-milling, relative to API milled alone, was due to hydrogen bond interactions between the drug and excipient. Co-spray drying sulfadimidine with the low Tg excipients, under the conditions specified, did not prove successful at mitigating disorder in the API with the API being amorphous across all composite systems. Moreover each API:excipient co-spray dried system required individual characterisation to determine their relative physical stabilities and vapour sorption properties. In conclusion, co-milling API with low Tg excipients which show good solubility in the amorphous drug is a promising strategy for preventing the undesirable generation of amorphous phase on co-milling.

Chapter 1

Introduction

ORIGIN AND SCOPE

The amorphous state is the highest energy level of a pharmaceutical solid material and the useful properties of amorphous solids, compared to the crystalline state, are exploited to improve the formulation profiles of active pharmaceutical ingredients (APIs) with low water solubility (Hancock and Zografi, 1997; Kaushal et al., 2004; Yu, 2001). As amorphous materials are thermodynamically unstable, there is a tendency to revert back to the crystalline form over time. Hence much effort has focused on better understanding the key factors for stabilising amorphous forms of drugs. Solid dispersions are the preferred method and are prepared by co-processing API with high glass transition temperature polymers which act to increase the T_g of the miscible system, compared to the pure amorphous drug (Zheng et al., 2012). By elevating the T_g, a key parameter for amorphous physical stability, the polymeric carrier kinetically acts as a crystallisation inhibitor (Hancock et al., 1995; Van den Mooter et al., 2001).

While the development of the amorphous form of pharmaceutical products remains a promising, but significant challenge to the pharmaceutical industry, a further challenge which is, perhaps, more commonly encountered, is the prevention of the unintentional generation of disorder in crystalline materials on processing. Amorphisation during routine pharmaceutical processing is undesirable as the disordered amorphous domain will differ, both from a processability and stability perspective, from its crystalline counterpart (Guinot et al., 1999; Vippagunta et al., 2001; Hancock and Parks, 2000). Ward and Schultz (1994) noted that milling induced solid state changes in salbutamol sulphate. When the milled drug was subsequently exposed to elevated temperature and relative humidity, the amorphous

phase crystallised which resulted in significant particle bridging and agglomeration which had the effect of cancelling out the desirable particle size reduction. The authors concluded that unintentional milling-induced solid state changes in salbutamol sulphate could significantly impact performance characteristics for inhalation delivery systems containing the API. Ticehurst et al. (2000) investigated the influence of milling on the crystallinity and physical stability of revatropate hydrochloride and noted that milled particles of the API agglomerated on storage. The authors attributed this size enlargement to crystallisation of amorphous regions generated during milling which resulted in an increase in the percentage of material outside the respirable range.

As high T_g excipients may be employed to increase the stability of amorphous solid dispersions, we hypothesise that it is conceptually possible to destabilise any API amorphous phase by instead co-processing with low T_g excipients. By exerting a T_g lowering effect, the excipient would facilitate recrystallisation so that any amorphous phase created will be only temporary and rapidly convert back to the crystalline form.

The scope of this thesis was:

- To investigate and characterise the effect of mechanical activation and spray drying on the solid state properties of APIs with particular emphasis on quantifying amorphous content.
- To explore the capacity of low glass transition temperature excipients to minimise amorphisation of drugs on co-milling.

- To evaluate and compare the influence of two mechanical operations (milling and dry mixing) on a model API co-processed with a series of dicarboxylic acids.
- To examine if the results and conclusions obtained from the co-milling and co-mixing data could translate and be applied to the corresponding systems co-processed by spray drying.

1.1 Polymorphism

Polymorphism is the ability of a solid material to exist in more than one form or crystal lattice structure (Aaltonen et al., 2003; Haleblian and McCrone, 1979). While polymorphs have the same chemical composition, they differ in their packing and geometric arrangements, which can affect important pharmaceutical physical and chemical properties, including melting point, apparent solubility, dissolution rate, and mechanical properties which can have direct impact on the quality, safety and efficacy of the final drug product formulation (Ford, 1989).

Polymorphs are generally divided into two groups: enantiotropic and monotropic (Threlfall, 1995). Monotropy refers to cases where only one polymorphic form is stable at all temperatures below the melting point. If another crystalline form is produced, it will eventually convert to the stable polymorph. This stable form has a higher temperature of melting, and enthalpy of fusion, compared to other less stable forms. Enantiotropy exists where one polymorph is stable over a certain temperature range and pressure while another polymorph is stable over a different temperature range and pressure. Drug substances can undergo phase transformations when exposed to a range of pharmaceutical processes, such as drying, milling, granulation, spray drying and compaction (Giron et al., 2004). It is generally the stable polymorphic form that is considered the most suitable as a lead candidate for development in order to avoid any late stage product failures due to conversion during manufacture and storage. For instance a more stable polymorphic form of the anti viral medicine ritonavir was discovered post production which resulted in development being ceased with serious commercial repercussions for key stakeholders (Bauer et al., 2001).

1.1.1 Pseudo-polymorphism

Pseudo-polymorphism refers to crystalline forms which have solvent molecules as part of their structure (Rodriguez-Sprong et al., 2004). Hydrates are pseudo-polymorphs where the solvent is water; solvates are pseudo-polymorphs where the solvent molecule is not water. Pseudo-polymorphs can form following crystallisation from solution or by exposure of a crystalline material to an environment containing water or solvent vapour.

Hydrates and solvates can be used as active pharmaceutical ingredients (APIs) if their state of hydration or solvation is proven to be maintained following exposure to all environmental conditions to which the substance might be exposed during its shelf life (Giron et al., 2004). As occurs with polymorphs, the physical stability of hydrates and solvates will depend on the relative humidity and temperature to which it is exposed, and the most stable form may transform as environmental conditions are varied (Singhal and Curatolo, 2004). For instance problems may occur if the solid form is exposed to a dry environment or to low relative humidity conditions, in which case a hydrate may transform to a crystal characterised by a lower state of hydration, including an anhydrous form, which may subsequently alter product performance (Giron et al., 2004).

1.2 Amorphous state

Amorphous solids lack the repeated long range three dimensional molecular ordering of crystalline materials, although they may exhibit some short range order. (Hancock and Zografi, 1997; Yu, 2001; Hilden and Morris, 2003). When compared to the crystalline state, amorphous solids have a disordered liquid-like structure and

are thermodynamically unstable. The presence of amorphous materials can be desirable or undesirable, depending on the unique properties of the high energy state. Approximately 40% of new chemical entities are poorly soluble, and this poor solubility presents an obstacle to formulation development (Sareen et al., 2012). The preparation and stabilisation of an API in its amorphous state is a viable approach to improve its solubility since amorphous solids generally exhibit higher apparent solubility than the crystal form of the same substance (Yu, 2001). However, disordered materials are inherently metastable and over time will tend to revert to a more thermodynamically stable, crystalline form (Hancock and Zografi, 1997; Yu, 2001).

Amorphous forms of materials can usually be prepared by rapid cooling of a melt (quench cooling), rapid precipitation from solution (spray drying and freeze drying), or by mechanical activation (milling) (Craig et al., 1999). Amorphisation occurs by virtue of the fact that these processes create conditions that can prevent crystallisation from occurring as the solid is formed, or they can mechanically disrupt the structure of an existing crystalline material.

The physical characterisation of amorphous materials differs to that of the corresponding crystalline form. As there is no long range three dimensional order associated with the amorphous state, the diffraction of X-rays is irregular compared to that in the crystalline state (Hancock and Zografi, 1997). Thus powder X-ray diffraction (pXRD) patterns of amorphous materials display broad halos, in contrast to characteristic Bragg peaks for a crystalline material (Surana and Suryanarayanan, 2000). Thermal analytical methods, such as differential scanning calorimetry, have been used widely to characterise amorphous pharmaceutical systems. Amorphous

materials will exhibit a glass transition temperature (T_g), a characteristic property used to assess the likely stability and suitability for use in pharmaceutical dosage forms (Hancock and Zografi, 1997). The T_g is discussed further in section 1.2.2. The irregular arrangement of molecules in the amorphous state results in the molecules occupying a large specific volume compared to the crystalline state and hence the density of an amorphous material is less than that of the crystalline form. Hancock and Zografi (1997) noted, however, that highly accurate density measurements are difficult and in many scenarios the magnitudes of differences between the crystalline and amorphous forms of a compound are small. Amorphous materials absorb significant amounts of water vapour from their surroundings relative to their crystalline counterparts (Andronis et al., 1997). Dynamic vapour sorption is used to probe the relative affinities of amorphous and crystalline materials for vapour at different environmental relative humidities or partial pressures. The study of vapour sorption properties of amorphous and crystalline materials by DVS is discussed further in section 1.5.

1.2.1 Polyamorphism/pseudo-polyamorphism

Polyamorphs are similar to crystalline polymorphs in that they represent distinct phases (Angell and Sare, 1970). The evidence of polyamorphism in pharmaceutical materials is limited. The best known example is that of ice, where amorphous samples produced by quench cooling from the liquid state have been shown to have different properties (Loerting et al., 2001). The different amorphous forms were characterised and showed clear differences by X-ray diffraction, density measurements and Raman spectroscopy. Winkel et al. (2007) reported two distinct

phases in amorphous carbonic acid and designated the two amorphous forms as α amorphous carbonic acid and β amorphous carbonic acid. The formation of the two high energy states depended on whether potassium carbonate and hydrochloric acid were prepared in freeze concentrated aqueous or methanolic solutions. The authors noted from infrared (IR) spectra that two different hydrogen bonding populations existed in crystalline α and β carbonic acid, which also existed in the two amorphous forms. Moreover the halo pattern by pXRD of β carbonic acid was broader and the halo peak (bump) maximum shifted to higher 2θ degree values. The concept of 'pseudo-polyamorphism' was coined by Hancock et al. (2002a) to describe amorphous materials that have different energetic and physical properties arising from different conditions of production. Depending on how an amorphous material is generated and stored, it should be possible to isolate amorphous materials which have different physical properties (Hancock, 2007). Surana et al. (2004) evaluated the effect of different processing conditions on the physical stability of amorphous trehalose. There was no variability in the glass transition temperature of the amorphous sugar on spray drying, freeze drying, dehydration and melt quenching. However significant differences were noted in terms of vapour sorption properties and crystallisation tendencies for the amorphous form of the drug produced by different methods. The authors noted that the melt quenched sample was the most resistant to crystallisation, the spray dried and freeze dried samples showed similar crystallisation tendencies while the amorphous state produced by dehydration showed the greatest propensity to crystallise. Hence pseudo-polyamorphs, or amorphous forms of the same material with different physical properties, need to be thoroughly characterised and their properties and

physical stabilities evaluated and understood if they are to be incorporated into pharmaceutical dosage forms.

1.2.2 Glass transition temperature

The glass transition is the single most characteristic feature of amorphous solids and represents the temperature where the molecules exhibit a major change in mobility (Hancock et al., 1995). Figure 1.1 presents a schematic diagram of the enthalpy (H) or specific volume (V) as a function of temperature where a melt is cooled. The melt usually crystallises at T_m , where there is large decrease in V and H. However, if the cooling rate is too fast to permit crystallisation, H and V may follow the equilibrium line of the liquid beyond T_m into the supercooled region. If the temperature is lowered further, the molecules may not have sufficient time to rearrange themselves and a change in slope occurs as the material enters the glassy state. This change in molecular motion as the material enters the non equilibrium glassy state is the glass transition temperature (T_g).

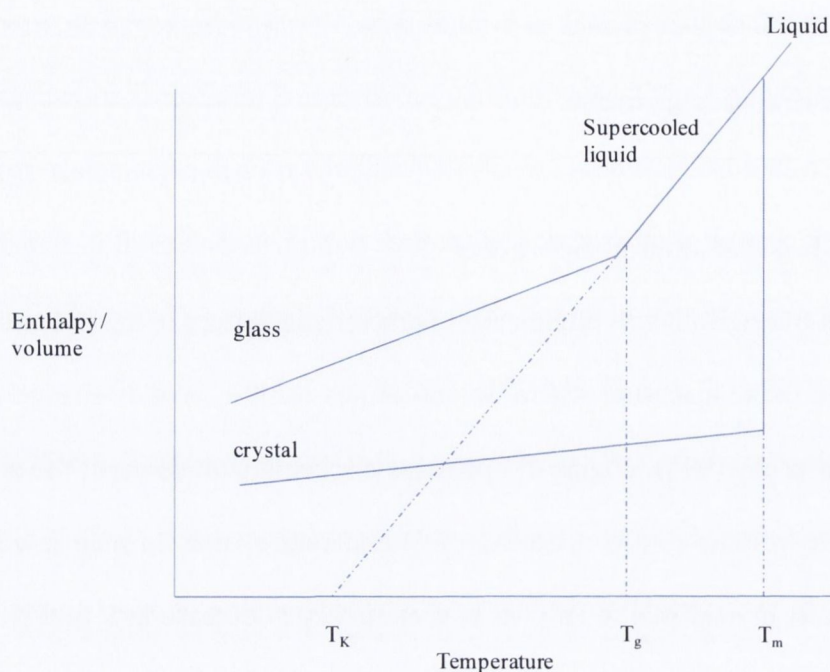


Figure 1.1 Schematic diagram of the variation of enthalpy (or volume) with temperature as a melt is cooled. T_m is the melting temperature and T_g is the glass transition temperature. Modified from Hancock and Zografi (1997).

The Kauzmann temperature (T_K) is below the melting point of the crystalline material and below the T_g of the amorphous material. It has been suggested that the T_K represents the temperature at which molecular motions responsible for the majority of unwanted physical changes in pharmaceutical products can be considered to be negligible over a product's shelf life (Hancock et al., 1995; Hatley, 1997). Thus the T_K can be used as an indicator of the storage conditions appropriate for amorphous pharmaceutical preparations to ensure physical stability. The T_K can be roughly estimated from the T_g ; storing an amorphous solid 50K below T_g is often sufficient to lower the risk of crystallization due to negligible molecular mobility at this temperature (Hancock and Zografi, 1997; Hatley, 1997).

It has been noted that the ratio T_g/T_m (in degrees Kelvin) calculated for several pharmaceutical solids was between 0.7 and 0.85 (Fukuoka et al., 1989; Kerc and

Srcic, 1995). The apparent constancy of the ratio indicates that the T_g can be estimated by the melting point data and is particularly useful for systems where the T_g is difficult to detect.

Molecular dispersions of a miscible drug/carrier system will typically display a T_g which is intermediate to that of the two pure amorphous components (Janssens and Van den Mooter, 2009). The relationship between the T_g of the composite ($T_{g_{mix}}$) and the composition of the mixture is described by the Gordon Taylor equation (Gordon and Taylor, 1952) in combination with the Simha-Boyer rule (Simha and Boyer, 1962).

$$T_{g_{mix}} = (w_1 T_{g1} + K w_2 T_{g2}) / (w_1 + K w_2) \quad \text{eq. 1.1}$$

where w is the weight fractions of each component, T_g the glass transition temperature, subscripts 1 and 2 represent amorphous compounds with the lower and higher T_g in the mix, and K is a constant that can be estimated with the Simha-Boyer rule (equation 1.2).

$$K = \rho_1 T_{g1} / \rho_2 T_{g2} \quad \text{eq. 1.2}$$

where ρ_1 and ρ_2 are the densities of amorphous components 1 and 2, respectively.

The equation was originally devised to describe T_g changes in polymer blends (Gordon and Taylor, 1952). However it has also been successfully employed in predicting the T_g of amorphous composites containing small molecules (Lobmann et al., 2011; Tajber et al., 2005). Systems which display deviations from the theoretical Gordon Taylor values are often associated with phase separation, strong specific interactions or the presence of an additional additive such as water (Gupta et al., 2005).

1.3 Solid dispersions

The term ‘solid dispersion’ refers to the dispersion of one or more active ingredients in an inert carrier or matrix at the solid state (Chiou and Riegelman, 1971). Dispersing an API in an amorphous carrier at the molecular scale not only increases its solubility and dissolution rate but can also prevent its recrystallisation over time (Repka et al., 2008; Leuner et al., 2000). The preparation of solid dispersions is the method of choice to stabilise the amorphous form of a drug (Zheng et al., 2012).

The improved physical stability of amorphous drugs in solid dispersions, relative to the amorphous drug alone, has been attributed to several factors. The T_g is a key factor governing the stability of amorphous phases. High T_g polymers act to increase the T_g of the miscible mixture resulting in a reduced molecular mobility at storage temperatures (Yoshioka et al., 1994). Van Den Mooter et al. (2001) noted that the physical stability of amorphous ketoconazole formulated as a solid dispersion with polyvinylpyrrolidone K25 was greatly enhanced compared to the pure amorphous drug. The composites displayed single T_g values, which increased gradually with higher amounts of polymer, indicating the anti-plasticising effect (see section 1.4.2 below) of the polymer additive. No specific structural interactions between the two components occurred and the authors concluded that the improved physical stability of the composite was due to the T_g elevating effect of the polymer.

Ivanisevic (2010) investigated the long term physical stability of 12 amorphous dispersions over a period of 9-22 months and compared the tendency for recrystallisation with that of the pure amorphous APIs. Nine drug/polymer systems

were miscible throughout the duration of the study and remained amorphous, whereas three phase separated systems recrystallised within 1-2 months. In contrast, the APIs selected for the study were very unstable as pure amorphous forms and crystallised within days.

Despite the obvious advantages, the number of pharmaceutical products on the market based on solid dispersions is limited (Laitinen et al, 2012). Amorphous API:polymer dispersions tend to be hygroscopic and the plasticising effect of water can cause phase separation and crystallisation. Moreover poor miscibility between components often results in large amounts of polymer being required for sufficient drug loading (Serajuddin, 1999).

1.4 Stability of the amorphous state

1.4.1 Crystallisation from the amorphous state

Amorphous systems are thermodynamically unstable and hence convert back to the energetically favourable crystalline form with time (Vasconcelos et al., 2007). The glass forming ability of a material is generally screened using thermal methods of analysis such as differential scanning calorimetry (DSC) and crystallisation behavior evaluated on cooling of a melt followed by reheating (Baird et al., 2010; Nascimento et al., 2005). Crystallisation from the amorphous state is a result of two independent events which have different temperature dependencies, nucleation and growth (Bhugra and Pikal, 2007). Nucleation is thermodynamically favoured at high rates of supercooling and growth is favoured at higher temperature or at lower degrees of supercooling (Hancock and Zografi, 1997). Between the glass transition temperature and the melting temperature there is a small window where the events

of nucleation and growth overlap. In the region of overlap an amorphous material is undergoing nucleation in a region of high growth and will crystallise (Trasi and Taylor, 2012; Figure 1.2). For compounds where the nucleation zone is at a much lower temperature than the growth zone, it is possible to quench the supercooled liquid into a glass. During the cooling process it is possible to have quenched in nuclei which are unable to grow during rapid cooling. However if the sample is reheated and passes through a temperature zone where growth is favoured then crystallisation will occur. If a compound has very low nucleation and growth rates then it may not crystallise during cooling and heating.

Baird et al. (2010) developed a classification system to assess the tendency of 51 organic glasses to crystallise upon supercooling from the melt. Class 1 compounds crystallise on cooling from the melt due to overlapping nucleation and growth. Class 2 compounds form a glass on cooling because growth rates are very low at low temperature where nucleation predominates. Class 3 compounds fail to crystallise on cooling and heating due to separated nucleation and growth rates or just overall low nucleation and growth rates. This is illustrated in Figure 1.2 below.

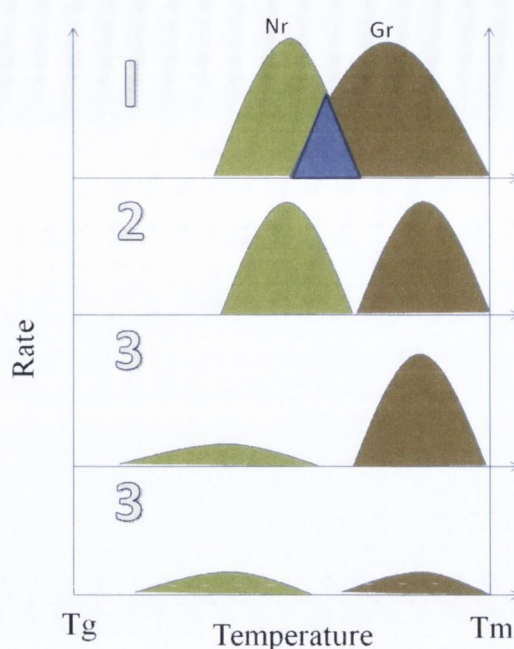


Figure 1.2 Schematic of different rates of nucleation (Nr) and growth (Gr) and hence crystallisation rates for class 1, 2 and 3 compounds on cooling and heating from the melt (adapted from Trasi and Taylor, 2012). Highlighted in blue for class 1 compounds is where nucleation and growth overlap and these compounds crystallise on cooling from the melt.

1.4.2. Plasticisation

The T_g of an amorphous solid can be decreased by the addition of a plasticiser (e.g. water) or guest molecule into the matrix (Claes and Zografis, 1990). Plasticisation refers to an increase in molecular rotation and movement which results in a reduction in the T_g of the amorphous phase (Heljo et al., 2012; Burnett et al., 2004; Hancock and Zografis, 1994). Water, for example, has a very low T_g of 136K (Haque and Roos, 2003) and, from the Gordon Taylor equation, it is clear that even a small increase in the amount of water in a mixture will significantly reduce the overall composite T_g . The extent of T_g reduction depends on the concentration of the plasticiser and its interaction with the amorphous material (Burnett et al., 2004). In this thesis it was anticipated that co-processing of the drug and excipient would

result in API:excipient composite systems so that the low T_g property of the excipient could be exploited. The low T_g excipient would function to lower the composite API:excipient T_g, relative to the T_g of the pure amorphous drug alone, and act to destabilise the amorphous form of an API. This concept, with respect to co-milling is illustrated in Figure 1.3. The terms ‘plasticising effect’ and ‘T_g lowering effect’ are used interchangeably in this thesis.

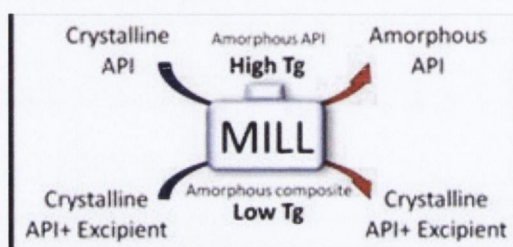


Figure 1.3 Schematic of mitigating amorphisation of API on co-milling with low T_g excipient.

1.4.3 Structural interactions

Intra and intermolecular hydrogen bonding are important considerations, in addition to the composite T_g, when considering the stability of an amorphous drug in a composite system, compared to the amorphous drug alone. IR spectroscopy can be used to study molecular interactions between components. In particular IR is very sensitive to hydrogen bonding (the strongest of all intermolecular interactions) as the peak position of the X-H bond (with X = oxygen, nitrogen or carbon) is very sensitive to the strength of association (Tang et al., 2002, Kaushal et al., 2008). Unbounded X-H displays a sharp peak on the IR spectrum of a molecule. This peak becomes broader and is shifted to lower wavenumber when hydrogen bonding

occurs with an acceptor atom. The stronger the hydrogen bond, the weaker is the X-H bond and the greater is the peak shift to lower wavenumber.

Tang et al. (2002) investigated the differences in hydrogen bonding tendencies by IR in the crystalline and amorphous states of seven dihydropyridine analogues. The authors concluded that, for some compounds hydrogen bonding was stronger in the crystalline state while for others it was stronger in the amorphous state. An appreciation of the difference in molecular interactions in the amorphous phase compared to the crystalline counterpart is helpful in understanding the behaviour of these systems. Marsac et al. (2006) compared the physical stability of felodipine, which has stronger hydrogen bonds in the amorphous state, with nifedipine which has stronger hydrogen bonds in the crystalline state. As expected, felodipine was noted to be more stable in the amorphous form than nifedipine, with slower crystallisation kinetics. In another study, a strong correlation between hydrogen bonding in molecules and crystallisation from the amorphous state was found in the case of acetaminophen glass (Gunawan et al., 2006). The authors noted that the stronger the hydrogen bonding of the drug in the amorphous state, the lower was the tendency of the drug to crystallise.

Knowledge of hydrogen bonding interactions is useful in selectively targeting polymers or small molecule excipients with specific donor or acceptor groups which could selectively promote or disrupt hydrogen bonding, depending on the desirable final solid state form of the material (Bhugra and Pikal, 2007). Miyazaki et al. (2004) attributed the ability of polyacrylic acid (PAA) to stabilise amorphous dispersions of acetaminophen to the strength of the acid base interaction between

the hydroxyl group of the drug and the carboxyl group in PAA. This contrasted with the improved stability of the drug with polyvinylpyrrolidone (PVP) associated with hydrogen bond interactions.

Matsumoto and Zografi (1999) investigated the influence of PVP on the crystallisation behavior of indomethacin. The Tg of the amorphous dispersions did not differ significantly from the Tg of the amorphous drug, and consequently molecular mobility of the composites was only marginally decreased. The authors therefore concluded that the antiplasticising effect of the high Tg polymer did not play a major role in the enhanced stability of the amorphous system. Spectroscopic analysis revealed that the formation of carboxylic acid dimers, a prerequisite for indomethacin crystallisation, was inhibited with only 5% w/w PVP, due to the formation of hydrogen bonds between the drug and polymer.

1.5 Vapour sorption properties of crystalline and amorphous solids

Amorphous materials have greater vapour sorption potential compared to their crystalline counterparts, due to increased void space, free energy and/or surface area (Burnett et al., 2006). Dynamic vapour sorption (DVS) has routinely been used to study the interaction of water and organic solvents with pharmaceutical materials (Burnett et al., 2006). The instrument measures the sample mass change as the vapour environment surrounding the sample is varied in a controlled manner. A key feature of the DVS system is the incorporation of an optical detector for measuring the vapour pressure of water and organic solvents. The software has an inbuilt standard vapour pressure table for organic solvents and water and the DVS uses

mass flow controllers (MFC) to flow gas through the system to produce the desired relative humidity (RH) or partial pressure (P/P_0). In order to generate a certain RH or P/P_0 , one of the MFC flows a percentage of dry gas (nitrogen) and the other MFC flows a certain percentage of solvent (water or ethanol were used in this thesis) into the system (wet flow). By varying the proportions of dry gas and wet gas, the RH or P/P_0 around the sample is controlled.

DVS can be used to measure the hygroscopicity of a pharmaceutical material, which is the ability of solids to take up vapour from the atmosphere at constant temperature with changes in RH (Reutzel-Edens and Newman, 2006). It is a routine test during preformulation studies to determine the impact of vapour on the physical properties of a drug candidate and to evaluate the ability of the sorbed vapour to compromise the stability of an amorphous material. The European Pharmacopoeia classifies solids as nonhygroscopic (0-0.12% w/w), slightly hygroscopic (0.2-2% w/w), moderately hygroscopic (2-15% w/w) and very hygroscopic (>15% w/w) according to the % vapour uptake at 25°C and 80% RH.

The amount of vapour that is sorbed will depend on the polarity of the compound, its surface area and porosity, as well as the temperature and partial pressure of the environment (Newman et al., 2007). Of particular concern when exploiting the amorphous form of a drug is its stability during processing and storage. Sorbed vapour can act as a plasticising agent, and is thus capable of lowering the T_g of an amorphous material below the storage temperature and cause phase transitions. There is often a critical humidity at which the glass transition will occur at a

particular temperature and its identification is important from a physical stability perspective (Burnett et al., 2004).

DVS has been shown to be a very sensitive analytical technique in the quantification of amorphous content (Mackin et al., 2002b; Saleki-Gerhard et al., 1997). Four vapour sorption techniques have been developed to quantify amorphous contents below 5%. Methods 1-3, as described below, are based on the different vapour affinities for the amorphous and crystalline phases of a given compound. Method 4 is based on the formation of a stoichiometric hydrate.

Method 1 involves measuring the water uptake of a partially amorphous material at a particular humidity and comparing it to a calibration curve measured with samples of known amorphous contents (Saleki-Gerhardt et al., 1994). Samples with known amounts of amorphous content are obtained by preparing physical mixtures, of varying proportions, of 100% crystalline and 100% amorphous standards of the material. The method assumes that uptake of the crystalline material is negligible compared to the amorphous phase.

Method 2, and the method used in this thesis, requires a recrystallisation event to occur in the course of DVS analysis in order to quantify the amorphous content (Mackin et al., 2002b). The sample is initially dried and then subjected to a P/P_0 (water or organic solvent) below the P/P_0 where sample recrystallisation occurs. The sample is then exposed to an elevated P/P_0 which forces recrystallisation. Here excess vapour sorbed by the amorphous phase can no longer be accommodated and is expelled, resulting in a mass loss in the DVS profile. The newly crystallised sample is finally exposed to the same P/P_0 as before (below where recrystallisation

occurs). Provided the sample has fully recrystallised, the difference in uptake between the amorphous and crystalline material is directly related to the amorphous content in the sample.

Method 3 uses organic vapours to quantify amorphous content. The method is based on the assumption that an amorphous material will have a greater organic vapour sorption capacity than the crystalline material (Young et al., 2007). The percentage uptake for a partially amorphous standard is compared to known amorphous content samples, as discussed for method 1. This method does not require a solvent induced crystallisation event. Young et al. (2007) noted the kinetics of octane sorption is relatively fast, when compared to water, so experimental throughput can be quicker when using organic vapours compared to moisture based experiments.

Method 4 is only suitable when the amorphous material forms a stoichiometric hydrate or solvate during vapour induced crystallisation (Buckton and Darcy, 1995). This limits the applicability of method 4. A benefit of this method is that it does not require any amorphous standards.

1.6 Drug-excipient solubility

Solubility parameters are based on regular solution theory (Hildebrand, 1950; 1962). Solubility parameters are used as estimates of molecular similarity between components and can be applied to low molecular weight organic materials (Hancock et al., 1997). The Hildebrand solubility parameter has been described as a non-discriminating method of characterising the properties of pharmaceutical solids

(Barton, 1984). It is easily calculated using Fedors group contribution method (Fedors, 1974). Its principal advantage is that a large number of functional groups have been evaluated and, secondly, it is a very fast and usable method as it only requires knowledge of the chemical structure of the compound. Greenhalgh et al. (1999) highlighted a trend in terms of increasing degrees of immiscibility with increasing differences in Hildebrand solubility parameter between the two components in amorphous dispersions. Solid dispersions consisting of components with similar solubility parameters are expected to display good miscibility/solubility in the amorphous state. Yoo et al. (2009) noted a correlation between amorphous miscibility/physical stability of binary solid dispersions and differences in Hildebrand solubility parameters ($\Delta\delta$). The smaller the $\Delta\delta$ the greater was the potential to have a miscible amorphous system.

The solubility of an API in an excipient and *vice versa* can be determined experimentally by thermal methods. A first method is based on the principle that when a mixture has a drug-polymer composition above the solubility of the drug in the polymer, the saturated amorphous solid phase is in apparent equilibrium with undissolved crystals of API (Theeuwes et al., 1974). This fraction of unsolubilised drug will exhibit a melting endotherm when the saturated amorphous phase with excess API is heated by DSC. The solubility is then obtained by plotting the measured melting enthalpy as a function of drug composition and extrapolating it to zero enthalpy (Gramaglia et al., 2005). A second method is known as the ‘melting point depression’ method (or scanning method). This thermal technique, introduced by Tao et al. (2009) is based on the measurement of the dissolution endpoint of API in API/polymer mixtures prepared by milling. The plot of the dissolution endpoint

as a function of composition gives the solubility curve of the crystalline solute in the amorphous polymer. For an additive to exert a T_g modifying effect, good solubility between the two components must exist so that they mix at the molecular level (Marsac et al., 2009, Rumonder et al., 2009).

1.7 Milling

Pharmaceutical solid materials for incorporation into formulations/final dosage forms are rarely crystallised at the optimum particle size. It is estimated that approximately 40% of marketed APIs have 'low solubility' according to the Biopharmaceutical Classification System (BCS) (Van Arnum, 2011). The BCS is scientific framework for classifying drug substances based on their aqueous solubility and intestinal permeability (Amidon et al., 1995). Particle size is critical in terms of its influence on dissolution rate, which is directly proportional to surface area (Nernst and Brunner, 1904). A reduced particle size leads to an increased dissolution rate, and higher bioavailability has been reported for a number of BCS class II and class IV compounds (Horter and Dressman, 2001). Comminution is a generic term for particle size reduction and terms such as grinding, milling, pulverisation and dispersion have been used synonymously (Parrot, 1974). Milling also has applications in deagglomeration, blending, and mixing of formulations. For instance, xemilofibran, an anti-thrombotic drug, forms agglomerates during processing and is milled to achieve the required particle size specifications (Mackin et al., 2002a).

Milling is a highly energetic process capable of causing structural changes in milled materials, such as changes in crystal morphology, an increase in the number of

crystal defects, polymorphic transformation, and partial or complete amorphisation (Willart and Descamps, 2008). Amorphisation upon milling is often unintentional and frequently undesirable as the amorphous form will tend to revert back to the more energetically favoured crystalline state (Buckton and Darcy, 1999). Mackin et al. (2002b) noted that the milled form of an experimental drug failed the blend content uniformity test when compared with the unmilled form of the API having similar particle size. Analysis by DVS revealed that milling had generated a partially amorphous form of the drug. The amorphous material created during milling recrystallised after a few days. Following recrystallisation the batches did not exhibit the same physical properties as the unmilled actives and resulted in drug product failing drug uniformity specifications. The authors suggested that the amorphous phase produced by milling recrystallised into a different polymorphic form of the drug, compared to the unmilled sample, resulting in changes in physical properties and blending characteristics.

The term ‘mechanical activation’ is used to describe the increase in energy of a solid material arising from mechanical stress (Smekal, 1942). Subjecting a crystalline material to mechanical stresses, primarily in the form of friction, attrition and fracture processes, results in structural disordering. Lattice defects, imperfections and crystal disordering are then associated with an increase in entropy and enthalpy (Huttenrauch et al., 1985). A constant change in energy, disorder or activity is called static activation, whereas a non-constant change in energy is referred to as dynamic activation. Milling is a highly dynamic process and transient periods of amorphisation and crystallisation has been reported (Balani et al., 2010; Gusseme et al., 2008). The high energy state is unstable and therefore once the

mechanical process has ceased, deactivation, in terms of crystallisation and energy loss will occur with time. The rate of deactivation will depend on the activation conditions and the material properties (Huttenrauch et al, 1985). The final solid state form will never reach an ideal structure free of defects; this irreversible output of energy has been referred to as ‘anergy’ (Huttenrauch et al., 1985). These points are illustrated in Figure 1.4 below.

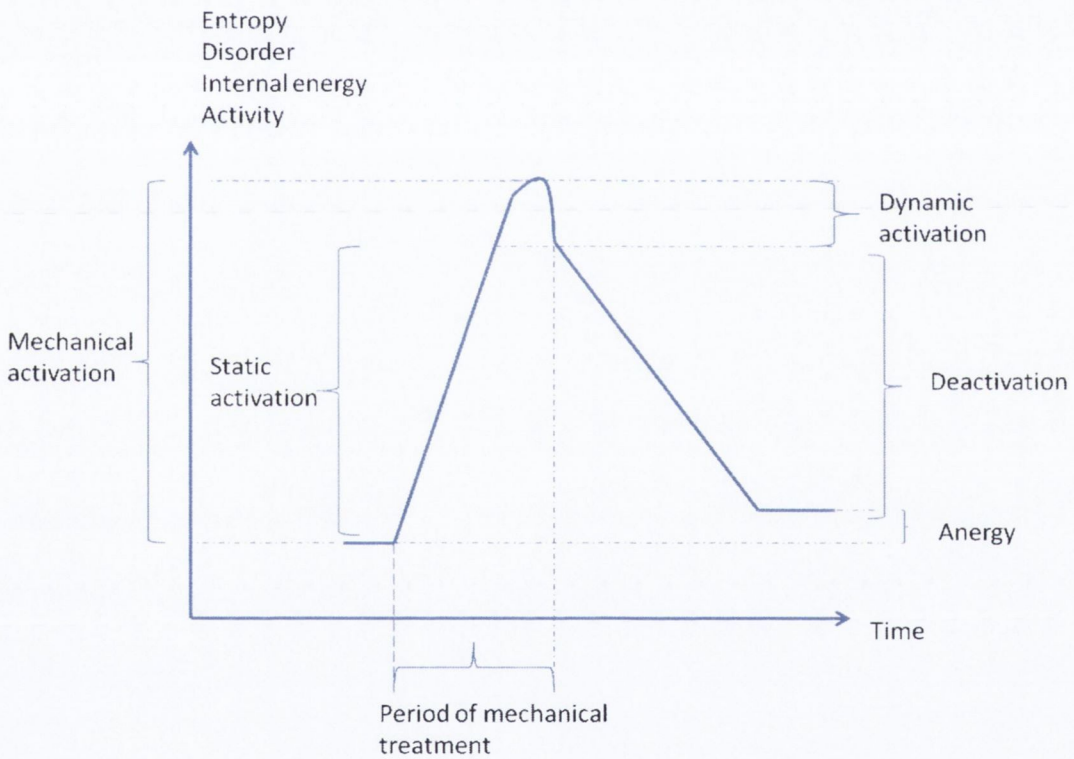


Figure 1.4 Schematic illustration of energy changes that occur during and after mechanical activation (adapted from Huttenrauch et al., 1985).

1.7.1 Co-milling

Co-milling refers to the milling of two or more materials together and is a simple and effective method of improving the physiochemical properties of various APIs (Shakhtshneider et al., 1996). Co-milling the poorly water soluble drug nifedipine with polyvinylpyrrolidone (PVP), sodium dodecyl sulphate, hydroxypropylmethylcellulose (HPMC) polyethylene glycol (PEG) and urea improved the dissolution rate of the drug (Friedrich et al., 2005). This was not only due to particle size reduction but also resulted from the ability of the carriers to prevent re-aggregation of finely divided drug particles. Co-milling nifedipine with PVP and with HPMC reduced the tendency of crystallisation of the amorphous drug, relative to physical mixtures of API and polymer, due to hydrogen bonding interactions between the API and polymer.

Co-milling enables the possibility of obtaining solid dispersions with unique properties and functionalities compared to the individual systems alone. Caron et al. (2011) produced amorphous dispersions of sulfadimidine and sulphathiazole by co-milling. The co-milled amorphous dispersions displayed better dissolution rates in aqueous media compared to the physical mixtures of unprocessed API and excipient, and compared to physical mixtures of API and excipient which were milled separately. Co-milling has been also employed in the preparation of amorphous solid dispersions of poorly water soluble drugs such as sulfamerazine and sulfadiazine (Caron et al., 2013), glicazide (Barzegar-Jalali et al., 2010), indomethacin (Watanabe et al., 2003), and piroxicam (Shakhtshneider et al., 2007). Formulating the compounds as solid dispersions combined the benefits of an

increase in solubility, maximal surface area of the active and an improvement in wettability.

Co-milling has been used in the preparation of co-amorphous binary systems of API with small molecules instead of polymers. Chieng et al. (2009) prepared co-amorphous indomethacin/ranitidine hydrochloride systems by co-milling and noted that API amorphisation occurred more rapidly on co-milling, compared to amorphisation of the individually milled drugs under the same milling conditions. Alleso et al. (2009) reported that co-milling of naproxen and cimetidine resulted in an amorphous mixture while milling naproxen alone did not cause amorphisation of the drug. In both studies the authors noted that the 1:1 molar co-amorphous systems were the most physically stable despite not having the highest composite T_g , and attributed the enhanced physical stability to intermolecular interactions between the two components.

Caron et al. (2007) co-milled mannitol ($T_g = 13^\circ\text{C}$) with trehalose ($T_g = 120^\circ\text{C}$) and produced amorphous molecular dispersions, with intermediate composite T_g values, when the weight fraction of mannitol was ≤ 0.65 . At higher weight fraction of mannitol, a two phase system of amorphous trehalose:mannitol and crystalline α mannitol was produced. In another study, Dudognon et al. (2006) co-milled budesonide (10, 30, 50, 70% w/w) with lactose ($T_g = 114^\circ\text{C}$) and produced amorphous systems with single T_g values between those of the pure milled compounds. The elevated T_g of the composite systems, relative to budesonide milled on its own, has the potential to enhance the stability of the amorphous form of budesonide.

1.8 Dry mixing

Mechanical activation is often considered to occur due to the fracture or breakage of a solid. However this is not a prerequisite for solid state changes to be induced in a material. In some mechanical operations routinely used in the pharmaceutical industry, such as size and shape sorting and blending the particles may be subjected to stresses below the threshold level required for fracture or breakage. For example, it has been shown that dry mixing activated griseofulvin at its surface resulting in a subsequent increase in apparent solubility (Mosharraf and Nystrom, 1999). Hockerelt et al. (2009) demonstrated that dry mixing of griseofulvin with mm-sized glass beads in a tumbler mixer was capable of completely amorphising the drug without any associated reduction in particle size. It was postulated that the process led to repeated deformation of the particles which eventually evolved into a crystalline to amorphous transformation in the drug.

1.9 Solid state amorphisation

Solid state amorphisation refers to amorphising a solid without passing through the liquid state at any point (Suryanarayana, 2001). Amorphous phase formation on milling is highly dependent on the milling conditions and the properties of the material. The two most critical variables which determine the nature of the final product are the milling energy, governed by the ball to powder ratio selected and speed or rotation, and the milling temperature (Shakhtshneider and Boldyrev, 1999). However there remains uncertainty regarding the actual mechanism of amorphisation by milling.

A ‘melt quench’ theory is proposed, whereby the mechanism of amorphisation is associated with a heating effect due to the balls in the milling chamber elevating the temperature of the system above the melting point of the compound (Shakhtshneider and Boldyrev, 1999; De Gusseme et al., 2008). The rapid return to ambient temperatures immediately after impact results in the quench effect. The ‘melt quench’ mechanism has been challenged based on milling experiments performed on fananserine (De Gusseme et al., 2008) and α lactose (Willart et al., 2004). In the case of fananserine, the API was noted to more easily amorphise at lower temperatures. This is counterintuitive to the hypothesis that the material amorphises via a melting step that occurs during the milling process; at lower temperature the gap between the milling temperature and the melting temperature of the compound is greater. In the case of α lactose, the absence of mutarotation of α lactose to the β isomer on milling was noted. Lactose displays a strong mutarotation effect when it is heated and melted, with the effect occurring both in aqueous solution and in the solid state. The absence of mutarotation on milling α lactose was highlighted as definitive evidence that the ‘melt quench’ mechanism was not a plausible mechanism for solid state amorphisation by ball milling.

Descamps et al. (2008) noted that amorphisation of a material on milling was promoted as the milling temperature was lowered and related this to the ‘driven alloy’ concept developed by Martin and Bellon (1997). According to the ‘driven alloy’ concept, during milling, there is a temperature independent disordering process caused by impact and attrition which increases the likelihood that amorphisation will occur. However the disordering effect needs to be weighed up against the counter argument that any increase in milling intensity will lead to an

increase in the milling temperature which will accelerate the propensity of any formed amorphous phase to crystallise. The tendency for crystallisation is viewed as a temperature dependent restoration process. Descamps et al. (2007, 2008) noted that the position of the T_g of a material relative to the milling temperature has a direct influence on whether polymorphic transformation or amorphisation is observed upon milling. Milling a material below its T_g favours amorphisation, and it was proposed by Descamps et al. (2008) that the disordering potential predominates, compared to the restoration component, when milling is performed below T_g . Cimetidine (Alleso et al., 2009), griseofulvin (Trasi et al., 2010), trehalose (Willart et al., 2001), glucose (Dujardin et al., 2008), lactose (Willart et al., 2007), sulphathiazole (Hu et al., 2010), sulfamerazine (Zhang et al., 2002) and piroxicam (Shakhtshneider, 1997) were found to completely amorphise when milling was performed at temperatures below their respective T_g values. In contrast, when milling is performed at elevated temperatures above the T_g of a compound, the temperature dependent restoration process predominates over the disordering potential and the material is maintained in the crystalline solid state. Milling of mannitol and sorbitol (Willart et al., 2007) and indomethacin (Otsuka et al., 1986) resulted in crystalline products but of a different polymorph when milling was performed at temperatures above the T_g s.

1.10 Spray drying

Spray drying is a one step, continuous process that converts a bulk liquid into powder. It is both a robust and scaleable process with broad application in the chemical, food and pharmaceutical industries (Master, 2002). It consists of 5 stages – atomisation, droplet gas mixing, drying of droplets, separation of dry particles

from the drying gas and collection of the dried product. The primary feature of the process is the formation of a spray which provides a high droplet area exposed to heat, resulting in a fast and efficient process. The bulk liquid is converted to droplets using an atomizing nozzle. A twin fluid nozzle atomiser was used in the Buchi-290 spray drier in this thesis. These nozzles tend to produce smaller droplets with a broader distribution when compared to rotary atomizers and are therefore preferred for pharmaceutical applications targeting small particle size (Snyder and Ballesteros, 2008). The orifice diameter will influence the size of the final particles. The diameter orifices of the tip and cap used in this study measured 0.7mm and 1.5mm respectively.

Spray drying applications in the pharmaceutical industry date to almost 50 years ago and has been used to produce functional excipients, to stabilise proteins and to produce API where control over solid state form, particle size and morphology is required (Snyder and Ballesteros, 2008). By modifying different operating parameters, it is possible to fine tune both the solid state form and solid state properties of the spray dried material (Bianco et al., 2012; Buckton et al., 2002). Spray drying frequently results in the amorphisation of API (Corrigan et al., 1984; Tajber et al., 2005; Caron et al., 2011). Co-spray drying of paracetamol, a physically very unstable amorphous drug with a low T_g, with hydrophilic polymers was recently shown to inhibit crystallisation of the drug (Zhao et al., 2012). IR studies did not indicate any specific interactions between API and polymer and the expected stability associated with a high composite T_g was not observed. The authors suggested that the loss of water from droplets, associated with the speed of evaporation during the spray drying process may have contributed to preventing

crystallisation of the drug. Corrigan et al. (2004) noted that co-spray drying salbutamol sulphate with lactose, which are both amorphous when spray dried alone, resulted in amorphous composites. In contrast co-spray drying the API with PEG resulted in composite systems of varying crystallinity, which was found to be dependent on the weight ratio of polymer to drug. The authors highlighted that the formation and physical stability of amorphous composites produced by spray drying was dependent on whether the T_g of one of the components was sufficiently high to elevate the composite T_g above that of the storage temperature.

Chapter 2

Materials and methods

2 Materials and Methods

2.1 Materials

Material	Supplier/manufacturer
Acetonitrile, HPLC grade	Fisher Scientific, Ireland
Adipic acid	Sigma Aldrich, Ireland
Budesonide	Kemprotec Ltd., UK
Ethanol 99.5%	Cooley Distillery, Ireland
Ethanol \geq 99.8% for DVS	Sigma Aldrich, Ireland
Glass beads (5mm)	Sigma Aldrich, Ireland
Glutaric acid	Sigma Aldrich, Ireland
Malic acid	Fluka Chemika, Switzerland
Mannitol	Sigma Aldrich, Ireland
Nitrogen gas (high purity, oxygen free)	BOC gases, Ireland
Pimelic acid	Sigma Aldrich, Ireland
Potassium bromide	Spectrosol, Ireland
Salbutamol sulphate	Camida Ltd. Ireland
Silica gel	Merck, Germany
Succinic acid	Sigma Aldrich, Ireland
Sulfadimidine	Sigma Aldrich, Ireland
Triethylamine	Sigma Aldrich, Ireland
Water, deionised	Millipore Elix advantage purification system

2.2 Methods

2.2.1 Milling

Ball milling was performed with a PM 100 high energy planetary mill (Retsch, Germany) at room temperature or in a cold room with a temperature of $4 \pm 1^\circ\text{C}$. 2.5 g of material was placed in stainless steel milling jars of 50 cm^3 volume with three stainless steel balls of diameter 20 mm, corresponding to a ball to powder mass ratio of 40:1. The speed of the solar disk was set at 400 rpm. Every 20 minutes of milling was followed by a pause period of 10 minutes to avoid overheating

2.2.1.1 Sulfadimidine and sulfadimidine:excipient composites

Total milling time of sulfadimidine (SDM) and SDM:excipient co-milled composites was kept constant at 15 hours (h) corresponding to an effective milling time (discounting the pause periods) of 10 h. SDM was comilled with the dicarboxylic acids glutaric acid (GA), adipic acid (AA), succinic acid (SA), and malic acid (MA) and the sugar alcohols mannitol (MAN) and xylitol (XYL) at different weight percentages of excipient ($X_{\text{excipient}}$). The following weight percentages of excipient were used :

$$X_{\text{GA}} = 5, 10, 20, 30, 40, \text{ and } 50;$$

$$X_{\text{AA}} = 20, 30, 50, 70;$$

$$X_{\text{SA}} = 50;$$

$$X_{\text{MA}} = 50;$$

$$X_{\text{MAN}} = 4, 10, 20, 40, 50, 60, 80;$$

$$X_{\text{XYL}} = 20, 40, 50, 60.$$

2.2.1.2 Salbutamol sulphate and salbutamol sulphate:excipient composites

Total milling time for milled salbutamol sulphate (SS) and co-milled SS:excipient composites was kept constant at 3 h, corresponding to an effective milling time of 2 h.

SS was co-milled with GA at different weight percentages of excipient ($X_{GA} = 5, 20, 35, 50$). SS was also co-milled with 21% w/w (corresponding to the solubility of AA in amorphous SS – see section 2.2.14.2) and 50% w/w AA, and 22% w/w (corresponding to the solubility of PA in amorphous SS - see section 2.2.14.2) and 50% w/w PA. API:excipient co-processed systems are named in accordance to the % weight fraction of each component. For instance SS95:GA5 refers to a system comprised of 95% w/w SS and 5% w/w GA.

2.2.1.3 Budesonide and budesonide:glutaric acid co-milled composite

Total milling time for milled budesonide and the co-milled budesonide:glutaric acid system ($X_{GA} = 50$) was 18 h, corresponding to an effective milling time of 12 h.

2.2.2 Dry mixing

Dry mixing experiments of SS and SS:excipient systems were performed using a Turbula mixer operating at 64 rpm (360 ml tubes, W.A. Bachofen, Switzerland) based on the method used previously by Hockerfelt et al. (2009). The API and API:excipient fractions were mixed with glass beads in the weight proportion 1:99 of powder to beads. A total powder content of 0.78 g was used for the dry mixing experiments. Experiments were performed at different times, ranging from 2 h to 24 h. SS was dry mixed with GA, AA and PA at excipient weight fractions corresponding to the solubility of each excipient in the amorphous drug (section 2.2.14.2). The 24 h mixes were also performed at 50% w/w excipient.

2.2.3 Spray drying

All systems were spray dried as solutions using a Büchi-290 Mini Spray Dryer (Büchi Laboratoriums-Techniq AG, Flawil, Switzerland). The conditions used for spray drying the various systems are presented in Appendix I. All feed solutions were freshly prepared prior to spray drying. A sonicator (Fisher Scientific FB 15053, Dublin, Ireland) was used to aid dissolution. All experiments were conducted in the open mode configuration using compressed air as the drying medium. A standard size cyclone was used. Samples were collected from the collecting vessel and cyclone of the spray dryer using a small brush and antistatic gun (Zerostat[®]3, Sigma Aldrich, UK). SDM was co-spray dried with the dicarboxylic acids GA, AA, SA, and with MAN. The following weight percentages of excipient ($X_{\text{excipient}}$) were used:

$$X_{\text{GA}} = 10, 20, 50, \text{ and } 60;$$

$$X_{\text{AA}} = 20, 50, 60;$$

$$X_{\text{SA}} = 50;$$

$$X_{\text{MAN}} = 4, 10, 20, 40, 50, 60, 80.$$

2.2.4 Freeze drying

SS:GA mixtures of various weight fractions ranging from 95:5 to 50:50 were dissolved in deionised water and stirred at room temperature to yield aqueous solutions with a concentration of 5% w/w total solid. The solutions were then sonicated for 10 minutes and filtered through a 0.45 micron syringe filter to ensure the absence of any residual crystals. The resulting aliquots (5 ml) were then poured into 50 ml plastic tubes, which were immersed in liquid nitrogen for 15 min and then loaded into a VirTis wide mouth filter seal glass flasks and attached to one of the manifold ports of a benchtop VirTis 6K freeze-dryer model EL (SP Scientific, USA). A Vacuum of 29-31 mtorr was obtained

by the use of an Edwards 5 RV5 rotary vane dual stage mechanical vacuum pump (Edwards, England). After 48 hours of freeze drying the tubes were removed and capped.

2.2.5 Melt quench

Samples were melt quenched by heating the material in an aluminium pan in the DSC at $10^{\circ}\text{C min}^{-1}$ beyond the melting point of the material, and then rapidly immersing the molten material in liquid nitrogen. Samples were subsequently reheated in a DSC at $10^{\circ}\text{C min}^{-1}$.

2.2.6 Physical mixtures

For comparison purposes, physical mixtures (50:50 w/w) of individually milled and spray dried API and excipient were prepared. The separately processed materials (total weight of 0.5g) were placed in 15 ml amber glass jars and mixed in a Turbula mixer (2 L, W.A. Bachofen, Switzerland) at 55 rpm for 10 minutes. The physical mixtures contained 50% w/w excipient and were immediately characterised on recovery of the samples from the Turbula mixer.

2.2.7 Thermal analysis

2.2.7.1 Differential scanning calorimetry

Differential scanning calorimetry (DSC) experiments were conducted using a Mettler Toledo 821^e with a refrigerated cooling system (LabPlant RP-100). Nitrogen was used

as the purge gas. Sealed aluminium pans with three vent holes were used throughout the study, and sample weights varied between 5 and 13 mg. The system was calibrated for temperature and cell constant using indium and zinc. A heating rate of $10^{\circ}\text{C min}^{-1}$ was implemented in all DSC measurements. Analysis was carried out and monitored by Mettler Toledo STAR^c software (version 6.10) with a Windows NT operating system ($n \geq 2$).

2.2.7.2 Modulated temperature differential scanning calorimetry (MTDSC)

Measurements of the heat capacity of amorphous and crystalline SDM were obtained using a modulated temperature DSC (MTDSC). Experiments were conducted on a DSC Q200 (TA Instruments, United Kingdom) in aluminium pans with 1 pinhole, and sample weights were between 2 and 6 mg ($n \geq 2$). The instrument was calibrated for temperature and cell constant using high purity indium. Heat capacity readings were calibrated using sapphire. The parameters used were the same as those reported by Caron et al. (2011): heating rate, $1^{\circ}\text{C min}^{-1}$; amplitude of modulation, 1°C ; period of modulation, 120 s. The glass transition temperatures of the SDM:MAN co-milled systems were obtained using a heating rate of $1^{\circ}\text{C min}^{-1}$; amplitude of modulation, 1°C ; period of modulation, 60 s.

2.2.7.2.1 Quantification of amorphous content by MTDSC

Amorphous content quantification from MTDSC measurements were performed by comparing the enthalpy of crystallisation to the enthalpy of melting. As these thermal events inevitably occur at different temperatures, it is necessary to correct for this

temperature dependence of the enthalpy values by taking account of the heat capacity difference between the solid and liquid state (equation. 2.1) (Lefort et al., 2004).

$$\% \text{ amorphous content} = 100 \times \frac{\Delta H_c}{\Delta H_m(T_m) - (T_m - T_c)\Delta C_p} \cdot \frac{1}{(1-\alpha)} \quad \text{Eq. 2.1}$$

where ΔH_c and ΔH_m are the enthalpies of recrystallisation and melting, T_c and T_m are their corresponding temperatures. The term α refers to the fraction of amorphous sample which does not crystallise upon heating and it is obtained from the ratio of the enthalpy of melting of the amorphous sample to that of the crystalline sample.

2.2.7.3 High performance differential scanning calorimetry (HyperDSC)

High performance DSC (HyperDSC) experiments were performed with a Perkin-Elmer Diamond DSC Pyris1 with HyperScan. Helium flow was set at $60 \text{ mL}\cdot\text{min}^{-1}$, and the heating rate employed was $300^\circ\text{C min}^{-1}$. Sample weights between 2 and 6 mg were placed in aluminium pans with three vent holes. The instrument was calibrated for temperature using high purity indium.

2.2.7.4 Thermal annealing and heating rate experiments

The protocol for the thermal annealing experiments conducted on the SDM:MAN co-spray dried systems was adapted from Mao et al. (2010). The experimental procedure is detailed below and was performed in the MTDSC. Isothermal annealing was performed at 30°C and 50°C .

- Equilibrate at 25°C
- Ramp 10°C min⁻¹ to 70°C
- Isothermal for 5 minutes
- Ramp 10°C min⁻¹ to 0°C
- Ramp 10°C min⁻¹ to 70°C
- Isothermal for 5 minutes
- Ramp 10°C min⁻¹ to 0°C
- Ramp 10°C min⁻¹ to 30°C / 50°C
- Isothermal for 60, 120, 240 or 480 min
- Ramp 10°C min⁻¹ to 0°C
- Ramp 10°C min⁻¹ to 80°C

Heating rate experiments on the SDM:MAN co-spray dried systems were performed using heating rates of 2, 10 and 20°C min⁻¹. The experimental protocol is shown below and was performed in the MTDSC.

- Equilibrate at 25°C
- Ramp 10°C min⁻¹ to 70°C
- Isothermal for 5 minutes
- Ramp 10°C min⁻¹ to 0°C
- Ramp 2, 10 or 20°C min⁻¹ to 80°C

2.2.7.5 Thermogravimetric analysis (TGA)

TGA experiments were conducted on a Mettler Toledo TG 50 apparatus. Weighed samples (5–10 mg) were analysed in open aluminium pans placed on a Mettler MT5 balance. Samples were heated at a scanning rate of 10°C min⁻¹ under nitrogen purge.

Mass loss of the samples recorded was analysed by the Mettler Toledo STARe software (n=2).

2.2.8 Powder X-Ray Diffraction (pXRD)

PXRD measurements were performed on samples placed on a low background silicon sample holder using a Rigaku Miniflex II desktop X-ray diffractometer (Rigaku, Tokyo, Japan). The pXRD patterns were recorded from 5° to 40° on the 2 theta scale at a step of 0.05° s⁻¹. The X-ray tube composed of Cu anode ($\lambda_{\text{CuK}\alpha} = 1.54 \text{ \AA}$), was operated under a voltage of 30 kV and current of 15 mA.

2.2.8.1 Quantification of amorphous content by pXRD

Quantification methods by pXRD were based on the principle that the integrated peak area is proportional to the degree of crystallinity (Byard et al., 2005; Shah et al., 2006). As pXRD measures properties specific to crystalline materials, a reduction in peak area with the concomitant appearance of a diffuse halo is linked to a reduction in crystallinity, which then can be associated with an increase in disorder or amorphous content (Zimper et al., 2010). An estimation of the degree of crystallinity of milled SDM was based on integrating the areas of Bragg peaks from the entire sample following milling (A_p) and comparing this to the commercial sample (A_c) (equation. 2.2).

$$\% \text{ amorphous content} = 100 \times \left(1 - \frac{A_p}{A_c} \right) \quad \text{Eq. 2.2}$$

Quantification of crystalline content of SS:excipient co-milled systems by pXRD was performed by Kieran Gallagher. The amorphous standard was prepared by milling the API for 2 hours and the crystalline reference standard was obtained by placing SS as received in the DVS at 90% RH until no mass loss events were observed in the kinetic profile. The method employed was based on that reported by Clas et al. (1995). Zinc oxide was used as an internal standard to determine if there were variations in peak position and intensity. Different weight fractions of crystalline SS (X_c) ($X_c = 0.2, 0.25, 0.5, 0.75, 0.9$) were prepared by mixing the relevant quantities of crystalline and amorphous reference samples (total mixed sample weight 100 mg) with 10 mg Zinc oxide using an agate mortar and pestle. This procedure was repeated once to produce a second independent set of reference standards for each weight fraction. Each set of reference standards was analysed by pXRD three times, giving a total of six results for each weight fraction. The pXRD peak used for the quantification of crystalline SS in each sample was at approximately $15.3^\circ 2\theta$, and was selected due to the lack of interference across all diffraction patterns. Rigaku Peak Integral software was used in the determination of peak intensity for each sample using the Sonnefeldt-Visser background edit procedure. Quantification results for binary systems are expressed in terms % amorphous content of the API.

2.2.9 Scanning electron microscopy (SEM)

Visualisation of particles was performed by SEM and images were recorded on a Mira Tescan XMU microscope (Tescan s.r.o., Czech Republic). Resolution: 3 nm at 30kV, accelerating voltage: 5kV, specimen stage: 300 nm by 330 nm (Compucentric),

detector: secondary electron. Before analysis, the samples were fixed on aluminium stubs and coated with gold under vacuum.

2.2.10 Infrared spectroscopy

2.2.10.1 Fourier Transform Infra-Red Spectroscopy (FTIR)

Infrared spectra were recorded on a Nicolet Magna IT 560 ESP spectrophotometer equipped with MCT/A detector, working under Omnic software version 4.1. A spectral range of 650–4000 cm^{-1} , resolution 2 cm^{-1} , and accumulation of 64 scans were used in order to obtain good quality spectra. A potassium bromide disk method was used with 1% (w/w) sample loading. Disks were prepared by compression under 8 tons for 2 min.

2.2.10.2 Near Infrared Spectroscopy (NIR)

Analysis by NIR was performed via collaboration with researchers in the National University of Ireland Galway. NIR spectra were collected in glass vials (15 × 45 mm) on a PerkinElmer Spectrum One fitted with an NIR reflectance attachment. The method was similar to that previously described by Hu et al. (2010). Spectra were collected with interleaved scans in the 10000–4000 cm^{-1} range with a resolution of 8 cm^{-1} , using 32 co-added scans. Sample vials were shaken and repositioned between triplicate measurements of each sample.

NIR data analysis was carried out using the Unscrambler v.9.8 software (Camo, Norway). Pre-processing methods, standard normal variate (SNV) transformation, and second derivative calculations (a window size of 21 points and second order polynomial) were used separately or combined. Partial least-squares (PLS) regression was used to create calibration models for quantitative analysis, and its performance was

evaluated using the correlation coefficient (R^2) and the root mean-square error (RMSE). RMSE is termed as the root-mean square error of calibration (RMSEC) for the calibration set and that of prediction (RMSEP) for the prediction set.

2.2.10.2.1 Quantification of amorphous content by NIR

Quantification of amorphous content of milled SDM was carried out by preparing amorphous/crystalline binary physical mixtures of SDM over the composition range of 0-100 % crystallinity and mixed uniformly for 3 minutes using a vortex mixer (Type 37600). The optimal calibration model was obtained by using a combination of SNV and 2nd derivative pretreatments in the 6850 – 6400 cm^{-1} spectral region, which gave a good linear relationship ($R^2=0.999$) between the calculated and the measured amorphous content with 2 PLS factors. Quantification results in binary systems are expressed in terms % amorphous content of the API.

2.2.11 Dynamic vapour sorption (DVS)

Sorption isotherms and kinetic profiles of the unprocessed, processed and co-processed systems were obtained using DVS (Advantage, Surface Measurement Systems, Alpert, U.K.). The temperature was $25.0 \pm 0.1^\circ\text{C}$ (lowered to $5.0 \pm 0.1^\circ\text{C}$ for SDM milled at 4°C), and either ethanol or water was used as the probe vapour (Appendix II). Samples were dried at 0% P/P_0 initially. SDM, BUD, SS and API:excipient containing systems were subjected to step changes of 10% P/P_0 up to either 50%, 70%, or 90% P/P_0 , and the reverse for desorption. Second/third sorption cycle isotherms were also determined. Co-mixed samples for SS:excipient systems were initially exposed to step changes of 10% RH up to 90% RH. Further samples were then simply exposed to

humidities below and above the threshold crystallisation RH, the humidity at which crystallisation and mass loss first occurred on the initial DVS run. The final P/P₀ value was system specific and was determined on the basis of when crystallisation was complete for each system. Absence of a mass loss in the second sorption cycle indicated full crystallisation. The sample mass was allowed to reach equilibrium, defined as $dm/dt \leq 0.002$ mg/min over 10 min, before the P/P₀ was changed (Tewes et al., 2010). Sample weights were between 8–15 mg.

2.2.11.1 Amorphous content quantification by DVS

Amorphous content calculations were performed using equation 2.3, as described previously by Balani et al. (2010).

$$\% \text{ amorphous content} = 100 \times \frac{\Delta m \cdot m_s}{m_d} \cdot \frac{1}{\Delta m_{100}} \quad \text{Eq. 2.3}$$

where Δm is the difference in the mass uptake (%) of the API between the first and second sorption cycles at a system specific RH, m_s is the sample mass in the DVS, m_d is the mass of the API in the overall sample mass, and Δm_{100} is the difference in mass uptake (%) between the first and second sorption cycles of the amorphous standard at a system specific RH. All DVS experiments were performed at least in duplicate. Quantification results by DVS for binary systems are expressed in terms of API amorphous content.

2.2.12 Surface area by BET

Specific surface area of spray dried powders was measured by gas adsorption using a Micromeritics Gemini VI surface area and pore size analyzer (Micromeritics, U.K.).

Adsorption measurements were performed with nitrogen gas as the analytical (adsorptive) gas and helium as the reference gas for free space measurements. Prior to analysis the samples were degassed under nitrogen gas, using a Micromeritics SmartPrep degasser for 24 h at 25°C to remove residual solvent content (Ní Ógáin et al., 2011). The evacuation conditions used in the analysis were as follows: rate of 500mmHg min⁻¹, time 1 min. Equilibration time for adsorption was 10s. The amounts of nitrogen gas adsorbed at a range of relative pressures, 0.05<P/P₀<0.35, were determined in order to calculate surface area by the Brunauer, Emmett and Teller (BET) method.

2.2.13 High Performance Liquid Chromatography (HPLC)

The HPLC method for SS was adopted from that of Malkki et al., (1990). The analytical column used was a LiChrosorb RP-18 (250 mm length, diameter 4 mm, particle size 10 µm S/N 009897). The column was attached to a Waters 1525 Binary Pump with an in built degasser, a Waters 717 plus autosampler and a Waters 2487 Dual λ Absorbance Detector. Samples were analysed using Breeze software Version 3.30. The mobile phase consisted of 0.02M phosphate buffer containing 750 µl triethylamine per 1 litre and acetonitrile (95/5 v/v). Phosphate buffer was adjusted to pH=3.0 after adding triethylamine. Separation was carried out isocratically at ambient temperature (about 22°C) and a flow rate of 1.5ml/min, with UV detection at 265 nm. The measured retention time for SS was approximately 4.9 min (n=2).

2.2.14 Solubility studies

2.2.14.1 Solubility determination of excipients in sulfadimidine by thermal analysis

The solubility of GA and AA and MAN in SDM were estimated by thermal analysis. First, API/excipient mixtures containing 40, 50, 60, 70, and 80% w/w of crystalline excipient were milled using the same milling conditions as described in section 2.2.1.1. The resulting powders were then melted on a heating plate at 200°C under nitrogen atmosphere, subsequently quenched to 25°C, and kept at this temperature for 2 days. At this stage, a mixture of crystalline excipient and amorphous API saturated with excipient was obtained, which was confirmed by pXRD. The melting enthalpy of the resulting crystalline phase was then determined by DSC and the average of two values plotted as a function of excipient mass fraction. A high heating rate (20°C min⁻¹) was used in order to prevent crystallisation of the API and gradual dissolution of the crystalline excipient in the amorphous API upon heating.

2.2.14.2 Solubility determination of excipients in salbutamol sulphate by thermal analysis

The solubilities of GA, AA and PA in amorphous milled SS were estimated by thermal analysis and will be referred to as Sol_{excipient} hereafter (e.g. Sol_{GA} refers to solubility of GA). Firstly, amorphous API:crystalline excipient mixtures containing between 50% and 90% w/w of crystalline excipient were manually mixed using a pestle and a mortar. The resulting powders were then heated on a heating plate at 160°C under nitrogen atmosphere, subsequently quenched to 25°C and kept at this temperature for 2 days. At this stage a mixture of crystalline excipient and amorphous API saturated with excipient

was obtained, which was confirmed by pXRD. The melting enthalpy of the resulting crystalline phase was then determined by DSC at $20^{\circ}\text{C min}^{-1}$ from 25°C to 180°C for SS:AA and 130°C for SS:GA and SS:PA, respectively, and the average of two values plotted as a function of excipient mass fraction.

2.2.14.3 Hildebrand solubility parameter

The Hildebrand solubility parameter was determined utilizing the Fedors group contribution method (Fedors, 1974). The solubility parameter for SDM as well as the individual excipients was calculated. The calculation involves the summation of molar vaporisation enthalpies of structural fragments in the material. The molecular volume can be derived from its density or alternatively in an additive fashion similar to that of the molar enthalpies. The Hildebrand solubility parameter was determined from equation 2.4 below:

$$\delta = \left[\frac{\Delta E_v}{V_m} \right]^{1/2} \quad \text{Eq. 2.4}$$

where ΔE_v is the energy of vaporisation and V_m is the molar volume.

Calculated Hildebrand solubility parameters are displayed in Appendix III.

2.2.15 Statistical analysis

Two sample t tests were carried out by Minitab statistical software release 13.32, Minitab Inc. Significance level was $\alpha < 0.05$.

Chapter 3

Characterisation and quantification of
amorphous content in mechanically
activated and spray dried active
pharmaceutical ingredients

3.1 Introduction

The impact of three common unit operations on the solid state characteristics of three APIs was explored in this chapter. The APIs chosen were sulfadimidine (SDM) which has a T_g of $\sim 78^\circ\text{C}$ (Caron et al., 2011), salbutamol sulphate (SS) which has a T_g of $\sim 122^\circ\text{C}$ (Griesdale et al., 2010) and budesonide (BUD) with a T_g of $\sim 90^\circ\text{C}$ (Dudognon et al., 2006). Their selection was based on their elevated T_g s, well above that of ambient temperature, which has been shown to be an indicator of ease of amorphisation by milling (Descamps et al., 2007). Each of the APIs was subjected to both milling and spray drying. Moreover SS was exposed to dry mixing with glass beads. The processed systems were characterised by pXRD, thermal analysis, DVS and SEM. A number of complementary techniques were used to quantify amorphous content and to enable changes in crystallinity on processing to be exposed. The comparison, the applicability and the usability of each quantification method is discussed. The objective was to explore the interrelationship between processing (via milling, dry mixing and spray drying), ease of amorphisation and crystallisation tendency of an API. Particular emphasis was focused on the different vapour sorption properties and crystallisation kinetics of amorphous forms of the same drug produced by the different modes of mechanical activation or by spray drying.

3.2 Sulfadimidine

3.2.1 PXRD and thermal analysis of unprocessed, milled and spray dried sulfadimidine

Figure 3.1 displays the pXRD patterns of unprocessed, milled (10 hours) and spray dried SDM. Unprocessed SDM displayed well defined Bragg peaks, characteristic of a crystalline material. Milled SDM revealed fewer Bragg peaks which were broader and of lower intensity against a halo background. Spray dried SDM was pXRD amorphous.

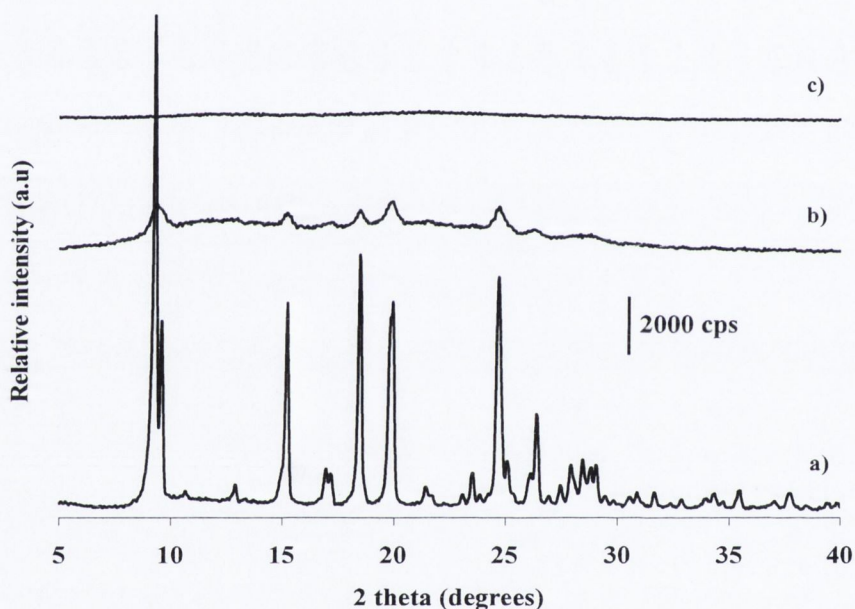


Figure 3.1 PXRD patterns of a) SDM unprocessed, b) SDM milled for 10 hours, c) SDM spray dried.

Thermal analysis by HyperDSC (at a heating rate of $300^{\circ}\text{C min}^{-1}$) of unprocessed SDM revealed a single endothermic peak at 198°C attributed to the melting of the API. The thermograms of the milled and spray dried materials displayed three main features, as seen in Figure 3.2. First, a step change in heat capacity was observed at $\sim 80^{\circ}\text{C}$, attributed to the T_g of SDM. Secondly, an exothermic crystallisation at 89°C for the milled sample and nearly 50°C higher, at 137°C , for the amorphous spray dried sample was observed. The minor endotherm after the T_g for the spray

dried sample could be due to enthalpic relaxation. Thirdly, milled and spray dried SDM melted at $\sim 197^{\circ}\text{C}$.

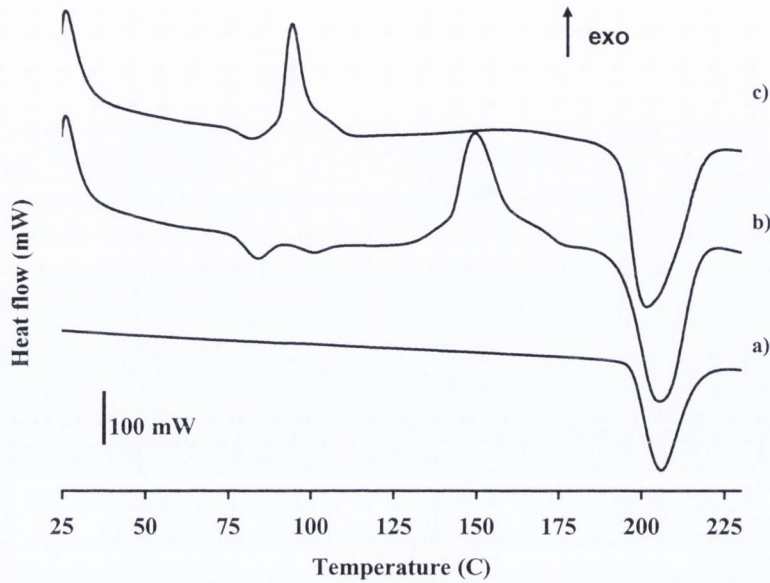


Figure 3.2 HyperDSC scans of a) SDM unprocessed, b) SDM spray dried, c) SDM milled.

Conventional DSC scans (heating rate of $10^{\circ}\text{C min}^{-1}$) were also performed on the unprocessed, milled and spray dried SDM. The scans are displayed in Figure 3.3.

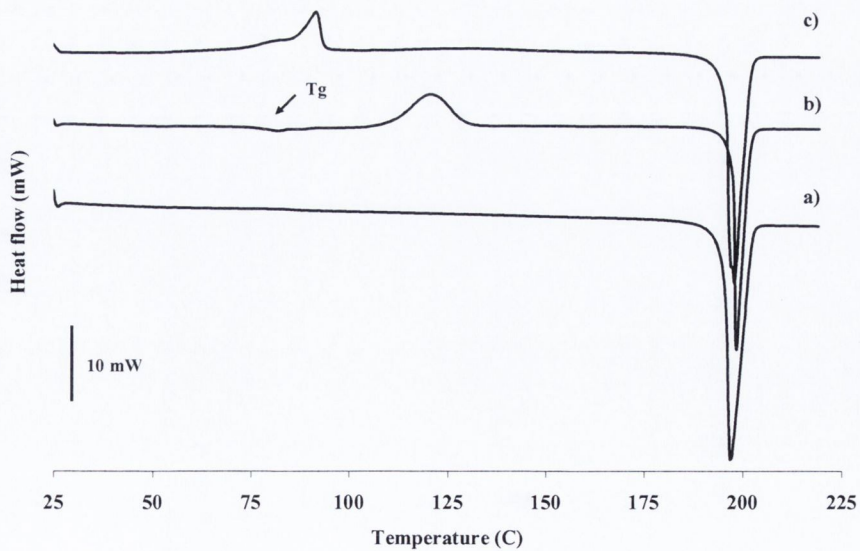


Figure 3.3 DSC scans of a) SDM unprocessed, b) SDM spray dried, c) SDM milled.

A T_g at 78°C was observed for the spray dried material but the baseline shift was less pronounced compared to the corresponding HyperDSC run. One of the most significant benefits of using fast scanning rates is the increase in sensitivity (Gabbott, 2008). This is because the same amount of energy flows through the sample over a shorter period of time, which then increases the heat flow signals. The fast scanning rate also had the advantage of separating T_g and crystallisation exotherms. A T_g could not be observed for the milled sample at the slower heating rate, its detection masked by the overlapping crystallisation exothermic peak at 78°C. Moreover a small leading shoulder can be observed before the main crystallisation event for the milled API. The crystallisation peak for the spray dried material occurred at 110°C, which was ~30°C lower than the exotherm in the fast scan run.

3.2.2 FTIR analysis

SDM, like other related sulphamonomethoxyl compounds, has strong characteristic bands in the region 3390 – 3425 cm⁻¹ due to the N-H stretching vibrations and a number of strong absorption bands at 1360 – 1315 cm⁻¹ due to the asymmetric stretching vibration of the SO₂ group (Socrates, 2001). The spectra for the crystalline, milled and spray dried drug are displayed in Figure 3.4. In addition to a general broadening of the peaks in the processed samples, changes in peak position was also evident compared to that of the unprocessed material. The decrease in spectral resolution and broadening of peaks is associated with the loss of the ordered, three dimensional crystal lattice structure on processing (Kaushal et al., 2008). This phenomenon was more pronounced for the fully amorphous spray dried material compared to partially crystalline milled material. Crystalline SDM displayed

characteristic peaks at 3442 and 3342 cm^{-1} for the asymmetric and symmetric (anilino) stretching vibration (Yang et al., 2005). The spectrum of milled SDM contained a small peak or shoulder at 3471 cm^{-1} which was not present in the unprocessed drug. This could be due to weakly bonded or a small fraction of non hydrogen bonded NH, as it is at higher wavenumber compared to the average hydrogen bonded NH (3442 cm^{-1}). Moreover the peak position is within the range observed for non hydrogen bonded NH stretches in other systems (Tang et al., 2002). The spectral peaks at 3442 and 3342 cm^{-1} were also shifted to higher wavenumber in the spray dried sample. The low frequency region (1000–400 cm^{-1}) of all three systems was similar which indicates that the overall structure of the molecule did not change dramatically despite the increased disorder within the processed material.

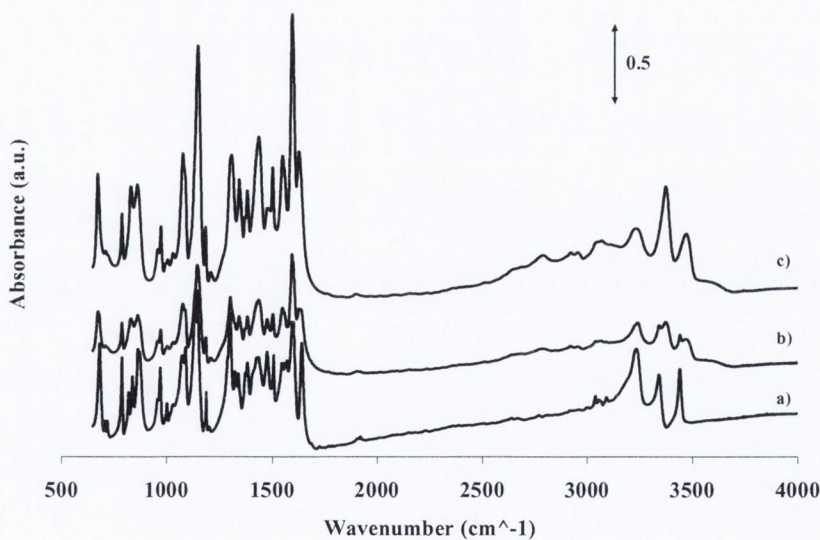


Figure 3.4 FTIR spectra of a) SDM unprocessed, b) SDM milled for 10 hours, c) SDM spray dried.

3.2.3 SEM

SEM analysis was carried out on SDM unprocessed, SDM milled for 10 hours and SDM spray dried (Figure 3.5).

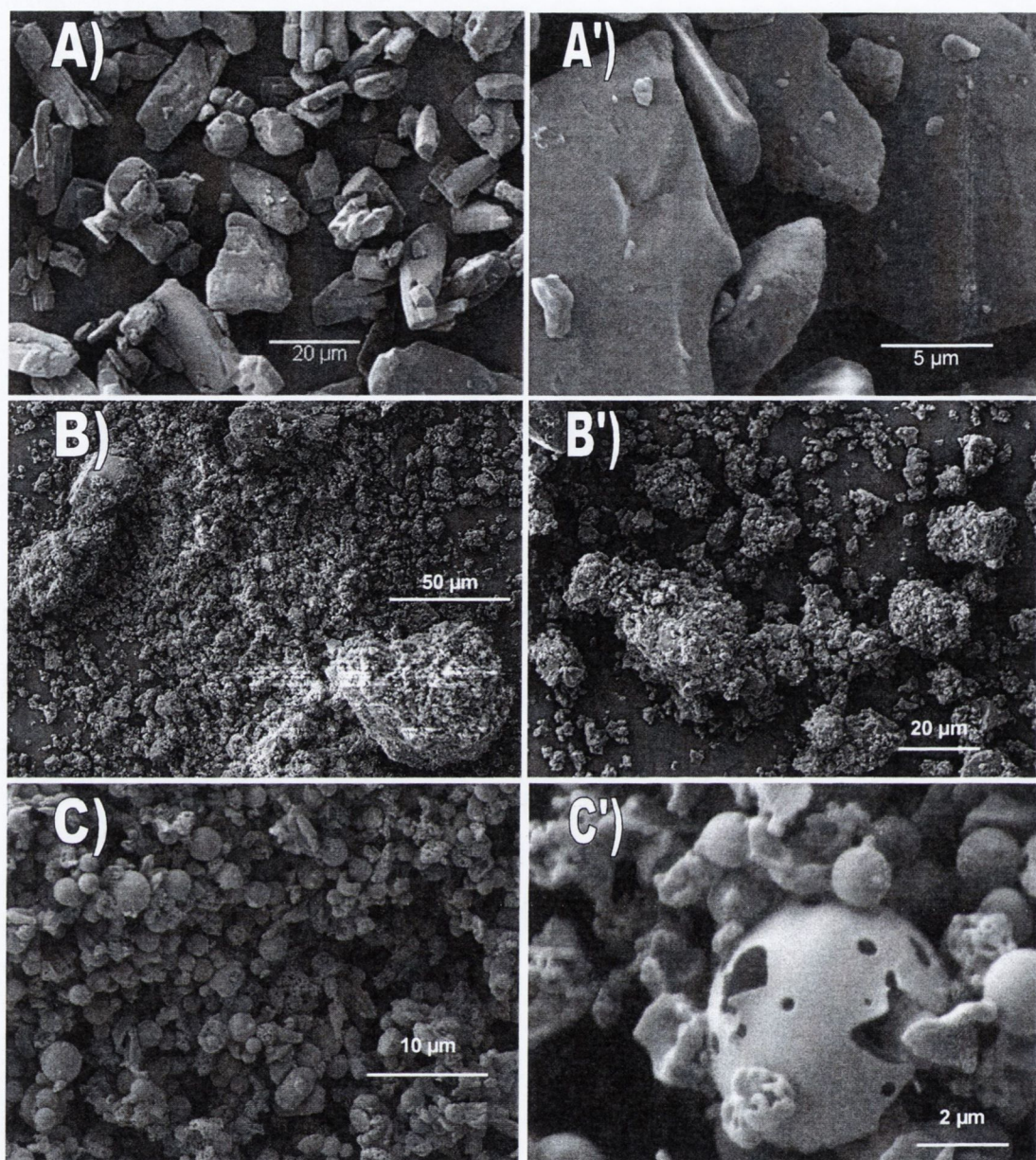


Figure 3.5 SEM micrographs of: A & A') SDM unprocessed, B & B') SDM milled for 10 hours, C & C') SDM spray dried.

The unprocessed material was characterised by irregular shaped particles with a number of surface located fines. SEM of the milled and spray dried API revealed that the primary morphologies were not preserved and the micron scale structures were very different. The milled material showed a high degree of surface roughness with large agglomerates present. The spray dried material consisted of a mixture of porous and non porous spherical particles.

3.2.4 Quantification of amorphous content in milled sulfadimidine

3.2.4.1 Vapour sorption analysis and amorphous content quantification by

DVS

Quantification of amorphous content of milled SDM by DVS was determined by a method similar to that developed by Mackin et al. (2002b) where the difference in mass uptake between the first and second sorption cycles at a particular partial pressure correlates with amorphous content. This method required a vapour induced crystallisation. Water was initially chosen as the probe molecule. SDM could not be completely amorphised by milling under the conditions used, even for up to 20 hours (Appendix IV), and hence the spray dried material was used as the 100% amorphous reference. As indicated in Figure 3.6, water was unable to induce crystallisation in the spray dried material. The amorphous material took up ~4.3% mass at 90% RH during the first sorption cycle. There were no mass loss events in the sorption cycles and pXRD performed on the sample after the second DVS cycle confirmed the material was still amorphous.

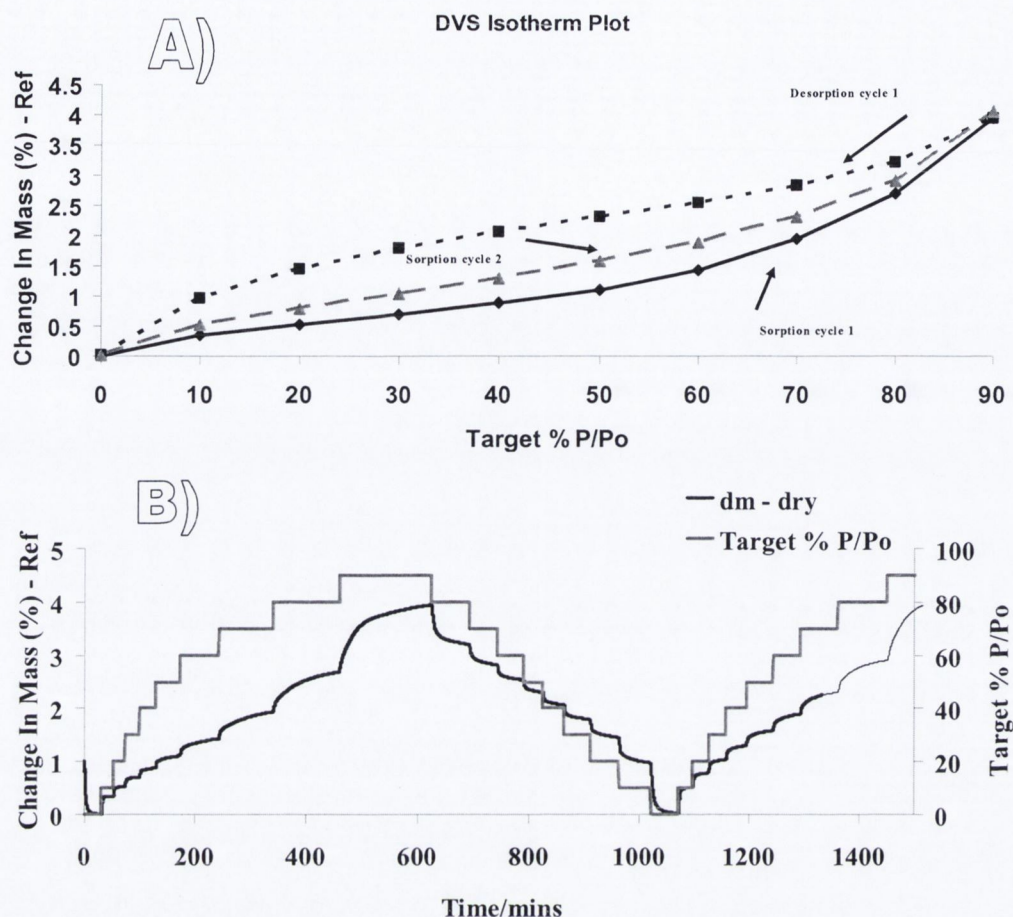


Figure 3.6 A) DVS isotherm plot of spray dried SDM, B) DVS kinetic profile of spray dried SDM. Water was used as the probe molecule.

In order to induce crystallisation by DVS, the amorphous drug was subjected to an ethanolic environment. Materials which have low affinities for water can be investigated with organic vapours to induce crystallisation (Shah et al., 2004). This is because water uptake by hydrophobic materials will be restricted to surface adsorption, limiting water access to the amorphous bulk. In contrast, non aqueous vapours would have enhanced access to the amorphous regions and can be used to induce crystallisation (Samra and Buckton, 2004). It was therefore postulated that by subjecting SDM to an ethanolic environment, the organic vapour would penetrate the powder bed, undergo bulk absorption, plasticise the API and induce

crystallisation. Ethanol did indeed induce crystallisation in both milled and spray dried SDM. The spray dried material underwent a single step crystallisation process at 40% P/P₀, represented by a sharp mass loss (Figure 3.7A). The milled API, in contrast, was observed to undergo an ethanolic vapour induced, multi step crystallisation process with a mass loss first observed at 30% P/P₀ (Figure 3.7B).

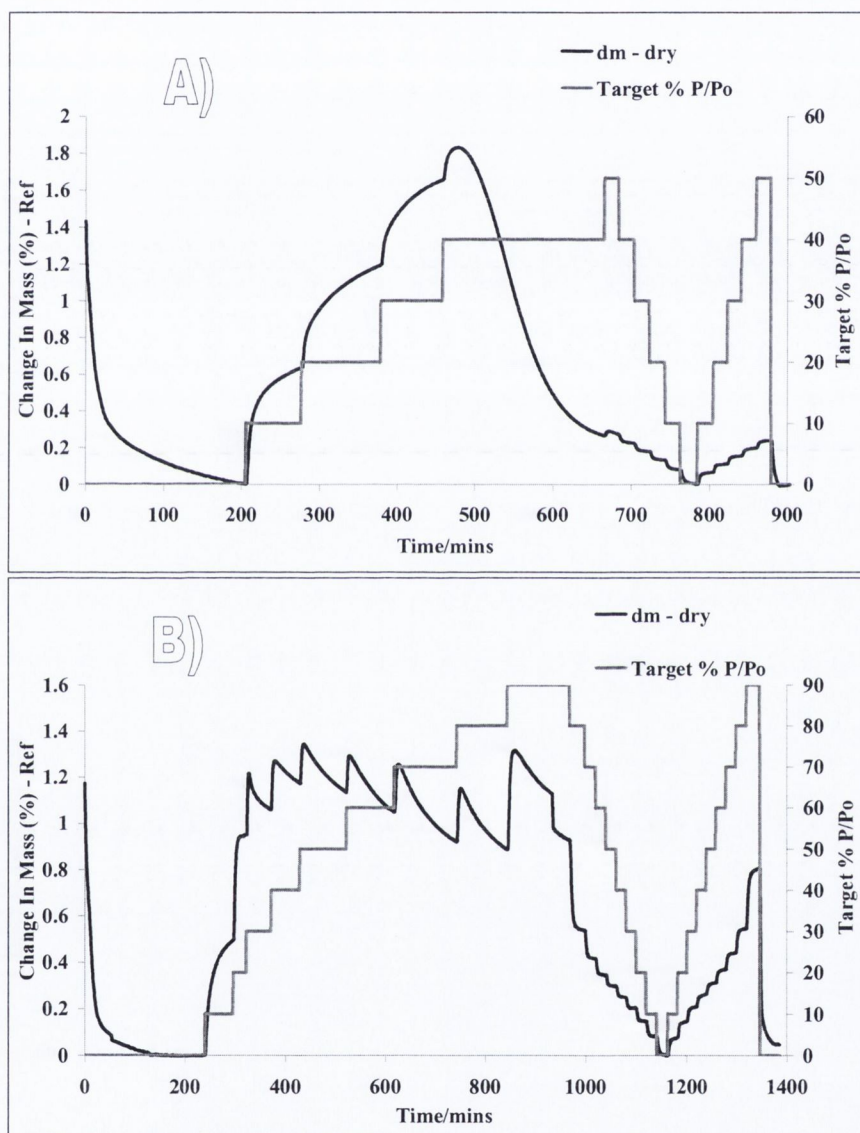


Figure 3.7 Ethanol vapour sorption kinetics of A) spray dried SDM and B) milled SDM.

It was assumed that the unprocessed API was 100% crystalline. To test this, SDM was placed in the DVS and subjected to both an ethanolic and water based

environment up to a P/P_0 or RH of 90% (Figure 3.8). There were no mass loss events in either profile and this was taken as proof that the API was crystalline and could be used as the 100% crystalline standard in subsequent quantification calculations.

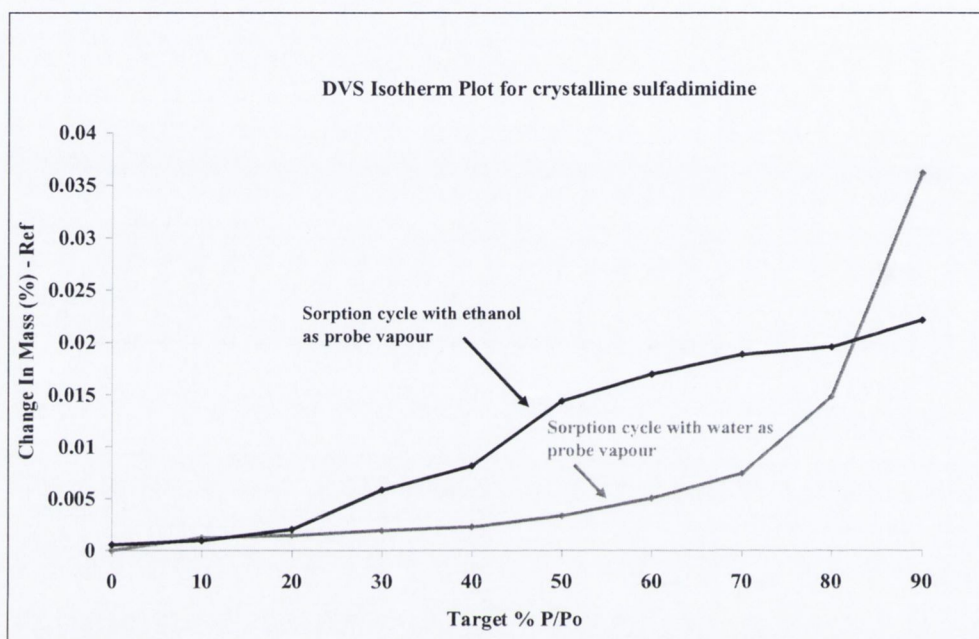


Figure 3.8 DVS isotherm plot (1st sorption cycles) for SDM unprocessed, using water and ethanol as probe vapour.

Physical mixtures of 100% crystalline/100% amorphous API were prepared over a concentration range from 0-100% amorphous content and analysed by DVS under an ethanolic environment (Figure 3.9A). The unprocessed crystalline drug had a % mass uptake of <0.01% w/w at 20% P/P_0 . As the milled material started to crystallise at 30% P/P_0 , the difference in mass uptake at 20% P/P_0 was used in the quantification calculations (highlighted in Figure 3.9A). A relationship between ethanol uptake before and after crystallisation and % amorphous content was observed. A linear fit of the response (ethanol uptake at 20% P/P_0) and independent

variable (% amorphous content) resulted in an R^2 of 0.9949 (Figure 3.9B). An amorphous content of $76 \pm 3\%$ for milled SDM was determined by DVS.

The quantification results by DVS are independent of the crystallisation kinetics provided the method has been developed to allow the sample to reach equilibrium at each partial pressure and the sample has crystallised completely (Mackin et al, 2002b). The absence of mass loss in the second sorption cycles was taken as confirmation that the amorphous material had fully crystallised.

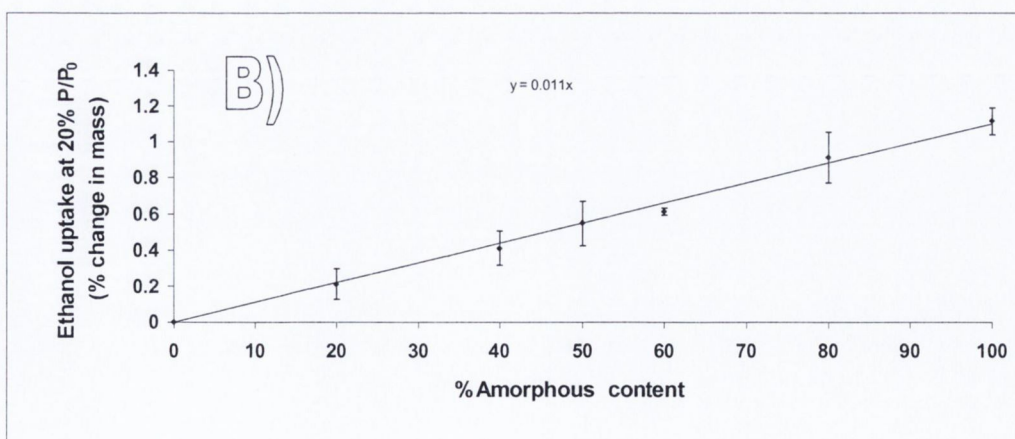
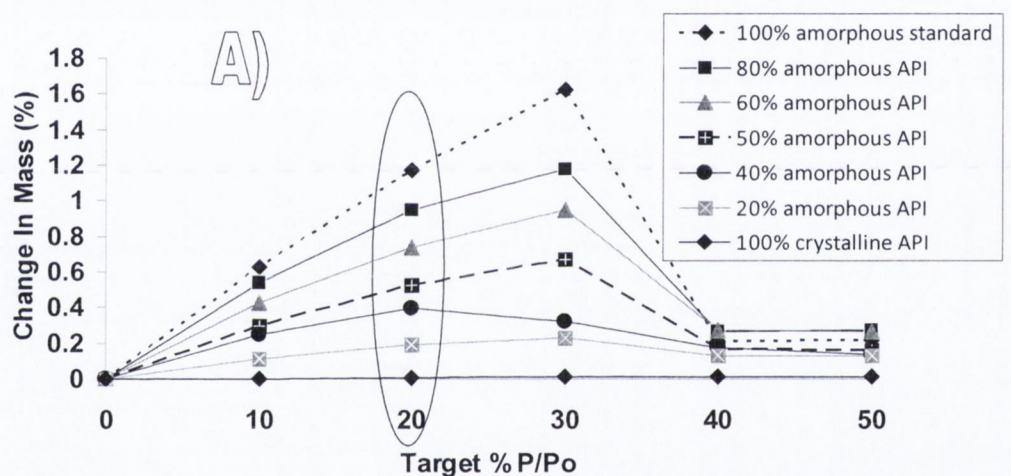


Figure 3.9 A) DVS sorption isotherm plots (1st cycle) for a range of known amorphous contents of SDM (change in mass at 20% P/P₀ highlighted); B) Calibration curve of ethanol uptake at 20% P/P₀ versus % amorphous content.

3.2.4.2 Amorphous content quantification by pXRD

The method of quantification by pXRD was based on integrating the areas of Bragg peaks from the entire sample following and milling and comparing this to unprocessed API, as previously described in section 2.2.8.1. The crystallinity of unprocessed SDM was taken to be 100%, based on the DVS data, and was used as the crystalline standard. The calculated amorphous content for milled SDM by pXRD was $88 \pm 2\%$.

3.2.4.3 Amorphous content quantification by MTDSC

Amorphous content of milled SDM was quantified by MTDSC using Eq. 2.1, as described in section 2.2.7.2.1. The input variables for the equation are displayed in Table 3.1.

Table 3.1 Enthalpies of crystallisation (ΔH_c) and melting (ΔH_m), their corresponding temperatures (T_c and T_m), difference in heat capacity of amorphous and crystalline SDM (ΔC_p) and the fraction of SDM which does not crystallise on heating (α).

Input variable	ΔH_c (J/g)	ΔH_m (J/g)	T_c (°C)	T_m (°C)	ΔC_p (J/g/°C)	α
Value	37	123	82	196	0.676	0
	33	120	81	196	0.676	0
	30	115	80	197	0.676	0

An amorphous content of $81 \pm 2\%$ was determined for milled SDM by MTDSC.

3.2.4.4 Amorphous content quantification by NIR

The NIR spectra (Figure 3.10) of the unprocessed and spray dried amorphous SDM exhibited clear differences in the $7000 - 6400 \text{ cm}^{-1}$ and $5150 - 4400 \text{ cm}^{-1}$ spectral

regions, with bands at 6806, 6604, 4876, 4776 and 4490 cm^{-1} being specific to the crystalline form of the API. Thus NIR was a suitable technique to quantify the amorphous content in milled SDM. The RMSEC and RMSEP values were 0.89% and 1.33%. The amorphous content value of milled SDM by NIR was determined to be $84 \pm 1\%$.

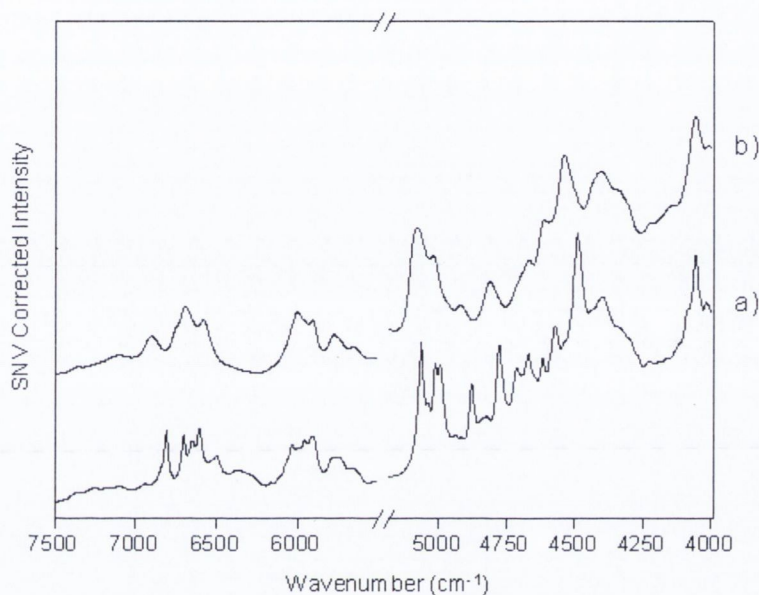


Figure 3.10 NIR spectra of a) SDM unprocessed, b) SDM spray dried.

3.2.4.5 Comparative analysis of amorphous content quantification by different methods for sulfadimidine milled at room temperature

Table 3.2 summarises the amorphous content of milled SDM as quantified by pXRD, MTDSC, NIR and DVS.

Table 3.2 Summary of amorphous content of milled SDM as quantified by pXRD, MTDSC, DVS and NIR.

System	% Amorphous content (\pm S.D)	Method
SDM milled	88 (2)	pXRD
	81 (2)	MTDSC
	84 (1)	NIR
	76 (3)	DVS

Good agreement was obtained for all four characterisation methods. XRD has traditionally been one of the most widely used techniques to quantify amorphousness due to accessibility and availability of instrumentation, relative simplicity and the capability to detect directly molecular order (Liu et al., 2009). The challenges associated with its use as a quantitative technique include preferred orientation, complex scattering patterns and reproducible sample preparation (Liu et al., 2009). The amorphous content value, as determined by pXRD, was the highest of the quantification techniques used in this work. Milling for long periods can give rise to an amorphous phase as well as nanocrystallites which can be beyond the detection limit of the X-ray (Bates et al., 2006). These nanocrystallites can contribute to the halo pattern and potentially bias upwards the amorphous content. Quantification methods by pXRD also have difficulty in detecting amorphous material in powder samples unless it accounts to as much as 10% of the total weight (Saleki-Gerhardt et al., 1994).

Amorphous content by MTDSC is based on heat capacity measurements and enthalpies of crystallisation and melting. Zimpler et al. (2010) noted that, in contrast to pXRD measurements, the change in heat capacity at the T_g can be used as a direct measure of amorphous material rather than be representative of a combination of true amorphous and otherwise disordered material. Measurements based on heat capacity can lower the detection limit to ~1%, which is considerably better than that of conventional DSC (~10%) (Lehto et al., 2006). A disadvantage of the method is that it is not applicable to all materials, and in particular for those which degrade on melting. The method could be applied to SDM because the API does not undergo degradation on melting.

NIR is a non invasive technique and recognised as being highly sensitive to small amounts of amorphous material (Hogan and Buckton, 2001). Spectroscopic measurements are often capable of detecting amorphous contents as low as 1% of the total sample (Lehto et al., 2006). Moreover spectra can be directly collected on solid samples without the requirement for any sample preparation and it is regarded as a quick method of analysis (Bai et al., 2004; Luner et al., 2000). The method has an advantage over thermal methods in that it is non destructive. It has an advantage over XRD methods because the amorphous phase gives specific, albeit broadened signals (Shah et al., 2006).

DVS is based on the different sorption capabilities of amorphous and crystalline materials. This is related to the structural features of both systems, one being a highly organised, tightly arranged crystal lattice, the other highly disordered with a larger surface area and void space where moisture can accumulate (Hancock and Zografi, 2007). Burnett et al. (2009) have demonstrated that the differences in sorption capacity between crystalline and amorphous phases can be used to detect amorphous contents below 1%.

3.2.5 Sulfadimidine milled at 4°C.

The API was also milled in a cold room at $4 \pm 1^\circ\text{C}$. It was anticipated that processing at the lower temperature would promote amorphisation due to the greater difference in the operating temperature and the T_g of the drug. Descamps et al. (2006) investigated the transformation of pharmaceutical compounds upon milling and noted that decreasing the milling temperature leads to an increase in the amorphisation tendency. The pXRD patterns of unprocessed SDM and the drug milled at RT and at 4°C are displayed in Figure 3.11. Amorphisation was promoted

on milling at the lower temperature, with the Bragg peaks highlighted being less intense against the halo background.

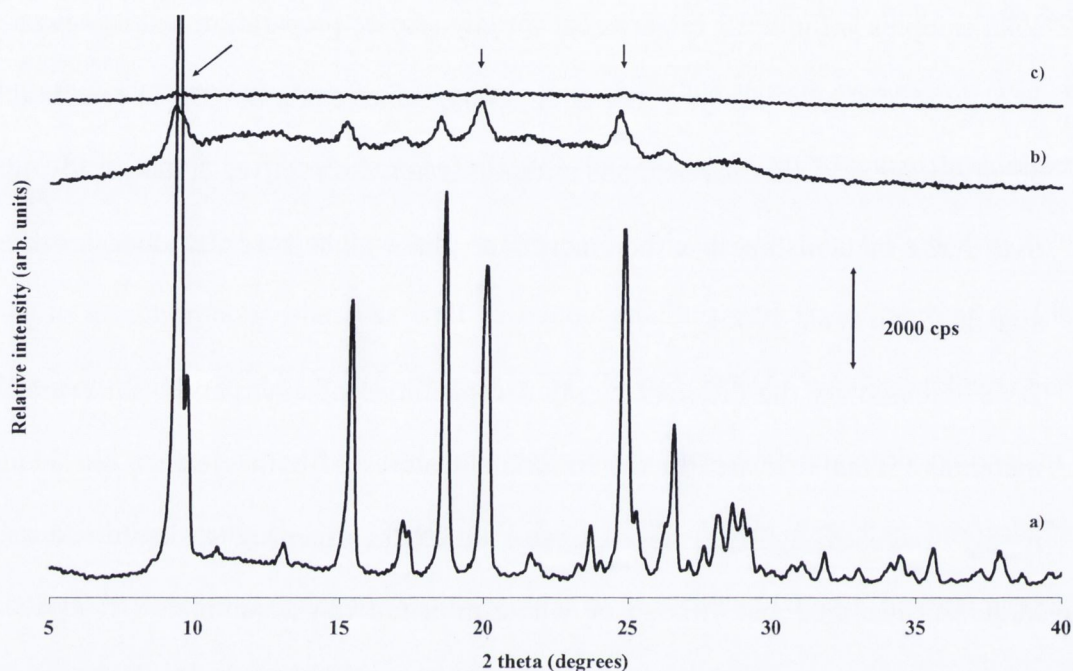


Figure 3.11 PXR D patterns of a) SDM unprocessed, b) SDM milled for 10 hours at RT, c) SDM milled for 10 hours at 4°C.

Quantification of amorphous content of the drug milled at 4°C was also carried out by pXR D, MT DSC, DVS and NIR and the results are displayed in Table 3.2.

Table 3.2 Summary of amorphous content of milled SDM at 4°C, as quantified by pXR D, MT DSC, DVS and NIR.

System	Amorphous content (\pm S.D)	Method
SDM milled at 4°C	96 (3)	pXR D
	91 (2)	MT DSC
	94 (1)	NIR
	63 (4)	DVS

The difference in % mass uptake between the first and second sorption cycles was less for the drug milled in a cold room at 4°C, compared to the drug milled at RT resulting in a lower calculated amorphous content (63% v 76%). This was unexpected because amorphous content, on the basis of the other quantification techniques, was greater for the lower temperature milled system. Variations in moisture uptake between two systems could be due to differences in amorphous content or due to changes in surface properties. It was then investigated if the surface area of the two milled systems differed. A material with a larger surface area would be expected to have a higher vapour affinity. The BET surface area of the unprocessed drug, spray dried amorphous material, and the material milled at the two different temperatures are displayed in Table 3.3.

Table 3.3 The impact of processing on the surface area of SDM.

Sample	BET surface area (m ² /g) ± S.D.
SDM unprocessed	0.7009 ± 0.0291
SDM spray dried	5.02015 ± 0.1554
SDM milled at RT	5.2532 ± 0.4011
SDM milled at 4°C	4.7637 ± 0.3545

Processing by milling and by spray drying both resulted in a large increase in surface area, relative to the unprocessed drug. However the BET surface area results for the API milled at RT and at 4°C were not statistically significantly different ($p > 0.05$).

The operating temperature is another variable that can interfere with the amount of vapour sorbed at any particular relative humidity or partial pressure. Hancock and Dalton (1999) investigated the effect of temperature on water vapor sorption of

several amorphous pharmaceutical sugars. It was noted that a reduction in temperature caused an increase in water vapor sorption at any given RH provided that the sugar remained amorphous. The authors proposed that the vapour sorption was an exothermic process and at lower temperatures sugar:vapour interactions were preferred over sugar:sugar and water:water interactions. Therefore DVS on the two milled drugs was performed at a lower temperature of 5°C. Interestingly the amorphous content of the drug milled at 4°C was calculated to be $87 \pm 2\%$ when the partial pressure profile was obtained at the lower temperature. Moreover this was in good agreement with the quantification results based on the other methods. The result, however, for the drug milled at RT but quantified at the lower temperature ($80 \pm 5\%$), was not statistically significantly different ($p > 0.05$) compared to the result obtained when the DVS was performed at ambient temperature. It would also have been expected that sorption uptake, and hence calculated amorphous content values, would have been greater for this system when analysed by DVS at the lower temperature. It is therefore suggested that the sample milled at 4°C partially crystallised when placed in the DVS at ambient temperature leading to an underestimation of the amorphous content.

3.3 Salbutamol sulphate

3.3.1 PXRD and thermal analysis of unprocessed, milled, dry mixed and spray dried salbutamol sulphate

SS raw material displayed Bragg peaks characteristic of a crystalline material. The API was identified as pure form 1 with characteristic diffraction peaks of this solid state form apparent at 10.7, 11.9 and 12.6 2 theta (Palacio et al., 2007). SS, in

contrast, was amorphous when processed by milling for two hours, by dry mixing with glass beads for 8 hours and when spray dried from water (Figure 3.12).

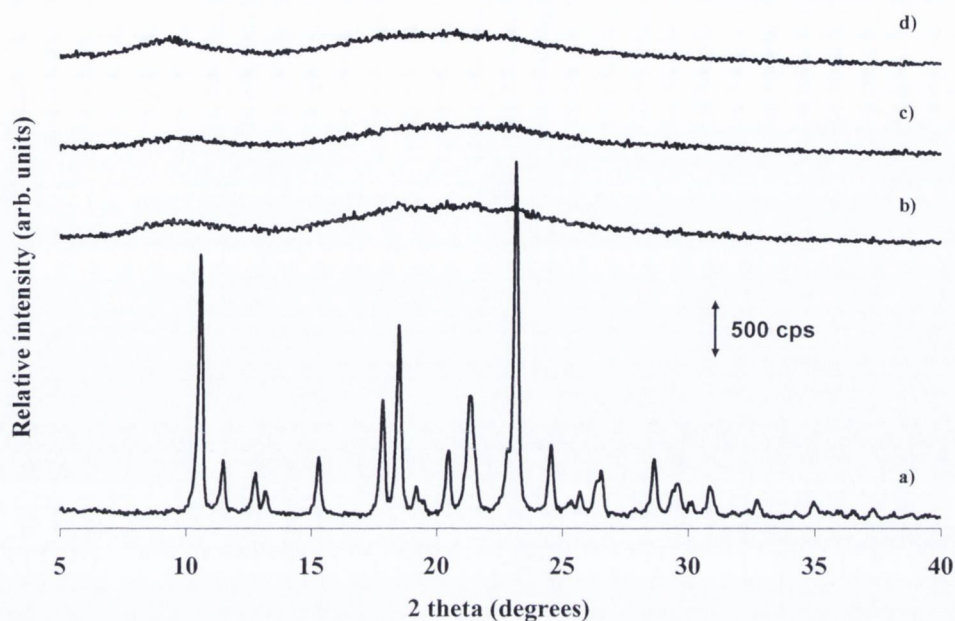


Figure 3.12 PXRD patterns of a) SS raw material, b) SS milled for 2 hours, c) SS dry mixed for 8 hours and d) SS spray dried from water.

The corresponding DSC thermograms are displayed in Figure 3.13. SS raw material revealed a single endothermic event with a temperature onset of 185°C. Both milled and spray dried SS displayed a broad endothermic event between 30-100°C believed to be due to loosely bound moisture (mass loss of 2% and 0.7% was noted for the milled and spray dried drug by TGA analysis from 25-100°C). SS raw material had a mass loss of 1.1% by TGA between 25-100°C. The glass transition temperature of milled, dry mixed and spray dried SS occurred at 120°C and is highlighted in Figure 3.13. The melting of the processed drugs coincided with thermal degradation of the API, and was confirmed by significant mass loss by TGA analysis. The degradation profiles differed for each of the processed drugs and were at a lower temperature relative to the unprocessed crystalline drug.

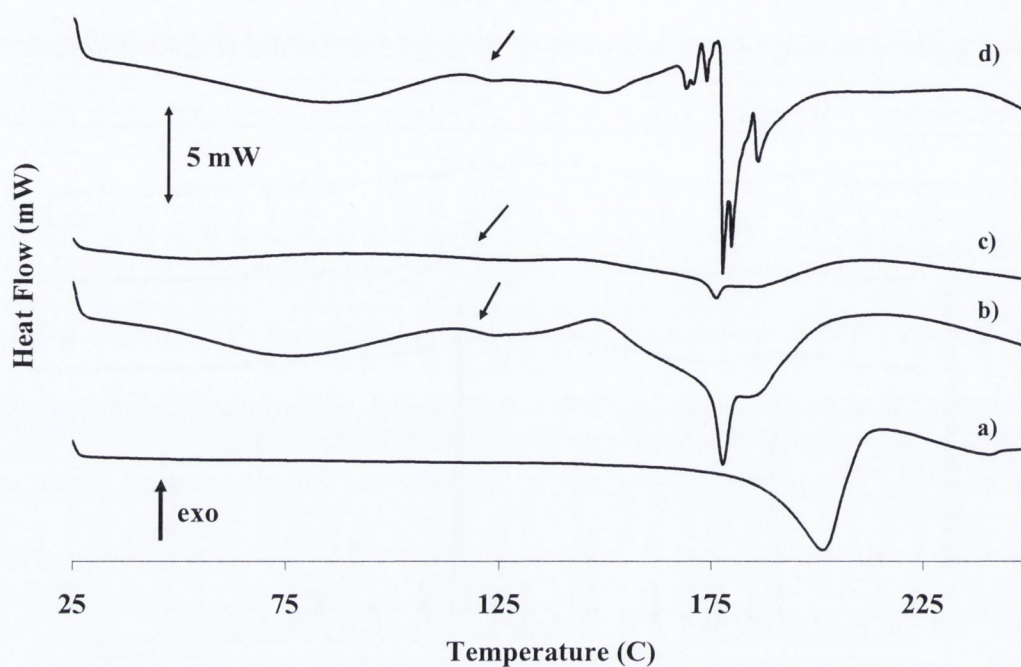


Figure 3.13 DSC thermograms of a) SS raw material, b) SS milled for two hours and c) SS dry mixed for 8 hours and d) SS spray dried. Highlighted with arrows is the glass transition temperature of processed SS.

3.3.2 Vapour sorption analysis

The water sorption kinetic profile for SS raw material is shown in Figure 3.14. SS took up around 0.3% mass at 50% RH followed by a series of sharp mass losses at higher RH. The vapour uptakes for the second and third sorption cycles were comparable with no mass loss events evident. The average % mass uptake at a specific RH from the second and third sorption cycles was then taken as the reference value for crystalline SS. The initial mass losses are attributed to crystallisation events, associated with the API raw material containing a small, but quantifiable amount of amorphous content.

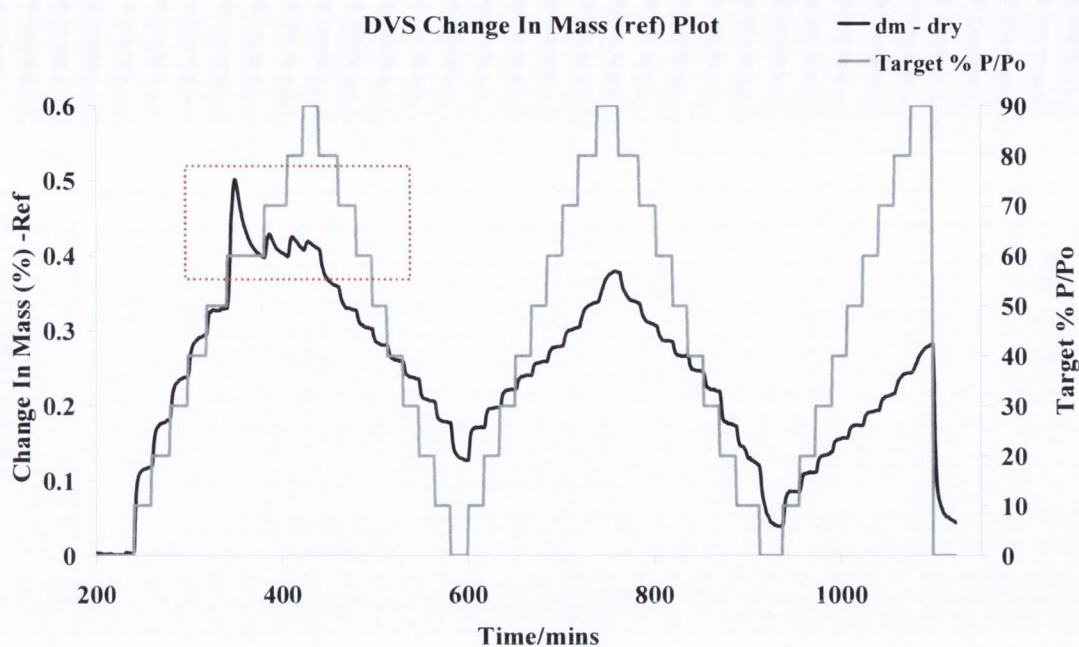


Figure 3.14 Vapour sorption kinetics of SS raw material. Highlighted are mass loss events due to crystallisation of amorphous material. Water was used as the probe vapour.

As the API was supplied in micronised form, it was assumed that this was the root cause of the amorphous content present. The method of quantification by DVS was the same as that employed for SDM and involved comparing the difference in % mass uptake between the first and second sorption cycles. The milled drug was used as the amorphous standard for these calculations. The sorption properties for dry mixed and milled SS are displayed in Figure 3.15.

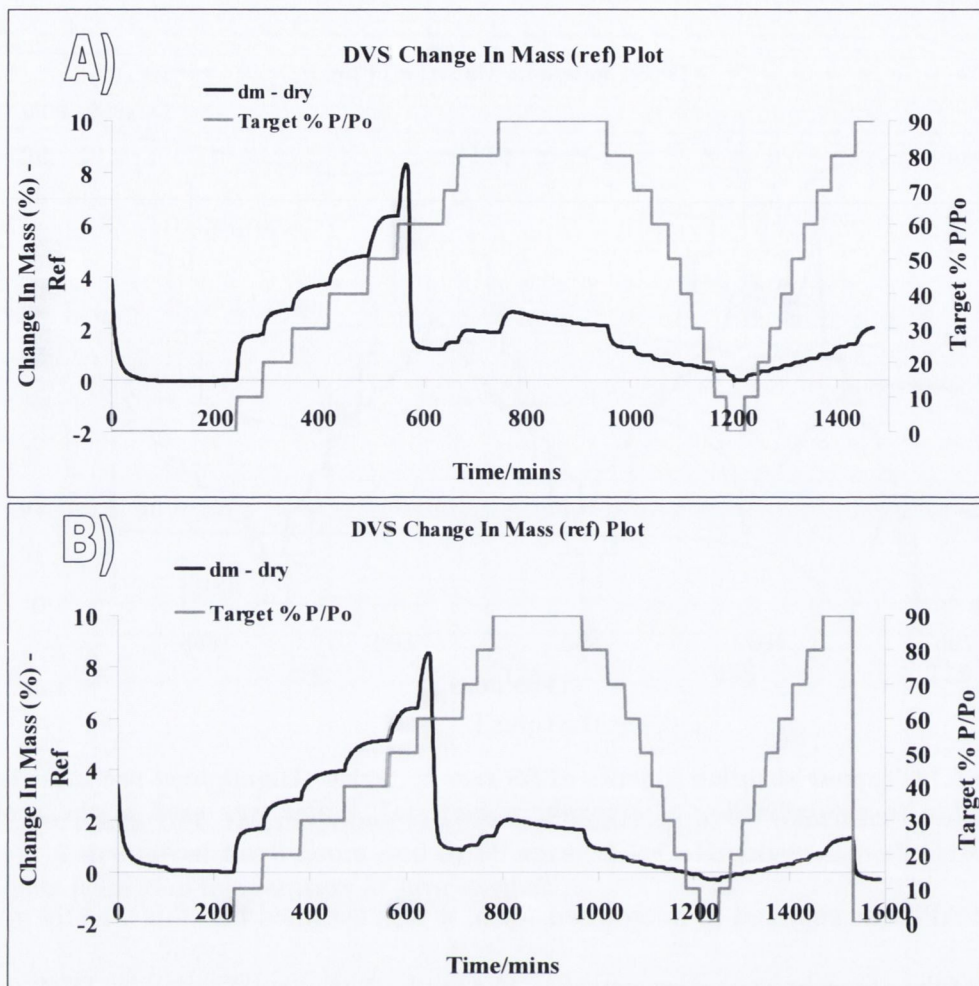


Figure 3.15 DVS sorption kinetics of A) SS dry mixed for 8 hours and B) SS milled for 2 hours.

Both processed materials lost nearly 4% mass during the initial drying step. This was followed by a % mass uptake of approximately 6% at 50% RH. Further elevating the RH resulted in a very sharp, steep mass loss due to an amorphous to crystalline transformation of the drug. Additional mass losses at 70%, 80% and 90% RH indicated that crystallisation was not fully complete after the initial mass loss at 60% RH. Second sorption cycles for both milled and mixed API were almost super-imposable and no mass loss here indicated that samples had fully crystallised. When the excess vapour is expelled during the amorphous to crystalline transition the API changes to a non-hygroscopic solid as confirmed by

the lower vapour uptake during the second sorption cycle. Comparing the % mass uptake at 50% RH for crystalline and milled amorphous SS, with that of the drug as received, revealed an amorphous content of $4 \pm 1\%$ for SS raw material.

The spray dried material was also exposed to a DVS humidity profile and the kinetic profile is displayed in Figure 3.16.

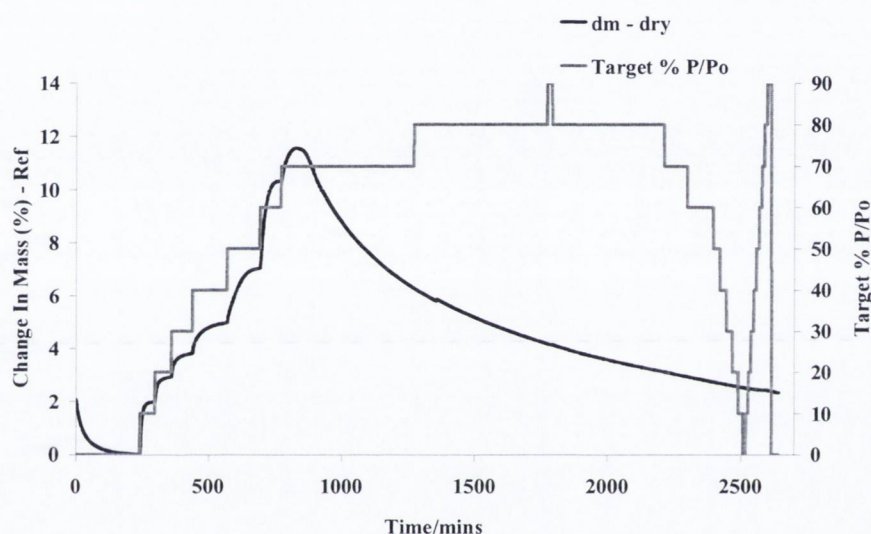


Figure 3.16 DVS kinetic profile for amorphous spray dried SS.

The profile differed considerably to that of the milled drug. Firstly the spray dried material started to crystallise at 70% RH, compared to 60%RH for the milled drug. The kinetics of crystallisation was also different for the spray dried drug, with the moisture ejection on crystallisation being much slower and not complete (2% change in mass) after the first desorption cycle. Moreover the ejection of moisture is still occurring even during the second sorption cycle. Columbano et al. (2002) investigated the crystallisation of amorphous spray dried SS by DVS and NIR and noted that the ejection of water on crystallisation was very slow and water remained associated with the particles for several days. They postulated that the released

moisture was not displaced by the particles but was trapped within the material. The method of amorphous content quantification by DVS used in this work required that the sample has fully crystallised during the first sorption cycle. Crystallisation was relatively quick and ran to completion for the milled material, but this was not the case for the spray dried amorphous drug. These differences are attributed to pseudopolymorphs, or amorphous forms of the same compound having different physical properties dependent on their method of production.

3.3.3 SEM analysis

SEM micrographs of unprocessed, milled, spray dried and dry mixed SS are displayed in Figure 3.17 below.

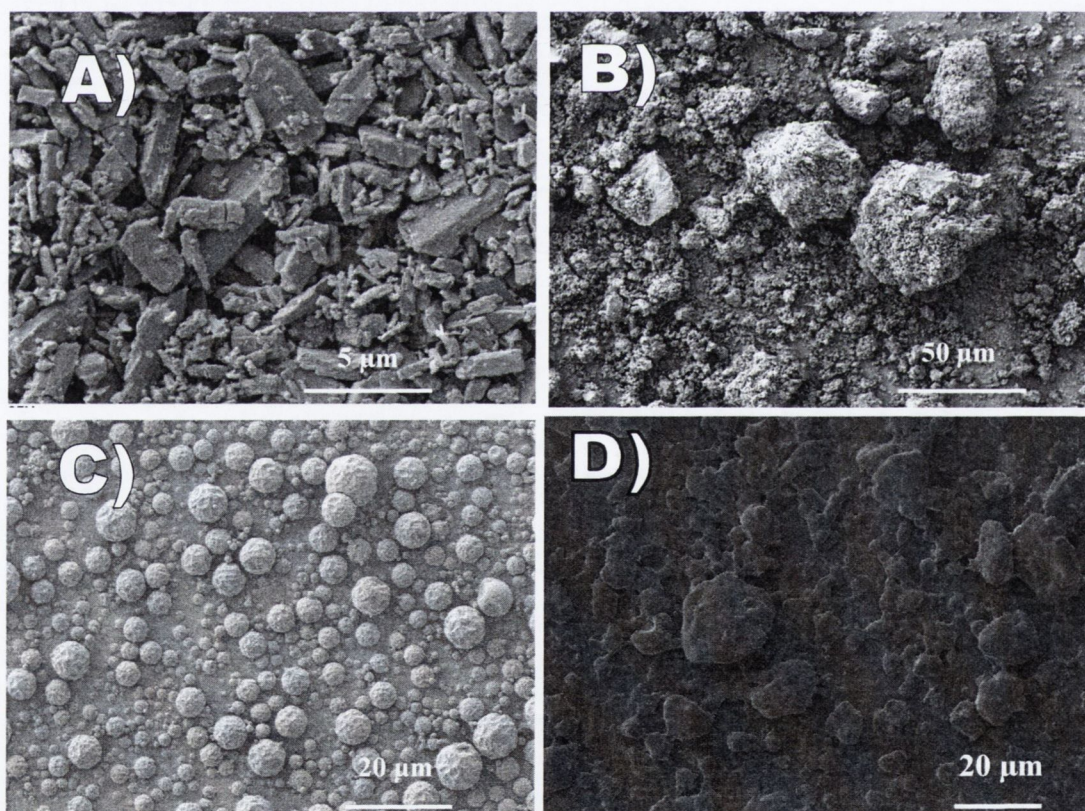


Figure 3.17 SEM micrographs of A) SS raw material, B) SS milled for 2 hours, C) SS spray dried, D) SS dry mixed for 8 hours.

SS raw material consisted of irregular shaped particles with a large number of fines. Milling the API resulted in coarse agglomerated particles of varying magnitude. As was observed for SDM, milling significantly disrupted the primary structure of the drug particles. Spray drying from aqueous solution resulted in spherical uniform particles. The surface of the particles had some dimpled, shrunken areas similar to that reported by Chawla et al. (1994), Columbano et al. (2002), Corrigan et al. (2004) and Muhammed et al, (2010). The dry mixed material consisted of fused irregular shaped particles.

3.4 Budesonide

3.4.1 PXRD and thermal analysis of unprocessed, milled and spray dried budesonide.

Budesonide (BUD) was milled for 12 hours, and the drug was also spray dried as a 1% w/v solution from 95:5 v/v ethanol:water (Appendix I). Unprocessed BUD was crystalline. The drug processed by either milling or spray drying was pXRD amorphous (Figure 3.18).

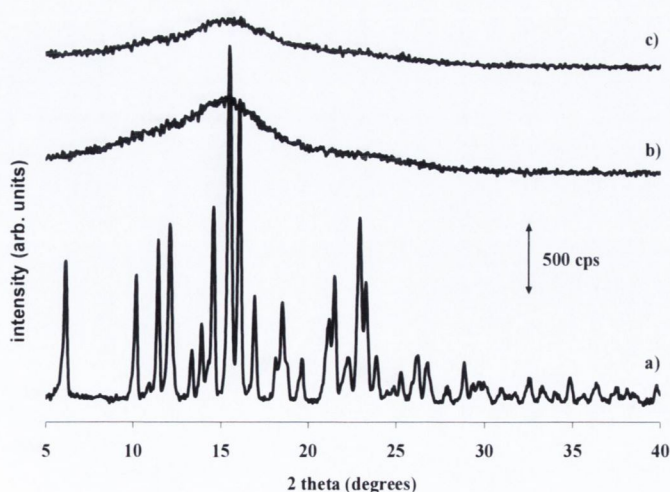


Figure 3.18 PXRD patterns of a) BUD unprocessed, b) BUD milled for 12 hours, c) BUD spray dried.

DSC analysis for the unprocessed API revealed a single melting endotherm at 248°C (Figure 3.19). A glass transition at 87°C for the spray dried drug was observed. The T_g of milled BUD could not be identified by conventional DSC due to the overlapping exotherm, but has been reported to be ~90°C (Dudognon et al., 2006). The crystallisation profiles for the processed drugs were different. The milled drug displayed a bimodal exotherm with a temperature onset of the first exotherm at 90°C. The spray dried material underwent a single step crystallisation with a higher temperature onset of 119°C.

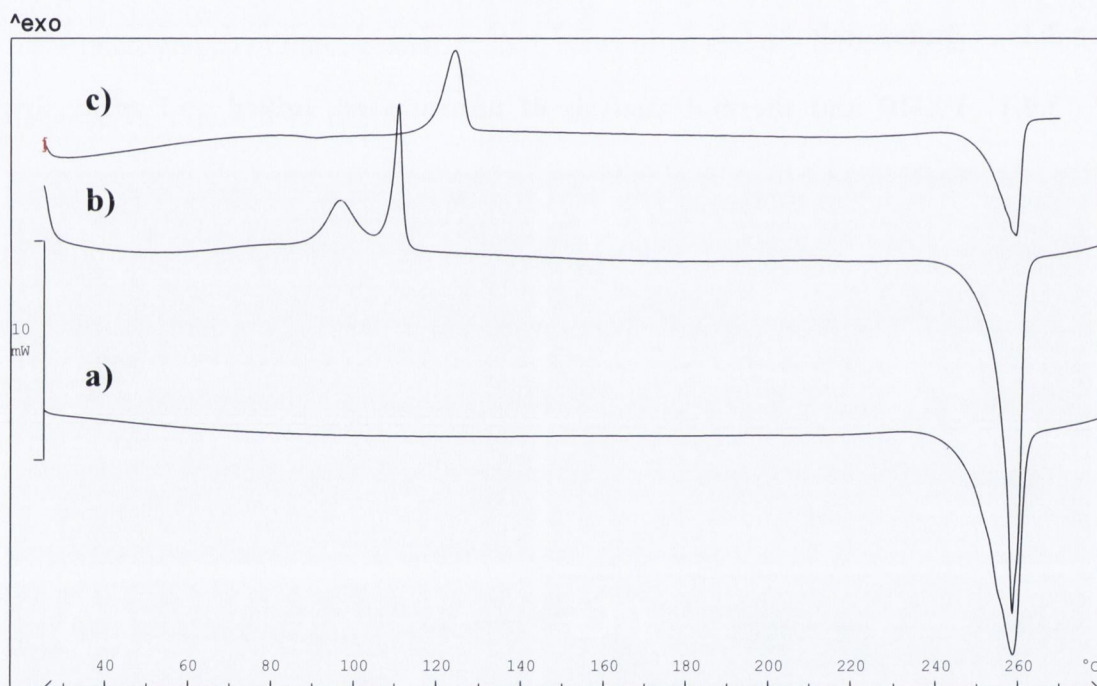


Figure 3.19 DSC thermograms of a) BUD unprocessed, b) BUD milled for 12 hours, c) BUD spray dried.

Chattoraj et al. (2012) investigated the crystallisation behaviour of ten different organic compounds produced by milling. In particular they focused on the mechanistic basis of single peak (unimodal) and two peak (bimodal) crystallisation profiles. They noted that the mode of crystallisation of an amorphous phase

depends on the relative position of the crystallisation onset temperature (T_c) with respect to the T_g . For each compound investigated, a bimodal exotherm was noted when T_g and T_m were close together. In contrast unimodal crystallisation occurs when T_c is well above T_m . For instance, when felodipine was milled for one hour, the T_c was approximately the same as the T_g and bimodal crystallisation behaviour was observed. However milling for 4 hours shifted the T_c $\sim 20^\circ\text{C}$ higher than T_g and a single crystallisation peak was identified. The reason why T_c and T_g are so close together is related to crystal nuclei or seeds that survive the milling operation. These seeds then induce rapid surface crystallisation which is subsequently followed by crystallisation of the bulk and amorphous particles free from these crystal nuclei (Chattoraj et al., 2012). This process then leads to the appearance of a bimodal exothermic process on thermal analysis. In this work, the T_g and T_c for spray dried BUD differed by $\sim 35^\circ\text{C}$ and a unimodal exotherm was observed. The T_g of amorphous BUD and the onset of crystallisation of the milled drug differed by only $\sim 3^\circ\text{C}$ and the milled drug was noted to undergo bimodal crystallisation. Interestingly a shoulder peak was also noted for milled SDM, as alluded to earlier, when analysed at $10^\circ\text{C min}^{-1}$, and no T_g could be observed because of the overlapping crystallisation exotherm (Figure 3.3). However the faster scanning rate of $300^\circ\text{C min}^{-1}$ enabled sufficient separation of T_g and T_c so that the shoulder peak was no longer apparent, with a unimodal exotherm present in the scan.

3.4.2 SEM

SEM micrographs of BUD unprocessed, milled and spray dried are displayed in Figure 3.20. The unprocessed API was composed of rough irregular shaped particles. The milled material was composed of larger agglomerates, of no regular

shape. The spray dried material was composed of spherical particles with relatively smooth surfaces.

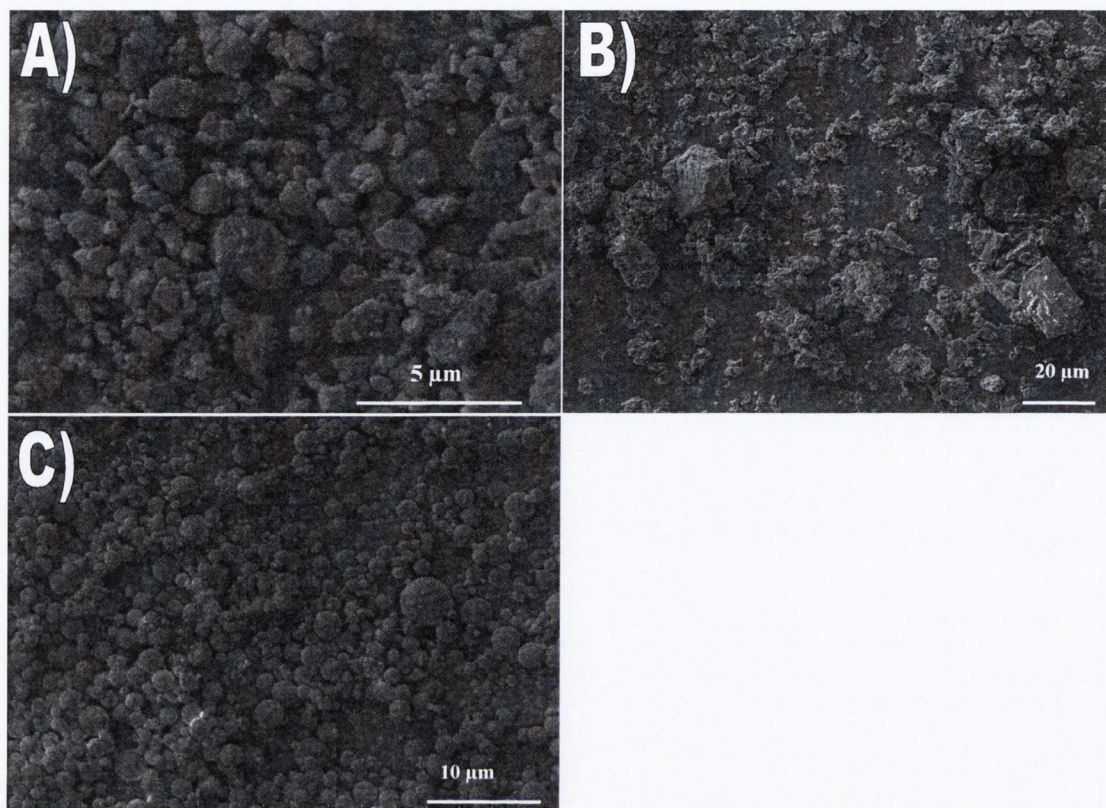


Figure 3.20 SEM micrographs of a) BUD unprocessed, b) BUD milled and c) BUD spray dried.

3.4.3 Vapour sorption analysis

The DVS sorption profiles for milled BUD, in both water and ethanolic environments, are displayed in Figure 3.21. Water was unable to sufficiently plasticise the amorphous milled drug to cause crystallisation, despite a % change in mass of 4.5% at 90% RH (Figure 3.21A). The first and second sorption cycles were super-imposable with no mass loss events observed. PXRD confirmed that the sample was still amorphous at the end of the second sorption cycle. When BUD was exposed to an ethanolic environment, a sharp mass loss was noted at 20% P/P₀ attributed to crystallisation of the API (Figure 3.21B). Mass loss events were also noted at all higher P/P₀ steps indicating that crystallisation was not complete on

exposure to 20% P/P₀. The second sorption cycle was characteristic of a fully crystalline material with no mass loss events associated with crystallisation events apparent.

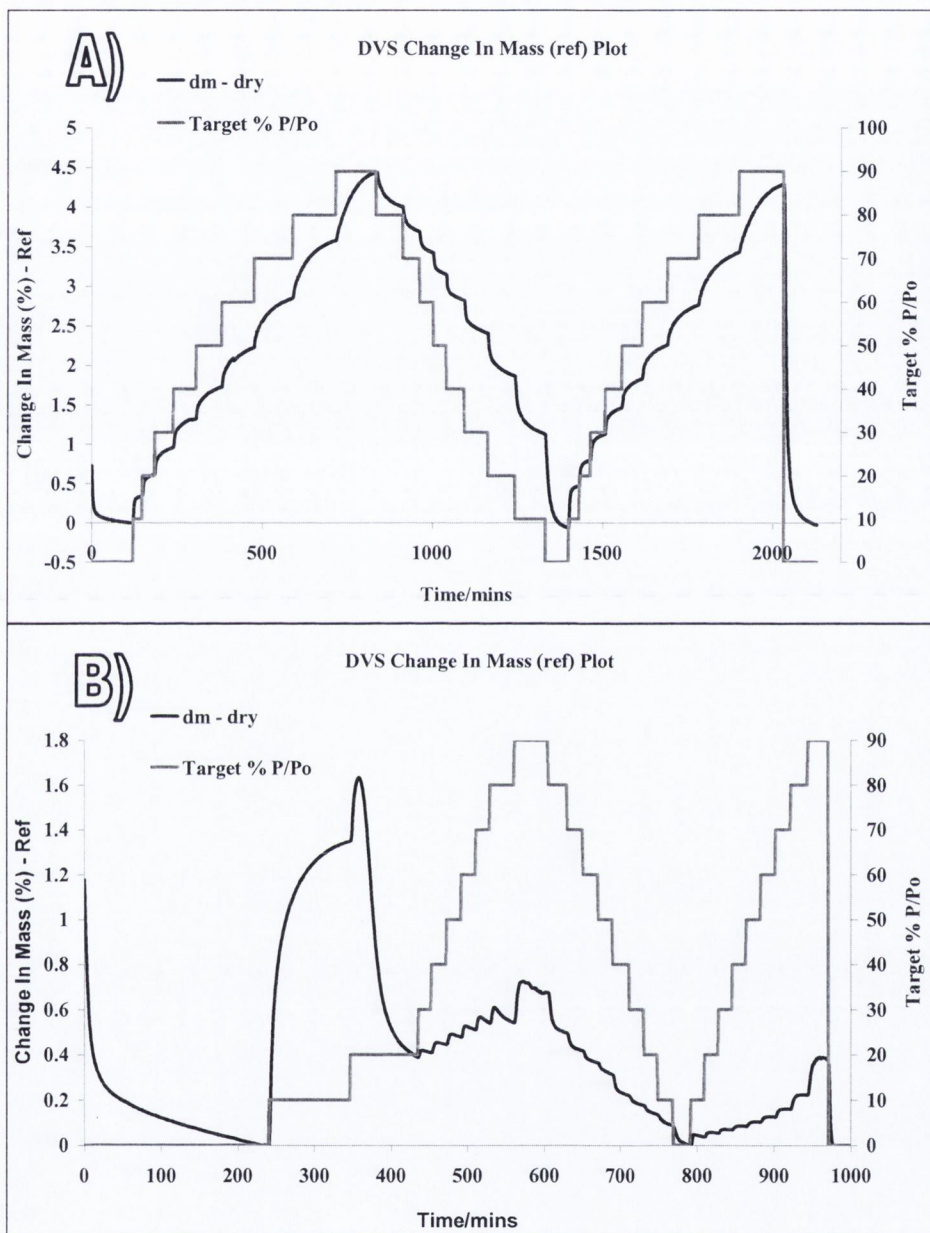


Figure 3.21 DVS kinetic profiles of milled BUD with A) water as probe molecule, B) ethanol as probe molecule.

DVS isotherm plots of BUD spray dried, milled and unprocessed under an ethanolic environment are displayed in Figure 3.22. The crystalline drug had a % mass

uptake of less than 0.2% at 80% P/P₀. Although both milled and spray dried BUD were pXRD amorphous, the drug processed by the two methods displayed different vapour sorption properties, attributed to pseudo-polyamorphism. The spray dried material crystallised between 30 and 40% P/P₀ compared to between 10 and 20% P/P₀ for the milled drug. This enhanced physical stability was consistent with the thermal data with the spray dried material crystallising at a higher temperature.

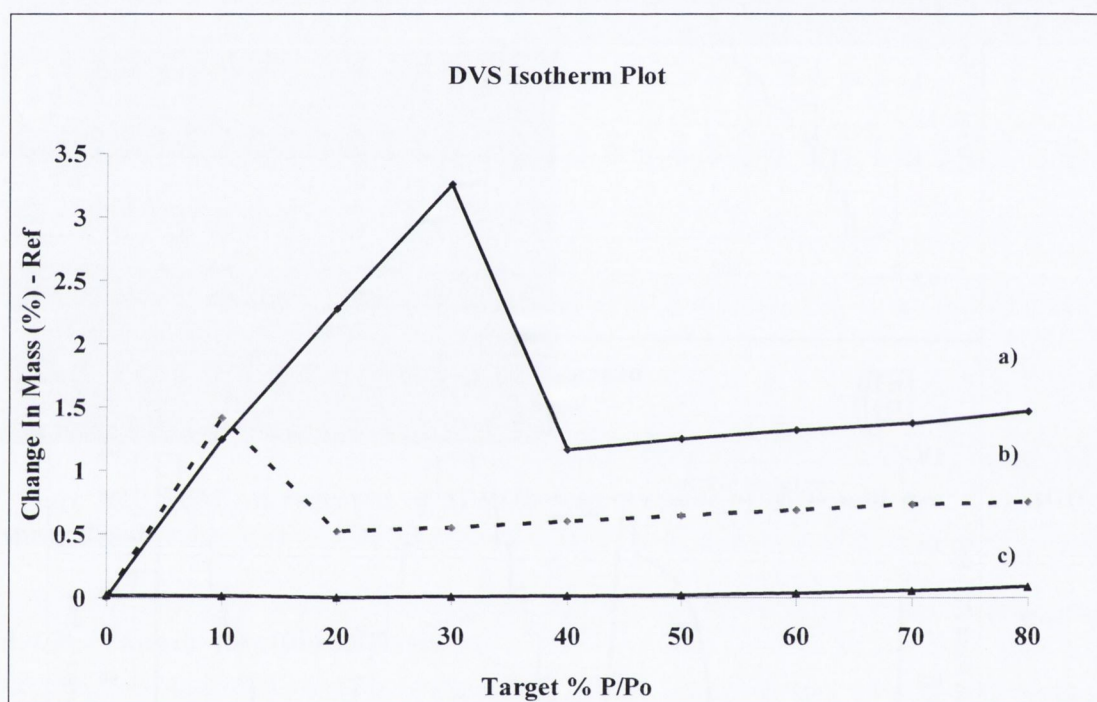


Figure 3.22 DVS isotherm plot, with ethanol as the probe vapour of a) budesonide spray dried, b) BUD milled, c) BUD unprocessed.

3.5 Conclusion

The effects of mechanical activation and spray drying on the solid state properties and degree of crystallinity of three model APIs were evaluated. Spray drying resulted in a crystalline to amorphous transformation in all three drugs. Milling, under the conditions specified, completely amorphised both SS and BUD, although

SDM was only partially amorphised on milling at RT and in a cold room at 4°C. Milling and dry mixing are two mechanical operations which, although differing considerably in terms of energy input, were capable of completely amorphising SS. The dry mixing process took considerably longer than milling (8h v 2h) to amorphise the drug, most probably due to the milder conditions to which the API particles are exposed. The different physical properties of the amorphous APIs, which were generated by different processes, was attributed to pseudopolymorphism.

The study highlighted the applicability of using multiple complementary techniques, based on diffraction, thermal, vapour sorption and spectroscopic properties, in quantifying amorphous character in a processed drug. The accuracy of the quantification analysis by DVS was shown to be potentially dependent on the process used to generate the amorphous standard. In the case of SDM, the spray dried amorphous drug was used in the generation of a calibration model to quantify amorphicity in the milled drug. This did not interfere with the quantification results, with values in good agreement with those obtained across all methods of analysis. In the case of SS and BUD, the physical stability and sorption properties of the amorphous standards differed according to the process to which they were initially exposed. Therefore, when quantifying amorphous content, the amorphous standard should ideally be prepared by a process matching that which the material was initially exposed to. It was highlighted that organic solvents are an effective alternative to water in inducing crystallisation in amorphous materials by DVS. For hydrophobic APIs like SDM and BUD, the % mass uptake and plasticising effect of ethanol was greater than water for the milled and spray dried materials and induced amorphous to crystalline transformations in both drugs.

When characterising and quantifying amorphicity in a processed drug, care should be exercised when interpreting results based on a single method. One method of quantification will never have universal application and for complete investigations and most accurate results, several methods should be used complementarily.

Chapter 4

Investigation of the capability of low glass transition temperature crystalline dicarboxylic acids to minimise amorphisation of sulfadimidine on co-milling

4.1 Introduction

The aim of this work was to evaluate the capability of a series of low T_g dicarboxylic acids to minimise the amorphisation of API on co-milling. It was hypothesised that the excipient would exert a T_g lowering effect, resulting in a system with a composite T_g lower than that of the T_g of the API alone. This would then facilitate the crystallisation of a drug which becomes amorphous on milling. The API selected was SDM which has a T_g of 78°C and which was previously shown, in chapter 3, to predominantly amorphise upon milling at room temperature. The excipients chosen were GA, AA, SA and MA. Based on the co-milling data obtained for SDM, GA was also co-milled with another API, BUD. All milling and co-milling experiments involving SDM were performed for 10 hours, and milling experiments involving BUD were performed for 12 hours. Amorphous content quantification following co-milling was carried out by DVS and/or NIR owing to ease of analysis and their known abilities to quantify very low levels of amorphous content (Hogan and Buckton, 2001).

4.2 Sulfadimidine co-milled with glutaric acid

4.2.1 Glutaric acid

The pXRD patterns of unprocessed and milled GA are displayed in Figure 4.1. The excipient was crystalline, and of the same polymorphic form, following milling for 10 hours. Bragg peak intensity was noticeably lower for the processed excipient, possibly due to crystallite size reduction and the introduction of defects arising from the milling operation (Khatirkar and Murty, 2010).

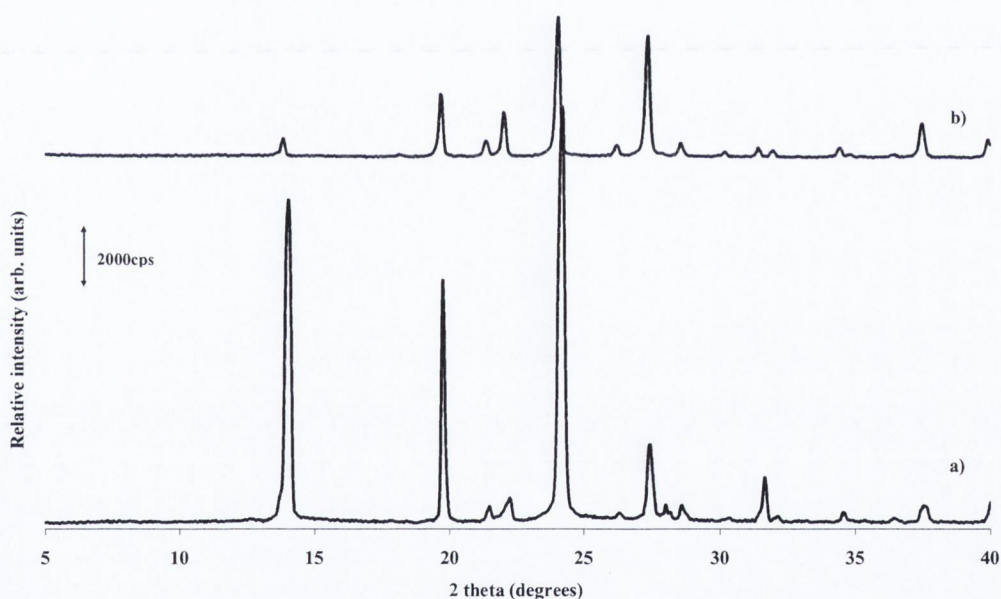


Figure 4.1 pXRD patterns of a) GA unprocessed, b) GA milled for 10 hours.

Thermal analysis of GA unprocessed revealed a two step endothermic event with a temperature onset of 73°C (Figure 4.2). This was followed by a second endotherm at 98°C ascribed to melting of the crystalline excipient. The DSC scan for the milled material also

displayed two thermal events, although the first endotherm was more symmetrical with a higher onset temperature of 77°C. Two crystalline forms are known for the GA, namely the lower energetic β form and a metastable α form. Grip and Samuelson (1984) reported the polymorphic transition temperature in GA to be at 63°C, while McNamara et al. (2006) and Ha et al. (2009) noted a solid solid transformation at around 75-76°C.

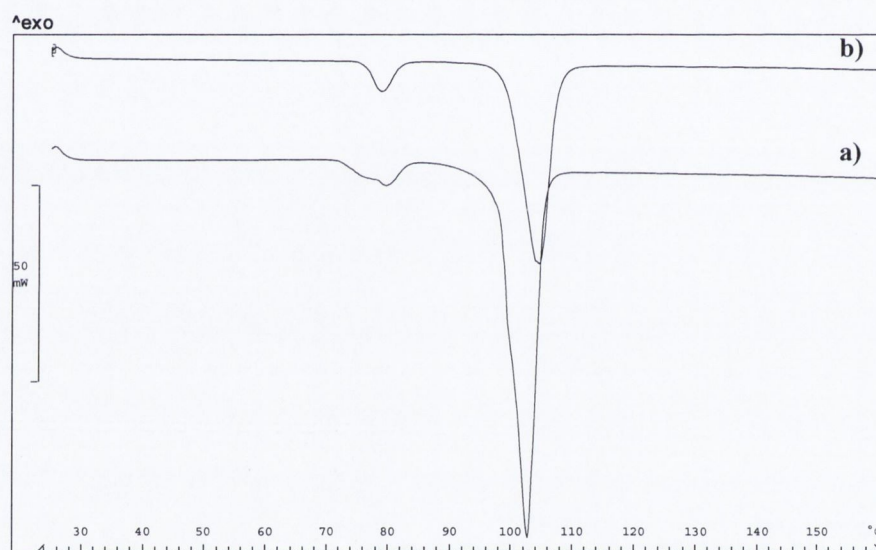


Figure 4.2 DSC thermograms of a) GA unprocessed, b) GA milled for 10 hours.

The unprocessed excipient was heated up to 85°C (a temperature intermediate to the transition of interest (~75°C) and melting (~98°C)), then removed from the DSC, and analysed by pXRD. The same process was repeated for the milled excipient. The Bragg peak positions were identical at both temperatures for the unprocessed material indicating that the same crystalline form of the excipient existed before and after the endotherm at

73°C. The two step endotherm was therefore attributed to a two step transformation process. The first step may represent a $\beta - \alpha$ transition, followed immediately by a melting and reconversion of the α crystals to the original β form. The pXRD pattern obtained at 85°C for the milled material indicated the presence of a new solid state form (Figure 4.3).

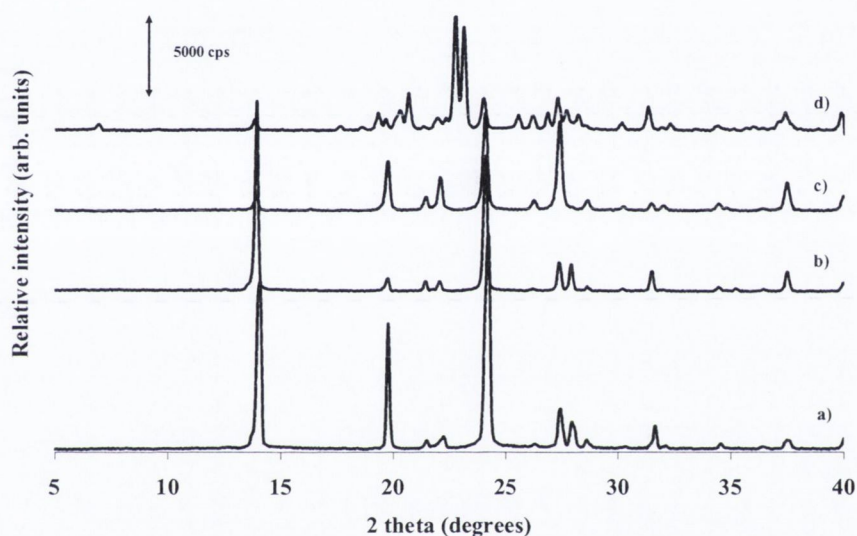


Figure 4.3 PXRd patterns of a) GA unprocessed, b) GA unprocessed when heated to 85 °C in the DSC and subsequently removed for analysis by pXRd, c) GA milled for 10 hours, d) GA milled for 10 hours and heated to 85°C in the DSC and subsequently removed for analysis by pXRd.

The single crystal XRD patterns (Ha et al., 2009) indicated that the transition at $\sim 77^\circ\text{C}$ in the milled excipient represented a transformation from the β form to a mixture of the two polymorphs. The system, obtained on heating the milled excipient to 85°C , contained predominantly the α polymorph, with the Bragg peak at 24.5 2θ representative of a trace amount of the β form.

4.2.2 PXRD and thermal analysis of sulfadimidine:glutaric acid co-milled composites

Figure 4.4 displays the pXRD patterns obtained for SDM unprocessed, SDM milled and SDM:GA co-milled composites. As previously discussed, SDM was partially amorphised when milled alone for 10 hours with an amorphous content of $76 \pm 3\%$, as determined by DVS. With $X_{GA} \geq 10\%$, characteristic peaks of SDM were observed with higher intensity compared to when the API was milled alone. Moreover the halo pattern was less pronounced, suggesting amorphisation had been reduced. No shifts in peak position or new peaks were noted.

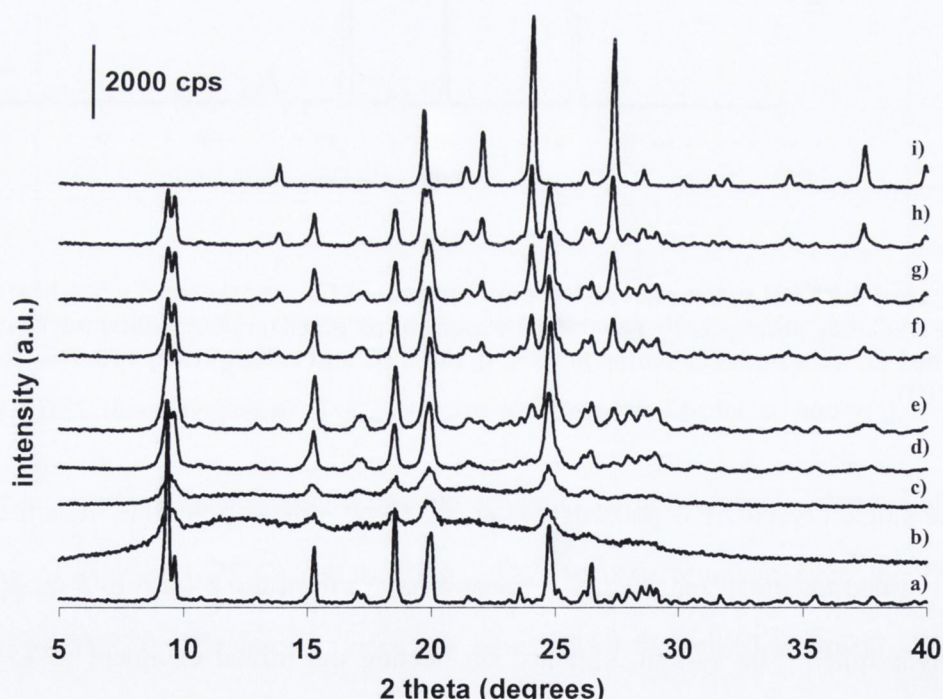


Figure 4.4 PXRD patterns of unprocessed, milled and co-milled SDM:GA systems: a) unprocessed SDM; b) milled SDM; c) $X_{GA} = 5$; d) $X_{GA} = 10$; e) $X_{GA} = 20$; f) $X_{GA} = 30$; g) $X_{GA} = 40$; h) $X_{GA} = 50$; i) milled GA.

Milled SDM displayed an exothermic peak at 80°C and a melting endotherm at 198°C. No crystallisation exotherms were seen in the DSC thermograms following co-milling with $\geq 10\%$ w/w GA (Figure 4.5). An endothermic peak gradually evolved just below 80°C, attributed to the solid-solid transformation that occurs in GA (McNamara et al., 2006).

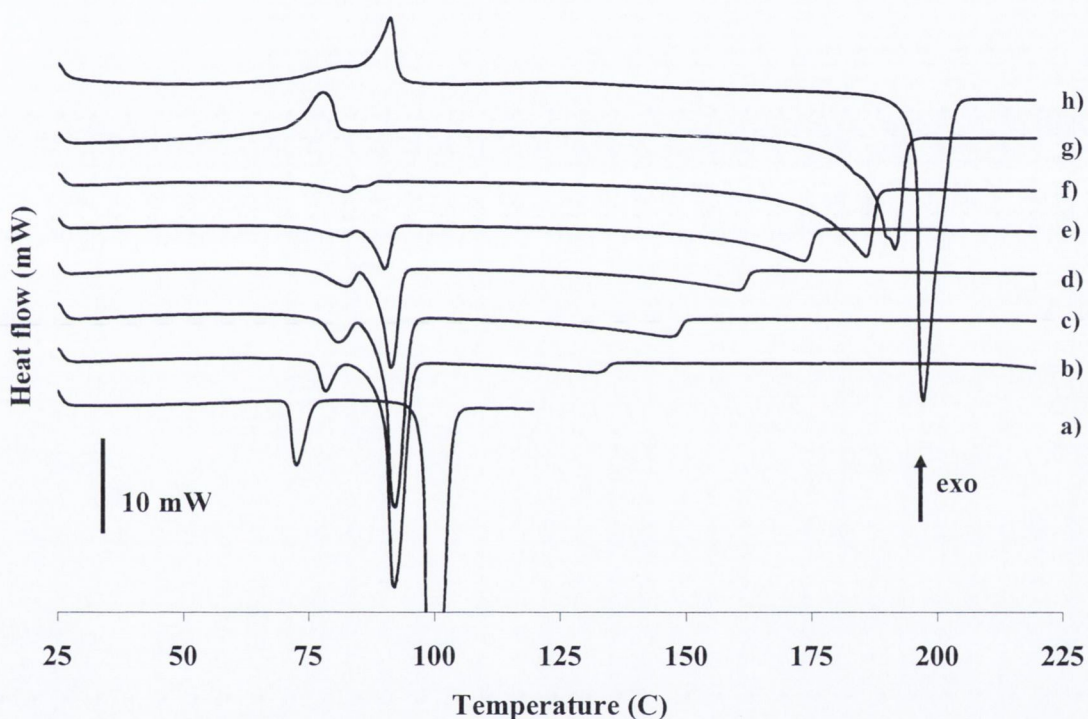


Figure 4.5 DSC scans of milled and co-milled SDM:GA systems: (a) GA milled; (b) $X_{GA} = 50$; (c) $X_{GA} = 40$; (d) $X_{GA} = 30$; (e) $X_{GA} = 20$; (f) $X_{GA} = 10$; (g) $X_{GA} = 5$; and (h) SDM milled.

The thermograms displayed a low temperature melting at 90°C which was constant across all binary compositions and was at a lower temperature compared to the melting of the excipient (99°C) and the drug (197°C). The presence of a depressed skewed melting of API suggests an interaction between the API and excipient on melting.

No evidence of transient amorphisation was observed following intermediate analysis at various time points (3, 5, 7, 10 hours) of SDM co-milled with GA, with both API and excipient appearing crystalline across all time points (Figure 4.6). The difficulty with observing an amorphous state by pXRD following extraction of a powder sample from the mill is that once milling is ceased, amorphisation stops and immediate crystallisation is possible prior to diffraction analysis.

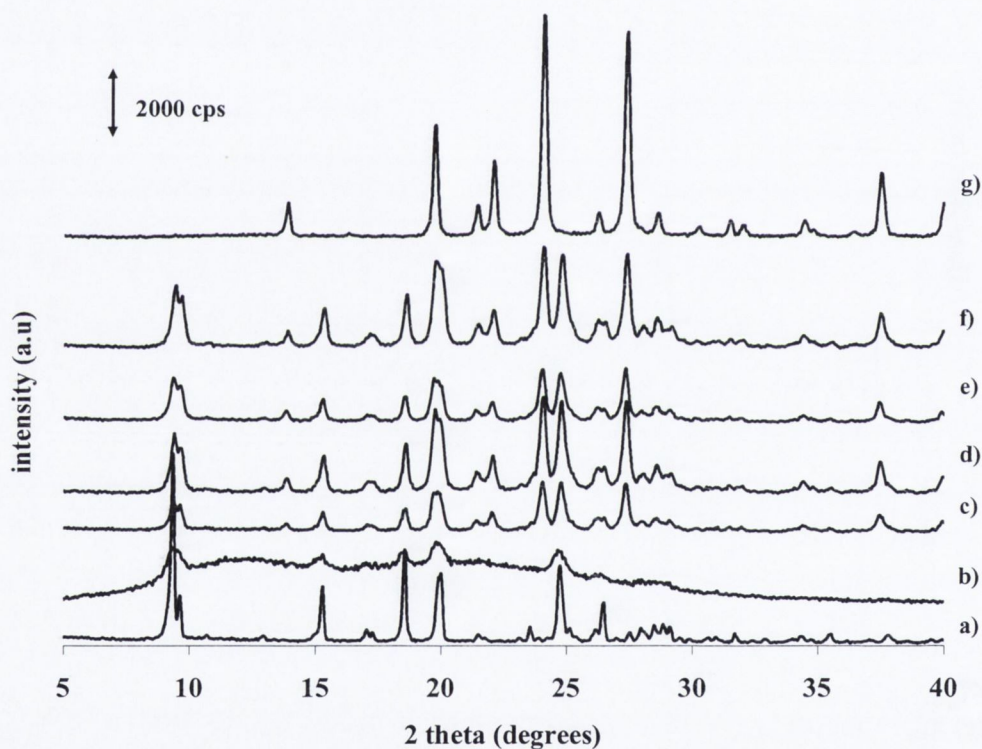


Figure 4.6 pXRD patterns of SDM unprocessed, SDM milled, GA milled and SDM50:GA50 co-milled for different time periods; a) SDM unprocessed, b) SDM milled for 10 hours, c) SDM50:GA50 co-milled for 3 h, d) SDM50:GA50 co-milled for 5 h, e) SDM50:GA50 co-milled for 7 h, f) SDM50:GA50 co-milled for 10 h, g) GA milled for 10 h.

4.2.3 Quantification of amorphous content

4.2.3.1 DVS

The method of quantification for the co-milled composites by DVS was similar to that employed for the API milled alone. Ethanol was used as the probe molecule as it was observed in chapter 3 that subjecting the milled API to an ethanolic environment resulted in crystallisation of the drug. Amorphous content calculations were performed using equation 2.3, as described in section 2.2.11.1.

An interesting observation for the SDM:GA co-milled system was that with only 5% w/w excipient, SDM started to crystallise at 20% P/P₀ (Figure 4.7A). Even the minimum weight fraction of GA used in the co-milling experiments had the effect of lowering the P/P₀ at which the API started to crystallise and hence the mass uptake at 10% P/P₀ was used for these particular composite quantification calculations. Mass loss at higher P/P₀ was also noted. Again it is highlighted that the quantification results are independent of the crystallisation kinetics, provided the method allows the sample to reach equilibrium at each partial pressure and the sample has crystallised (Mackin et al., 2002b). For all systems, crystallisation was complete before the start of the second sorption cycle. As seen in Figure 4.7B, a mass loss was observed at 50% P/P₀ for the co-milled system with $X_{GA} = 30$ indicating some degree of amorphicity (9%) was still present (Table 4.1). Figure 4.7C shows a two cycle sorption profile for the SDM50:GA50 co-milled system and represents typical moisture behaviour for a crystalline material. The amount of moisture sorbed was very small and there were no mass loss events evident in the sorption cycles. API

amorphisation was indeed eliminated on co-milling with 50% w/w GA. Amorphous content values for SDM:GA co-milled systems, as quantified by DVS, are displayed in Table 4.1 below and all SDM:diacid co-milled quantification results are discussed later in section 4.8.

Table 4.1 API amorphous content of SDM:GA co-milled systems as quantified by DVS

System	% amorphous content (\pm S.D)
SDM milled	76 (3)
SDM95:GA5	78(2)
SDM90:GA10	30 (5)
SDM70:GA30	9 (5)
SDM50:GA50	0 (0)

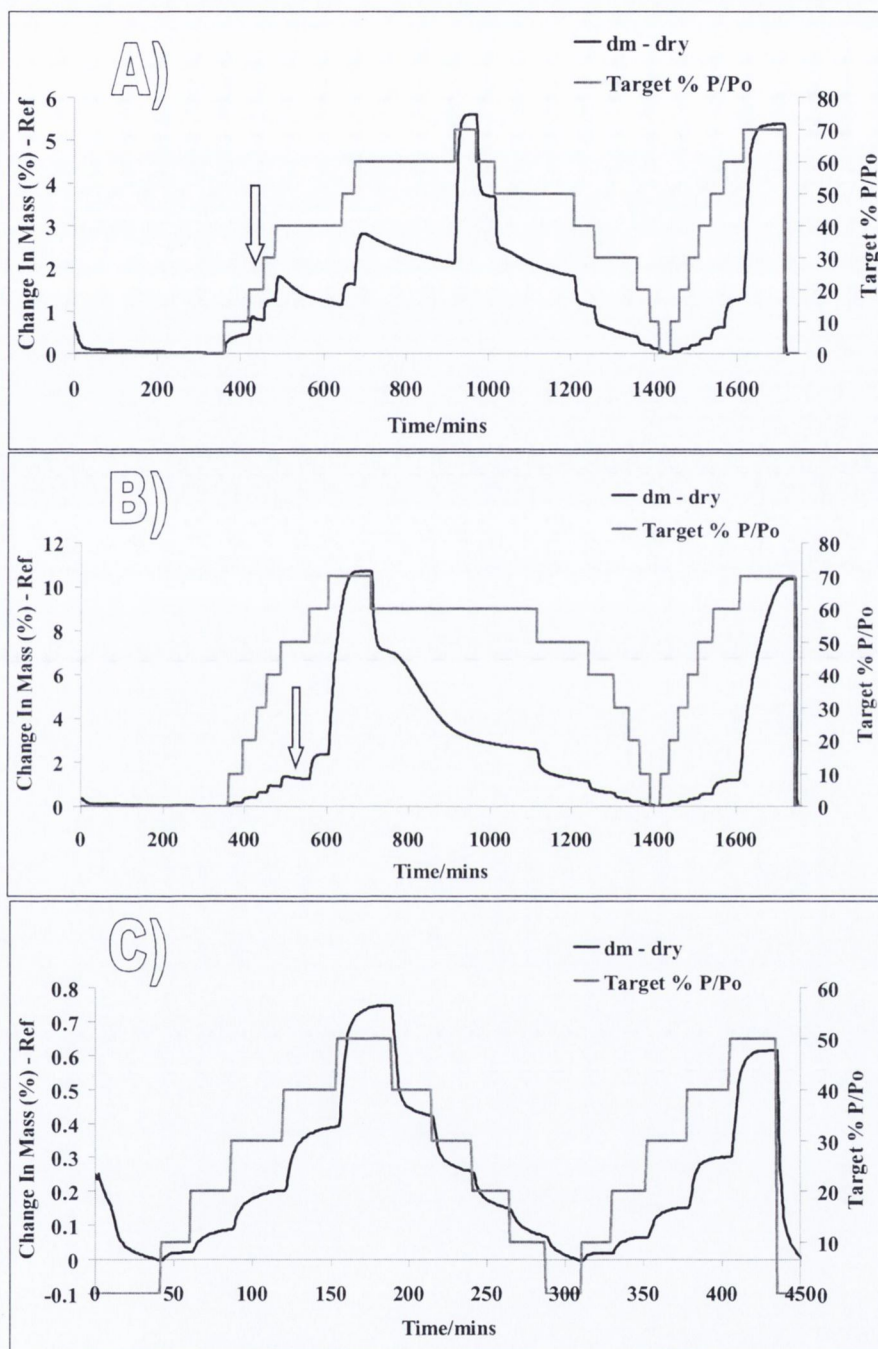


Figure 4.7 Ethanol vapor sorption kinetics of co-milled SDM:GA composites: (A) $X_{GA} = 5$; (B) $X_{GA} = 10$; and (C) $X_{GA} = 50$. Arrows indicate where mass loss was first observed to occur. No mass loss events were observed in the profile for the SDM50:GA co-milled system.

4.2.3.2 NIR

Amorphous (spray dried) / crystalline physical mixtures of SDM were diluted step wise with increasing amount of milled GA and NIR spectra collected before and after each step of dilution were used to build the calibration models. From Figure 4.8, it can be seen that the spectral region of $6850 - 6400 \text{ cm}^{-1}$ displayed characteristic bands for SDM, with no interference from GA, and thus this region was used for the PLS modelling. Quantification results by NIR indicated that API amorphous content was lowered to 10% on co-milling with 30% w/w GA and lowered to just 4% on co-milling with 50% w/w GA. The amorphous content values of SDM on co-milling with GA, as quantified by NIR, are listed in Table 4.2 below and all SDM:diacid co-milled quantification results are discussed later in section 4.8.

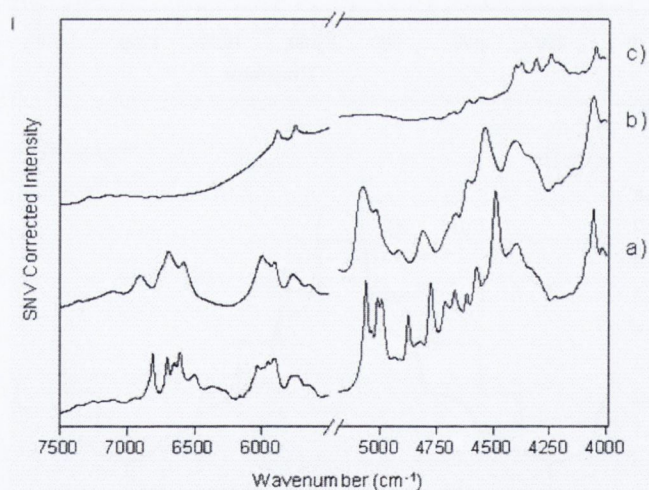


Figure 4.8 NIR spectra of a) SDM unprocessed, b) SDM spray dried and c) GA milled for 10 hours.

Table 4.2 API amorphous content of SDM:GA co-milled systems as quantified by NIR

System	% amorphous content (\pm S.D)
SDM milled	84 (1)
SDM95:GA5	76 (1)
SDM90:GA10	27 (1)
SDM70:GA30	10 (1)
SDM50:GA50	4 (1)

4.2.4 Physical mixture of milled sulfadimidine and milled glutaric acid

A physical mixture of milled SDM and milled GA (50:50 w/w) was prepared and the crystallinity of the system was evaluated by pXRD and DVS. It can be observed from Figure 4.9 that co-milling greatly enhanced the crystallinity of the API compared to the corresponding physical mixture. The Bragg peak at 9.62° theta, and highlighted in Figure 4.9, is more defined in the co-milled system, compared to the physical mixture, an indicator of higher crystallinity.

The DVS kinetic profile for the physical mixture is displayed in Figure 4.10. An amorphous content of 33% (30%, 36%) for the API in the physical mixture was determined using equation 2.3, as described in section 2.2.11.1. This was unexpectedly low, based on the pXRD patterns, and the fact that the drug milled alone had a DVS amorphous content of $76 \pm 3\%$. The system had a % change in mass comparable to the API milled alone during the first sorption cycle. Mass uptake during the second sorption cycle was,

however, higher than anticipated which resulted in the low amorphous content value reported. This could be due to the physical mixture system having a ~39% change in mass at the end of the first sorption cycle, compared to <1.6% for the milled drug alone (Figure 3.7B in chapter 3). It may be that large uptake in moisture could interfere with surface properties and potentially distort quantification results obtained by DVS.

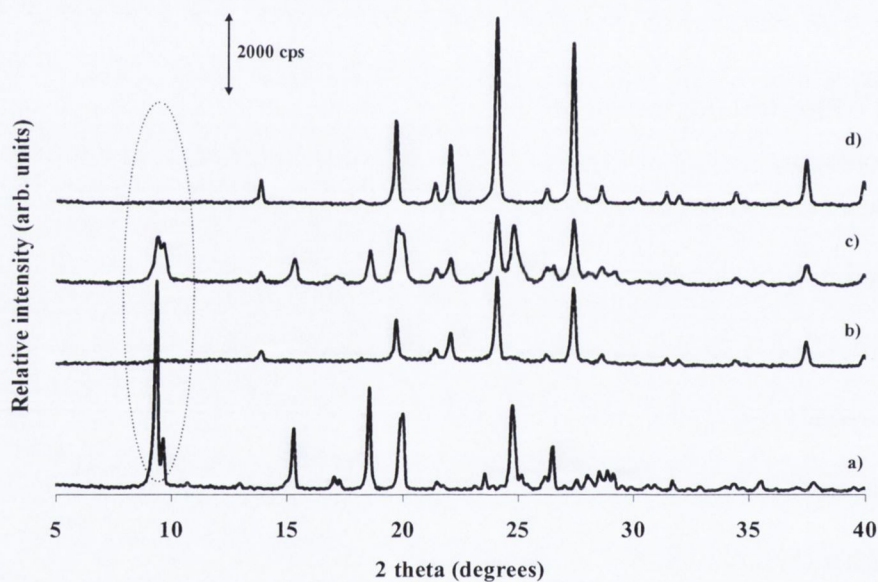


Figure 4.9 PXR D patterns of a) SDM unprocessed, b) SDM50:GA50 physical mixture, c) SDM50:GA50 co-milled for 10 hours, d) GA milled for 10 hours. Highlighted is a characteristic Bragg peak of the API at 9.6 2 theta.

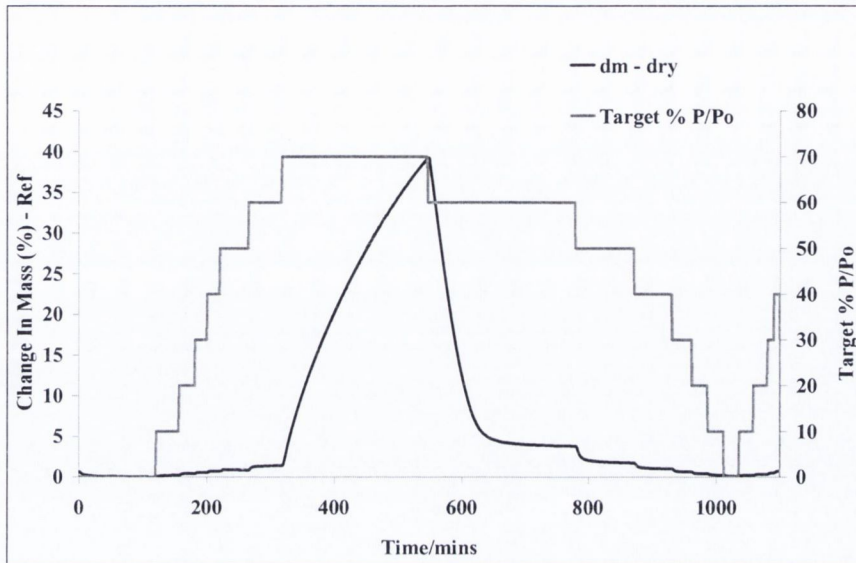


Figure 4.10 DVS kinetic profile of SDM50:GA50 physical mixture.

4.3 Adipic acid

The pXRD patterns and DSC scans for AA unprocessed, and AA milled for 10 hours, are displayed in Figure 4.11 below. AA is monomorphic (Ng et al., 2010). The retention of all Bragg peaks with the absence of an amorphous halo coupled with the lack of a glass transition or recrystallisation exotherm in the DSC scans was consistent with the excipient being crystalline at the end of the milling operation.

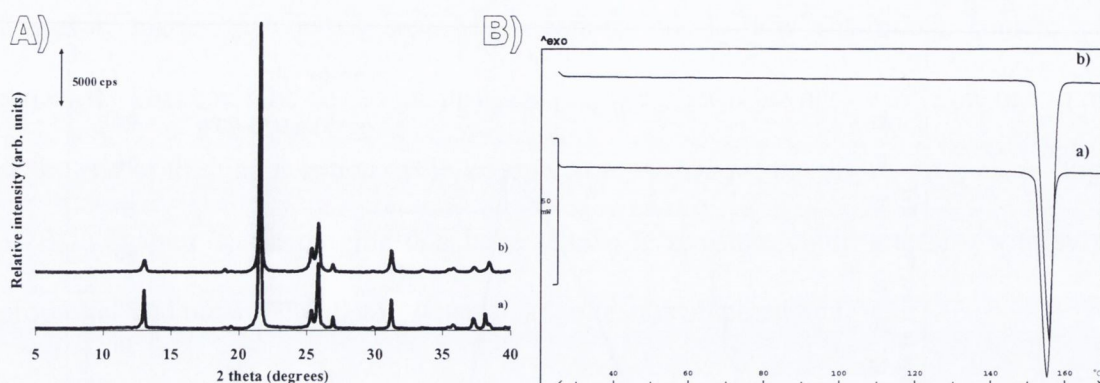


Figure 4.11 A) PXR D patterns of a) AA unprocessed and b) AA milled for 10 hours. B) DSC thermograms of a) AA unprocessed and b) AA milled for 10 hours.

4.4 Succinic acid

SA exhibits dimorphism constituting the stable β form at room temperature and the metastable high temperature α form (Chikhalia et al., 2006). Both forms melt over a very narrow temperature range with negligible differences in their heats of fusion (Chikhalia et al., 2006). pXR D enables identification of the two polymorphs with the α form having characteristic Bragg peaks at 22.5 and 27 2 theta. Both the unprocessed excipient and the milled sample were identified as the β form (Figure 4.12A). Characteristic peaks of the excipient were retained after milling although a reduction in intensity was noted. DSC analysis of the unprocessed and milled excipient revealed an endothermic event at 187°C, ascribed to melting of the crystalline material (Figure 4.12B).

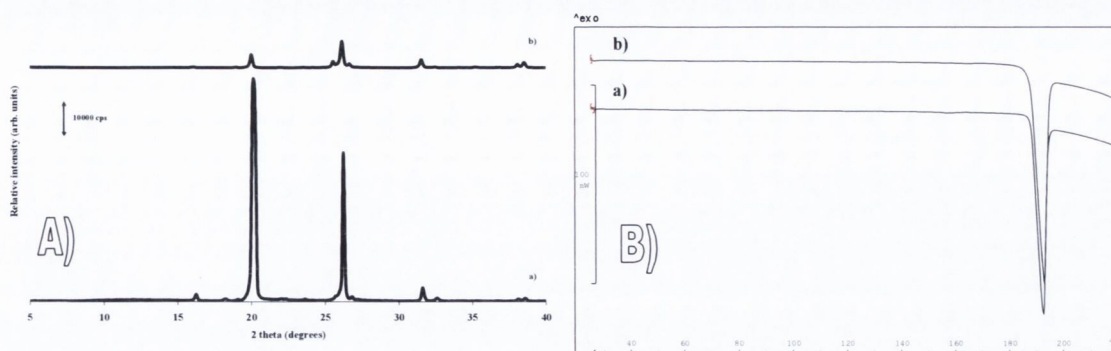


Figure 4.12 A) XRD patterns of a) SA unprocessed, b) SA milled for 10 hours. B) DSC thermograms of a) SA unprocessed, b) SA milled for 10 hours.

4.5 Malic acid

MA is a hydroxylated derivative of succinic acid. DSC scans of the unprocessed, milled and melt quenched sample are displayed in Figure 4.13. The unprocessed and milled excipient displayed a single melting endotherm at 131°C and 124°C, respectively. This depression in melting temperature for the milled excipient, coupled with a 15% reduction in the enthalpy of fusion following mechanical activation (247 v 210 J/g) could be due to milling induced disorder and crystallite size reduction. The melt quenched sample revealed a T_g at -15°C. The sample subsequently recrystallised at 19°C and melted at 118°C.

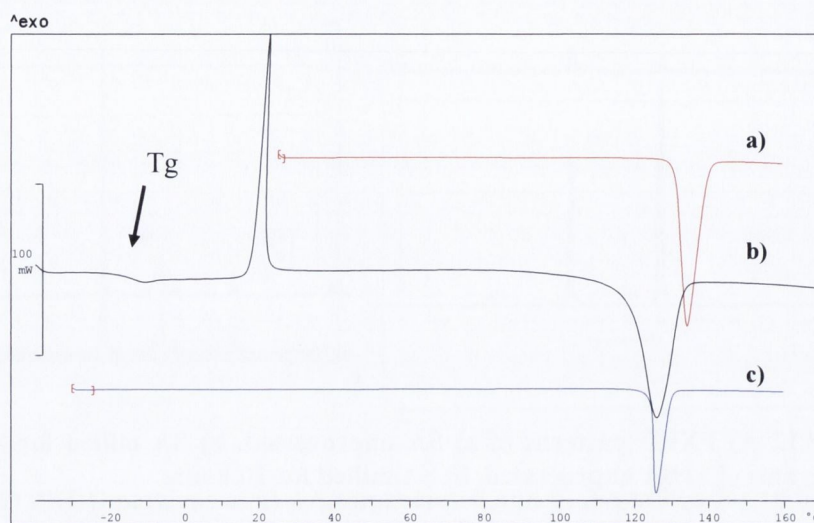


Figure 4.13 DSC scans of a) MA unprocessed, b) MA melt quenched, c) MA milled for 10 hours. Highlighted is the Tg of the melt quenched sample.

The pXRD patterns for unprocessed and milled MA are displayed in Figure 4.14. The excipient was crystalline after milling but peaks were of lower intensity and broader.

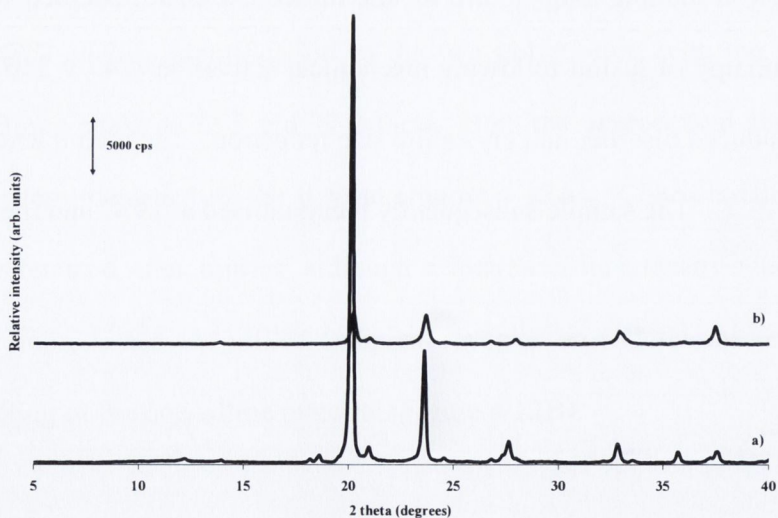


Figure 4.14 pXRD patterns of a) MA unprocessed and b) MA milled for 10 hours.

4.6 Glass transition temperatures and solubility parameters of sulfadimidine and the dicarboxylic acids

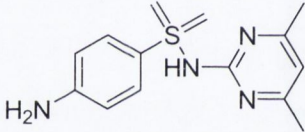
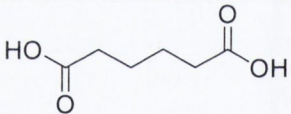
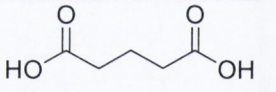
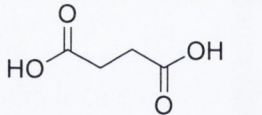
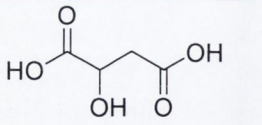
The dicarboxylic acids investigated were crystalline in nature and, except for MA (which amorphised upon melt quench), were resistant to amorphisation when milled or spray dried (Appendix IV). SA undergoes degradation on melting and hence it was not possible to perform the usual melt quench experiment. No T_gs or crystallisation exotherms were observed in the thermograms of melt quenched GA or AA (Appendix IV).

The theoretical T_g values for GA, AA and SA were calculated using the $T_g = T_m \times 0.7$ rule (Fukuoka et al., 1989; Kerc and Srcic, 1995) and are displayed in Table 4.3. Lin et al. (2009) compared the values obtained by this method against those determined experimentally for a number of compounds and found a generally good agreement between the estimated and experimental values, with an average prediction error of approximately 5.9%. T_g values for five compounds investigated in this work could be determined experimentally by DSC, in addition to the $T_g = T_m \times 0.7$ rule; values for SDM differed by 22K (351K by DSC v 329K calculated), values for BUD differed by 5K (360K by DSC v 365K calculated), values for SS differed by 72K (393K by DSC v 321K calculated), values for MA differed by 24K (258K by DSC v 282K calculated) and values for MAN differed by 22K (286K by DSC v 308K calculated).

The solubility parameters for SDM and the dicarboxylic acids were calculated using Fedors group contribution theory (Appendix III) and values are displayed in Table 4.3. SDM and GA would be expected to be most miscible of all the binary component systems. The

difference in the Hildebrand solubility parameter for the API and excipient ($\Delta\delta$) was only $0.1 \text{ MPa}^{1/2}$, compared to a difference of $0.8 \text{ MPa}^{1/2}$ for SDM and AA and $1.3 \text{ MPa}^{1/2}$ for SDM and SA. MA differs structurally with SA by just an extra hydroxyl group on its alkyl backbone, but this resulted in a much greater $\Delta\delta$ of 8.0 (Table 4.3).

Table 4.3 Summary of solubility parameters, melting point values, Tg values, molecular weights and chemical structures for SDM and the dicarboxylic acids. $\Delta\delta$ is the difference of the Hildebrand solubility parameter between API and excipient.

System	Hildebrand solubility parameter ' δ ' ($\text{MPa}^{1/2}$)	$\Delta\delta$	Tm (K)	Tg (K)	Mw ($\text{g}\cdot\text{mol}^{-1}$)	Chemical structure
Sulfadimidine	25.7	NA	470	351 (329*)	278.33	
Adipic acid	24.9	0.8	425	298*	146.14	
Glutaric acid	25.8	0.1	370	259*	132.11	
Succinic Acid	27.0	1.3	460	322*	118.09	
Malic acid	33.7	8.0	404	258 (283*)	134.09	

*Tg values determined by the $T_g = T_m \times 0.7$ rule

4.7 Sulfadimidine co-milled with adipic acid, succinic acid and malic acid

SDM was co-milled with AA, SA and MA, with the objective to see if comparable results as those observed with GA could be obtained. Amorphous content was quantified by DVS and NIR, as for the SDM:GA systems. The pXRD patterns for the individual excipients as well as the co-milled composites with $X_{\text{excipient}} = 50\%$ are displayed in Figure 4.15. Focusing on Bragg peaks at approximately 9.6, 15.1, 18.1 and 24.9 2θ there is an indication that, relative to the API milled alone, amorphisation was reduced on co-milling with AA but was promoted on co-milling with SA and MA.

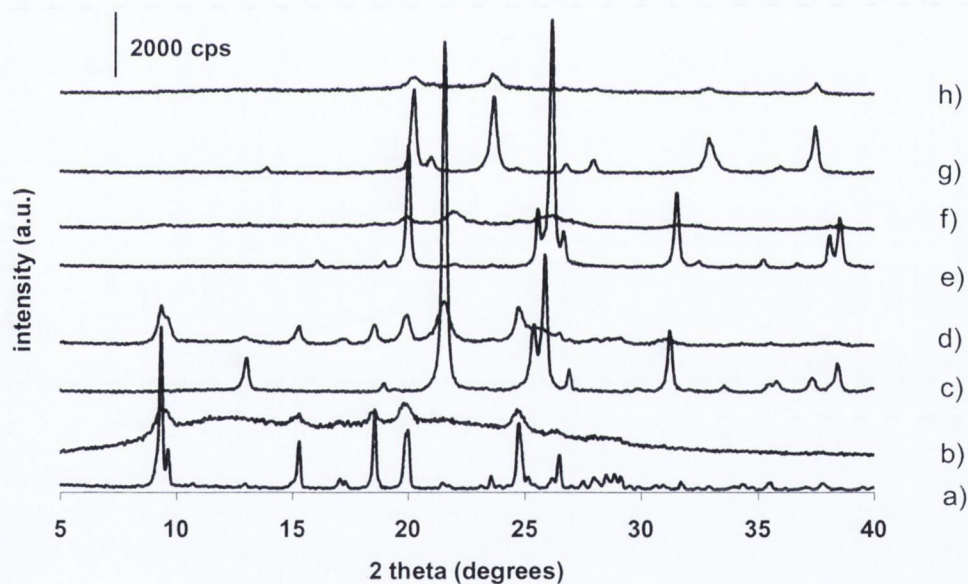


Figure 4.15 pXRD patterns of (a) unprocessed SDM; (b) SDM milled; (c) AA milled; (d) comilled SDM50:AA50; (e) SA milled; (f) comilled SDM50:SA50; (g) MA milled; and (h) comilled SDM50:MA50.

The corresponding DVS sorption profiles for these co-milled systems are shown in Figure 4.16. The difference in mass uptake at 20% P/P₀ for the SDM:AA system, and at 30% P/P₀ for the SDM:MA and SDM:SA systems was used for these DVS amorphous content calculations, in contrast to 10% P/P₀ which was used for the SDM:GA co-milled systems. This was because crystallisation occurred at higher P/P₀ values for these co-milled composites. The capacity of the SDM:MA system to sorb ethanol increased noticeably between 20% and 30% P/P₀ and measurements at 10% or 20% P/P₀ would have significantly underestimated the amorphous content for this system. Amorphous content quantification by NIR was carried out in a manner similar to that described for SDM:GA systems and the RMSEC values for the calibration models obtained with each excipient were between 0.31 and 1.34. API amorphous content values for SDM50:AA50, SDM50:SA50 and SDM50:MA co-milled composites are displayed in Table 4.4 below and are discussed in detail in section 4.8.

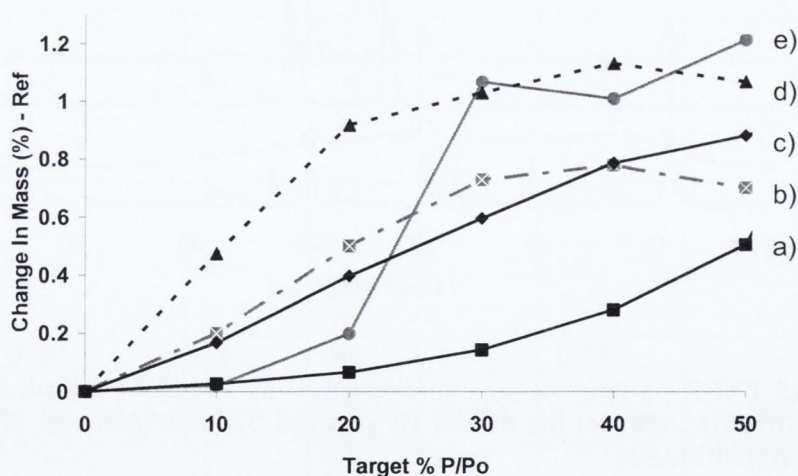


Figure 4.16 Sorption isotherms (first cycle) of milled SDM and co-milled composites of SDM with excipients: (a) SDM50:GA50; (b) SDM50:SA50; (c) SDM50:AA50; (d) SDM milled; and (e) SDM50:MA50. Error bars are omitted for clarity.

Table 4.4 API amorphous content of SDM50:AA50, SDM50:SA50 and SDM50:MA50 co-milled systems as quantified by DVS and NIR.

System	% Amorphous content (\pm S.D)	
	DVS	NIR
SDM milled	76 (3)	84 (1)
SDM50 : AA 50	54 (2)	52 (1)
SDM50 : SA 50	62 (2)	96 (1)
SDM50 : MA50	114 (5)	100 (1)

4.8 Comparison of API crystallinity on co-milling with a series of dicarboxylic acids

Amorphous content values for the SDM:diacid co-milled systems are displayed in Table 4.5. In order to assess whether co-milling SDM with a number of low Tg dicarboxylic acids could mitigate amorphisation in the API, it was first necessary to know how much amorphous content was generated when the API was milled alone. The general agreement between the four quantification methods (ranging from 76%-88% by pXRD, MTDSC, DVS and NIR in chapter 3) gave a reliable indicator of the amorphous content in the milled API and provided a basis on which to compare the effects of co-milling with the selected dicarboxylic acids.

Amorphous content for SDM, relative to the API milled alone, was more than halved following co-milling with 10% w/w GA and completely eliminated following co-milling with 50% w/w GA, as quantified by DVS. NIR results displayed very good agreement, although 4% amorphous content was still detected for the 50:50 co-milled system. Of the excipients investigated, SDM has the most comparable solubility parameter with GA with a $\Delta\delta$ of only 0.1, as previously mentioned (Table 4.3). GA also has a low calculated Tg value

(-14°C). Quantification results by DVS and NIR were in very good agreement for the SDM50:AA50 co-milled system. AA, after GA, was the second most effective excipient at mitigating API amorphisation on co-milling. Although MA has a theoretical T_g value of -15°C, which is very similar to GA, co-milling SDM with this excipient completely amorphised the API, as quantified by both DVS and NIR. Interestingly it was noted earlier that MA has the poorest miscibility of all the excipients with SDM (Table 4.3). The amorphous content value of 114% by DVS (Table 4.5) was attributed to complete amorphisation of the API and partial amorphisation of MA.

Table 4.5 Summary of API amorphous content of SDM:diacid co-milled systems as quantified by DVS and NIR.

System	% Amorphous content (±S.D)	
	DVS	NIR
SDM milled	76 (3)	84 (1)
SDM95 : GA5	78 (2)	76 (1)
SDM90 : GA10	30 (5)	27 (1)
SDM70 : GA30	9 (5)	10 (1)
SDM50 : GA50	0 (0)	4 (1)
SDM50 : AA 50	54 (2)	52 (1)
SDM50 : SA 50	62 (2)	96 (1)
SDM50 : MA50	114 (5)	100 (1)

For all systems investigated, the rank order of difference of Hildebrand solubility parameter between API and excipient correlated with the degree of crystallinity of API on co-milling. Quantification results by DVS and NIR were not in agreement for the SDM:SA system (Table 4.5). Based on the pXRD pattern (Figure 4.15), the API was

predominantly amorphous and hence the DVS result would appear to have underestimated the amorphous content. NIR was therefore considered the more appropriate quantification technique for this particular system.

4.9 Physical mixture of milled sulfadimidine with milled adipic acid, succinic acid and malic acid

The pXRD patterns obtained for the physical mixtures of milled SDM with milled excipient, obtained with $X_{\text{excipient}} = 50\%$ w/w, are displayed in Figure 4.17. The API, as indicated by the Bragg peak highlighted, was predominantly amorphous in the physical mixtures. DVS was used to quantify the amorphicity of the API in the physical mixtures and results are illustrated in Table 4.6. The SDM50:MA50 system had a % change in mass of ~47% after the first sorption cycle (Figure 4.18A) and as discussed for the SDM50:GA50 physical mixture system, such a large mass uptake may have interfered with the sorption behaviour of the system in the second cycle. The API amorphous content (56%) was again significantly lower when compared to the drug milled alone (76%), despite the sorption uptakes being comparable in the first cycle. The SDM:AA and SDM:SA physical mixtures had a % change in mass of $\leq 2\%$ at the end of the first sorption cycle and the quantification results for these systems were closer to the value of ~76% for the SDM milled alone.

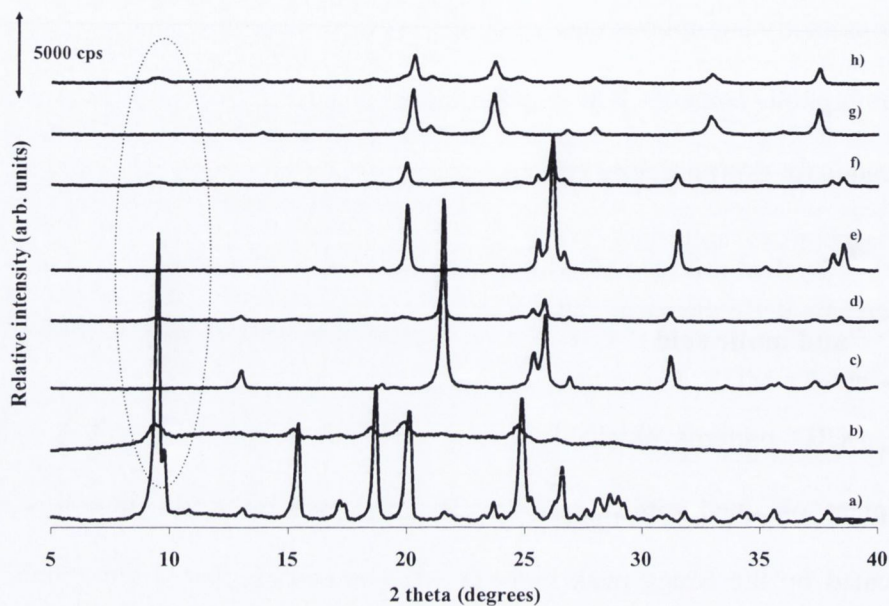


Figure 4.17 PXRD patterns of a) SDM unprocessed, b) SDM milled, c) AA milled, d) SDM50:AA50 physical mixture, e) SA milled, f) SDM50:SA50 physical mixture, g) MA milled, h) SDM50:MA50 physical mixture.

Table 4.6 Summary of API amorphous content in physical mixtures ($X_{\text{excipient}} = 50\%$ w/w) as quantified by DVS. The amorphous content of the API is also included for comparison purposes.

System	% amorphous content range or (\pm S.D.)/(range)
SDM milled	76 (3)
SDM50:AA50	69.5 (65,74)
SDM50:SA50	73.5 (72,75)
SDM50:MA50	56 (52, 60)

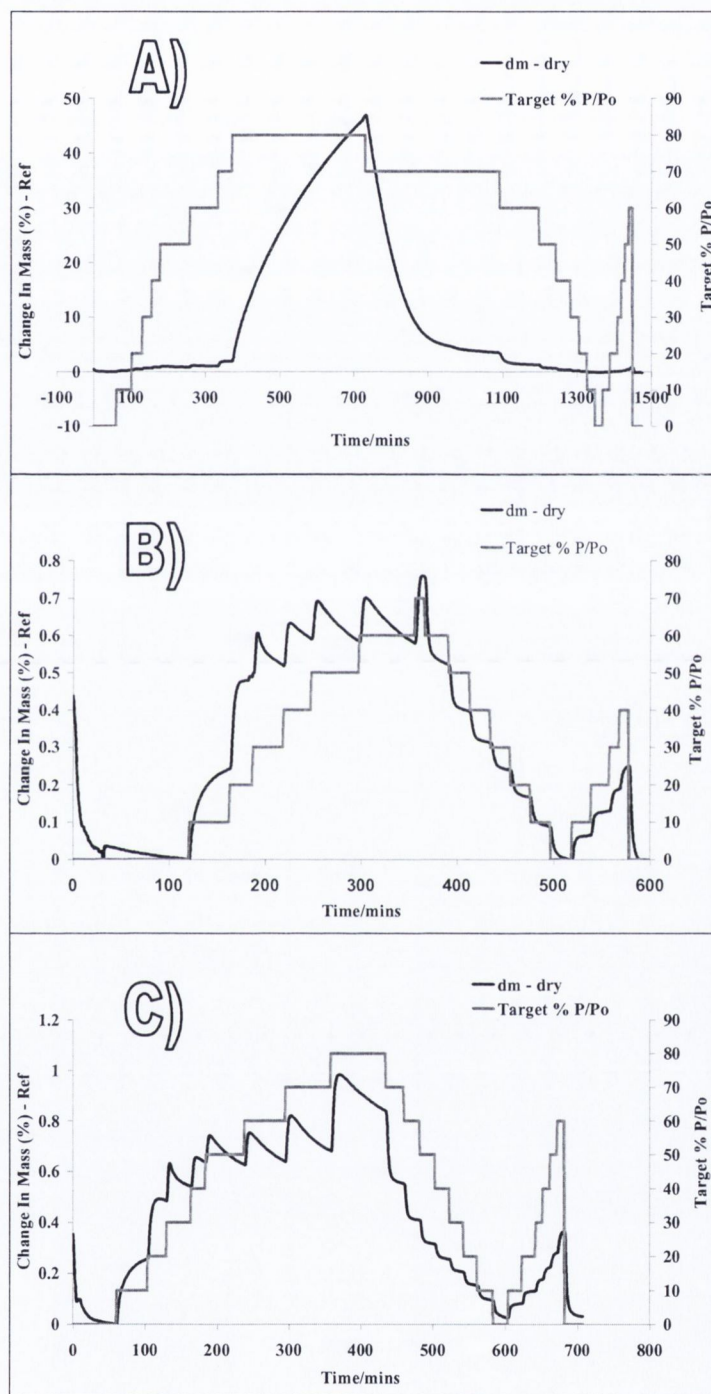


Figure 4.18 DVS kinetic profiles of a) SDM50:MA50 physical mixture, b) SDM50:AA50 physical mixture, c) SDM50:SA50 physical mixture.

4.10 Characterisation by FTIR

FTIR measurements on the individual components, their physical mixtures and the corresponding co-milled composites were undertaken. Particular attention was focused on the wavenumber regions of 3000 – 3500 cm^{-1} (OH and NH stretching vibrations), 1600 – 1800 cm^{-1} (C=O vibration) and 1200 – 1400 cm^{-1} (OH bends and CH stretches), as changes in hydrogen bonding networks would be reflected in peak shifts in these regions (Socrates, 2001). For this work, particular attention was focused was on the SDM:GA and SDM:MA systems because of the divergence in results obtained on co-milling with these two excipients.

Figure 4.19 displays the spectra of SDM, SDM milled, GA milled, SDM50:GA50 co-milled, SDM50:GA50 physical mixture, SDM50:MA50 co-milled, SDM50:MA50 physical mixture and milled MA. SDM, like other related sulfa compounds has strong characteristic bands in the region 3390 – 3425 cm^{-1} due to the N-H stretching vibrations and a number of strong absorption bands at 1360 – 1315 cm^{-1} due to the asymmetric stretching vibration of the SO_2 group (Socrates, 2001). Milling of the API, as discussed in section 3.2.2, resulted in a broadening of peaks consistent with a less ordered structure (Anderton, 2003). The extra shoulder peaks at 3414 cm^{-1} and 3471 cm^{-1} are likely due to a small fraction of non hydrogen bonded NH which is present in the amorphous material (Tang et al., 2002). The C=O stretch at 1695 cm^{-1} is the characteristic feature of the GA spectrum and its position is very sensitive to H bonding and its molecular environment. No peak shifts to either higher

or lower wavenumber were observed for this or any of the key peaks of SDM in the spectra for either the co-milled composite or the physical mixture.

The C=O stretch in milled MA, and also in the spectra of the physical mixture, exists as an intense band and is split into two peaks at 1700 cm^{-1} and 1740 cm^{-1} respectively, suggesting that there are two populations of interactions occurring with this functional group. The shoulder of the carbonyl band was no longer resolved following co-milling and a pronounced peak shift to 1729 cm^{-1} was observed. The free OH stretch in MA at 3523 cm^{-1} was much broader and at lower wavenumber for the co-milled composite compared to that present in the spectrum of the excipient or the physical mixture. This, in addition to differences in the $1440 - 1395\text{ cm}^{-1}$ and $960 - 880\text{ cm}^{-1}$ region where OH bending peaks occur, suggests interactions between the API and excipient.

The difference in the FTIR spectra for the SDM:GA and SDM:MA systems could be related to the additional hydroxyl group on the alkyl chain of MA, which should provide additional hydrogen bonding possibilities. It is conceivable that this networking of interactions and hydrogen bonding between the multiple functional groups available could immobilise the amorphous API and prevent its crystallisation. Kadoya et al. (2008) studied the effect of molecular interactions on amorphous binary solids involving amines and hydroxyl carboxylic acids and related this to their propensity for crystallisation. The authors noted that the length of the diacid alkyl chain had limited effects on the T_g of the mixtures but that the introduction of a hydroxyl group had a large effect on reducing component mobility. It should be noted however that amorphous MA could not be

analysed by FTIR owing to lack of physical stability and hence it was not possible to determine categorically whether shifts in peak position were due to interactions between SDM and MA or because of a crystalline to amorphous transition in the excipient.

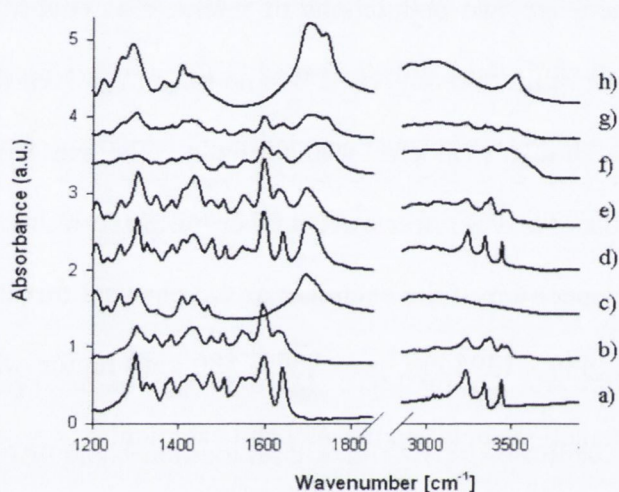


Figure 4.19 FTIR spectra of (a) SDM unprocessed; (b) milled SDM; (c) milled GA; (d) comilled SDM 50:GA50; (e) physical mixture SDM50:GA50; (f) comilled SDM 50:MA50; (g) physical mixture SDM50:MA50; and (h) milled MA.

4.11 Co-milling milled sulfadimidine with excipient

To investigate if the excipients were promoting crystallisation from an amorphous state, as opposed to physically shielding the API from the stresses of the milling operation, milled SDM was co-milled with 50% w/w milled GA and 50% w/w milled MA. Here the API and excipient were first milled separately. The milled API, now predominantly amorphous, was then co-milled with the milled excipient. The pXRD patterns are displayed in Figure 4.20 below.

When milled SDM was co-milled with milled GA (50% w/w), API crystallisation occurred, therefore eliminating the possibility that the excipient was exerting a protecting or shielding effect. Co-milling milled SDM with 50% w/w MA did not cause crystallisation of the API and indicates that the presence of seed crystals is not the likely mechanism behind the observed results.

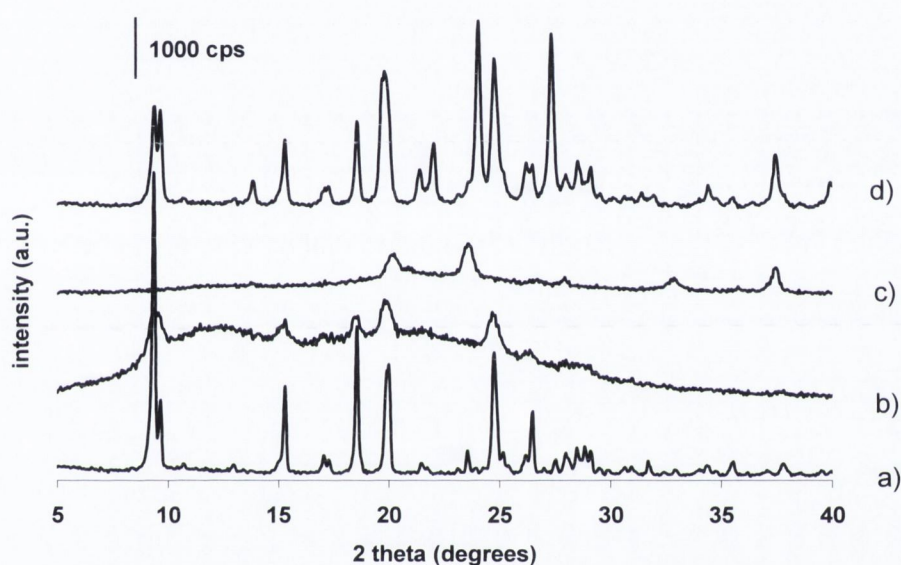


Figure 4.20 PXRD patterns of a) SDM unprocessed, b) SDM milled, c) milled SDM co-milled with milled MA (50% w/w), d) milled SDM co-milled with milled GA (50% w/w).

4.12 Solubility determination of glutaric acid and adipic acid in amorphous sulfadimidine by thermal analysis

Due to the effectiveness of GA and AA at reducing amorphisation of SDM on co-milling, their respective solubilities in the API were determined by thermal analysis, as described in section 2.2.14.1. A linear relationship was observed between the composition and the enthalpy of fusion in both cases and the solubility of the excipient in amorphous API was

estimated as the zero enthalpy interception point by extrapolation (Figure 4.21). The solubilities of crystalline GA and AA in amorphous SDM were determined to be 34% and 20%, respectively. The presence of a single T_g value intermediate to that of the API and excipient was taken as an indicator of a mixed system while a phase separated amorphous system will display two distinct T_g values. The melt miscibility of the SDM:GA and SDM:AA systems was confirmed by the presence of a single intermediate T_g value in the melt quenched samples. Solubility of SA in SDM could not be determined by this method due to significant mass loss (chemical degradation or sublimation) upon melting. In the case of MA, the excipient showed immiscibility with SDM during melt quenching experiments. SDM and MA also had the largest $\Delta\delta$ ($8.0 \text{ MPa}^{1/2}$).

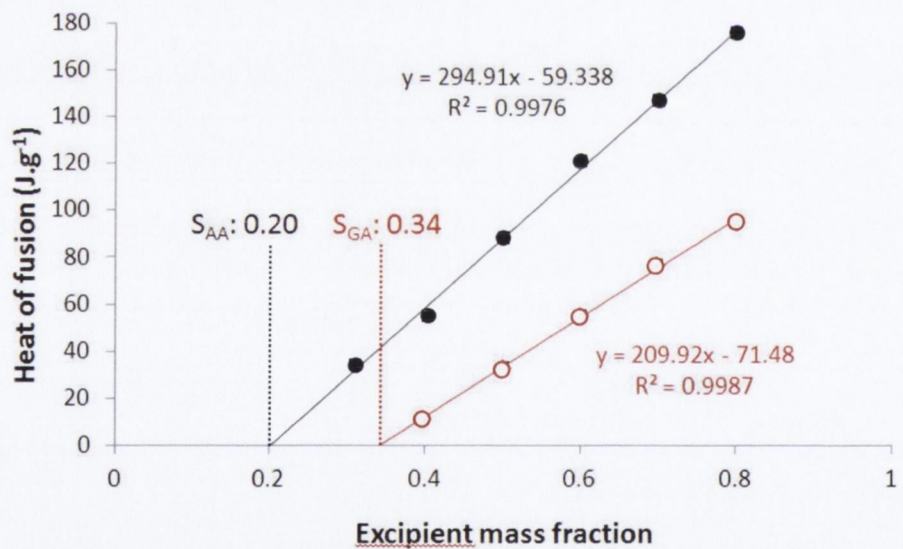


Figure 4.21 Plot of GA mass fraction (open symbols) and AA mass fraction (closed symbols) against heat of fusion determined by thermal analysis. S_{AA} and S_{GA} refer to the solubility of AA and GA in SDM respectively.

Figure 4.22 displays a plot of experimental Tg of melt quenched samples and % crystallinity of co-milled systems as quantified by DVS as a function of GA and AA mass fraction.

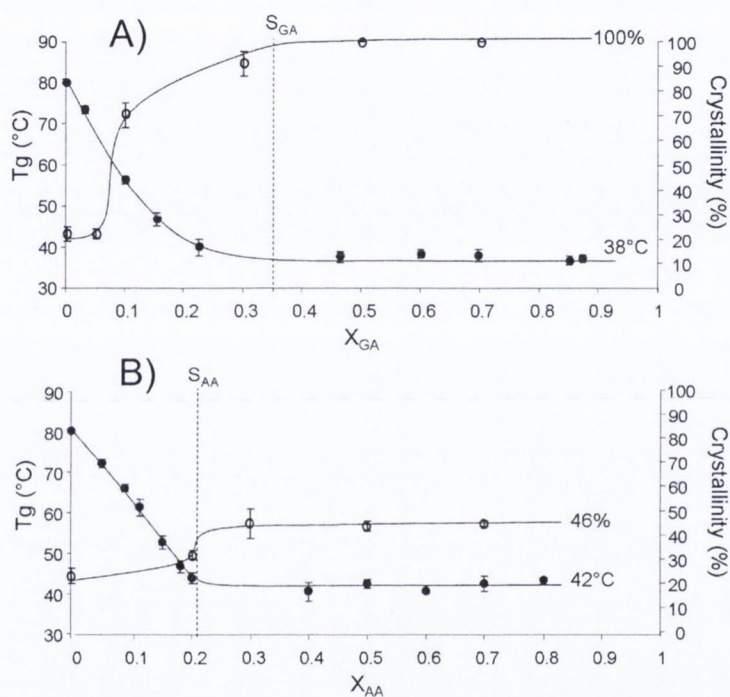


Figure 4.22 Plot of experimental Tg (closed symbols) of melt quenched samples and % crystallinity (open symbols) of co-milled systems as quantified by DVS as a function of A) GA mass fraction and B) AA mass fraction. S_{AA} and S_{GA} are the experimental solubilities of excipient in API.

At excipient weight fractions corresponding to S_{GA} , and just beyond S_{AA} , the crystallinity of the co-milled systems approached near maximum and then levelled off. Interestingly the co melt quenched systems, at S_{GA} and S_{AA} , had Tg minimum values of 38°C and 42°C respectively. Nevertheless co-milling SDM with GA was more effective at mitigating

amorphisation of the API. This suggests that additional factors, in addition to solubility and T_g, may have a role to play in the observed results. Trasi and Taylor (2012) recently investigated the effects of polymer additives on amorphous APIs and noted that effects on API mobility, as manifested by changes in T_g, could not fully explain changes in crystal growth rates. The authors suggested that interactions between the drug and additive, are very important in determining the extent of crystal growth inhibition. Differences in interaction strength in amorphous blends of SDM:AA and SDM:GA might explain the differences in results, despite the T_g being reduced to almost the same extent.

4.13 Budesonide co-milled with glutaric acid

Previous work demonstrated that BUD had a T_g of ~90°C and that the API could be completely amorphised when milled for 12 hours. The drug was co-milled with 50% w/w GA for 12 hours and the pXRD patterns obtained are displayed in Figure 4.23. The crystallinity of the API was markedly improved on co-milling with the excipient. The amorphous halo in the milled system was replaced by easily identifiable Bragg peaks corresponding to those of the API and the beta polymorph of the excipient. In contrast, no Bragg peaks were assignable to the API in the pXRD for the corresponding physical mixture with all peaks corresponding to β GA (Figure 4.23).

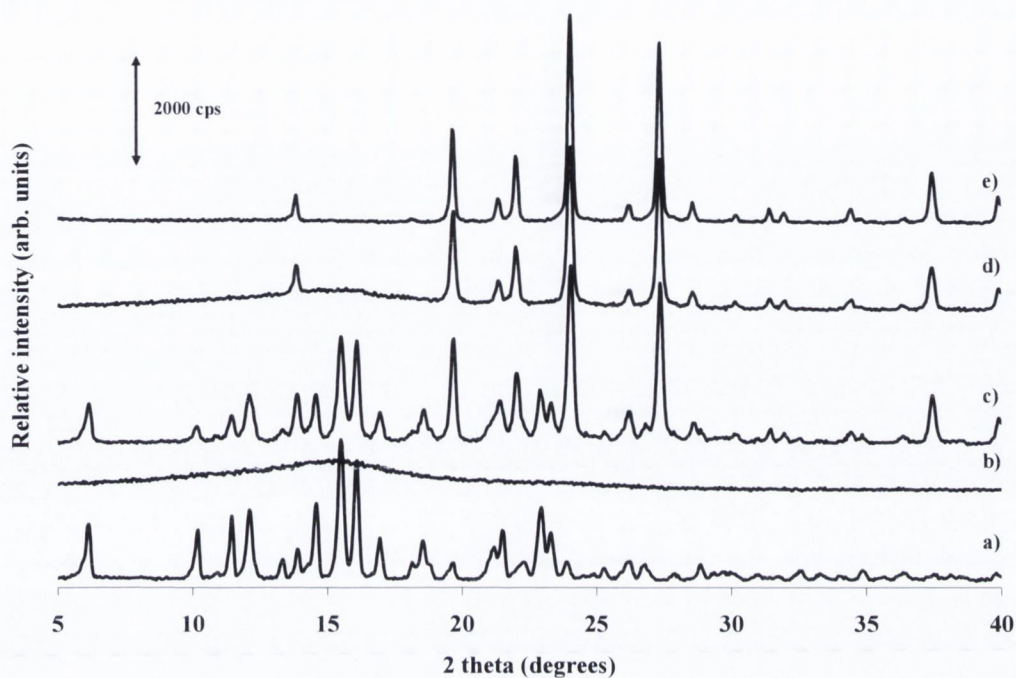


Figure 4.23 PXR D patterns of a) BUD unprocessed, b) BUD milled for 12 hours, c) BUD50:GA50 co-milled for 12 hours, d) BUD50:GA50 physical mixture, e) GA milled for 12 hours.

The corresponding DSC thermograms are displayed in Figure 4.24. Crystalline BUD melts at 248°C (chapter 3). The milled amorphous material crystallises via a two step process with a temperature onset of 108°C. As expected from the pXR D data, no crystallization exotherm was apparent in the thermogram for the co-milled system. The β to α transition in the excipient occurs at the same temperature in the co-milled system, as was observed for the excipient milled alone, but the melting onset of the excipient was depressed by 6°C. An exotherm was observed in the thermogram for the physical mixture, prior to the melting of the excipient, which is likely due to crystallisation of amorphous BUD. The melt of

BUD in the co-milled and physical mixture is obscured by the simultaneous degradation of the excipient at high temperatures.

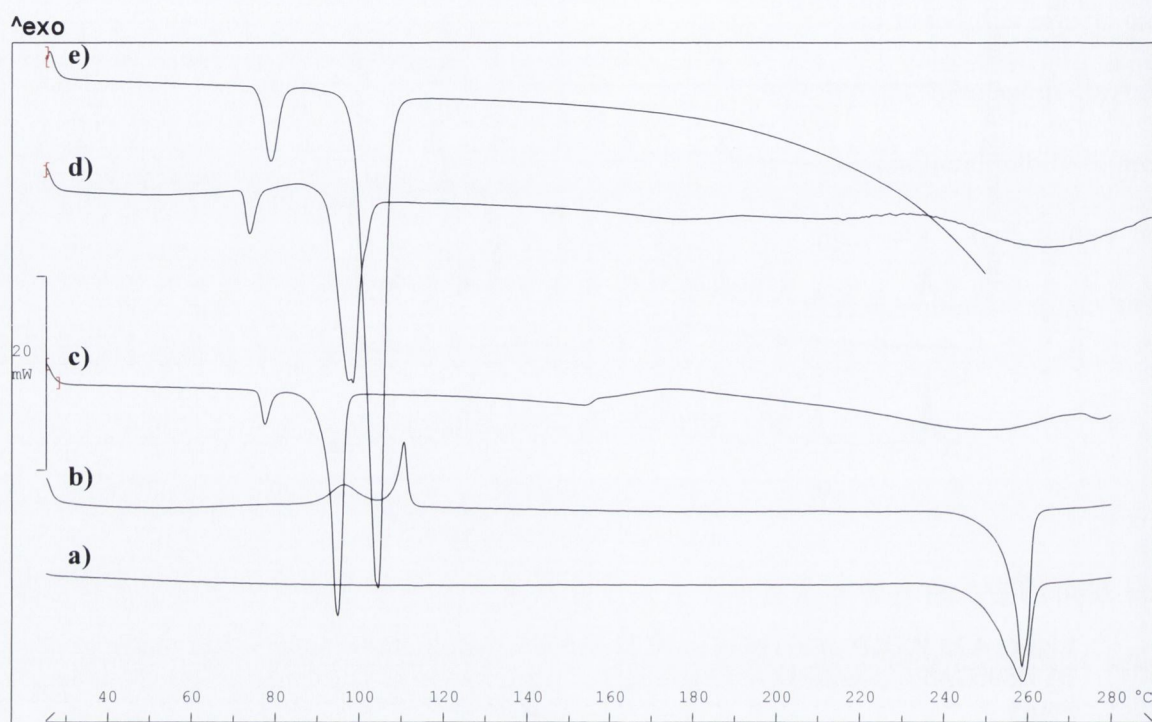


Figure 4.24 DSC thermograms of a) BUD unprocessed, b) BUD milled for 12 hours, c) BUD50:GA50 co-milled for 12 hours, d) BUD50:GA50 physical mixture, e) GA milled for 12 hours.

The amorphous content of BUD on co-milling with GA, as well as the API:excipient physical mixture, was determined by DVS. The milled drug was used as the 100% amorphous reference standard for quantification by DVS. A DVS isotherm plot of crystalline, milled, co-milled and physical mixture of BUD with 50% w/w GA is displayed in Figure 4.25. Comparing the % mass uptake difference between the first and second sorption cycles for the co-milled composite with that of the 100% crystalline and

amorphous standard, at 10% P/P₀, indicated that API amorphisation was eliminated in the composite system. API amorphous content in the physical mixture was 71 ±8%, again highlighting the impact that the actual process, compared to a physical mix of API and excipient, has on mitigating amorphisation of a milled drug.

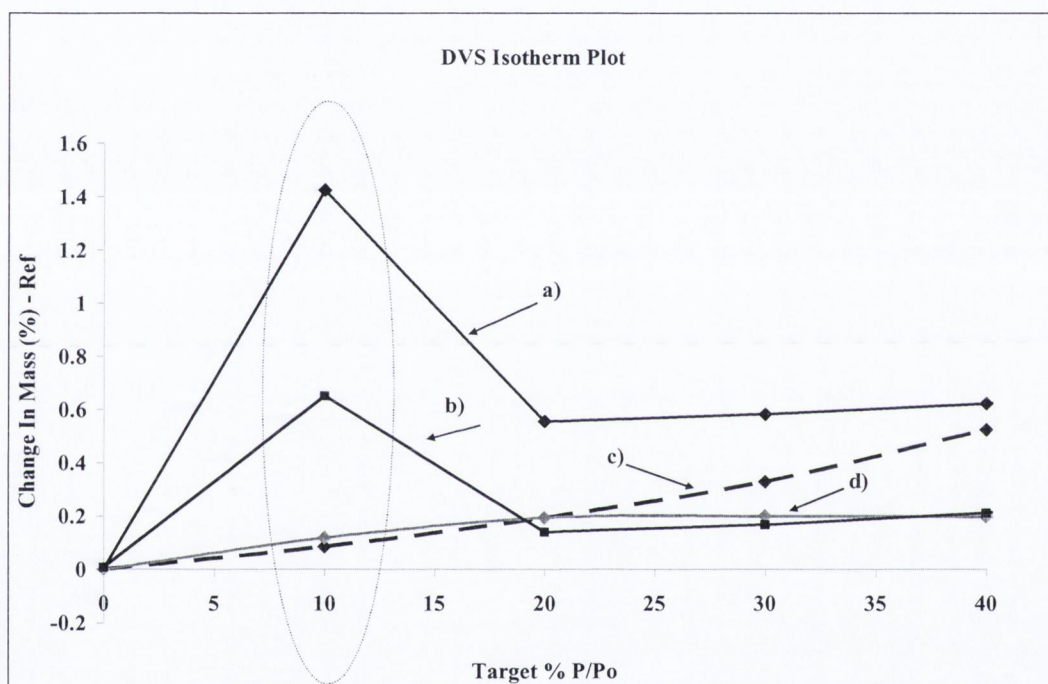


Figure 4.25 DVS isotherm plot of a) BUD milled for 12 hours, b) BUD50:GA50 physical mixture, c) BUD50:GA50 co-milled for 12 hours and c) crystalline BUD. Error bars are omitted for clarity.

The Hildebrand solubility parameter for BUD was calculated to be 25.9 MPa^{1/2} by Fedors group contribution method (Appendix III), and again was very similar to the value calculated for GA (25.8 MPa^{1/2}). Hence BUD and GA are likely to be soluble in each other

so that the low T_g of the excipient can be exploited to promote crystallisation of the amorphous API on co-milling.

4.14 Conclusion

We have shown that amorphisation of SDM and BUD could be completely eliminated following co-milling with 50% w/w GA. SDM was completely amorphised following co-milling with MA. These results could not be anticipated based solely on the fact that both excipients are crystalline and have low T_g values. The findings in this work show that excipients which have solubility parameters comparable to the API are more likely to exert a T_g lowering effect resulting in composite T_g values lower than that of the API alone, which can promote crystallisation from the amorphous state. We have shown, for the SDM:GA and SDM:AA systems, that at the solubility of excipient in amorphous API, the T_g of the co-melt quenched composites was at a minimum and the crystallinity of the respective co-milled systems at these concentrations of excipient were approaching near maximum.

Chapter 5

Reducing mechanical activation-induced amorphisation of salbutamol sulphate by co-processing with selected carboxylic acids

5.1 Introduction

It was previously demonstrated, in chapter 4, that co-milling SDM with a series of low T_g excipients was an effective strategy to minimise amorphisation of the drug. It was highlighted that excipients which showed good solubility in the API exerted a T_g lowering effect, resulting in composite T_g values lower than that of the API alone, which could mitigate amorphisation of the API. In contrast, a crystalline excipient (MA) which displayed very poor solubility in the API was found to promote amorphisation of the drug.

In this chapter we evaluate and compare, for the first time, the influence of milling and dry mixing on an API co-processed with low T_g excipients. SS was chosen because of its high glass transition temperature (120°C) and its propensity, as noted in chapter 3, to completely amorphise when milled for 2 hours or dry mixed with glass beads for 8 hours. The excipients chosen were GA, AA and PA, based on their low glass transition temperatures according to the $T_g = T_m \times 0.7$ rule (Fukuoka et al., 1989; Kerc and Srcic, 1995). The objective of the study was to see if co-processing SS with low T_g excipients, via two different modes of mechanical activation, could prevent or minimise amorphisation of the API.

5.2 Solubility determination of glutaric acid, adipic acid and pimelic acid in amorphous milled salbutamol sulphate

The solubilities of GA, AA and PA in the amorphous milled API at 25°C were determined by thermal analysis, as described in section 2.2.14.2. A linear relationship was observed between the composition and the enthalpy of fusion of the excipient for all three systems and the $Sol_{excipient}$ was estimated as the zero enthalpy interception point by extrapolation (Figure 5.1). The melting enthalpies of the pure excipients were omitted from the plot. This is because it is not appropriate to compare a system of ‘amorphous API and crystalline excipient’ where the endothermic peak represents a dissolution, to a system of ‘pure excipient’ where the endothermic peak is an actual melting event. Sol_{GA} , Sol_{AA} and Sol_{PA} were 35%, 21% and 22% respectively. It should be noted that the method of preparation of the mixtures of crystalline excipient and amorphous API saturated with excipient did not lead to drug degradation, as verified by HPLC (section 2.2.13).

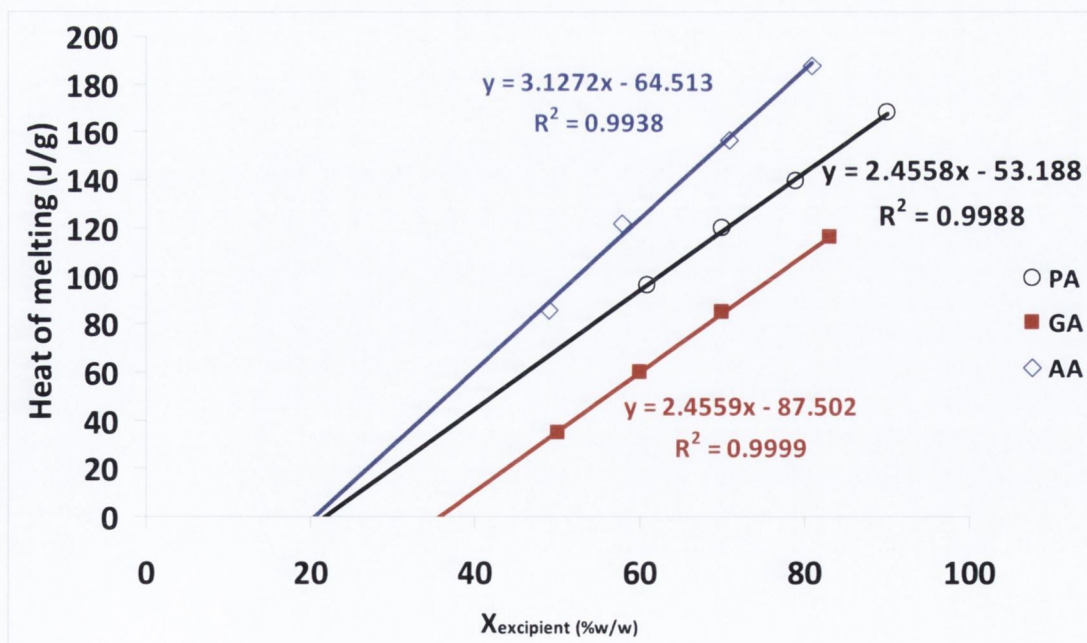


Figure 5.1 Plot of heat of melting versus AA mass fraction, PA mass fraction and GA mass fraction.

5.3 Salbutamol sulphate co-milled with glutaric acid

The pXRD patterns of SS raw material, SS milled for 2 hours and SS:GA co-milled composites are displayed in Figure 5.2. Milling was noted to completely amorphise the drug, as discussed previously in chapter 3. Co-milling with just 5% w/w GA, a concentration well below Sol_{GA} of 35%, resulted in an amorphous halo similar to that for the API milled alone. Processing at excipient concentrations close to, at, and above the Sol_{GA} revealed Bragg peaks specific to the API and indicated that the degree of amorphisation of SS was reduced.

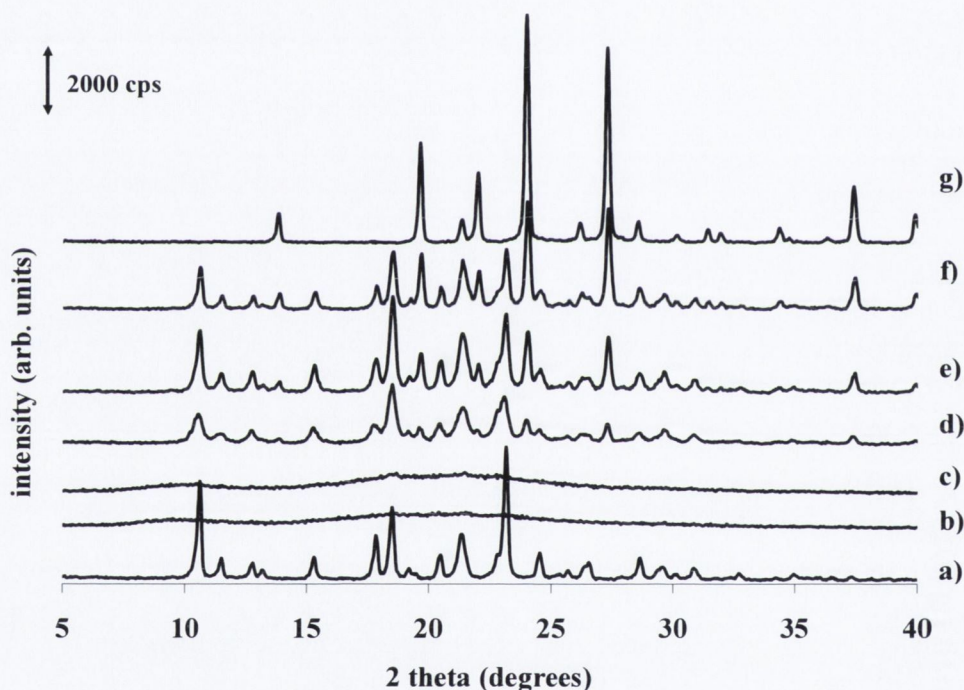


Figure 5.2 PXR D patterns of SS raw material, SS milled, GA milled and SS:GA co-milled composites. a) SS raw material, b) SS milled, c) SS95:GA5, d) SS80:GA20, e) SS 65:GA35, f) SS50:GA50, g) GA milled.

The DSC thermograms for SS raw material and the co-milled systems are displayed in Figure 5.3. An exotherm at around 125°C was observed for the SS95:GA5 co-milled system which was attributed to crystallisation of the amorphous API. No corresponding exothermic peak was present in the thermogram of the API milled

alone, suggesting that co-milling the drug with just 5% w/w GA generated a less thermally stable system than that of API milled on its own. No crystallisation exotherms were noted for the co-milled systems at higher weight fractions of excipient, as expected from the pXRD data. The thermal events between 70 – 105°C correspond to a polymorphic conversion in the excipient followed by its melting (McNamara et al., 2006). A melting endotherm at approx 90°C for all co-milled systems was noted and was at a lower temperature when compared to the melting of either the excipient (98°C) or drug (185°C). The melting of excess API at higher temperature is distorted by the simultaneous thermal degradation of the drug.

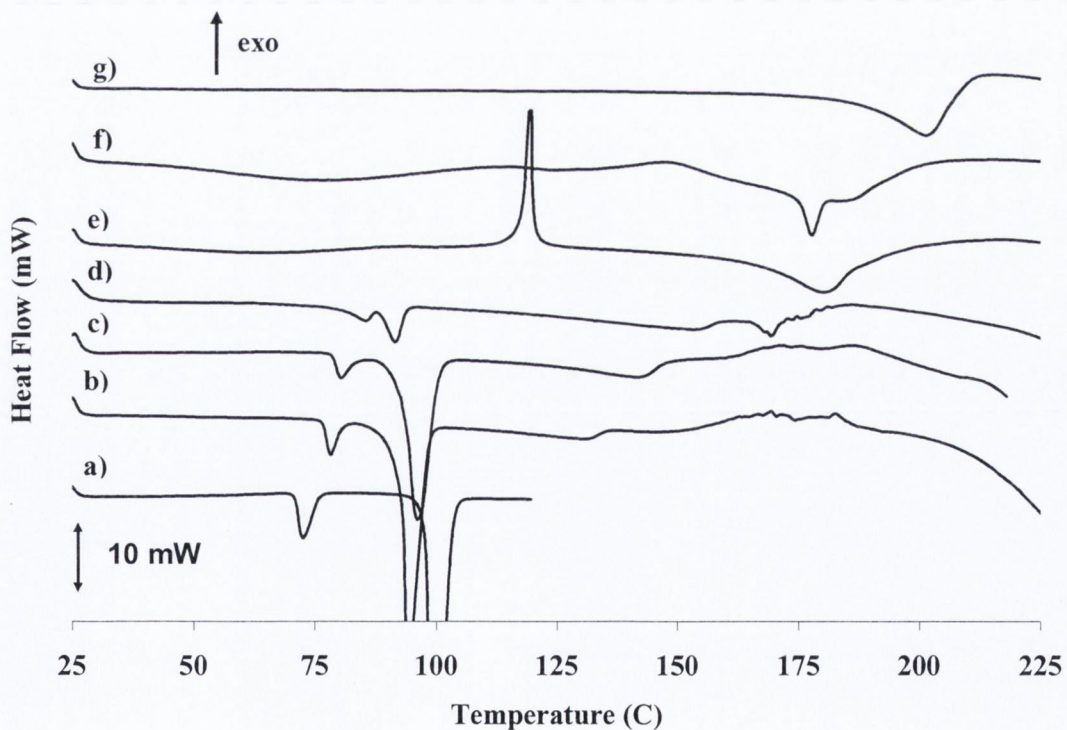


Figure 5.3 DSC thermograms of SS raw material, SS milled, GA milled and SS:GA co-milled composites. a) GA milled, b) SS50:GA50, c) SS65:GA35, d) SS80:GA20, e) SS95:GA5, f) SS milled, g) SS raw material.

DVS isotherm plots (with water as probe molecule) of SS milled as well as SS:GA co-milled composites are displayed in Figure 5.4. The SS95:GA5 system crystallised at a lower RH (between 40-50% RH) compared to the API milled alone (between 50-60%), indicative of a less physically stable system. The mass uptake at 40% RH was used in the quantification calculations and from Figure 5.4 it can be seen that uptakes were lower for the co-milled systems compared to the API milled alone. Amorphous content calculations were performed as described in section 2.2.11.

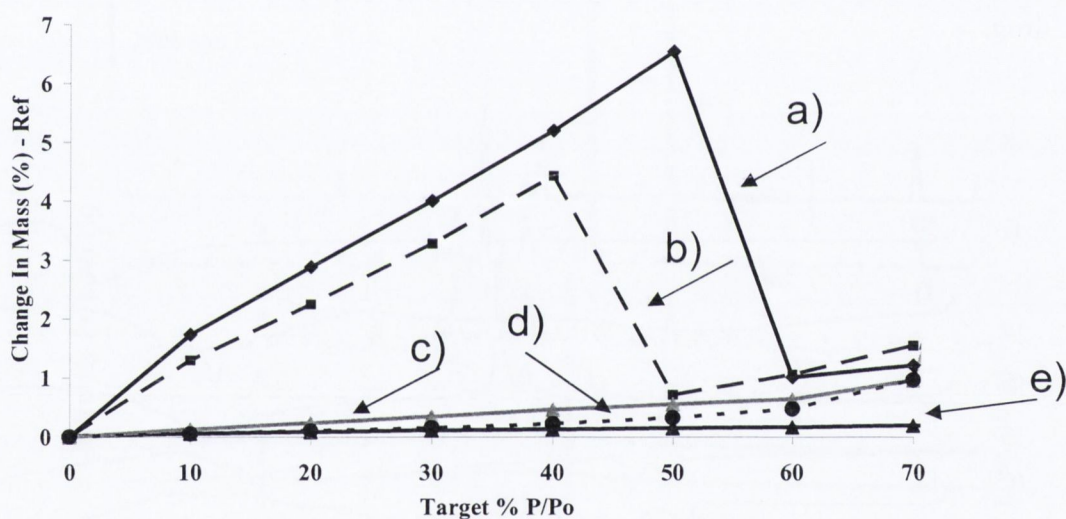


Figure 5.4 DVS Isotherm plots of SS milled and SS:GA co-milled composites. a) SS milled, b) SS95: GA5, c) SS80:GA20, d) SS65:GA35, e) SS50:GA50. Error bars are omitted for clarity.

PXRD was used as complementary quantification technique. The method of quantification was previously described in section 2.2.8.1. The calibration curve of peak intensity versus crystalline SS weight fraction (X_c) is displayed in Figure 5.5 and quantification results are listed in Table 5.1. The limit of detection was determined by the IUPAC method, as reported by Long and Winefordner (1983),

and corresponded to a crystalline weight fraction of 0.1. The limit of quantification was calculated, also by the IUPAC method, to be 0.18.

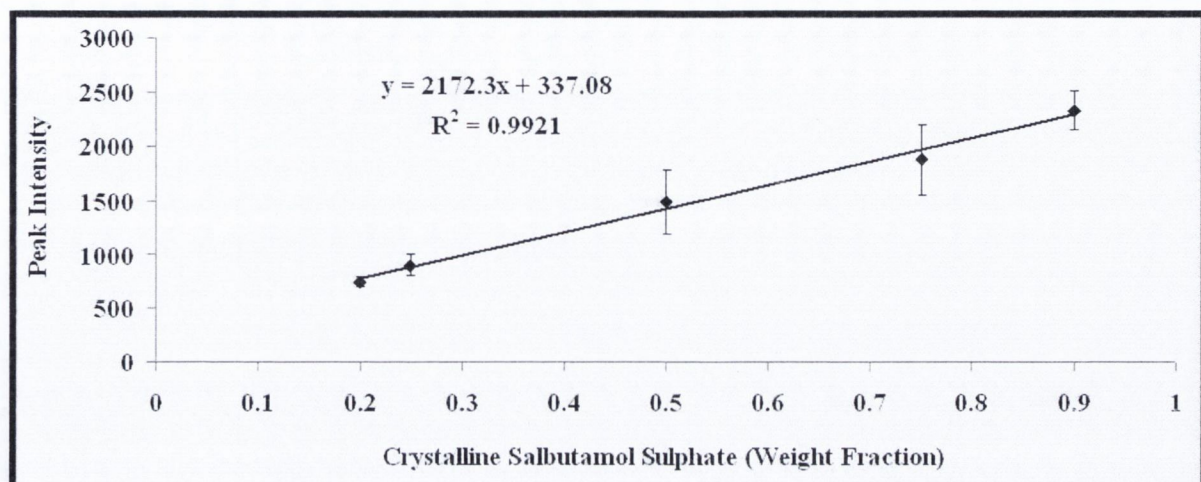


Figure 5.5 Calibration curve of peak intensity versus crystalline SS weight fraction

(X_c)

Table 5.1 Summary of amorphous content of SS raw material, SS milled and SS:GA co-milled systems as quantified by DVS and pXRD.

System	% Amorphous content (±S.D.)	
	DVS	pXRD
SS	4 (1)	0
SS milled	100	100
SS95:GA5	88 (3)	100
SS80:GA20	13 (6)	0
SS65:GA35	8 (4)	0
SS50:GA50	0	0

When comparing the two sets of quantification results by DVS and pXRD in Table 5.1, it should be acknowledged that, with pXRD it is difficult to detect amorphous content below 10%, whereas in the case of DVS, the detection limit is often lower

than 1% (Lehto et al., 2006). For instance, quantification results based on pXRD indicated that API amorphisation was eliminated on co-milling with just 20% w/w GA, in contrast to DVS which detected an amorphous content of 13%.

5.3.1 Physical mixture of milled salbutamol sulphate and milled glutaric acid

A physical mixture of milled SS and milled GA was prepared, as described in section 2.2.6, and the pXRD pattern obtained is displayed in Figure 5.6. All Bragg peaks corresponded to the excipient, which was taken as an indication that the API, in the physical mixture, was still amorphous. It is clear from the pXRD patterns that API crystallinity was higher in the co-milled system relative to the corresponding physical mixture.

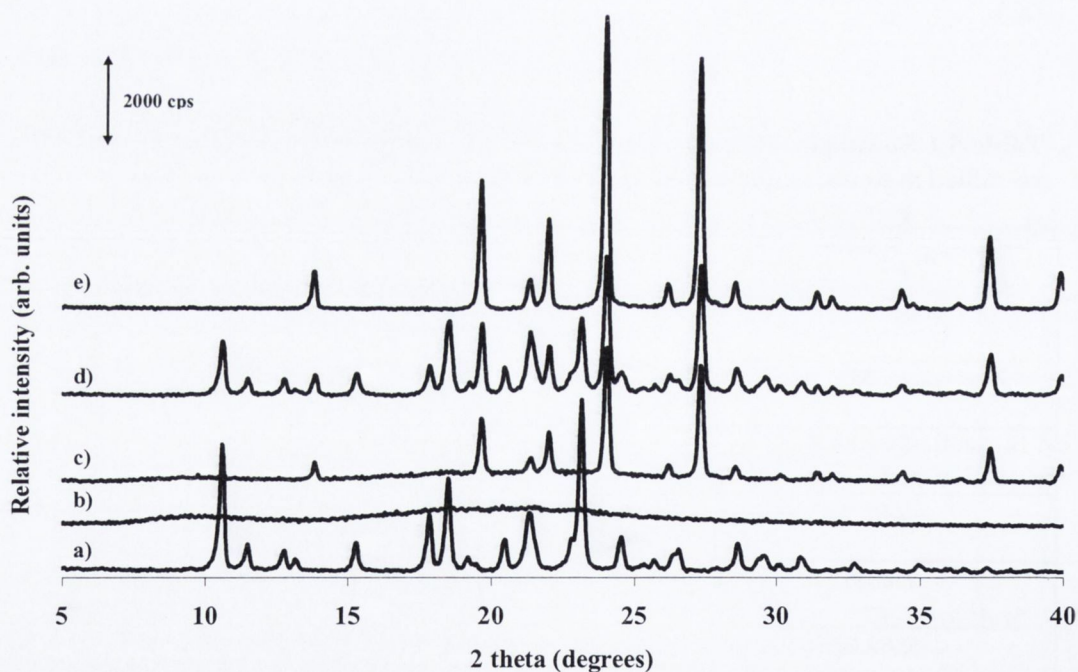


Figure 5.6 pXRD patterns of a) SS as received, b) SS milled for 2 hours, c) SS50:GA50 physical mixture, d) SS50:GA50 co-milled, e) GA milled for 2 hours.

The DVS kinetic profile for the physical mixture is displayed in Figure 5.7. Recrystallisation was observed to first occur at 50% RH, which was at a lower RH

compared to the API milled alone. Further mass losses were observed at 60% and 80% RH. The second cycle sorption behaviour was indicative of a crystalline material with no mass loss events evident. The difference in % mass uptake at 40% RH for the first and second sorption cycles was used in the quantification calculations. The % amorphous content of the API in the physical mixture was calculated to be 95% (n =2; 92, 98%). A very high API amorphous content was expected since the pXRD pattern of the physical mixture suggested the API was completely amorphous.

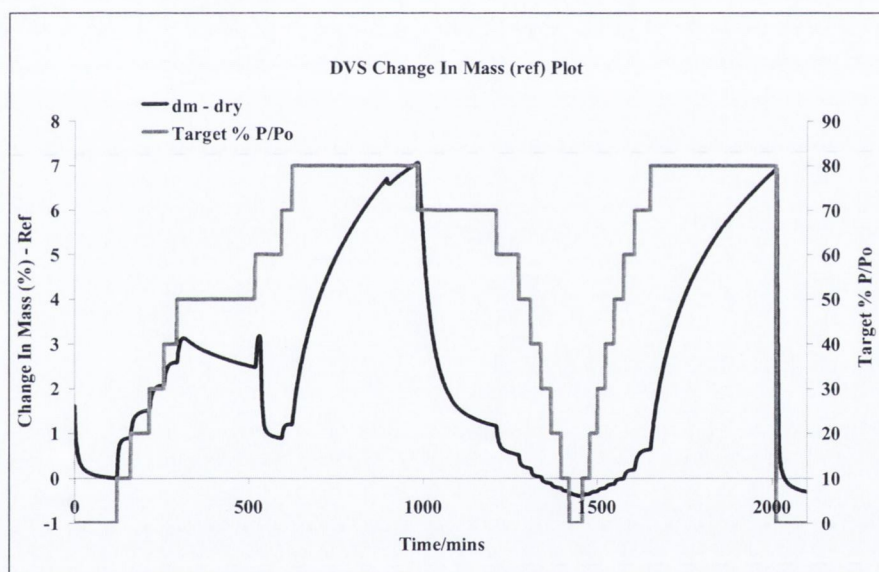


Figure 5.7 DVS kinetic profile for the SS50:GA50 physical mixture.

5.4 Pimelic acid

Pimelic acid (PA) is a pentanedicarboxylic acid reported to exhibit three different polymorphic forms, denoted as α , β , and λ (Ha et al., 2009). When compared to the pXRD patterns of the three modifications of PA (Burger et al., 1996; Ha et al., 2009), the unprocessed excipient and the milled excipient were identified as containing a mixture the α and β polymorphs (Figure 5.8a and b).

Thermal analysis by DSC of unprocessed PA, and PA milled for 2 h, revealed three solid-solid transformations (Figure 5.9). The first endothermic event occurred with a peak temperature onset of 55°C (observed under high magnification) for the milled excipient and at 86°C for the unprocessed excipient. In both cases, the thermal event was attributed to a $\beta - \alpha$ polymorphic transformation. The transformation was confirmed by heating the milled excipient to 70°C, and the unprocessed excipient to 95°C in the DSC (beyond the first endothermic peak in both cases), removing the material from the DSC and subsequently analysing it by pXRD. The patterns obtained in both cases were super-imposable and representative of the α form (Figure 5.8c). It was concluded that milling preferentially results in formation of the α polymorph, and any β PA which exists after milling converts to the α form at lower temperature. The second endotherm at ~97°C, in the DSC scans of both unprocessed and milled PA, was ascribed to the $\alpha - \lambda$ transition, and this final form melted at ~105°C. The three endothermic events, representing polymorphic transformation in PA, are consistent with the findings of Burger et al. (1996) and Ha et al. (2009). It should also be noted that PA could not be amorphised by either spray drying or by the melt quench method (Appendix IV). The T_g of PA was calculated to be -8°C by the T_g = T_m x 0.7 rule.

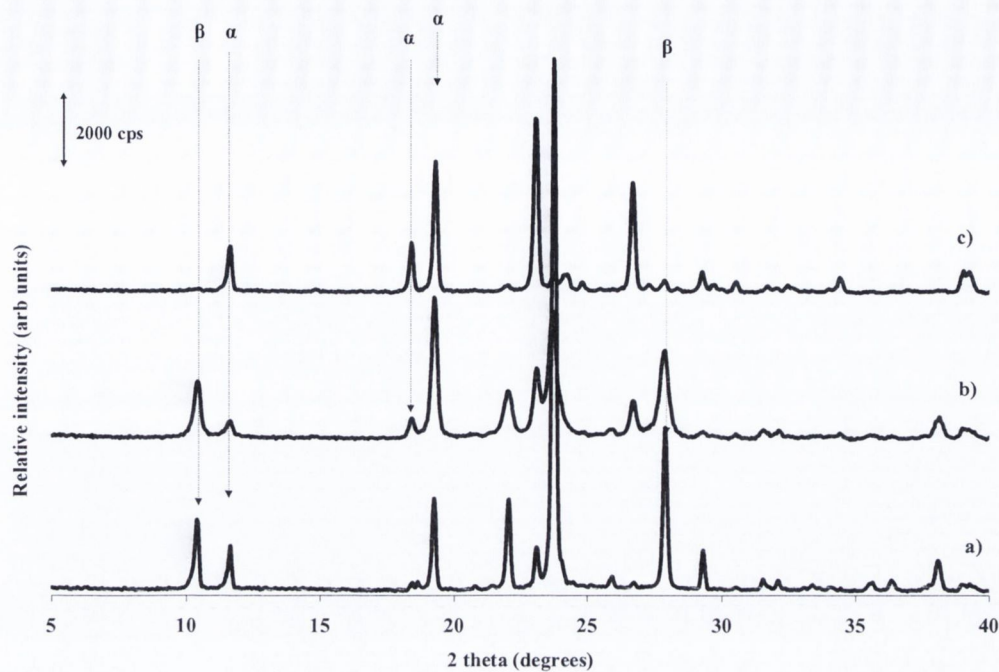


Figure 5.8 PXRD patterns of a) PA unprocessed, b) PA milled for 2 hours, c) PA after heating the unprocessed excipient to 95°C in the DSC and subsequently removing for analysis by pXRD. Highlighted are Bragg peaks characteristic of the α and β polymorphs of PA (Burger et al., 2006; Ha et al., 2009).

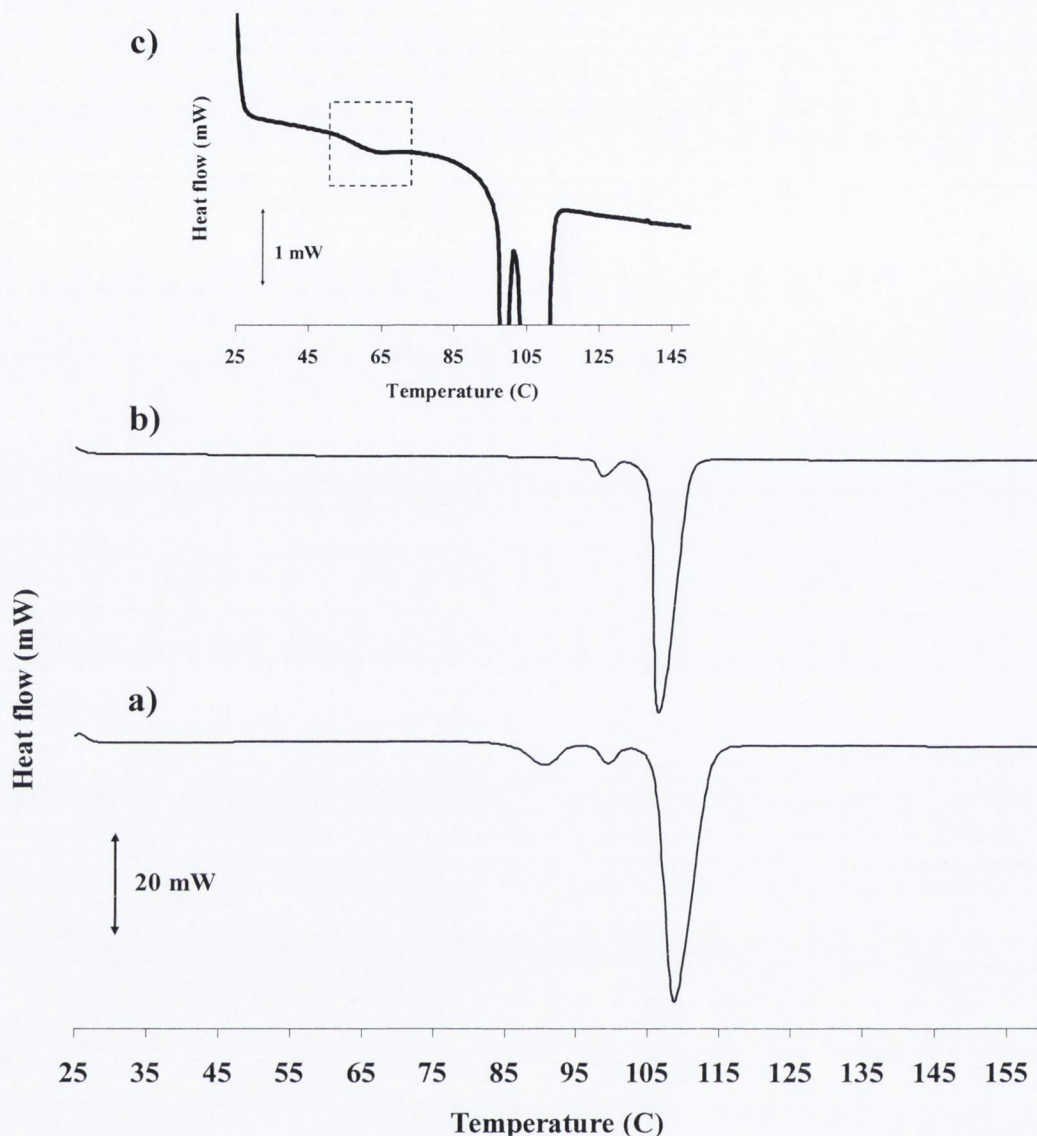


Figure 5.9 DSC scans of a) PA unprocessed, b) PA milled, c) PA milled, endotherm highlighted under magnification.

5.5 Salbutamol sulphate co-milled with adipic acid and pimelic acid

SS was co-milled at compositions corresponding to Sol_{AA} and Sol_{PA} (21% and 22% w/w), and above (50% w/w). The pXRD patterns of the co-milled systems are displayed in Figure 5.10 and the API amorphous content values, as quantified by DVS and pXRD, are displayed in Table 5.2. The presence of Bragg peaks in the co-milled systems, corresponding to the crystalline API, indicated that co-milling with

these excipients was effective at reducing the degree of amorphisation of the milled drug.

It was anticipated that maximal amorphisation reduction of SS on co-milling would be achieved at excipient weight fractions corresponding to Sol_{AA} and Sol_{PA} . This is because, at Sol_{AA} and Sol_{PA} , amorphous API produced during milling would be saturated with excipient, and these API:excipient composite systems therefore were expected to have the lowest possible composite T_g . However API amorphous content did change when $X_{excipient} > Sol_{PA}$ and Sol_{AA} , and as indicated in Table 5.2, a further amorphous content reduction of more than 15% was observed, in both cases, on co-milling with 50% w/w AA and PA. The purpose of using pXRD as a quantification technique in this study was to support the results of the analysis by DVS and demonstrate that the reduction in API amorphicity on co-milling at excipient weight fractions beyond $Sol_{excipient}$ could indeed be observed from an orthogonal method. Results from both DVS and pXRD illustrated that such a reduction in API amorphous content was observed (Table 5.2). Balani et al. (2010) previously co-milled SS with AA at different weight fractions of excipient and our quantification results by DVS are in agreement with the quantification results reported in that study. Moreover the authors noted an excipient concentration dependent effect on the amorphous content of the API on co-milling. A possible explanation is that the co-milling operation leads to amorphous SS, supersaturated with excipient, which conceptually could lead to a greater composite T_g reduction and promote further crystallisation from the amorphous state. The production of a supersaturated amorphous dispersion by co-milling was also extensively reported by Mahieu et al., (2013), Caron et al., (2007) and Willart et al., (2008).

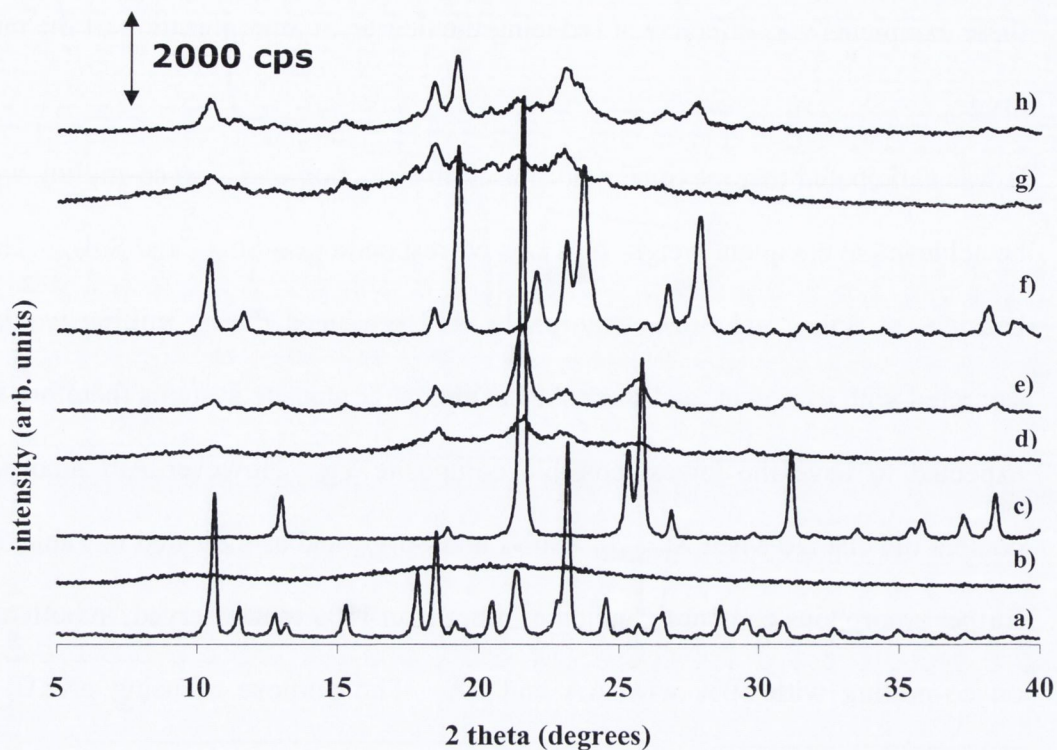


Figure 5.10 PXRD patterns of a) SS raw material, b) SS milled, c) AA milled, d) co-milled SS79:AA21, e) co-milled SS50:AA50, f) PA milled, g) co-milled SS78:PA22, h) co-milled SS50:PA50.

Table 5.2 Summary of amorphous content of SS:AA and SS:PA co-milled systems as quantified by DVS and pXRD.

System	% Amorphous content (\pm S.D.)	
	DVS	pXRD
SS79 : AA21	63 (2)	75 (7)
SS50 : AA50	46 (5)	62 (12)
SS78 : PA22	64 (2)	60 (15)
SS50 : PA50	42 (4)	48 (10)

5.5.1 Physical mixtures of milled salbutamol sulphate with milled adipic acid and with milled pimelic acid

Physical mixtures of milled SS with milled AA and with milled PA were prepared, as described previously in section 2.2.6. For SS:AA and SS:PA physical mixtures,

the API was amorphous with all Bragg peaks in the pXRD patterns assignable to those of the crystalline excipient (Figure 5.11). DVS kinetic profiles for the physical mixtures are presented in Figure 5.12. The SS:AA physical mixture underwent crystallisation at 60% RH, represented by a very sharp mass loss. In contrast, the SS:PA physical mixture commenced crystallisation at 50% RH. Therefore differences in % mass uptakes between sorption cycles at 50% RH for the SS:AA system and at 40% RH for the SS:PA system were used in the quantification calculations. The quantification results for SS:excipient physical mixtures are displayed in Table 5.3 and it can be seen that API amorphicity was not altered in the physical mixtures of the individually milled components, compared to the API milled alone.

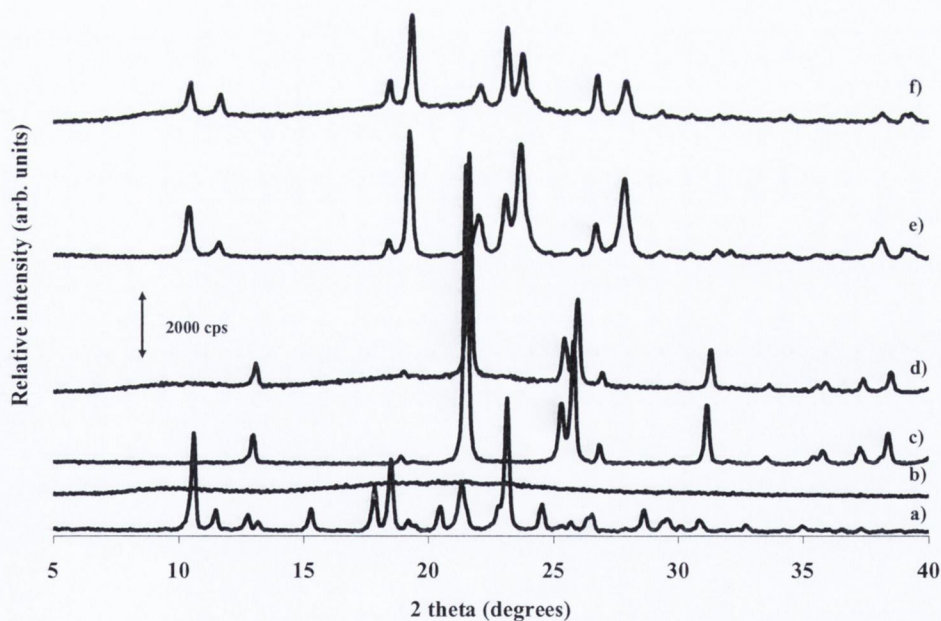


Figure 5.11 PXR D patterns of a) SS as received, b) SS milled for 2 hours, c) AA milled, d) SS50:AA50 physical mixture, e) PA milled, f) SS50:PA50 physical mixture.

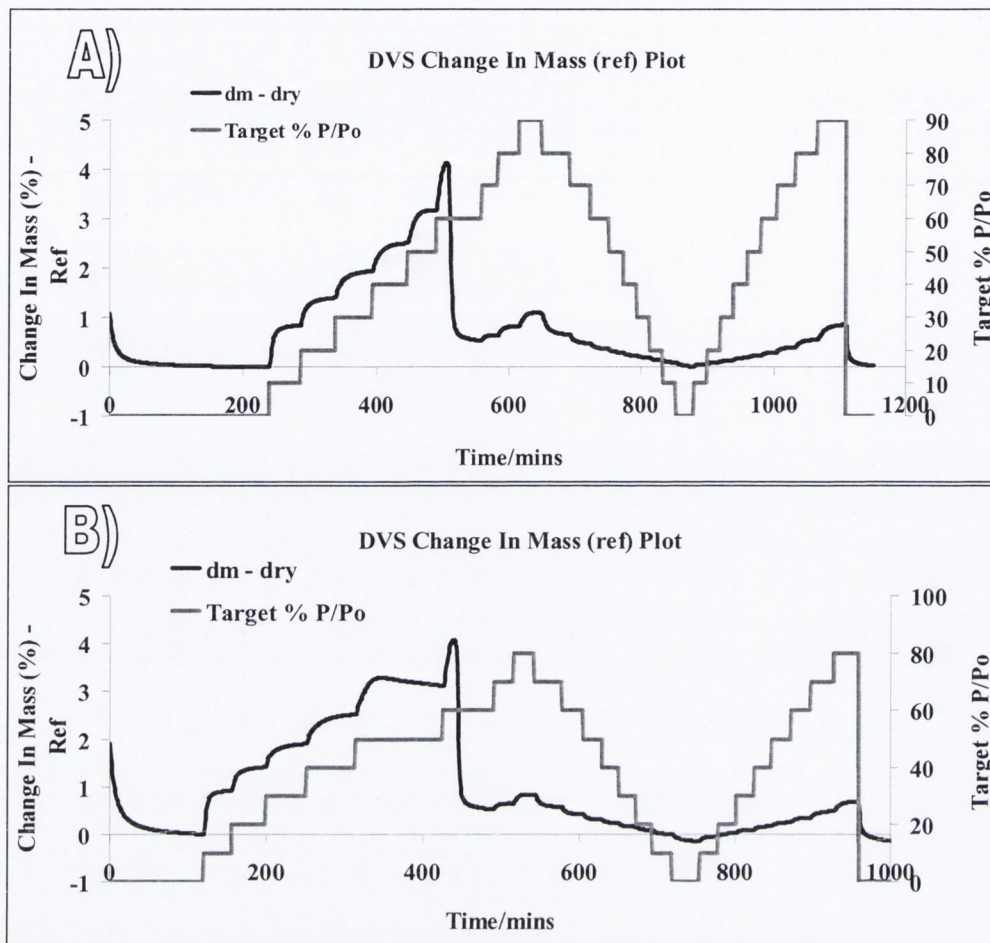


Figure 5.12 DVS kinetic profiles of A) SS50:AA50 physical mixture and B) SS50:PA physical mixture.

Table 5.3 Summary of amorphous content of SS:excipient physical mixtures as quantified by DVS.

System	% API amorphous content (range)
SS50:AA50 physical mixture	100.5 (97, 104)
SS50:PA50 physical mixture	92.5 (89, 96)
SS50:GA50 physical mixture	94 (90,98)

5.6 Salbutamol sulphate co-mixed with the dicarboxylic acids.

SS was co-mixed separately with the three dicarboxylic acids, at compositions corresponding to $Sol_{excipient}$ and for varying times. A plot of amorphous content

versus dry mixing time is shown in Figure 5.13. SS dry mixed was completely amorphous after 8 h, as discussed in Chapter 3. Co-mixing experiments were performed for as long as 24 h until a plateau was observed whereby no further changes in API amorphisation with mixing time were noted.

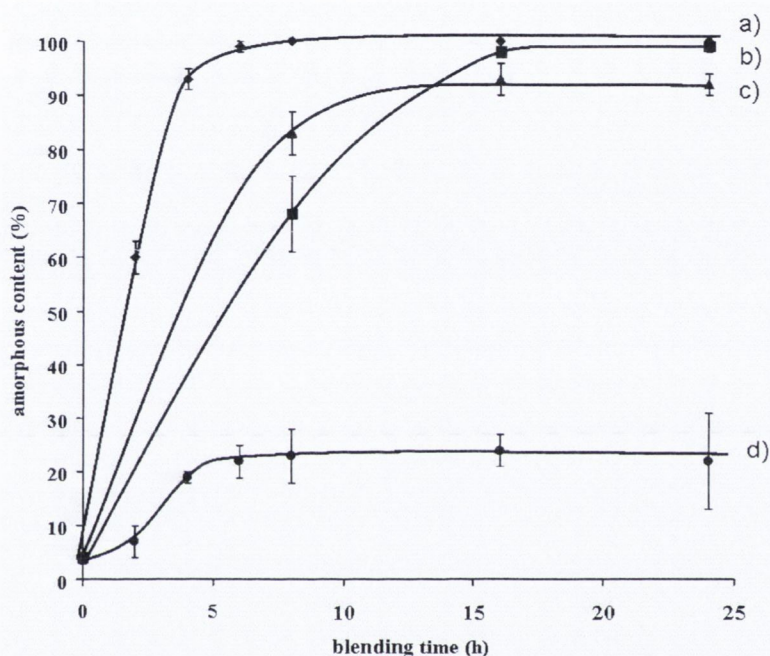


Figure 5.13 Plot of amorphous content (%) v mixing time (h) for SS dry mixed and SS:excipient co-mixed composites. a) SS dry mixed, b) SS:PA, c) SS:AA, d) SS:GA. The weight fraction of excipient corresponded to $Sol_{excipient}$.

API amorphous content of the co-mixed composites was quantified by DVS. The kinetic profiles for the SS:GA, SS:AA and SS:PA systems, after dry mixing for 24 h, are displayed in Figure 5.14 below.

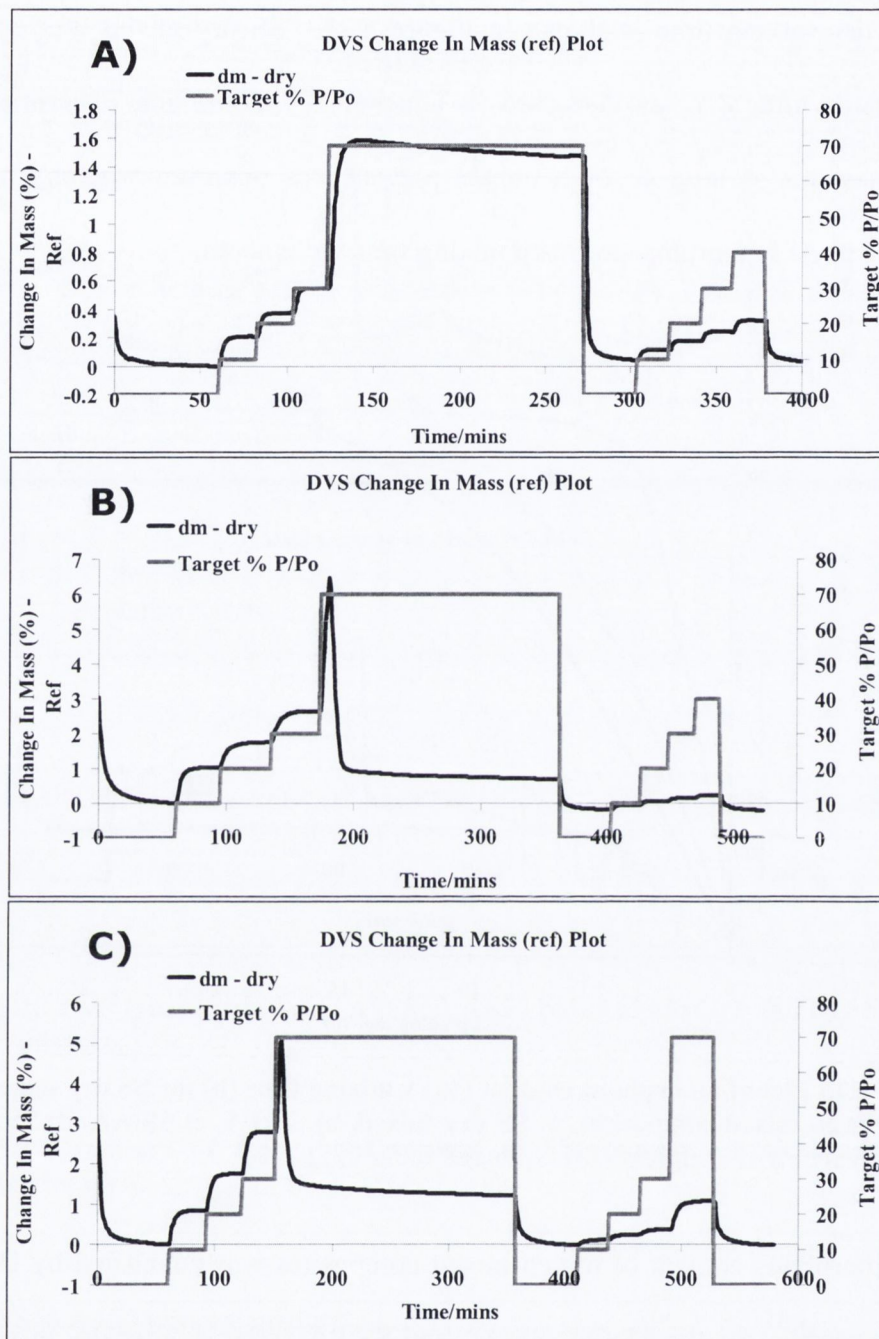


Figure 5.14 DVS kinetic profiles of SS:excipient co-mixed composites after mixing for 24 h. A) SS:GA, B) SS:AA, C) SS:PA. The weight fraction of excipient corresponded to $Sol_{excipient}$.

The mass loss at 70% RH during the first sorption cycle for the SS:GA dry mixed composite indicated that co-mixing did not completely eliminate amorphisation of the API. Mass uptakes and subsequent mass losses on crystallisation were higher for the SS:AA and SS:PA systems, compared to the SS:GA dry mixed system,

indicating these excipients were less effective at mitigating API amorphisation on co-milling. After 24 h, co-mixing SS with PA had a negligible effect on amorphisation of the API, co-mixing with AA lowered the amorphous content by $8 \pm 2\%$, whereas the co-mixed API composite with GA had an amorphous content reduction of more than 75%, relative to the API dry mixed alone. The quantification results indicated that GA was again the most effective excipient at mitigating API amorphisation on mechanical activation (Table 5.4).

The reduction of API amorphisation by co-mixing was, however, less pronounced when compared to the corresponding co-milled data. For instance co-milling SS with 35% w/w GA resulted in an API amorphous content of $8 \pm 4\%$, whereas an API amorphous content of $22 \pm 9\%$ was determined for the corresponding co-mixed system. For SS:AA composite systems, at Sol_{AA} , API amorphous content was determined to be $63 \pm 2\%$ following co-milling, compared to an amorphous content of $92 \pm 2\%$ on co-mixing. Again for SS:PA composite systems, at Sol_{PA} , API amorphous content was determined to be $63 \pm 2\%$ following co-milling, which was considerably lower compared to an API amorphous content of $100 \pm 5\%$ on co-mixing.

In order to assess whether a supersaturation effect occurred on co-mixing, as was proposed for co-milling, experiments were performed at excipient weight fractions of 50% w/w. No differences in API amorphous content on co-mixing at the two different concentrations of each excipient were noted (Table 5.4). Dry mixing is a much milder mechanical operation than milling and with less energy input the likelihood of obtaining a supersaturated state is less.

Table 5.4 Summary of amorphous content of SS:excipient co-mixed systems for 24 h, as quantified by DVS.

System	% API amorphous content (\pm S.D)
SS65:GA35	22 (9)
SS50:GA50	21 (4)
SS79:AA21	92 (2)
SS50:AA50	87 (4)
SS78:PA22	100 (5)
SS50:PA50	99 (1)

Amorphous SS, prepared by dry mixing, was then mixed with 35% w/w crystalline GA and samples were periodically removed over time and evaluated by pXRD. It was noted that Bragg peaks of excipient became less intense initially due to dissolution of the excipient in the amorphous API (Figure 5.15). No comparable reduction in Bragg peak intensity was noted when the excipient was dry mixed alone. After 3 h the system had recrystallised (Figure 5.15). It was therefore hypothesised that, upon mechanical activation, initial amorphisation of the API is preceded by dissolution of the excipient, which is solubility dependent, and acts to lower the composite T_g and promote crystallisation of the drug.

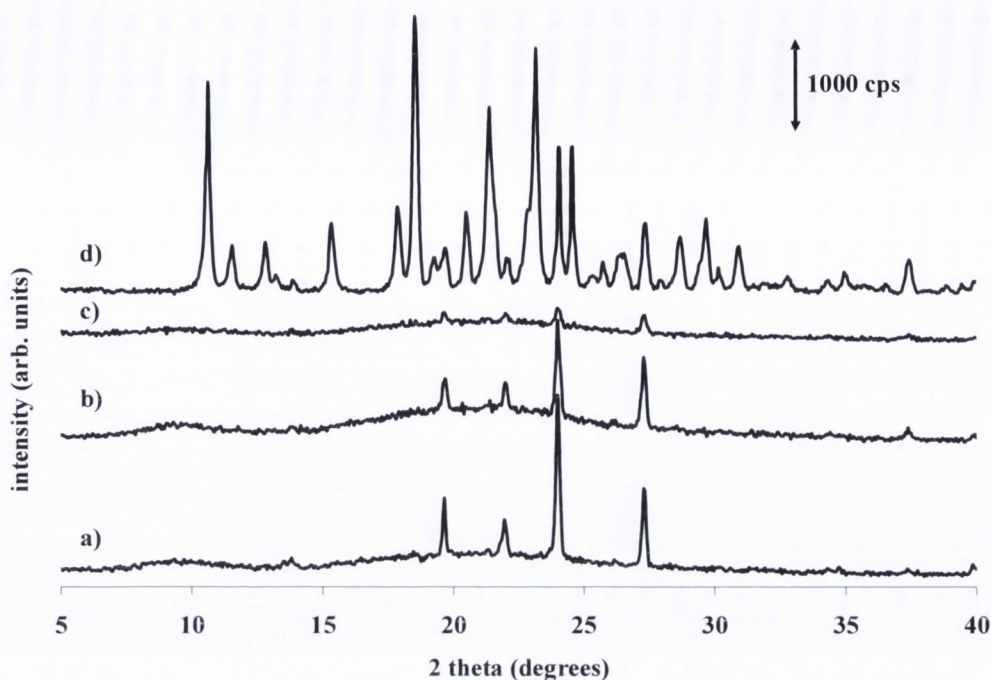


Figure 5.15 PXR D patterns of co-mixed composites of amorphous SS and crystalline GA. a) amorphous SS:GA at time 0, b) amorphous SS:GA at 1 h, c) amorphous SS:GA at 2 h, d) amorphous SS:GA at 3 h. The weight fraction of crystalline GA corresponded to Sol_{GA} .

5.7 Linking API crystallinity on co-milling to composite Tg lowering effect of excipient

If the dicarboxylic acids were indeed exerting a composite Tg lowering effect on co-milling, relative to the Tg of the amorphous API alone, then a Tg lowering effect would be observed for API:excipient amorphous systems. SS cannot be melted without degradation, therefore freeze drying was used to produce amorphous composites for each API:excipient system. Figure 5.16 displays a plot of experimental Tg of freeze dried samples and % crystallinity of co-milled systems as a function of GA weight fraction. With $X_{GA} < Sol_{GA}$ the composite systems were amorphous. With $X_{GA} > Sol_{GA}$ crystallinity associated with the excipient was observed. In accordance to what was reported in the study with SDM, the crystallinity of the SS:GA co-milled systems approached near maximum and then

levelled off at excipient weight fractions very close to Sol_{GA} . The freeze dried amorphous composites, at Sol_{GA} , had a T_g minimum value of 5°C . Amorphous composites at a composition corresponding to Sol_{GA} would be saturated with excipient and therefore exhibit the lowest possible composite T_g . Increasing the amount of excipient should have no further effect on the T_g and this is why the T_g curve flattens when $X_{GA} > Sol_{GA}$.

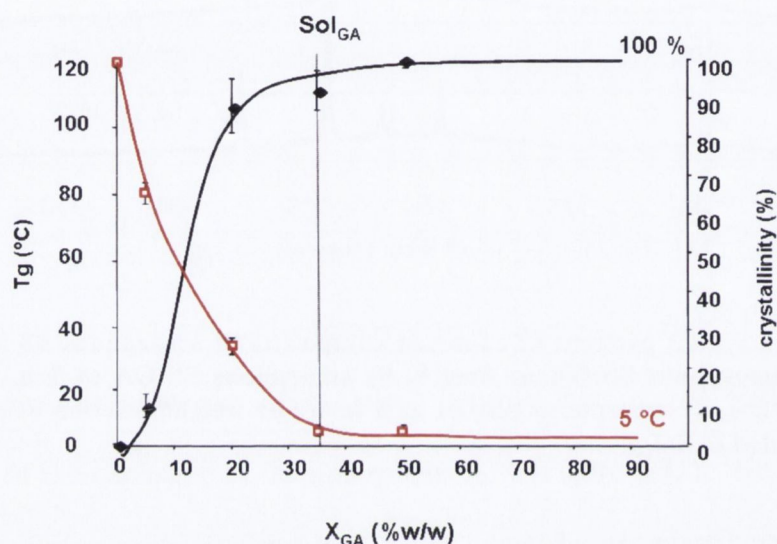


Figure 5.16 Plot of experimental T_g (open squares) of freeze dried samples and % crystallinity (closed triangles) of SS:GA co-milled systems. X_{GA} refers to the weight fraction of GA and Sol_{GA} is the solubility of GA in amorphous SS.

The identification of a single T_g value intermediate to that of the API and excipient was taken as an indicator of a mixed, single phase system (Qian et al., 2010). In contrast, a phase separated amorphous system will display two distinct T_g values. The detection limit for a second T_g will depend on the system under investigation and the experimental method employed. As GA, AA and PA are not amenable to amorphisation on their own, in this particular case phase separation of API and excipient in the amorphous state is unlikely. The miscibility of the SS:GA, SS:AA, and SS:PA systems were confirmed by the presence of a single T_g value in the freeze dried amorphous samples. At $Sol_{excipient}$, the SS:AA system had a T_g

minimum value of 34°C and the SS:PA system had a T_g minimum value of 31°C, respectively, indicating that only GA was capable of producing a composite with an intermediate T_g below that of room temperature (5°C). GA had the lowest calculated T_g value, it was the most soluble of the excipients in the API (35%), it produced the lowest composite T_g on freeze drying, and it proved to be the most effective excipient at mitigating amorphisation on both co-milling and co-mixing.

5.8 Conclusion

We have shown in this work that amorphisation of SS could be effectively eliminated on co-milling with 50% w/w GA, while it could be more than halved on co-milling with 50% w/w AA and PA. Dry mixing of SS with these low T_g excipients also resulted in a less disordered API, although the extent of reduction was less pronounced relative to the corresponding co-milled data. GA was the most effective excipient at mitigating API amorphisation on both mechanical co-processing techniques; it displayed the highest solubility of the excipients in the amorphous drug, and it exerted the most pronounced T_g lowering effect in the amorphous composites. The reduction in API amorphisation on co-mixing achieved at excipient concentrations corresponding to their solubility in the amorphous drug was the same compared to systems with 50% w/w excipient. In contrast, co-milling at the higher concentration of excipient produced a further reduction in API amorphisation. This is thought to be due to a supersaturation effect arising from the more energetic milling process, enabling more excipient to further lower the composite T_g, and promote crystallisation. We have shown that initial amorphisation of the API is preceded by dissolution of the excipient which induces a T_g lowering effect on the resultant composite and induces crystallisation of the

drug. Co-processing SS with low glass transition temperature dicarboxylic acids via two different modes of mechanical activation proved effective at mitigating amorphisation of the API.

Chapter 6

Co-milling and co-spray drying of
sulfadimidine:polyol and
sulfadimidine:diacid composites

6.1 Introduction

The co-processing of a drug with an excipient which has a low T_g, coupled with high solubility in the API, has been shown to be an effective strategy at mitigating amorphisation of the drug. Previous work has investigated the capacity of crystalline dicarboxylic acids to minimise amorphisation of SDM and SS by mechanical activation. In part 1 of this chapter we expand the excipients under investigation to the sugar alcohols or polyols. Mannitol (MAN) is a commonly used pharmaceutical excipient and it has a T_g below room temperature (13°C) (Caron et al., 2007). Xylitol (XYL) is a crystalline excipient with a documented T_g of -23°C (Carpentier et al., 2003). Both of these low T_g sugar alcohols were co-milled with SDM in order to assess and evaluate whether the degree of amorphisation of the API was lowered relative to the drug milled alone. Part 2 of this chapter examines the effect of co-processing SDM with MAN and with the dicarboxylic acids (GA, AA, SA) by another common unit process – spray drying. The objective was to investigate if co-spray drying the API with these low T_g excipients could help prevent amorphisation of the drug.

6.2 Sulfadimidine and mannitol co-milled composites

6.2.1 Mannitol

MAN exists in at least three polymorphic forms, termed α , β and δ . The β form is the most thermodynamically stable at room temperature (Burger et al., 2000). MAN unprocessed was identified as the β form by pXRD, with characteristic peaks occurring at 10.5 and 14.8 2θ (Hulse et al., 2009). Complete transformation from the stable β form to the metastable α form occurred after 10 hours of milling. Characteristic Bragg peaks of the α form were identified at 9.5 and 13.7 2θ (Hulse et al., 2009).

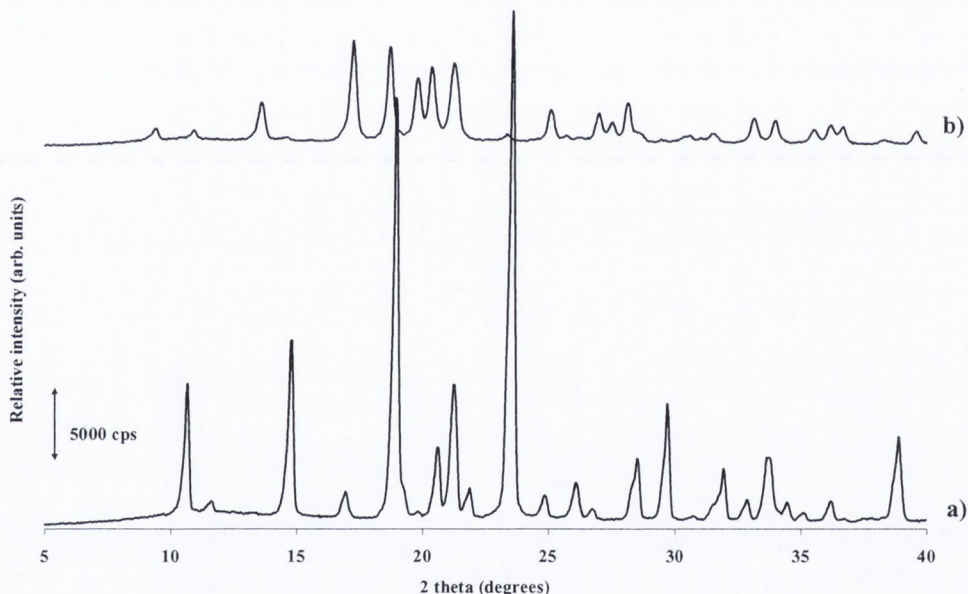


Figure 6.1 pXRD patterns of a) MAN unprocessed, b) MAN milled for 10 hours.

Thermal analysis of both unprocessed MAN (β) and MAN milled for 10 hours (α) showed a single endothermic peak with a temperature onset of 167°C (Figure 6.2). The two solid state forms were indistinguishable with respect to their melting temperatures, consistent with that reported by Burger et al., (2000). The T_g of the excipient was confirmed to be 13°C by the melt quench method, with MAN crystallising via a two step process at 23°C and 58°C (Figure 6.2).

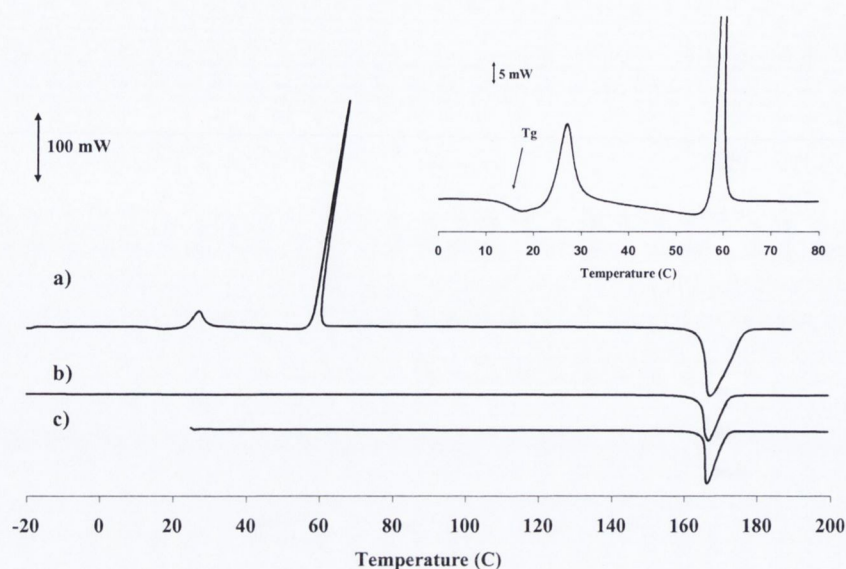


Figure 6.2 DSC thermograms of a) melt quench MAN, b) MAN milled for 10 hours, c) MAN unprocessed. The inset illustrates the Tg of melt quenched MAN and the two step crystallisation process.

FTIR spectroscopy is a useful tool to provide a fingerprint identification of the different polymorphs of MAN (Burger et al., 2000). Their different packing arrangements give rise to different intermolecular interactions and orientation of bonds, thereby producing different vibrational and stretching frequencies. In particular, significant differences are known to occur in the region of $3700\text{-}2500\text{ cm}^{-1}$ where O-H and C-H vibrations occur (Burger et al., 2000). Table 6.1 displays selected FTIR bands obtained for the unprocessed excipient, and the excipient after 10 hours of milling. The spectra were consistent with those quoted by Burger et al. (2010) and with the original classification by Walter Levy (1968).

Table 6.1 Spectroscopic comparison of characteristic stretching vibrations for unprocessed MAN, milled MAN for 10 hours and those of the Burger classification.

Burger classification		Experimental results	
β	α	MAN 'as received'	MAN after 10 hr mill
1210	1196	1210	1197
1081	1085	1080	1080
1019	1020	1019	1020
959	953	959	953
930	927	929	927
514	519	Not detected	Not detected

6.2.2 Solubility determination of mannitol in amorphous sulfadimidine

The solubility of MAN in amorphous SDM was determined by thermal analysis, as described in section 2.2.14.1. A linear relationship was observed between the composition and the enthalpy of fusion of the excipient and the $Sol_{excipient}$ was estimated as the zero enthalpy interception point by extrapolation (Figure 6.3). Sol_{MAN} was determined to be 4% w/w.

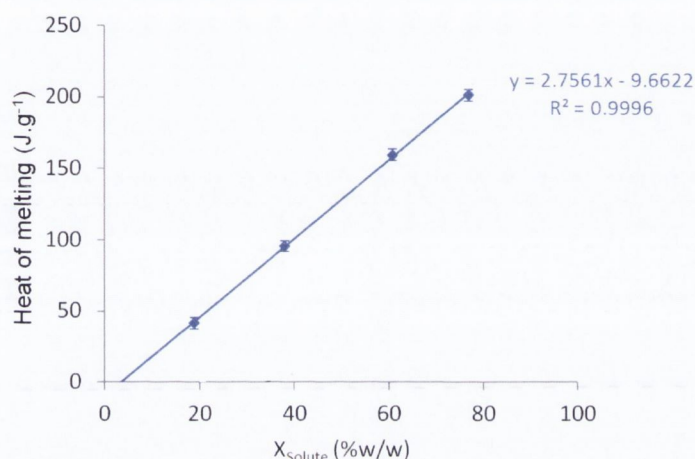


Figure 6.3 Plot of heat of melting versus MAN weight fraction (X_{solute}).

6.2.2.1 Hildebrand Solubility Parameter

The Hildebrand solubility parameter for MAN was determined by Fedors group contribution method, as described in section 2.2.14.3. The value obtained was $38.2 \text{ MPa}^{1/2}$, which is more than 12 units higher than the calculated solubility parameter for SDM ($25.7 \text{ MPa}^{1/2}$). Greenhalgh et al., (1999) identified a link between immiscibility problems in binary systems and differences in the solubility parameters and noted that a difference of $10 \text{ MPa}^{1/2}$ or greater between two components was a likely indicator of immiscibility.

6.2.3 PXRD and thermal analysis of sulfadimidine:mannitol co-milled composites

SDM and MAN were co-milled together for 10 hours at room temperature using different weight fractions of excipient. This ranged from a composition corresponding to the solubility of MAN in amorphous SDM (4%), up to 80% w/w excipient. The pXRD patterns for the co-milled systems are displayed in Figure 6.4. Characteristic Bragg peaks of SDM, at 9.6, 15.1 and 24.9 2 theta, and highlighted in Figure 6.4, became less intense with increasing amounts of excipient in the co-milled composites. This was taken as an indicator that amorphisation of SDM was promoted on co-milling with MAN. Bragg peaks of α and β MAN are evident in the patterns for the co-milled systems.

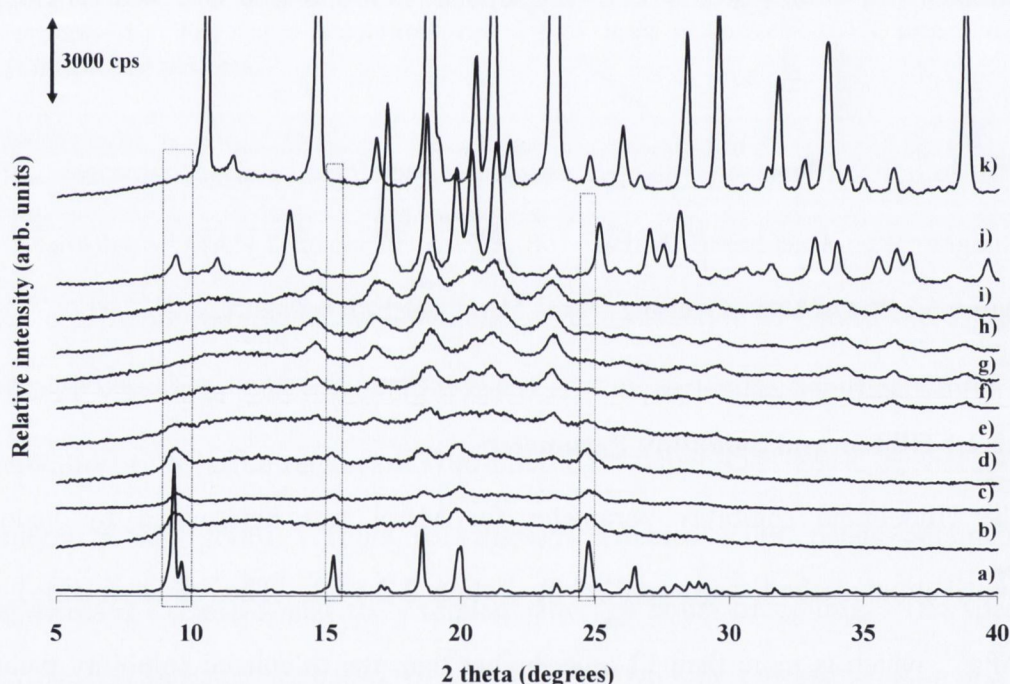


Figure 6.4 PXRD patterns of a) SDM unprocessed, b) SDM milled for 10 hours, c) SDM96:MAN4 co-milled, d) SDM90:MAN10 co-milled, e) SDM80:MAN20 co-milled, f) SDM60:MAN40 co-milled, g) SDM50:MAN50 co-milled, h) SDM40:MAN60 co-milled, i) SDM20:MAN80 co-milled, j) α MAN, k) β MAN. Characteristic peaks at 9.6, 15.1 and 24.9 2 theta of crystalline SDM are highlighted.

DSC thermograms of milled SDM and SDM:MAN co-milled systems are displayed in Figure 6.5. It can be observed that as the composition of MAN increased, the

recrystallisation exotherm of milled SDM was progressively shifted to higher temperature. This indicates a more thermally stable amorphous phase.

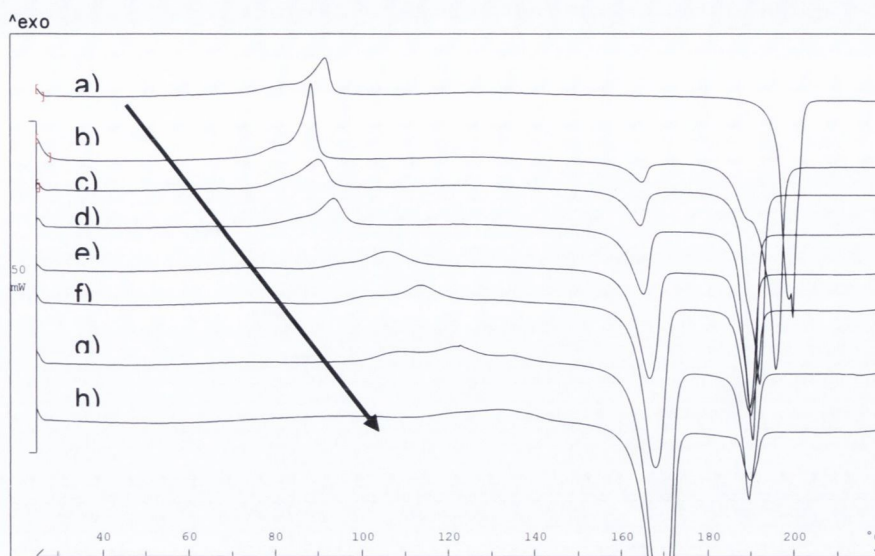


Figure 6.5 DSC thermograms of a) SDM milled for 10 hours, b) SDM96:MAN4 co-milled, c) SDM90:MAN10 co-milled, d) SDM80:MAN20 co-milled, e) SDM60:MAN40 co-milled, f) SDM50:MAN50 co-milled, g) SDM40:MAN60 co-milled, h) SDM20:MAN80 co-milled.

The melting endotherms for both MAN and SDM in the co-milled composites were shifted by about 4°C and 11°C, respectively, to lower temperatures relative to the pure, individual components milled alone. The melting onset temperature depression was observed initially at a composition of 4% w/w MAN (weight fraction corresponding to its solubility in the API), and remained constant thereafter, irrespective of the excipient weight fraction. This could reflect the limited solubility of MAN in SDM, as determined earlier to be 4%.

The T_g values of the composite systems could not be determined using conventional DSC, as the step change in heat capacity was masked by the exothermic crystallisation peak. Hence MTDSC was performed on the systems (section 2.2.7.2), and the reversing heat flow signals are displayed in Figure 6.6. The T_g of SDM milled alone was identified at 77°C. A single T_g , in the temperature range of 75-79°C was observed for the co-milled systems. The fact that the T_g did not shift to lower temperature in the co-

milled systems, despite the low T_g of the excipient, was not surprising considering the very low solubility of the excipient in amorphous SDM (4%). No T_g close to the value of amorphous MAN (13°C) was apparent. If MAN was amorphous, but had phase separated from the amorphous drug, then a T_g around 13°C would have been observed for the amorphous excipient. Amorphous MAN is known to be very unstable and displays a strong tendency to crystallise (Yu, 2001).

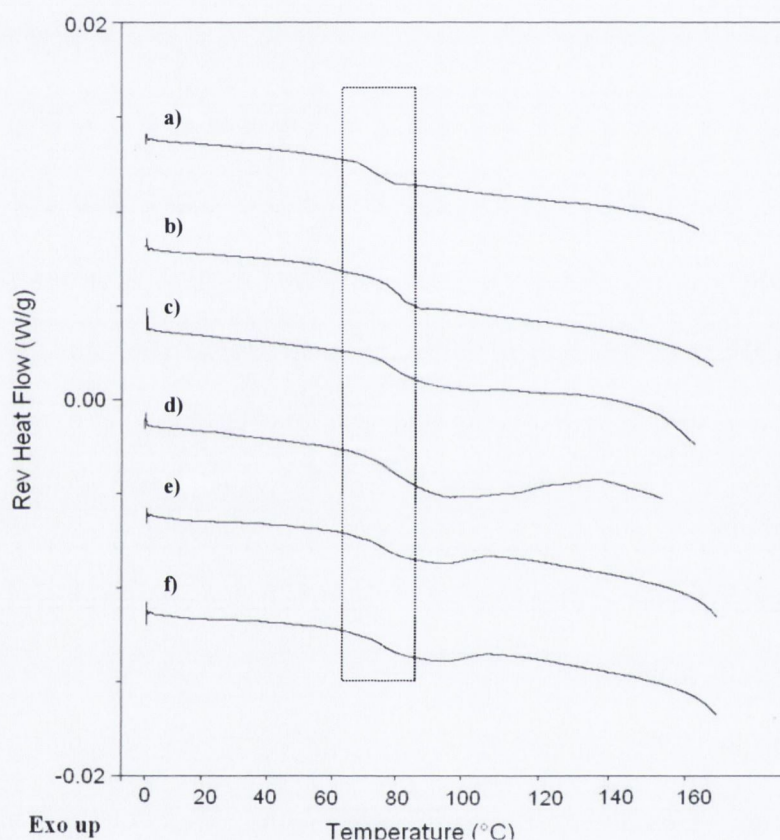


Figure 6.6 Reversing heat flow signals for a) SDM milled, b) SDM96:MAN4 co-milled, c) SDM90:MAN10 co-milled, d) SDM80:MAN20 co-milled, e) SDM60:MAN40 co-milled, f) SDM50:MAN50 co-milled.

6.2.4 Physical mixture of milled sulfadimidine and milled mannitol

A physical mixture of milled SDM and milled MAN (50:50 w/w) was prepared in order to evaluate the effect of the milling process, compared to a physical mix of the individually milled components, on the final solid state form of the drug. The

recrystallisation exotherm for SDM was shifted by 27°C to higher temperature for the co-milled system compared to the corresponding physical mixture (Figure 6.7). Moreover the pXRD pattern for the co-milled system displayed a more diffuse halo pattern, with the characteristic Bragg peak of the crystalline API more pronounced in the pattern for the physical mixture (highlighted in Figure 6.8).

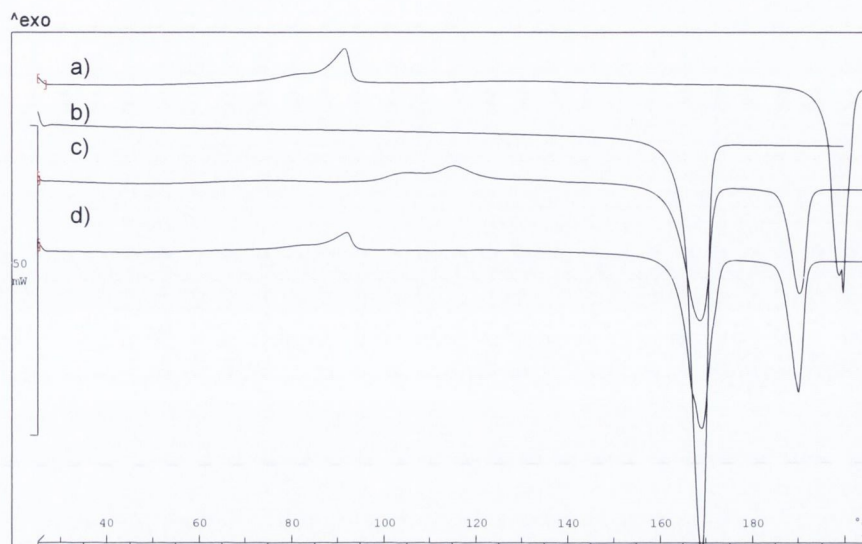


Figure 6.7 DSC scans of a) SDM milled for 10 hours, b) MAN milled 10 hours, c) SDM50:MAN50 co-milled, d) SDM50:MAN50 physical mixture.

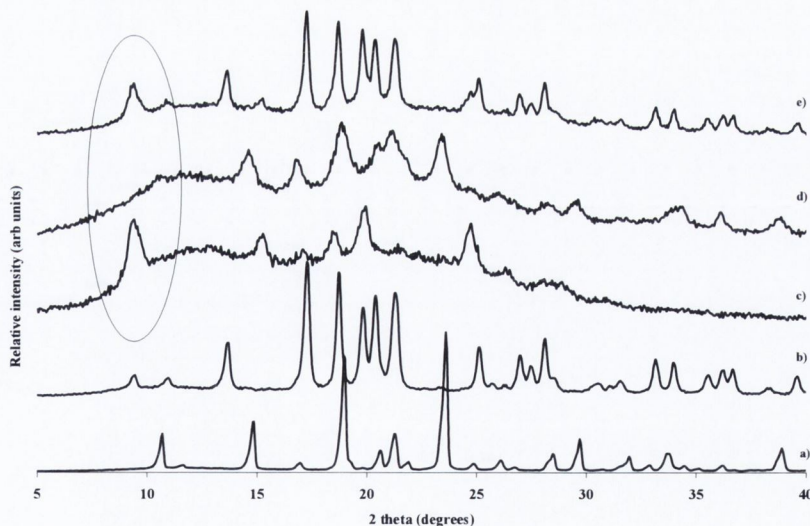


Figure 6.8 PXRD patterns of a) β MAN, b) α MAN, c) SDM milled, d) SDM50:MAN50 co-milled, e) SDM50:MAN50 physical mixture. Highlighted is a characteristic peak of crystalline SDM at 9.6 2 theta.

6.2.5 Quantification of amorphous content

DVS analysis was performed on co-milled systems at MAN weight fractions corresponding to its solubility in the drug (4%), and at higher weight fractions of 20% w/w and 50% w/w. Sorption/desorption kinetic profiles were also obtained for the physical mixture for comparative purposes (Figure 6.9). Ethanol was chosen as the solvent vapour as it induced crystallisation in the milled drug and enabled quantification of amorphous content of the API by DVS.

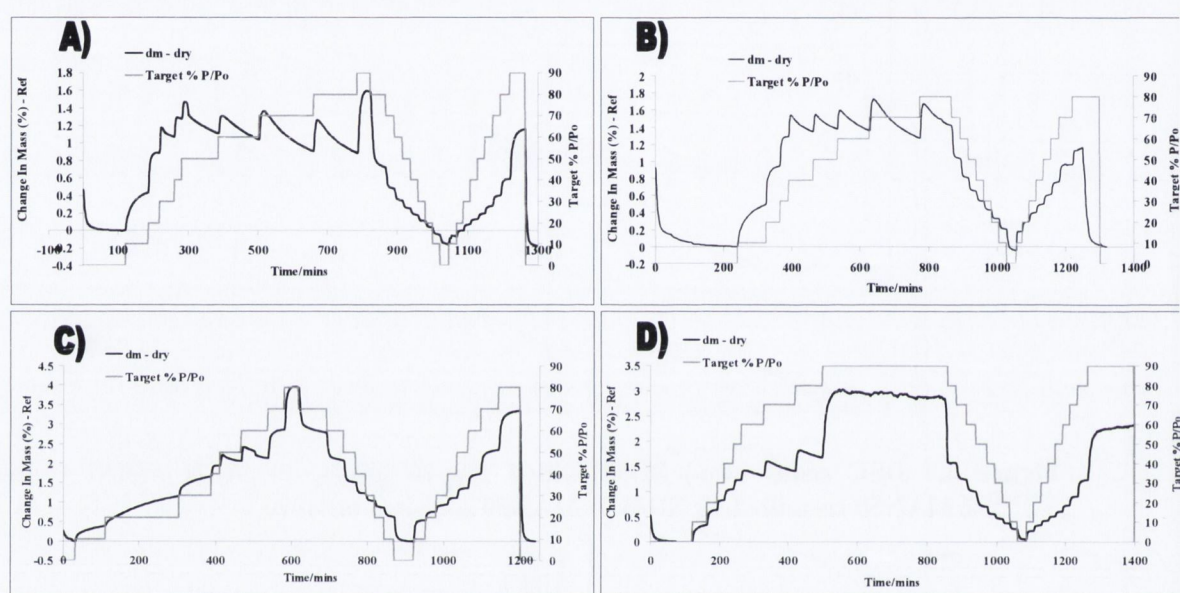


Figure 6.9 DVS kinetic profiles for a) co-milled SDM96:MAN4, b) co-milled SDM80:MAN20, c) co-milled SDM50:MAN50, d) Physical mixture of milled SDM50:milled MAN50.

The first onset of mass loss and hence crystallisation for milled SDM was previously observed to commence at 30% P/P₀ (section 3.2.4.1 in chapter 3). The critical humidity threshold for crystallisation for the SDM96:MAN4 co-milled system was also 30% P/P₀. However the SDM80:MAN20 system and the SDM50:MAN50 system started to crystallise at 40% and 50% P/P₀, respectively, indicating that co-milled composites with higher weight fractions of MAN were more resistant to an ethanolic vapour induced crystallisation. The physical mixture of milled drug and excipient took up considerably

less vapour compared to its co-milled counterpart (0.8% v 1.7% at 30% P/P₀). Amorphous systems are known to have greater sorption potential compared to crystalline materials and thus this result was expected from the pXRD data.

Quantification of amorphous content was performed by DVS, as previously discussed for other SDM:excipient systems, and the results are displayed in Table 6.2 below. The quantification results for SDM milled, SDM96:MAN4, and SDM80:MAN20 were not statistically significantly different ($p > 0.05$). API amorphous content was $96 \pm 2\%$ in the 50:50 co-milled systems, compared to $67 \pm 4\%$ in the corresponding physical mixture. Based on the pXRD, thermal and DVS data, it can be concluded that co-milling SDM with MAN promotes amorphisation of the API and leads to a more physically stable amorphous phase relative to the drug milled alone.

Table 6.2 Summary of amorphous content of milled SDM, SDM:MAN physical mixture and SDM:MAN co-milled systems as quantified by DVS.

System	Amorphous content % (\pm S.D)
SDM milled	76 (3)
SDM96:MAN4 co-milled	71 (1)
SDM80:MAN20 co-milled	77 (1)
SDM50:MAN50 co-milled	96 (2)
SDM50:MAN50 physical mixture	67 (4)

6.2.6 FTIR analysis

The FTIR spectra of milled SDM, unprocessed SDM, co-milled SDM:MAN at $X_{\text{MAN}} = 20\%$, 40% and 50% , and milled MAN are displayed in Figure 6.10.

SDM has an amino functional group associated with its structure, and MAN has six hydroxyl groups along its alkyl backbone. There are two important considerations when mixing between alcohol and amino containing compounds occurs (Takeda et al., 2003). The first effect is that the H-bond O-H...N is stronger than O-H...O and/or N-H...N because of the stronger tendency of N to donate its electrons and the electronegativity of the O atom. The hydrogen bond structure on mixing would therefore be more developed by introducing stronger types of H bonds, compared to hydrogen bonds occurring within or/and between like molecules. The second effect is that the number of lone pairs and H atoms that can participate in H bonding increases when the two components are mixed (Takeda et al., 2003).

As discussed previously, milled SDM has an additional peak at 3471 cm^{-1} , relative to the unprocessed drug, thought to be due to a proportion of non hydrogen bonded NH existing in the amorphous phase. This stretching vibration was shifted to lower wavenumber for the co-milled composites, the extent of the downward shift being dependent of the weight fraction of MAN present in the co-milled composites. A downward shift from 3471 cm^{-1} to 3466 cm^{-1} and 3461 cm^{-1} in the SDM80:MAN20 and SDM60:MAN40 systems were noted. For composites with higher weight fractions of MAN, the peak was much broader and masked by the strong band stretch for the hydroxyl groups.

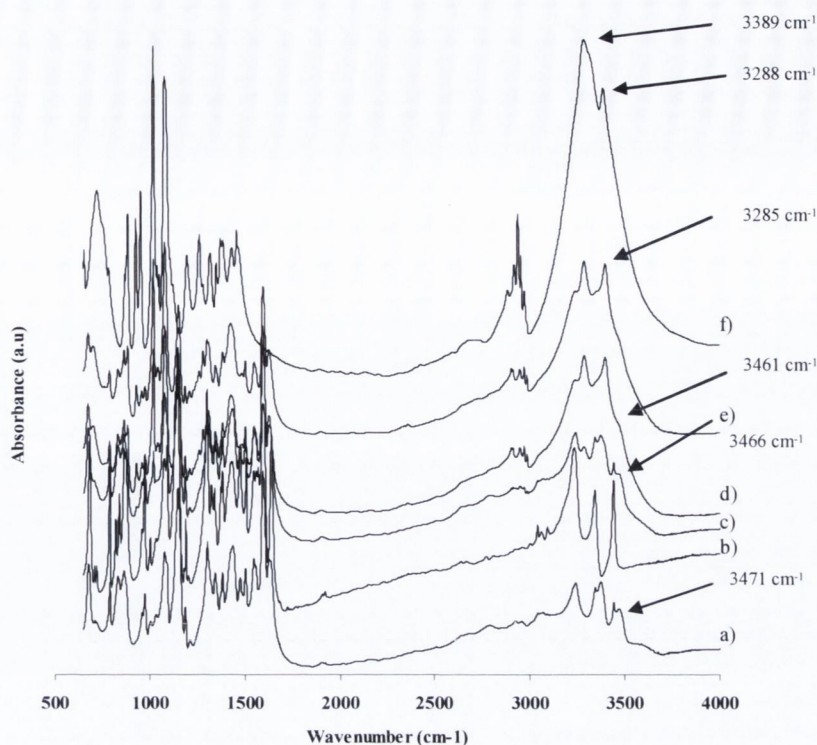


Figure 6.10 FTIR spectra of a) SDM milled for 10 hours, b) SDM as received, C) SDM80:MAN20 co-milled, d) SDM60:MAN40 co-milled, e) SDM50:MAN50 co-milled, f) MAN milled for 10 hours.

The hydroxyl stretching bands of α MAN occur at 3389 and 3288 cm^{-1} , the difference representing the strength and type of hydrogen bonding present. The band at lower frequency is much broader due to more pronounced intermolecular hydrogen bonding. In contrast, the higher energy peak is much sharper, consistent with an intramolecular hydrogen bonded O-H stretch. For the API:excipient co-milled spectra, the lower energy band was noticeably sharper compared to the corresponding band in the spectrum for the milled excipient, which could be due to less intermolecular hydrogen bond formation between MAN molecules in the co-milled composites. A concomitant decrease in wavenumber would be expected for one of the hydroxyl stretching modes in MAN if hydrogen bonding was occurring with the amino group in SDM. A downward shift in wavenumber was indeed observed for the lower energy vibrational mode (to 3285 cm^{-1}) and indicates that it is the hydrogen bond acceptor group. Hence it is possible that

hydrogen bond formation between hydroxyl groups in MAN and NH groups in SDM might explain the enhanced stability of the API amorphous phase on co-milling.

6.3 Sulfadimidine and xylitol co-milled composites

XYL was crystalline after milling for 10 hours by pXRD, and DSC revealed a single melting endotherm at 97°C. The T_g of the excipient was determined by the melt quench method, and evaluated to be -19°C (Figure 6.11).

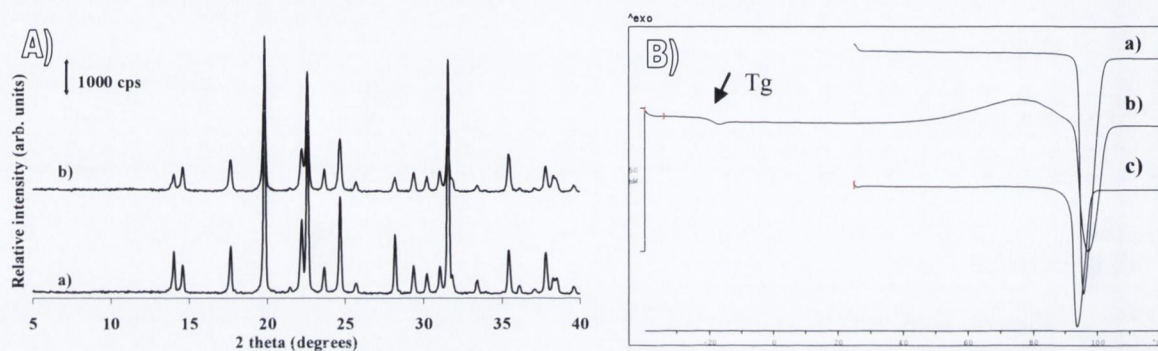


Figure 6.11 A) pXRD patterns of a) XYL unprocessed, b) XYL milled for 10 hours. B) DSC thermograms of a) XYL unprocessed, b) XYL melt quenched with T_g highlighted and c) XYL milled for 10 hours.

The pXRD patterns for the co-milled composites are displayed in Figure 6.12. As was observed for the co-milled systems with MAN, the characteristic Bragg peak of SDM at 9.6 2 theta became less pronounced as the weight fraction of XYL increased in the milled systems. All Bragg peaks for systems with $X_{\text{XYL}} \geq 40\%$ corresponded to the excipient.

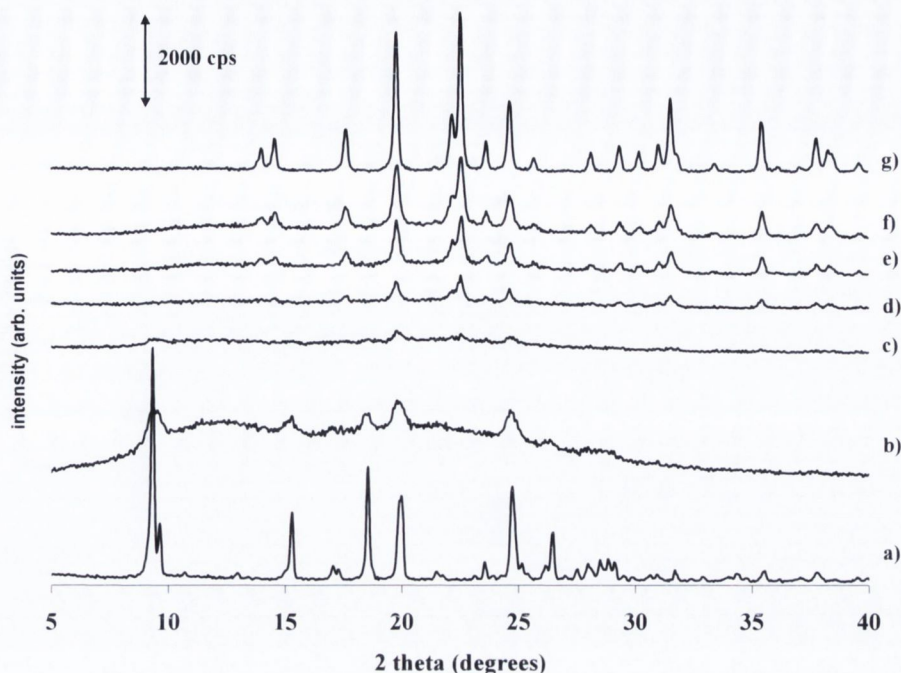


Figure 6.12 PXRD patterns of a) SDM unprocessed, b) SDM milled for 10 hours, c) SDM80:XYL20 co-milled, d) SDM60:XYL40 co-milled, e) SDM50:XYL50 co-milled, f) SDM40:XYL60 co-milled, g) XYL milled for 10 hours.

The calculated Hildebrand solubility parameter for XYL was 37.1. As the difference in the Hildebrand solubility parameter for SDM and Man ($\Delta 12.5 \text{ MPa}^{1/2}$) and SDM and XYL ($\Delta 11.4 \text{ MPa}^{1/2}$) were similar, it was assumed that the solubility of XYL in SDM would also be very small and not too dissimilar to the 4% value obtained for MAN in SDM. Based on this, and the fact that the pXRD data indicated that the excipient was not effective at mitigating amorphisation of the drug on co-milling, it was decided not to investigate further the SDM:XYL co-processed systems.

6.4 Sulfadimidine and mannitol co-spray dried composites

6.4.1 PXRD and thermal analysis

The PXRD patterns and DSC scans for MAN unprocessed and spray dried are displayed in Figure 6.13. Comparison with single crystal data (Figure 6.14; adapted from Hulse et

al., 2009) indicated that the spray dried excipient material contained a mixture of the α and β polymorph. The spray dried material melted at 167°C, a temperature identical to that of the unprocessed form.

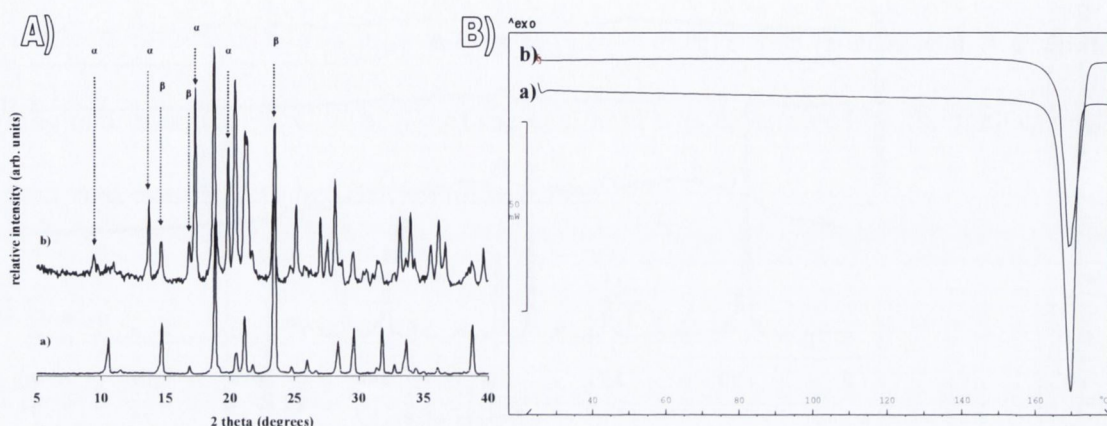


Figure 6.13 A) PXR D patterns, with characteristic Bragg peaks of the α and β polymorphs highlighted of a) β MAN unprocessed, b) spray dried MAN, B) DSC thermograms of a) β MAN unprocessed, b) spray dried MAN.

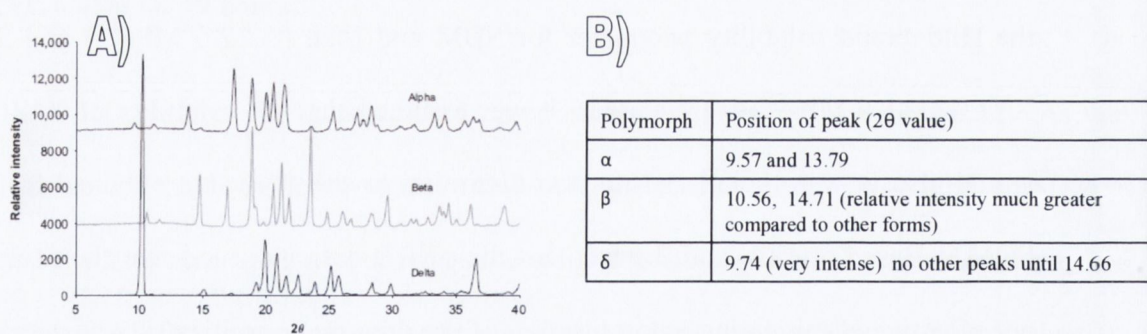


Figure 6.14 A) Single crystal XRD patterns for the three polymorphic forms of MAN and B) Table illustrating the position of key Bragg peaks specific to each polymorphic form of MAN (adapted from Hulse et al., 2009).

The PXR D patterns for the SDM:MAN co-spray dried systems are displayed in Figure 6.15. Co-spray drying at an excipient composition corresponding to Sol_{MAN} (4% w/w) resulted in an amorphous halo. The 90:10 system displayed some trace crystallinity associated with the excipient (circled in red in Figure 6.15). Crystallinity associated with

MAN in the 90:10 system was not surprising because $X_{MAN} > Sol_{MAN}$ and because MAN is very unstable in the amorphous state. The API was amorphous for all co-spray dried systems and Bragg peaks corresponding to all three polymorphs of MAN were apparent for systems with $X_{MAN} \geq 50\%$. Bragg peaks at 9.8 and 22.5 2θ were specific to the delta form of MAN (highlighted with arrows in Figure 6.15).

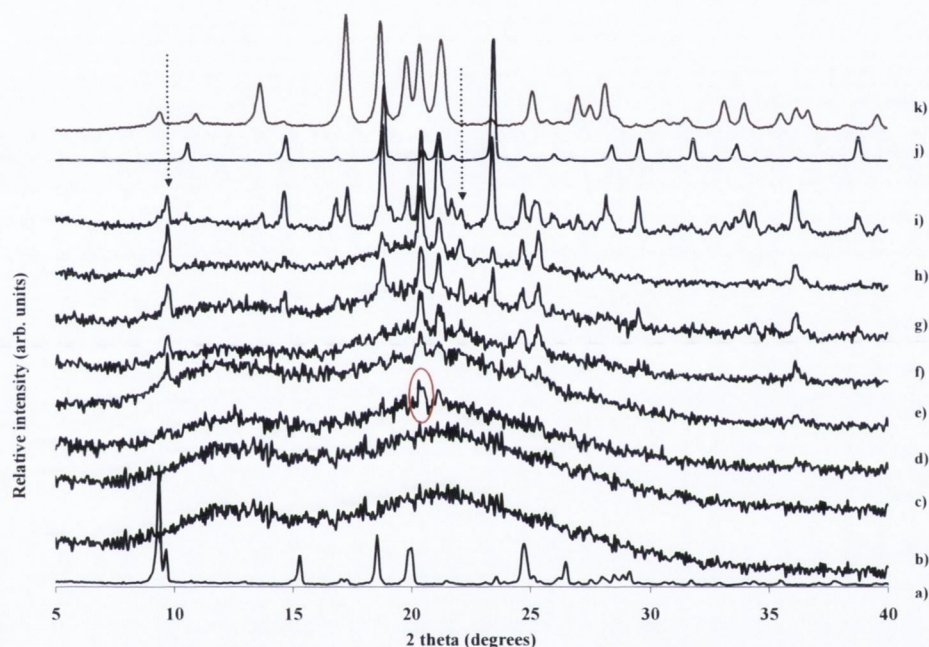


Figure 6.15 PXRD patterns (data normalised) of a) SDM unprocessed, b) SDM spray dried, c) SDM96:MAN4 co-spray dried, d) SDM90:MAN10 co-spray dried, e) SDM80:MAN20 co-spray dried, f) SDM60:MAN40 co-spray dried, g) SDM50:MAN50 co-spray dried, h) SDM40:MAN60 co-spray dried, i) SDM20:MAN80 co-spray dried, j) β MAN, k) α MAN. The dashed arrows indicate peaks corresponding to the δ polymorph of MAN.

The DSC thermograms are displayed in Figure 6.16. The scans are complex and are discussed, with reference to the 50:50 co-spray dried system, in terms of three events; (1) the endothermic event at $\sim 60^\circ\text{C}$, (2) the exothermic crystallisation events in the temperature region $80\text{--}140^\circ\text{C}$, and (3) the polymorphic transformation at $\sim 155^\circ\text{C}$. The melting events are similar to what was observed for the co-milled systems and are not discussed further.

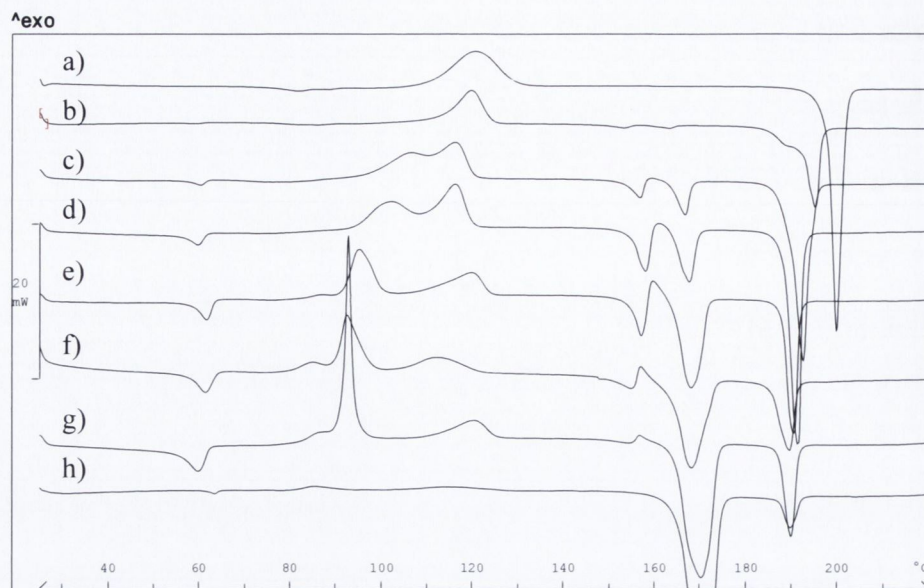


Figure 6.16 DSC thermograms of SDM spray dried and SDM:MAN co-spray dried systems; a) SDM spray dried, b) SDM96:MAN4, c) SDM90:MAN10, d) SDM80:MAN20, e) SDM60:MAN40, f) SDM50:MAN50, g) SDM40:MAN60, h) SDM20:MAN80.

6.4.1.1 Endothermic event

When a glass is stored below, but close to its T_g , it can lose excess enthalpy as it approaches a state of equilibrium, a process known as relaxation. When the sample is heated, the lost enthalpy is recovered at the T_g and manifests as an endotherm associated with the T_g , often referred to as an endothermic overshoot (Petrie, 1972). The endotherm at $\sim 60^\circ\text{C}$ was initially ascribed to an amorphous phase undergoing enthalpic relaxation associated with a glass transition. This was because the reversing signal of a MTDSC did not show the endothermic overshoot associated with relaxation (Figure 6.17). The conditions used for the MTDSC experiments are listed in section 2.2.7.2 in chapter 2.

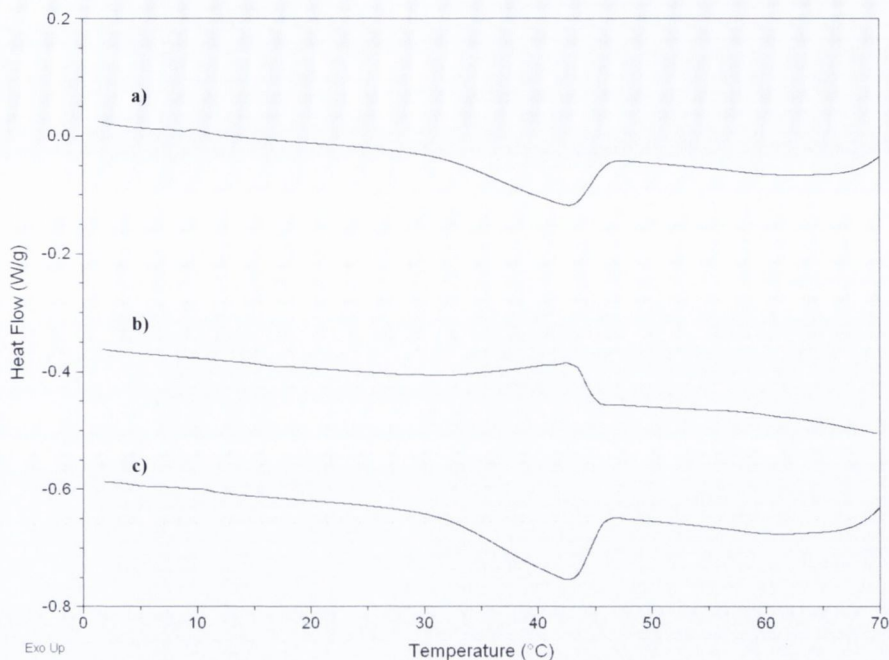


Figure 6.17 MTDSC scan of the SDM50:MAN50 co-spray dried system showing a) the total heat flow signal, b) the reversing heat flow signal and c) the non reversing heat flow signal.

6.4.1.1.1 Thermal Annealing and heating rate studies

Enthalpic relaxation below T_g and the subsequent recovery at T_g indicates the existence of molecular mobility (Hancock et al., 1995). The stability and shelf life of amorphous pharmaceuticals has been shown to be directly related to the time scale of molecular motions. Hence understanding enthalpic relaxation processes is important in developing amorphous formulations with sustained stability to prevent significant crystallization within their anticipated shelf lives (Hancock and Parks, 2000). The objectives of these studies were to study the factors influencing the enthalpic recovery in the SDM:MAN co-spray dried system and to use the data generated to better understand the nature of the endotherm observed in the DSC scan of the spray dried composites.

Experiments were performed based on work previously reported by Mao et al. (2010), and the experimental protocol is described in section 2.2.7.4 in chapter 2. Thermal history was accounted for by heating each sample to 343K and cooling back to 273K

prior to analysis. Enthalpic relaxation studies often show that longer annealing times at higher temperatures result in more pronounced endothermic overshoots and higher glass transition temperatures (Surana et al., 2004). Annealing the 50:50 co-spray dried sample for 480 mins, compared to non annealed samples did produce a more prominent endothermic overshoot (Figure 6.18A), and higher onset and midpoint T_g values, with effects being more pronounced at the higher annealing temperature of 323K (Figure 6.18B). Both onset and midpoint T_g values are used as indicators of T_g during annealing experiments (Mao et al., 2010).

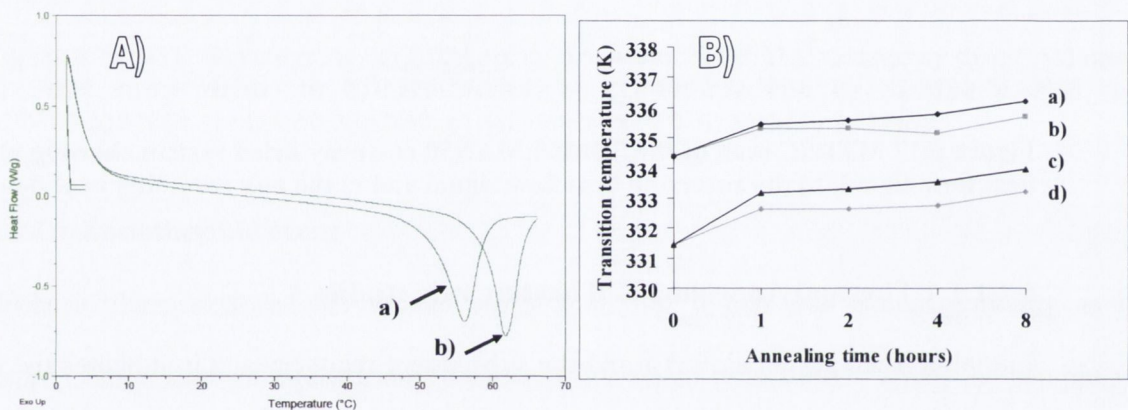


Figure 6.18 A) Effect of annealing on the endothermic event for the SDM50:MAN50 co-spray dried system; a) non-annealed, b) annealed for 480 minutes at 323K. B) Comparison of indicator values of T_g as a function of annealing time (480 mins) at 303K and 323K for the SDM50:MAN50 co-spray dried system; a) T_g midpoint annealed at 323K, b) T_g midpoint annealed at 303K, c) T_g onset annealed at 323K, d) T_g onset annealed at 303K.

Faster heating rates also tend to produce higher and broader T_g values and more pronounced endothermic overshoots in samples that are undergoing enthalpic relaxation (Mao et al., 2010). As can be seen from Figure 6.19 the endothermic event was shifted progressively to higher temperature with higher heating rates.

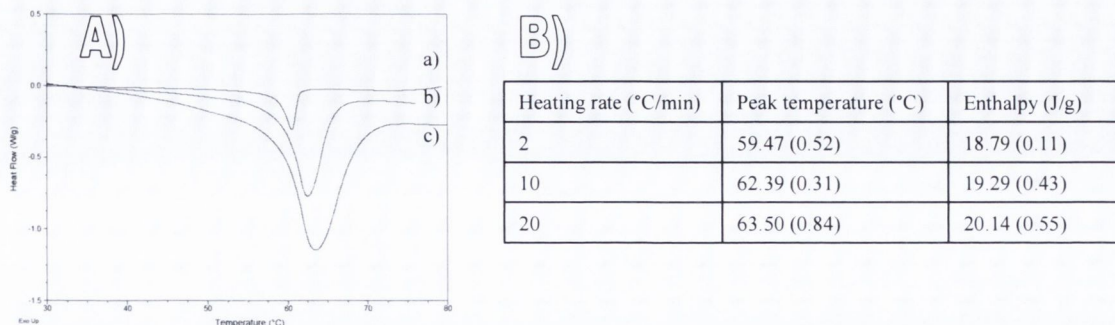


Figure 6.19 A) Influence of heating rate on the apparent glass transition and associated relaxation; a) $2^{\circ}\text{C min}^{-1}$, b) $10^{\circ}\text{C min}^{-1}$, c) $20^{\circ}\text{C min}^{-1}$. B) Peak temperature and enthalpic values of the endothermic transition as a function of different heating rates. Standard deviation in parenthesis.

6.4.1.1.2 Thermal cycling

Enthalpic relaxation is only observed upon heating an amorphous system from below T_g to above T_g . The SDM50:MAN50 co-spray dried system was then heated and cooled several times above and below the transition of interest at 60°C . Figure 6.20 indicates that the endothermic overshoot was apparent on both heating and cooling.

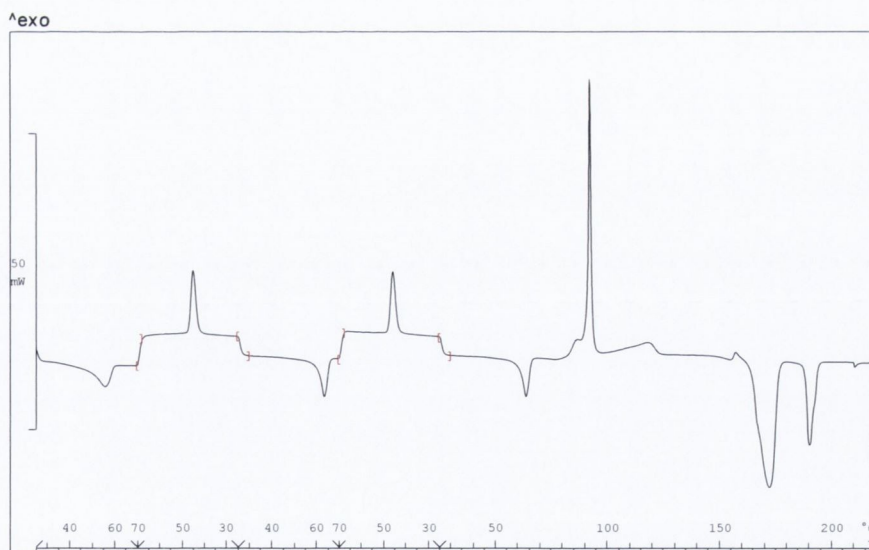


Figure 6.20 DSC thermogram of SDM50:MAN50 co-spray dried composite when subjected to the following thermal profile : 25-70-25-70-25-220°C at $10^{\circ}\text{C min}^{-1}$.

Hence the initial assumption that the endotherm represented a T_g and enthalpic relaxation was invalid. The spray dried sample was also heated in the DSC beyond the endotherm, to 80°C , subsequently removed and analysed by pXRD. The pattern did not show any

differences compared to the pattern obtained for the spray dried composite (data not shown). However it is possible that the temperature change that occurs upon removal of the sample from the DSC to the XRD instrument could induce the temperature sensitive transition. Hence it would have been useful to analyse the sample in a VTXRD instrument. The endotherm at 60°C was not reversible upon heating beyond the first exothermic peak at 105°C. Moreover as the sample recrystallised gradually upon storage, the enthalpy of the endothermic event became less, suggesting that a relationship existed between the event and the amorphous state of the system. Further work is required to elucidate if the transition represents the crossover of two different amorphous phases occupying different energy levels.

6.4.1.2 Exothermic event

The crystallisation event for amorphous spray dried API was represented by a single exothermic peak in the thermogram. On co-spray drying with 10% and 20% w/w MAN, a bimodal exotherm was observed. Two discrete exothermic peaks were identified in the thermograms for the co-spray dried composites with 40%, 50% and 60% w/w MAN. The 50:50 composite was heated to 105°C in the DSC (a temperature intermediate to the two exotherms), as well as to 130°C (a temperature above the second exotherm); both samples were subsequently removed and analysed by pXRD. The patterns obtained are displayed in Figure 6.21. All Bragg peaks of the pattern obtained at 105°C aligned to one of the three polymorphs of the excipient, while the higher temperature pattern was representative of both the API and excipient. The first sharp exothermic event was therefore ascribed to crystallisation exclusively of the excipient, and the second to that of the API. Moreover the temperature onset for the second exotherm in the

SDM50:MAN50 co-spray dried system was the same as the exothermic crystallisation for the API spray dried alone (110°C).

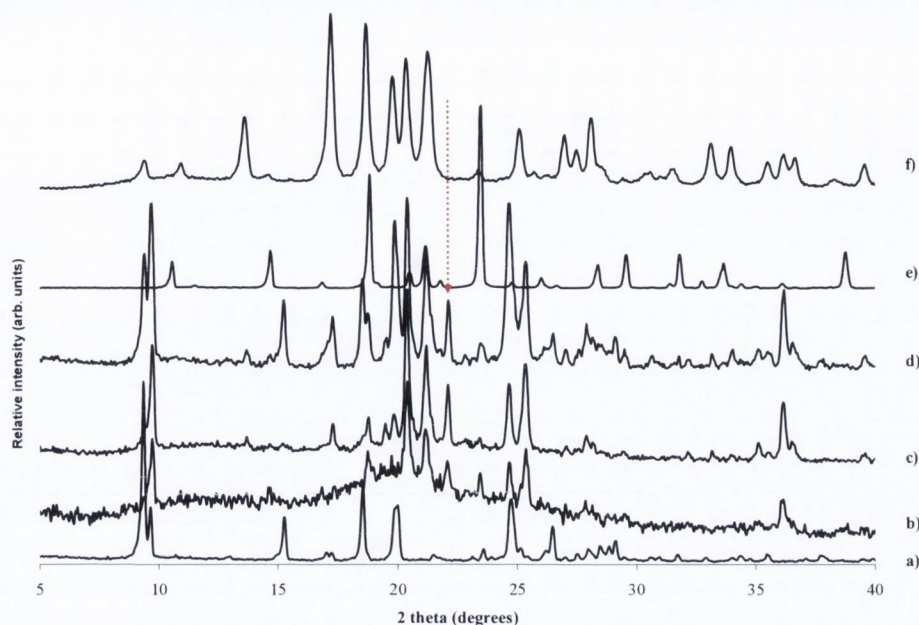


Figure 6.21 PXR D patterns of a) SDM unprocessed, b) SDM50:MAN40 co-spray dried at RT, c) SDM50:MAN40 co-spray dried heated to 105°C in the DSC and subsequently removed for analysis by pXR D, d) SDM50:MAN40 co-spray dried heated to 130°C and subsequently removed for analysis by pXR D, e) β MAN, f) α MAN. The dashed line highlights the Bragg peak specific to the δ form at 22.5 2 theta.

6.4.1.3 Polymorphic transformation

The polymorphic event at $\sim 155^\circ\text{C}$ was attributed to polymorphic transformation of δ MAN. The presence of this form on co-spray drying was confirmed by pXR D, as alluded to earlier. Yoshinari et al. (2002) reported a polymorphic transformation for δ MAN in the temperature range 140-155°C. They attributed these events to an initial melting of δ MAN, followed by its solidification to the stable β form and finally melting of this form at 167°C. No polymorphic transformation was observed in the DSC scans for either milled or spray dried MAN, because in both these individually processed systems, the δ form of MAN was not present.

6.4.2 DVS analysis

The DVS kinetic profiles for the SDM96:MAN4, SDM90:MAN10, SDM80:MAN20 and SDM50:MAN50 co-spray dried systems under water vapour are displayed in Figure 6.23. SDM spray dried alone did not crystallise when subjected to vapour humidities up to 90% RH, as discussed in chapter 3. For composites with $X_{MAN} < 50\%$, no mass loss events were apparent in either the first or the second sorption cycles, indicating that these spray dried composites were physically stable on exposure to such humidity profiles. In contrast, a very sharp expulsion of sorbed vapour occurred for the SDM50:MAN50 system at 50% RH. A second mass loss step was evident at 90% RH. The absence of any mass loss in the second sorption cycle confirmed that the system had fully crystallised (confirmed by pXRD).

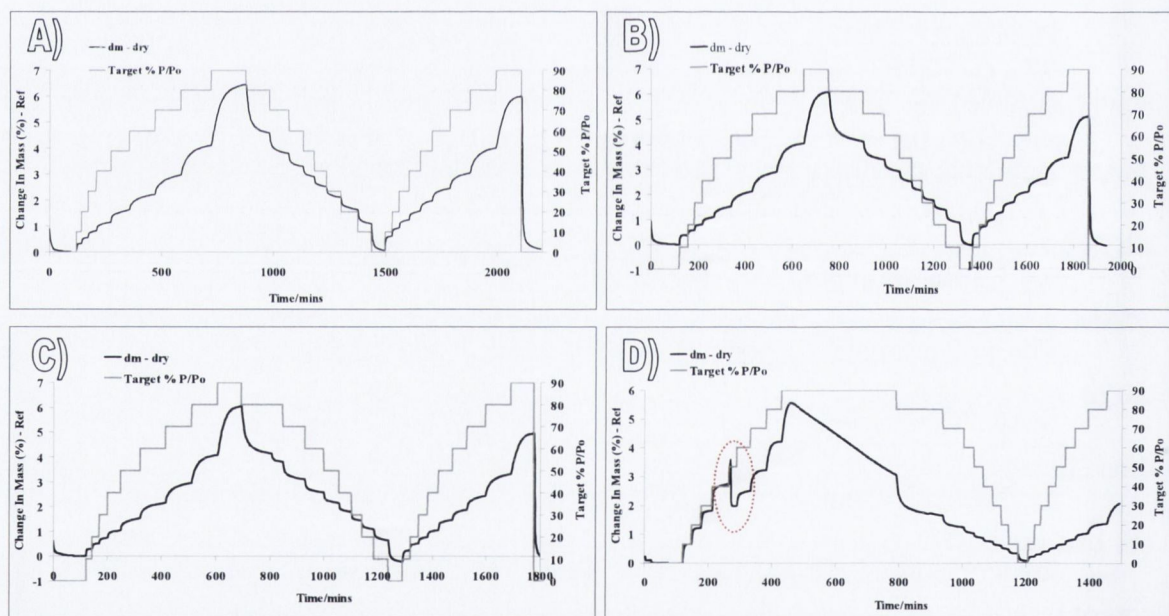


Figure 6.23 DVS kinetic profiles for SDM:MAN co-spray dried systems; A) SDM96:MAN4, B) SDM90:MAN10, C) SDM80:MAN20, D) SDM50:MAN50 (highlighted in red is the sharp mass loss event at 50 % RH).

As the two exotherms in the thermogram corresponded to crystallisation of MAN and SDM respectively, it was thought that the initial sharp mass loss at 50% RH in the sorption profile may correspond to MAN crystallisation. The expelled moisture could

then act as a plasticizing agent, lower the T_g of the API and result in the crystallisation of the drug at 90% RH. To test this, the sample was exposed to 50% RH, removed from the DVS apparatus and a pXRD pattern was obtained (Figure 6.24). The API was still amorphous but Bragg peaks of the excipient were of greater intensity. Moreover the enthalpy of the first exothermic peak (due to crystallisation of MAN) was reduced from 79 J/g in the thermogram prior to DVS analysis, to 15 J/g in the thermogram after exposure to 50% RH. The enthalpy of the second exothermic peak (35 J/g) in the DSC thermograms, prior to and after exposure to 50% RH, was not different. This indicates that the mass loss at 50% RH was associated exclusively with MAN crystallisation. Subjecting the co-spray dried system to 90% RH resulted in crystallisation of the API (Figure 6.24).

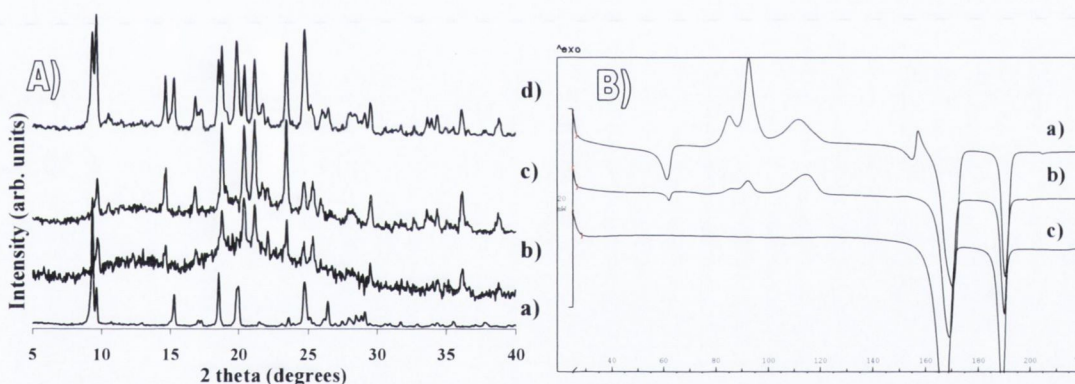


Figure 6.24 A) pXRD patterns (data normalised) of a) SDM unprocessed, b) SDM50:MAN50 co-spray dried, c) SDM50:MAN50 co-spray dried after exposure to 50% RH in the DVS, d) SDM50:MAN50 co-spray dried after exposure to 90% RH in the DVS. B) DSC thermograms of a) SDM50:MAN50 co-spray dried, b) SDM50:MAN50 co-spray dried after exposure to 50% RH in the DVS, c) SDM50:MAN50 co-spray dried after exposure to 90% RH in the DVS.

6.4.3 Physical mixture of spray dried sulfadimidine and spray dried mannitol

A physical mixture of spray dried SDM and spray dried MAN (50:50 w/w) was prepared and analysed by DSC. The thermogram for the physical mixture contrasted significantly to that of the co-spray dried composite, and simply displayed the T_g of the amorphous

API at $\sim 78^\circ\text{C}$, followed by a single exothermic event at $\sim 110^\circ\text{C}$ attributed to crystallisation of the amorphous drug, and finally melting of the two components at 168°C and 190°C (Figure 6.25).

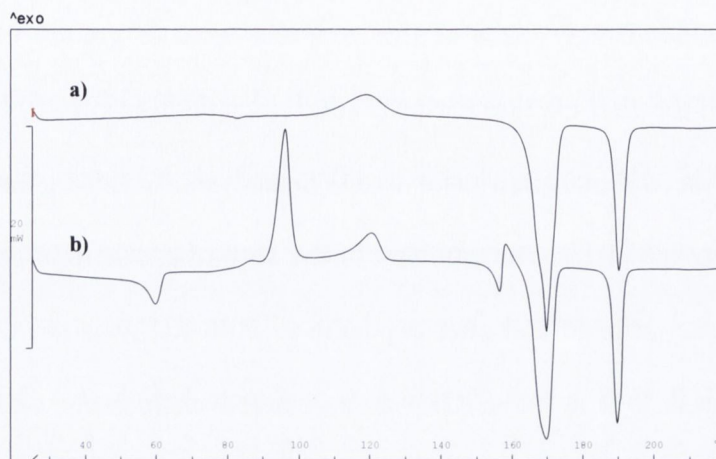


Figure 6.25 DSC thermograms of a) SDM50:MAN50 physical mixture and b) SDM50:MAN50 co-spray dried.

6.5 Glutaric acid and sulfadimidine:glutaric acid co-spray dried systems

GA underwent a polymorphic transformation on spray drying alone, from the stable β form to the metastable α form (Figure 6.26). The α polymorph melted at 97°C with no transformation occurring around 73°C , as seen for the unprocessed excipient.

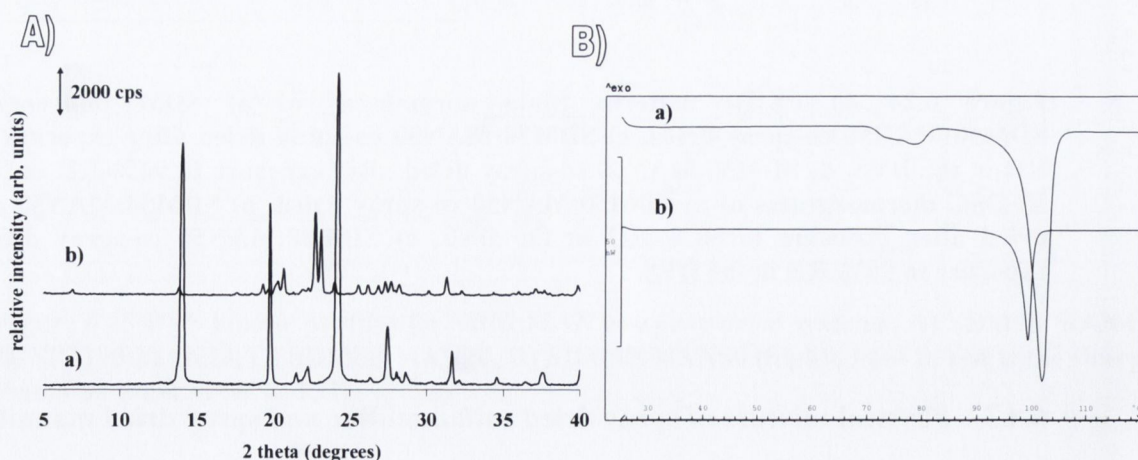


Figure 6.26 A) pXRD patterns of a) GA unprocessed, b) GA spray dried. B) DSC thermograms of a) GA unprocessed, b) GA spray dried.

The pXRD patterns obtained for the SDM:GA co-spray composites are displayed in Figure 6.27. The API was amorphous, irrespective of the weight fraction of excipient. At concentrations below Sol_{GA} (i.e. 34%), API:excipient amorphous composites were produced. At excipient weight fractions above Sol_{GA} , GA was crystalline and existed as the metastable α polymorph.

No powder was recovered on co-spray drying SDM with GA, with $X_{GA} = 30$ and 40. Inlet (78-90°C) and outlet temperatures (41-50°C) were elevated but no powder was again recoverable. These weight fractions of excipient correspond very closely to the solubility of the excipient in the amorphous drug and it is possible that the amorphous composite saturated with excipient is very hygroscopic and prevents the recovery of a powder sample on spray drying.

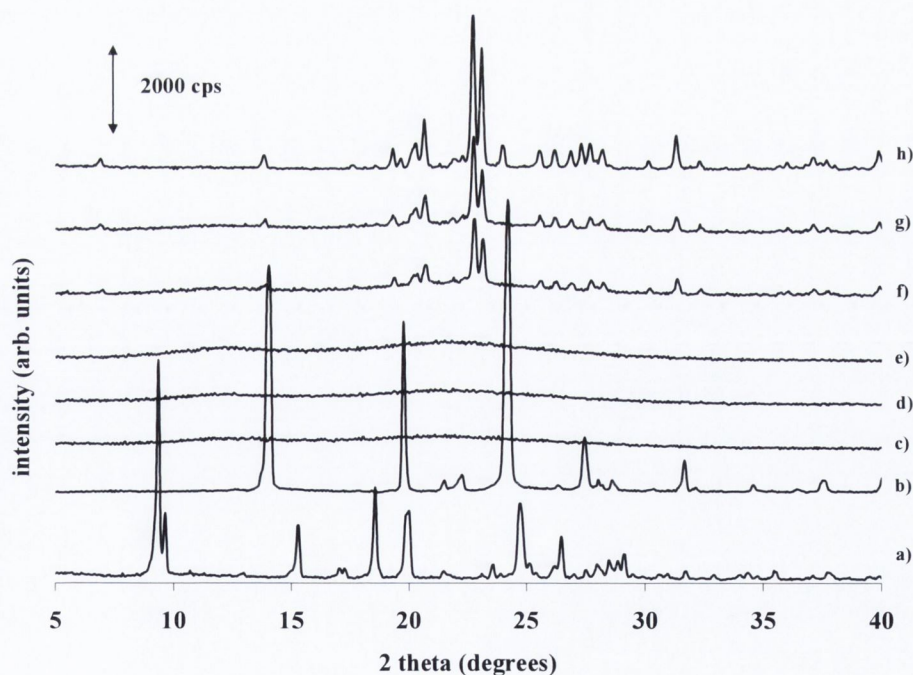


Figure 6.27 PXR D patterns of a) SDM unprocessed, b) GA unprocessed, c) SDM spray dried, d) SDM90:GA10 co-spray dried, e) SDM80:GA20 co-spray dried, f) SDM50:GA50 co-spray dried, g) SDM40:GA60 co-spray dried, h) GA spray dried (α polymorph).

The DSC thermograms of the spray dried systems are displayed in Figure 6.28. The crystallisation exotherm peak temperature, at $\sim 110^{\circ}\text{C}$ for the spray dried API, was shifted by 12°C to lower temperature for the 90:10 and 80:20 systems and by 42°C for the 50:50 and 40:60 co-spray dried systems. This indicates that amorphous phase in the co-spray dried composites is less physically stable when compared to amorphous SDM spray dried alone. The melting temperatures for both the excipient and API were at a lower temperature in the co-spray dried systems relative to the individual spray dried components.

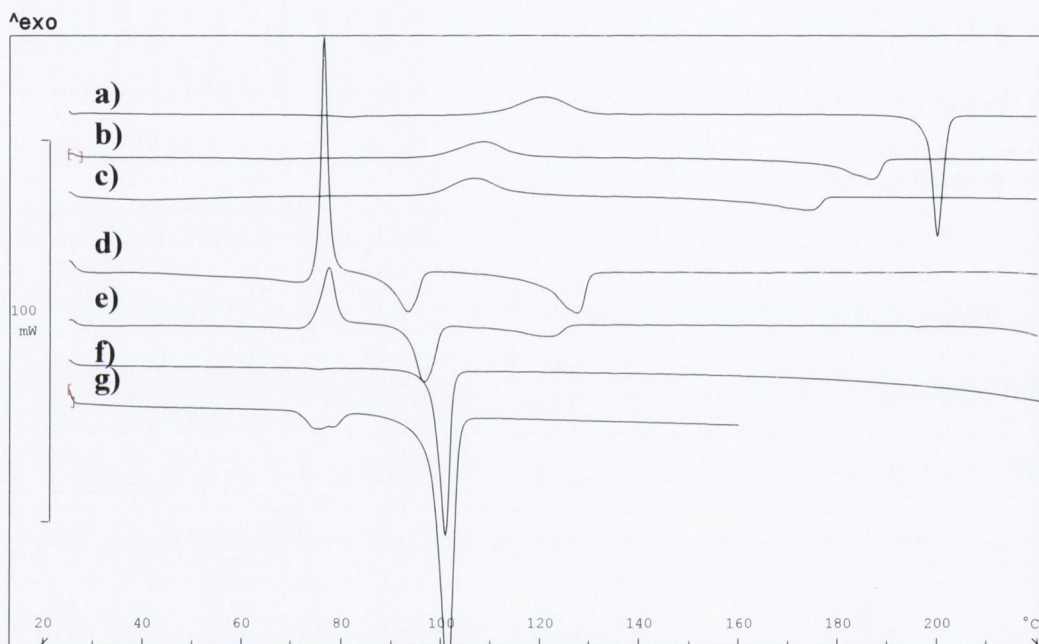


Figure 6.28 DSC thermograms of a) SDM spray dried, b) SDM90:GA10 co-spray dried, c) SDM80:GA20 co-spray dried, d) SDM50:GA50 co-spray dried, e) SDM40:GA60 co-spray dried, f) GA spray dried, g) GA unprocessed.

6.5.1 Physical stability

The 50:50 co-spray dried system was stored in a sealed dessicator at 4°C for up to 18 months and analysed periodically by pXRD (Figure 6.29). No change in polymorphic form of the excipient occurred after 18 months and the API was still amorphous. This is interesting when it is considered that α GA produced by spray drying is unstable and

converts to the stable β form within a few hours when stored under dessicated conditions at $\sim 4^{\circ}\text{C}$ (data not shown). Nolan (2008) noted that spray dried SDM was amorphous for 8 weeks when stored in dessicated conditions at 4°C before the system started to crystallise. Nevertheless in the co-spray dried composite both the amorphous form of the drug and the metastable polymorphic form of GA were stabilised.

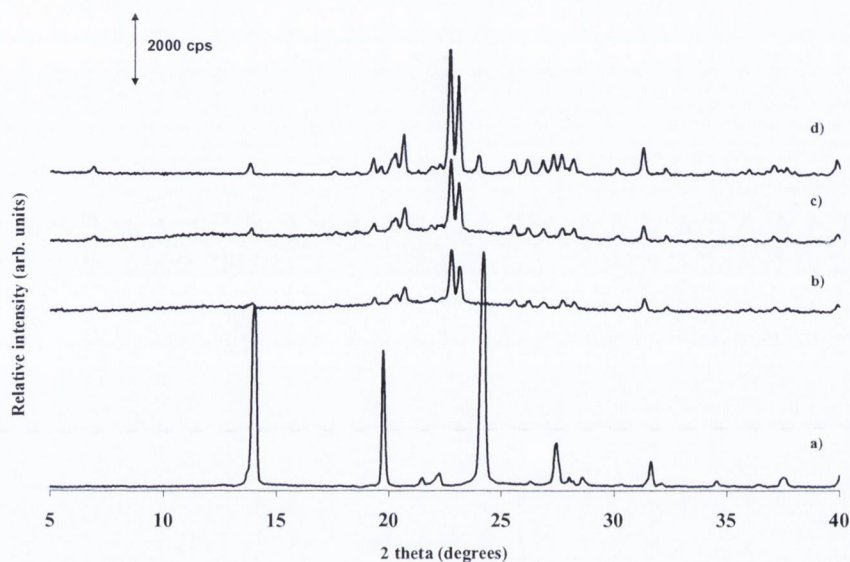


Figure 6.29 PXR D patterns of a) β GA, b) SDM50:GA50 co-spray dried, c) SDM50:GA50 co-spray dried after 18 months, d) α GA.

Accelerated physical stability studies by DVS, using water as the probe vapour, were performed on the 90:10 and 50:50 co-spray dried systems. For both systems, the API was amorphous prior to DVS analysis. Sorption/desorption kinetic profiles for these systems, SDM spray dried alone, as well as a combination isotherm plot are displayed in Figure 6.30.

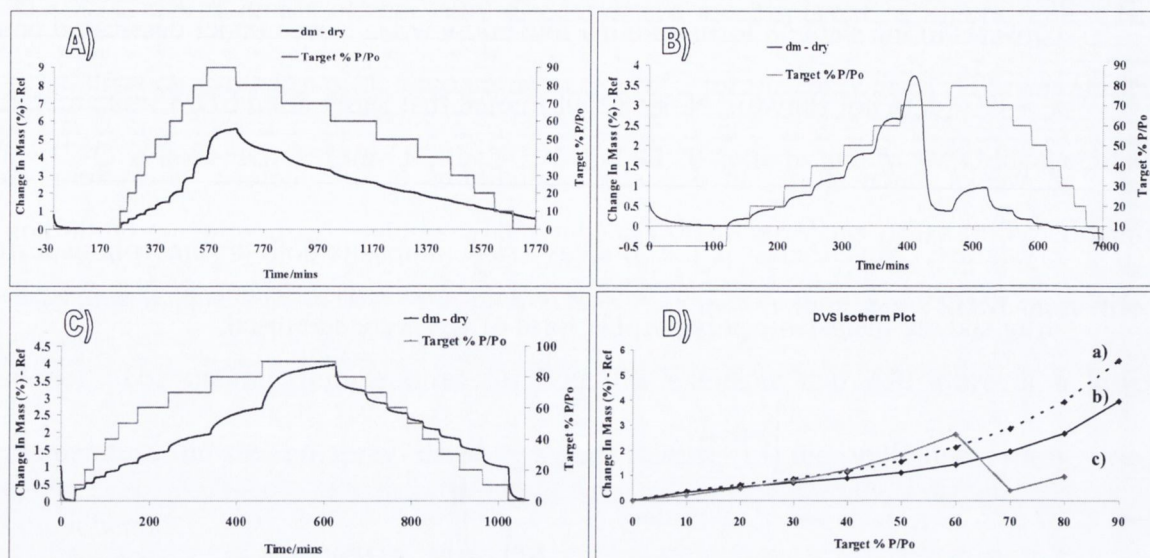


Figure 6.30 Sorption/desorption plot for A) SDM90:GA10 co-spray dried, B) SDM50:GA50 co-spray dried, C) SDM spray dried, D) Isotherm plot of a) SDM90:GA10 co-spray dried, b) SDM spray dried, c) SDM50:GA50 co-spray dried.

The 90:10 system had a mass uptake of 5.5% at 90% RH, compared to a mass uptake of 3.9% for the API spray dried alone. This could be due to the sorption properties of amorphous GA which exists in the spray dried composite, as indicated by pXRD. However the system did not undergo crystallisation, despite the extra sorption uptake, even when subjected to 90% RH. In contrast, a large mass loss at 70% RH was observed for the 50:50 system (Figure 6.30B and Figure 6.30D). DSC and pXRD confirmed that crystallisation of the API in the 50:50 system at elevated humidities was accompanied by polymorphic transformation of GA from the metastable α to the stable β form (Figure 6.31). The 50:50 system was the only sample which displayed residual crystallinity, associated with α GA, and this may have played a role at inducing further crystallisation in the system at high RH.

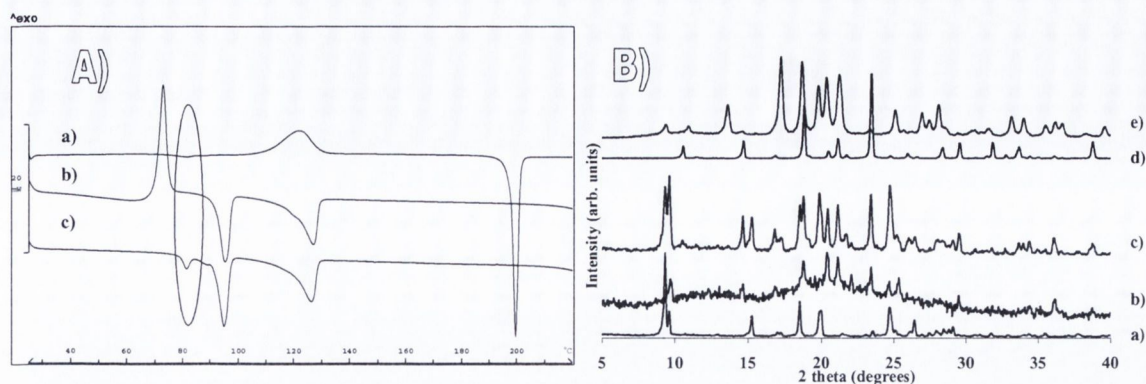


Figure 6.31 A) DSC thermograms of a) SDM spray dried, b) SDM50:GA50 co-spray dried, c) SDM50:GA50 co-spray dried after crystallisation in the DVS. B) PXRD patterns (data normalized) of a) SDM unprocessed, b) SDM50:GA50 co-spray dried, c) SDM50:GA50 co-spray dried after crystallisation in the DVS, d) β GA, e) α GA.

6.5.2 SEM analysis

It was unexpected that the SDM50:GA50 co-spray dried system was more stable than the API spray dried alone when stored at 4°C in a sealed dessicator (at least 18 months versus 8 weeks), considering the composite crystallised at a lower temperature when analysed by DSC. Moreover it crystallised on exposure to a RH of 70%, whereas the API itself remained amorphous when subjected to 90% RH in the DVS. SDM spray dried, as discussed in chapter 3, consisted of small spherical particles. GA unprocessed existed as coarse irregular shaped particles. GA spray dried consisted of fused agglomerates. The 90:10 system was composed of spherical particles. The image of the 80:20 system was representative of large particles with smaller spherical particles, possibly of the amorphous API. SEM of the 50:50 co-spray dried system revealed a single population of discrete particles, similar to the unprocessed excipient. The particles were irregular in shape and of much larger size compared to the individually spray dried systems, and compared to the unprocessed materials. No spherical particles attributable to the amorphous drug were apparent. The presence of the excipient in the spray dried composite may be such that it is exerting an encapsulating or shielding effect on the

amorphous API, sterically hindering it and inhibiting nucleation and growth. Forbes et al. (1998) noted that the distribution of a protein and excipient within a particle may not be uniform on spray drying and that the protein could preferentially locate at sites where crystallisation is not favoured and is stabilised in the amorphous form.

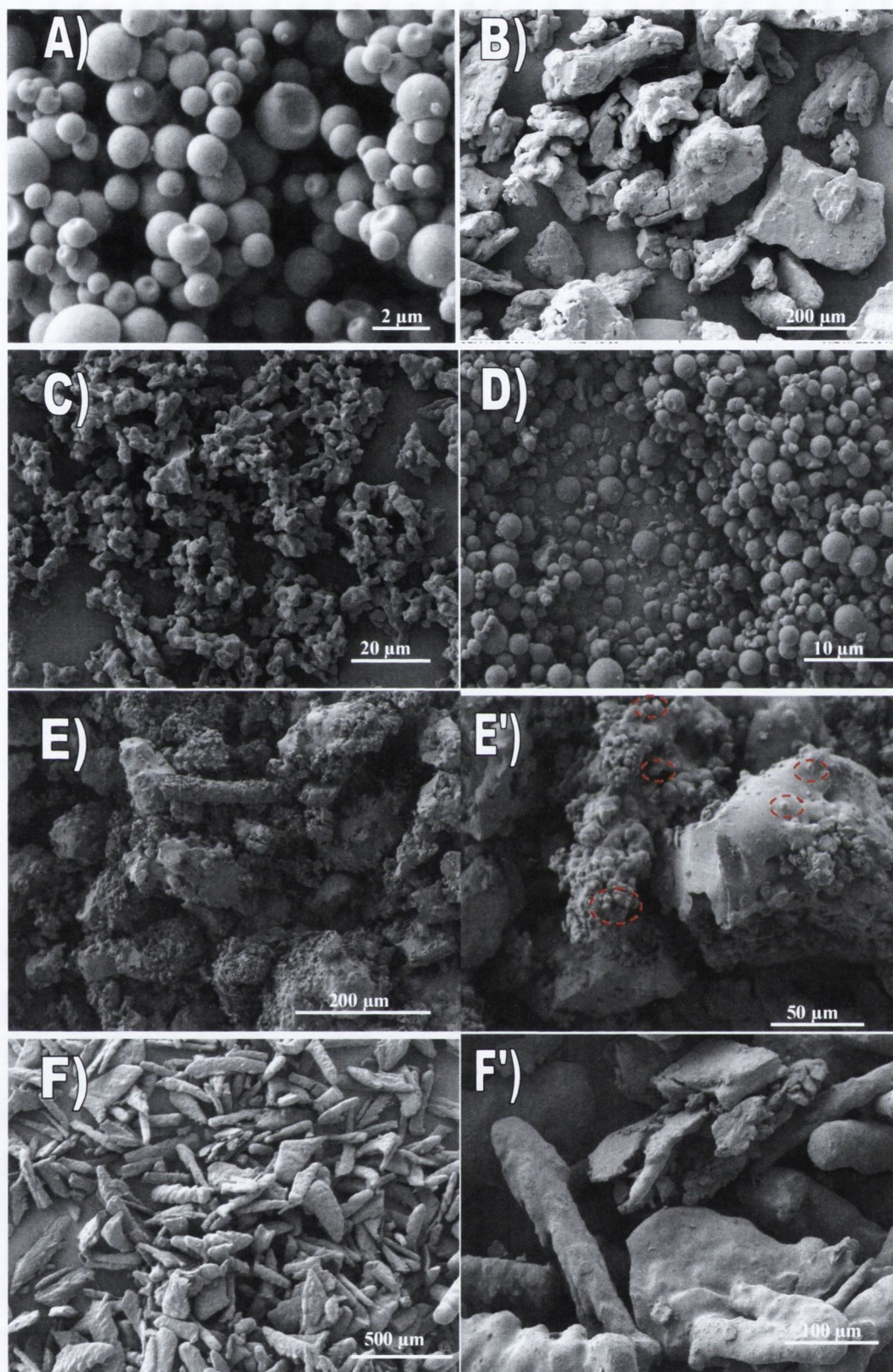


Figure 6.32 SEM micrographs of A) SDM spray dried, B) GA unprocessed, C) GA spray dried, D) SDM90:GA10 co-spray dried, E and E') SDM80:GA20 co-spray dried, F and F') SDM50:GA50 co-spray dried.

6.6 Sulfadimidine:adipic acid and sulfadimidine:succinic acid co-spray dried systems

The pXRD patterns of spray dried AA and SDM:AA co-spray dried composites are displayed in Figure 6.33. The excipient was crystalline when spray dried alone and of the same crystalline form as unprocessed AA. The 80:20 co-spray dried composite was the only system which was completely amorphous. The weight fraction of excipient in this 80:20 composite corresponded to the solubility of the excipient in the amorphous drug ($Sol_{AA} = 20\%$). When the weight fraction of AA was above Sol_{AA} , it was expected that Bragg peaks associated with crystalline excipient would be observed in the pXRD patterns. Indeed for all composite systems with $X_{AA} > 20$, the API was amorphous with Bragg peaks associated with crystalline AA apparent.

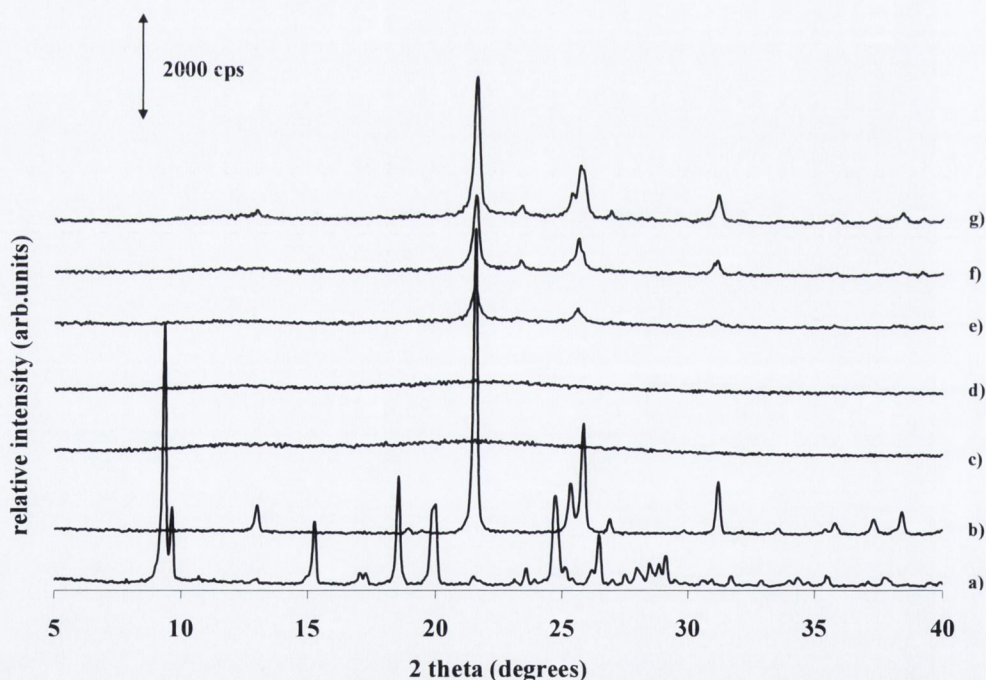


Figure 6.33 pXRD patterns of a) SDM unprocessed, b) AA spray dried, c) SDM spray dried, d) SDM80:AA20 co-spray dried, e) SDM60:AA40 co-spray dried, f) SDM50:AA50 co-spray dried, g) SDM40:AA60 co-spray dried.

The thermal behaviour of the co-spray dried systems are displayed in Figure 6.34 below. The spray dried excipient melted at 152°C. The exothermic crystallisation peak in the drug spray dried alone was shifted downwards by ~20°C in the 80:20 composite system. The melting peaks of the excipient and drug were 12 and 23°C lower than the melting of the pure components spray dried alone. Exothermic crystallisations occurred for all systems in the temperature range 100 – 109°C and were depressed to a lesser extent when compared to the corresponding SDM:GA co-spray dried systems. A low temperature melting at 139°C was observed for the 50:50 and 40:60 co-spray dried systems.

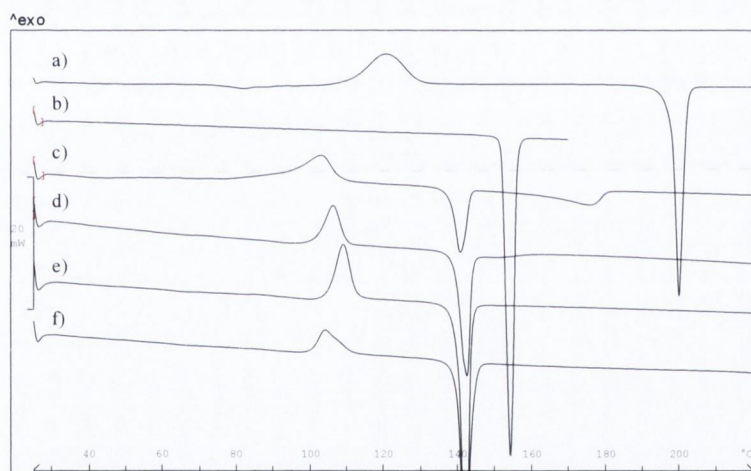


Figure 6.34 DSC thermograms of a) SDM spray dried, b) AA spray dried, c) SDM80:AA20 co-spray dried, d) SDM60:AA40 co-spray dried, e) SDM50:AA50 co-spray dried, f) SDM40:AA60 co-spray dried.

SDM was also co-spray dried with 50% w/w SA. The pXRD patterns and DSC thermograms are displayed in Figure 6.35. The API was amorphous in the composite system with the crystalline Bragg peaks being associated with the excipient. Spray dried SA melted with degradation at 187°C. The thermogram of the spray dried composite displayed an exothermic peak at 94°C, which was 26°C lower than the crystallisation of the spray dried API. A melting endotherm was observed at 166°C with degradation occurring at higher temperature.

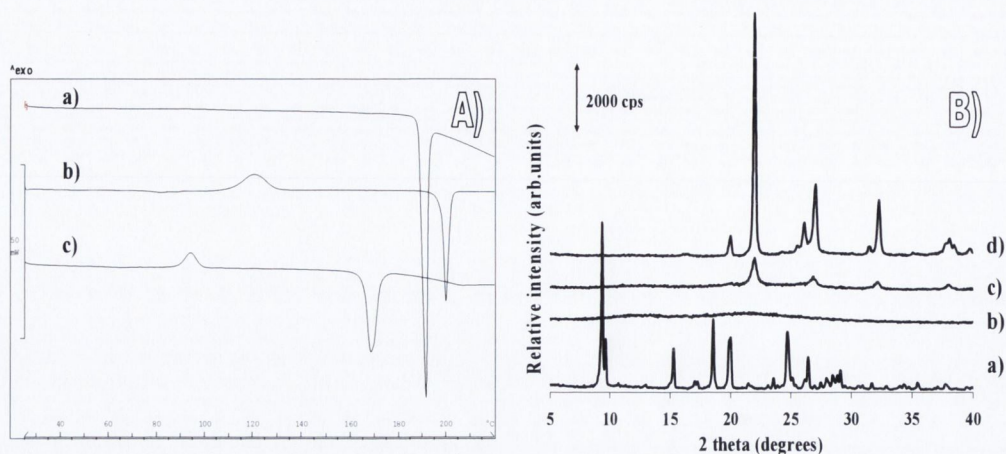


Figure 6.35 A) DSC thermograms of a) SA spray dried, b) SDM spray dried, c) SDM50:SA50 co-spray dried. B) pXRD patterns of a) SDM unprocessed, b) SDM spray dried, c) SDM50:SA50 co-spray dried, d) SA spray dried.

6.7 DVS analysis of sulfadimidine:diacid co-spray dried composites

DVS sorption isotherms for SDM spray dried and SDM co-spray dried with 50% w/w GA, SA and AA are displayed in Figure 6.36. As ethanol functioned as a plasticizer and induced crystallisation in the spray dried API, the co-spray dried systems were also exposed to an ethanolic environment. This allowed for comparability analysis across all systems and enabled determination of the threshold crystallisation P/P_0 for each processed system. Moisture sorption information for such composite systems is useful in predicting solid state stability and understanding the effects of sorbed vapours on the crystallisation tendencies of amorphous systems (Airaksinen et al., 2005).

Spray dried GA, AA and SA, when analysed individually by DVS, had vapour uptakes of <math><0.06\%</math> on exposure to 30% P/P_0 . The SDM:GA and SDM:SA co-spray dried composites had lower ethanol sorption uptakes (0.5% mass change in both cases), compared to the API spray dried alone (1.6%), at 30% P/P_0 . The excipients could be viewed as acting as shielding or protecting agents, limiting exposure of the amorphous drug to the surrounding vapour molecules. In contrast the uptake for the SDM:AA system was more than double that of the other composites (1.1% at 30% P/P_0).

The SDM:SA system started to crystallise between 30-40% P/P₀, similar to the API spray dried alone and subsequently underwent multiple crystallisation events at 40, 50, 60, 70 and 80% P/P₀. The SDM50:GA50 system underwent a single step crystallisation between 40-50% P/P₀. Despite having higher sorption capacity at low P/P₀, the first mass loss in the kinetic profile for the SDM50:AA50 system was at 70% P/P₀. This system had a much higher affinity for ethanol at 60% P/P₀ (3.4%) than would have been anticipated from the sorption behavior of the individually spray dried excipient (0.1%) and drug (0.3%, having recrystallised) at the same P/P₀.

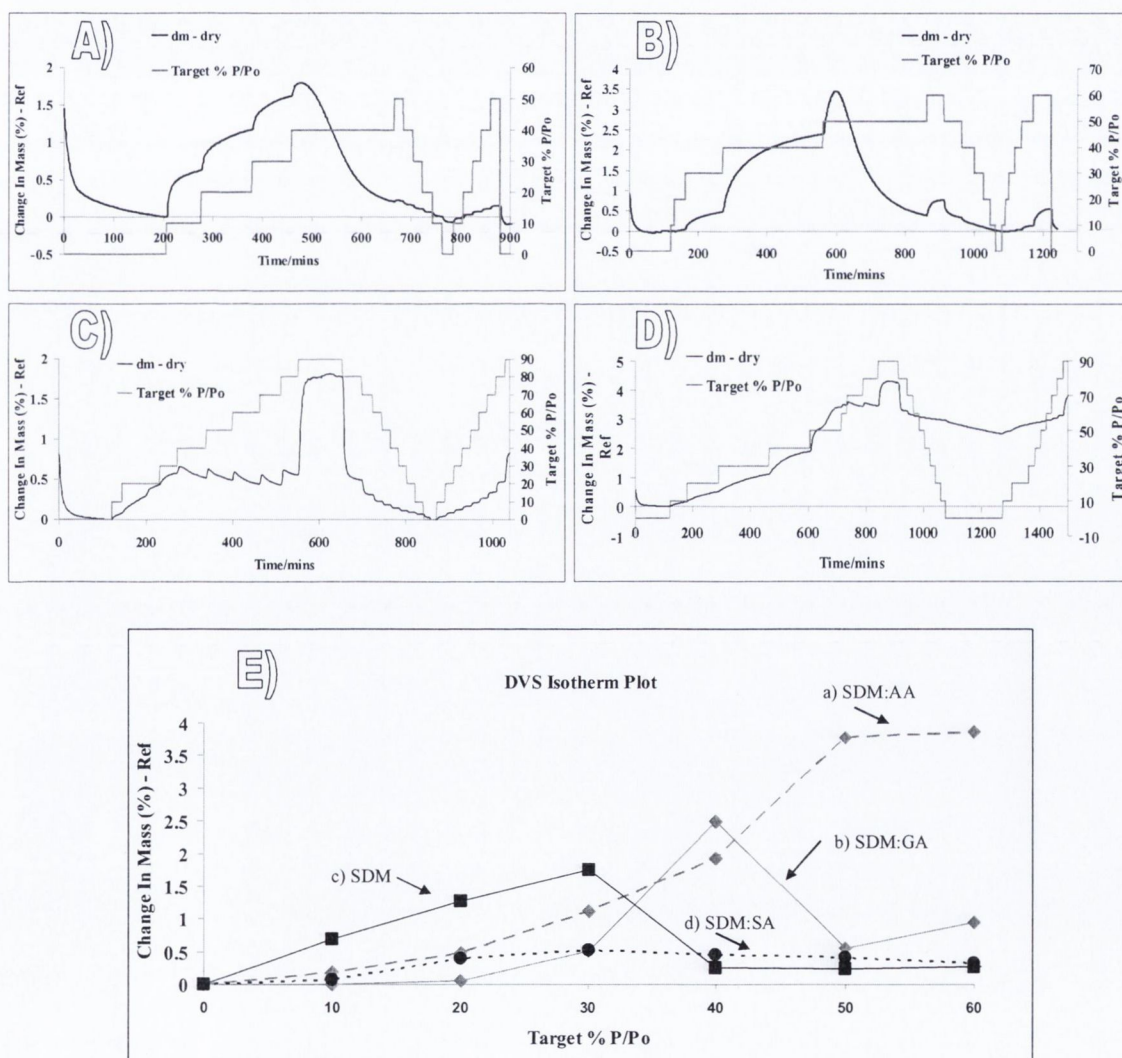


Figure 6.36 DVS kinetic profiles and isotherm plots of SDM spray dried and SDM:diacid co-spray dried composites. A) SDM spray dried, B) SDM50:GA50, C) SDM50:SA50, D) SDM50:AA50, E) Isotherm plot – 1st sorption cycles. $X_{\text{excipient}} = 50\%$ w/w.

Forbes et al. (1998) investigated the vapour sorption properties and physical stabilities of a series of spray dried sugar/protein composites and noted that the interaction of vapour with a co-processed complex may be very different depending on the excipient selected. Some excipients can function as crystallisation catalysts, while others can act as crystallisation inhibitors. Moreover the manner with which composites interact with vapour may differ significantly when compared to the behavior of the individual components. Stubberud and Forbes (1998) investigated the effects of additives on the moisture induced crystallization of amorphous materials. The authors noted that some excipients can act as internal desiccants and delay the onset of crystallisation. Other excipients can have an isolating or deaggregating effect and act to enhance the exposure of the amorphous drug to the surrounding vapours. The sorption behaviour of the API:diacid co-spray dried systems in this work were very different, found to be independent of the behaviors of the individually spray dried components, with each system requiring individual characterisation.

6.8 Conclusion

In this chapter we co-milled SDM with MAN and XYL, two sugar alcohols with low T_g values, below that of room temperature. The solubility of MAN in amorphous SDM was determined to be just 4% and hence the viability of exploiting the excipients low T_g was counteracted by the very poor miscibility of the two components. MAN had an unexpected stabilising effect on the amorphous API, with crystallization temperatures progressively shifted to higher temperatures with increasing amount of excipient. A single T_g, similar to the T_g of the amorphous API, was observed for the SDM:MAN co-milled composites.

The excipients selected were not effective at preventing or minimizing amorphisation of the API on co-spray drying. The API was amorphous across all co-spray dried composite systems, independent of the excipient composition. Amorphous composites were produced when the weight fraction of MAN, GA and AA was below their solubilities in the amorphous drug ($Sol_{MAN} = 4\%$, $Sol_{GA} = 34\%$, $Sol_{AA} = 20\%$). The metastable polymorphs of GA and MAN were produced when the excipient weight fraction, in the feed solution, exceeded Sol_{GA} and Sol_{MAN} . The affinities of the co-spray dried composites for the environmental vapour were system specific and each API:excipient composite required individual characterisation to understand their relative physical stabilities and sorption properties. In conclusion co-spray drying SDM with low T_g excipients, under the conditions specified, did not prove successful at mitigating disorder in the API with the drug being amorphous across all composite systems.

7.1 Introduction

This work explored the feasibility of co-processing API with low T_g excipients as a strategy for counteracting the unwanted generation of an unstable amorphous phase and preserving the crystallinity of a processed drug. An important component of this work was the quantification of amorphous content and a number of analytical techniques were utilised throughout the thesis for this purpose. Investigations were initially focused on SDM, with further studies performed on SS and BUD to see if results could be generalised to other APIs. A total of seven low T_g excipients were chosen; five dicarboxylic acids and two sugar alcohols, and processing techniques used were milling, dry mixing and spray drying.

7.2 Amorphisation of API on processing

Chapter 3 explored the impact of mechanical activation and spray drying on the solid state properties of three APIs. Spray drying amorphised all three drugs, milling completely amorphised BUD and SS, and dry mixing SS for 8 hours converted it to an amorphous form.

The glass forming ability and glass stability of organic molecules can be estimated from characteristic thermal descriptors from a typical DSC run, as illustrated in Figure 7.1. A useful indicator of a material's glass forming ability is the reduced glass transition temperature (T_{rg}).

$$T_{rg} = T_g/T_{melt} \quad \text{eq. 7.1}$$

It is expected that the closer the T_{rg} value is to 1, the easier the material is converted to a glass (Baird et al., 2010).

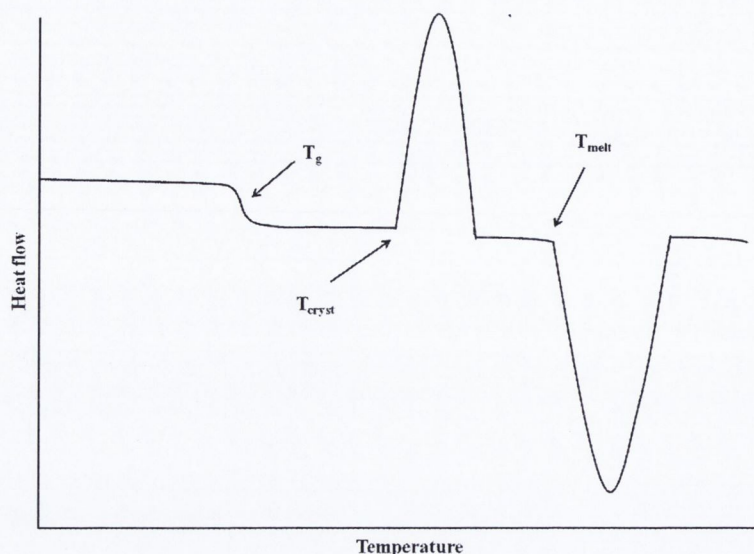


Figure 7.1 Schematic of parameters used to describe glass forming ability and glass stability of organic materials. T_{cryst} is the temperature onset of crystallisation, T_g is the midpoint of the glass transition temperature and T_{melt} is the melting temperature.

Zhou et al. (2002) evaluated the glass stability and crystallisation tendency of several pharmaceutical materials using the parameter ‘reduced temperature’ T_{red} . It was observed that lower T_{red} values corresponded with higher crystallisation rates and less stable glasses.

$$T_{\text{red}} = T_{\text{cryst.ons}} - T_g / T_{\text{melt}} - T_g \quad \text{eq. 7.2}$$

The reduced temperature is essentially an indicator of how far above the glass transition a material must be heated before spontaneous crystallisation occurs. It provides a platform for comparing the crystallisation tendencies of compounds having different T_g s.

Compounds with high melting temperatures and high melting enthalpies are more likely to display a strong tendency to crystallise from the amorphous state, either on cooling from a melt or upon reheating in the DSC. This is because more energy is expended in breaking the crystal lattice and therefore it is expected the driving forces of crystallisation to be greater compared to compounds with lower melting temperatures and small enthalpies of melting (Baird et al., 2010).

From Table 7.1 it can be seen that SS, of the three APIs in thesis, has a T_{rg} closest to 1 and hence would be expected to be the most easily amorphised of the APIs. This was indeed the case and the API was converted to an amorphous state after only 2 hours of milling and was selected as the only API to be dry mixed with glass beads (amorphised after 8 hours). No attempt was made to amorphise SDM or BUD by dry mixing because of the unlikelihood of achieving amorphisation within a reasonable period of time. Balani et al. (2010) noted that the SS could be fully transformed to a disordered state even after just 1 hour of milling. It was anticipated, based the T_{rg} data in Table 7.1, that SDM would amorphise more readily than BUD. However BUD underwent a crystalline to amorphous transformation after 12 hours of milling, whereas SDM could not be fully amorphised even after milling for up to 20 hours (Appendix IV). Caron et al. (2011) milled SDM for 10 hours and also noted residual crystallinity by pXRD. BUD had the highest melting point of the three APIs (531K), compared to a melting point of 475K for SS and 468K for SDM (Table 7.1) and may be viewed as having the strongest tendency to crystallise from the amorphous state.

Table 7.1 Glass forming ability, glass stability and melting parameters of SDM, SS and BUD.

Compound	T_{rg}	T_{red}	T_m (K)	ΔH_{fus} (J/g)
SDM	0.75	0.27	468	135
SS	0.83	NA	475	NA
BUD	0.67	0.20	531	NA

An association between ease of amorphisation by milling and the extent of the difference between the milling temperature and the T_g of the compound was noted. SS had the highest T_g (~120°C) and was most easily amorphised by milling,

whereas SDM had the lowest T_g (78°C) of the three APIs and could not be fully amorphised by milling. These observations may have useful implications regarding the optimisation of process parameters and conditions during production. For instance, the amorphisation tendency by milling may be hindered if the T_g of a compound is lowered due to plasticising effect of water from the environment. Moreover if amorphisation by milling is necessary and desirable but is not achievable at ambient operating temperatures, then lowering the temperature of milling can enhance the tendency for amorphisation. Hu et al. (2012) demonstrated that amorphous sulphathiazole could be produced by cryo-milling for less than 3 hours, whereas Caron et al. (2011) noted a polymorphic transformation of the drug when milled at room temperature for 10 hours. In Chapter 3 we demonstrated that amorphisation of SDM was enhanced by milling at the lower temperature.

7.2.1 Inter-comparison of the amorphous state of drugs produced by different processes

The influence of the processing technique on the solid state form of a drug is well documented in the literature. In contrast there is limited published data on the direct comparison of the amorphous form of a model compound produced by different preparative methods. Spray drying and mechanical activation by milling are viable processes capable of inducing crystalline to amorphous transformations in APIs in order to exploit the useful properties of the amorphous state.

Mechanical techniques and solvent based techniques, like spray drying, are fundamentally different and hence exposure to different stresses may result in different physical and chemical stabilities in amorphous materials. For instance, on a macro level, the amorphous material on spray drying is being formed from an

already existing disordered state (in solution) and is primarily subjected to thermal stresses. Amorphisation on mechanical activation, however, can be regarded as a direct transition from one solid state to another.

It was noted that the amorphous state of the APIs in this work, produced by different methods, had different relative physical stabilities. For instance, spray dried BUD recrystallised at a temperature 11°C higher than the corresponding amorphous milled form. Spray dried SDM crystallised at a temperature 30°C higher than the milled drug when heated in a DSC. Hence if the objective was to convert these APIs into amorphous forms which displayed the best physical stability, then spray drying would be the process of choice.

Bhugra and Pikal (2007) noted that the high temperature in spray drying versus the low temperature in freeze drying, as well differences in mechanical stresses, may result in different physical stabilities of the amorphous form of a compound. Tsukushi et al. (1994) reported that the amorphous form of cyclodextrin displayed different physical stabilities in the amorphous state according to whether the amorphous form was generated by milling the crystalline form or by quenching the melt. In another study, Patterson et al. (2005) examined the susceptibility of crystalline to amorphous conversions by ball milling and quench cooling for carbamazepine, dipyridamole, glibenclamide and indomethacin and noted results to be compound specific. The amorphous products were prone to crystallisation but differed according to their thermal histories and modes of production (Patterson et al., 2005).

Chapter 3 evaluated the sorption properties and crystallisation tendencies of the amorphous drugs under defined humidity conditions. Spray dried SDM and milled BUD would be considered as moderately hygroscopic according to the European

Pharmacopoeia hygroscopicity classification system (1999) because they have a moisture uptake of between 2-15% w/w at 25°C/80% RH, however neither API recrystallised on exposure to 2 sorption cycle humidity profiles up to 90% RH. It was noted that spray dried SS commenced crystallisation between 60-70% RH, whereas the milled amorphous material converted back to the crystalline form between 50-60% RH. The sorption uptakes prior to crystallisation at 50% RH, for milled and spray dried SS, were not however statistically significantly different ($p > 0.05$). Contrasting kinetic profiles were observed for the processed APIs. For instance, the extremely slow expulsion of moisture of spray dried SS on crystallisation, compared to the corresponding milled material was also noted by Griesdale et al. (2011). The authors highlighted how the quantification of amorphous content, when linked to the total mass loss on crystallisation of an amorphous standard may not be realistic and reliable if the material under investigation and the amorphous standard are produced by different processes.

The viability of using organic solvents like ethanol, as an alternative to water, where the intention is to plasticise the API so that its T_g is below that of the operating temperature and for crystallisation to be favoured, was demonstrated in Chapter 3. Water, as probe vapour, was not capable of sufficiently plasticising spray dried amorphous SDM or milled amorphous BUD. This was in contrast to ethanol which induced amorphous to crystalline transformation in both materials. This has useful implications for quantifying amorphicity in systems where a vapour induced crystallisation is necessary.

The morphology of the processed drugs varied considerably depending on which unit process the API was exposed to. Paluch et al. (2012) devised a novel morphological classification system for spray dried materials. Classification was

based on four variables, namely shape, surface properties, visual morphology and interior of the particle. Spray dried SDM was composed of spherical particles, with both smooth and crumpled surfaces, with populations of both non porous and porous particles with hollow interiors. Spray dried SS consisted of spherical, crumpled, non porous continuous particles whereas spray dried BUD particles were spherical, smooth, non porous and continuous. In contrast to the spray dried material, the morphology of the milled forms of each API were indistinguishable from each other. Hancock et al. (2002) noted that mechanical forces can destroy the primary particles of powders which can have significant impact on bulk powder flow properties. It is anticipated that the impact of the varying levels of amorphicity, as well as particle morphology on the rheological behaviour of processed powders will be investigated as future work.

7.3 Quantifying amorphous content in single and multi-component systems.

Any property that varies proportionally with the fraction of crystalline phase in crystalline/amorphous mixtures can be used to measure crystallinity (Pikal et al., 1978). The amorphous content of milled SDM was quantified using 4 different analytical techniques based on diffraction, thermal, spectroscopic, and vapour sorption properties. The use of multiple complementary techniques allowed for more thorough characterisation of the material. DVS is known to have excellent sensitivity (Shah et al., 2006) and because of its ease of use and applicability to both single and binary systems, was the primary method of quantification. An advantage of DVS, over pXRD and/or DSC was highlighted in chapters 3 and 5. SS, as received in micronized form, was initially analysed by DSC and a single melting/degradation event was noted. No exothermic peak in the thermogram was

observed. When the API was analysed by pXRD, strong characteristic Bragg peaks of form 1 were observed with no evidence of an amorphous halo pattern. However DVS was capable of detecting amorphous content in the API, due to mass loss events occurring during the first sorption cycle. An amorphous content of 4% for SS was quantified by DVS, which was beyond the capability of DSC and pXRD as quantification techniques, and proved important in subsequent quantification calculations.

Results in Chapter 3 and Chapter 4 highlighted the benefits of using multiple complementary techniques rather than relying on a sole method of quantification. DVS, if used in isolation, would have falsely indicated that milling SDM at the lower temperature resulted in a lower level of amorphisation compared to the system milled at RT. The sorption capacity of SDM milled at 4°C was less when DVS was performed at 25°C, compared to DVS experiments performed at 5°C. It was suggested that performing a DVS run at an elevated temperature relative to the milling temperature resulted in partial crystallisation of the API prior to analysis and resulted in an underestimation of the amorphous content. In Chapter 4, DVS indicated an API amorphous content of 114% on co-milling SDM with MA. The method of quantification by DVS used in this thesis assumes the excipient is crystalline and that change in vapour uptake, relative to the individual crystalline uptakes, is exclusively related to amorphisation of the API. For this composite system, MA became partially amorphised on co-milling and the additional vapour sorption due to the amorphous excipient resulted in an API amorphous content in excess of 100%. In chapter 5 pXRD was also used to quantify API amorphicity in binary systems with excipient. The isolation of peaks proved difficult and the separation of the amorphous scattering from the total diffraction was problematic.

In contrast to DVS, which displayed better sensitivity to subtle solid state changes, samples which had crystalline contents $\leq 13\%$ or $\geq 90\%$ could not be differentiated by pXRD from fully amorphous or fully crystalline systems.

An appreciation of the mechanisms by which a vapour and solid material interact may explain why the API amorphous content quantification results for the SDM:GA (33%) and SDM:MA (56%) physical mixtures (individually milled) in Chapter 4 deviated from what was expected ($\sim 76\%$). Newman et al. (2008) refined the definition of hygroscopicity to include such interactive mechanisms. These were identified as 1) adsorption at the surface without bulk penetration, 2) liquefaction of water on the surface of the solid, 3) absorption by penetration into the bulk portions of the solid. For materials that sorb more than 2% w/w mass the possibility of deliquescence should be investigated which could have significant effects on the properties of the solid. Deliquescent materials can undergo conformational change, surface area and surface properties may be altered, as well as the orientation of polar molecules, which can impact sorption and desorption kinetic profiles. The greater the vapour mass uptake the greater the potential effect on solid state properties (Newman et al., 2008).

Table 7.2. Comparison of API amorphous content (average), as quantified by DVS, and % mass uptakes after 1st sorption cycles for SDM:excipient (individually milled) physical mixtures ($X_{\text{excipient}} = 50$)

<i>Physical mixture</i>	<i>% mass uptake at end of sorption cycle 1</i>	<i>% API amorphous content</i>
SDM:GA	39	33
SDM:MA	47	56
SDM:AA	<1	70
SDM:SA	<1	74
SDM:MAN	2	67

SDM:GA and SDM:MA physical mixtures underwent bulk absorption and deliquescence during the first sorption cycles. This was indicated by large steep increases in vapour uptake over narrow P/P and the fact that the vapour content did not reach an equilibrium value with probe molecules continually being absorbed. In contrast, the SDM:AA, SDM:SA and SDM:MAN physical mixtures had a % change in mass of $\leq 2\%$ at the end of the first sorption cycle. The likelihood of problems associated with surface modifications with such small uptakes, compared to deliquescent materials, is considerably less. Quantification results for these systems were indeed closer to the anticipated API amorphous content result of $\sim 76\%$.

Yoshinari et al. (2002) investigated the impact of moisture on polymorphic transformations in mannitol. The authors noted that moisture induced a polymorphic transformation from the δ form to the β form which resulted in the excipient having a larger surface area and higher hygroscopicity. Polymorphism in a compound on exposure to elevated humidities could therefore result in different sorption profiles and mass uptakes compared to the original form and potentially impact quantification results by DVS. Hence evaluating the mechanism by which a solid material interacts with vapour, in addition to measuring vapour uptake at particular partial pressures, is important.

7.4 Mitigating API amorphisation on co-processing with low Tg excipients

Chapters 4 and 5 focused on investigating if co-milling (SDM, SS, BUD) and co-dry mixing API (SS) with low Tg dicarboxylic acids was a viable strategy for preventing or reducing amorphisation in the drug. It was highlighted that the

efficiency of the process, arising from the T_g lowering effect, was highly dependent on the solubility of the excipient in the amorphous API.

Of the five acids (GA, AA, PA, SA and MA) and two polyols (MAN and XYL) investigated across the co-processed systems, GA was the most effective at mitigating amorphisation. The solubility of GA in amorphous SDM and amorphous SS, determined by thermal methods, was very similar and in the range 34-35% w/w. When co-milling was performed at these weight fractions of excipient, the crystallinity of both SDM and SS was at near maximum and the corresponding amorphous miscible systems displayed the most pronounced T_g lowering effect.

The possibility of obtaining amorphous API supersaturated with excipient on co-milling SS with the diacids was discussed in Chapter 6. This supersaturation effect was not observed on co-mixing. Generating a supersaturated state on co-milling has potentially useful implications arising from the ability of excipient to lower the T_g of the composite to a greater extent and to more readily promote crystallisation of an amorphous drug (Figure 7.2).

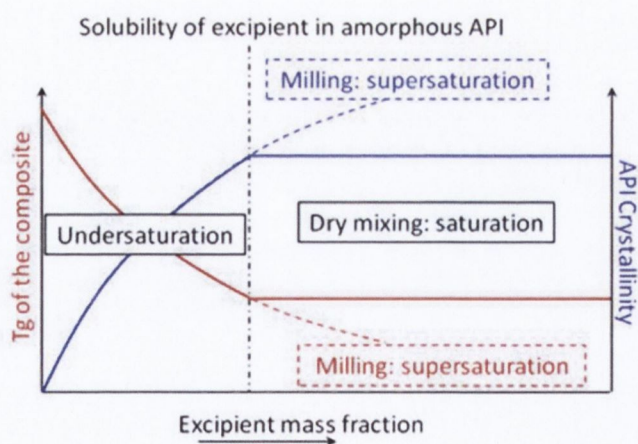


Figure 7.2 Schematic of API crystallinity and composite T_g v excipient mass fraction. Milling, in contrast to dry mixing, led to amorphous API supersaturated with excipient with consequent changes in API crystallinity.

SS amorphisation was lowered by more than 20% on co-milling at a concentration of 50% w/w AA and PA, relative to experiments performed at Sol_{AA} (21% w/w) and

Sol_{PA} (22% w/w). In contrast, no further reduction in API amorphicity was observed when dry mixing was performed at the higher concentration of excipient (Table 7.3).

Table 7.3 Summary of experimental solubilities, T_g minimum values of composite amorphous systems, and amorphous content values, as quantified by DVS, for co-milled and co-mixed SS:excipient systems. X_{excipient} refers to the weight fraction of excipient.

System	Sol _{excipient} (%)	T _g minimum (°C)	% Amorphous content (± S.D)			
			Co-milling (3 h)		Co-mixing (24 h)	
			X _{excipient} = Sol _{excipient}	X _{excipient} = 50 % w/w	X _{excipient} = Sol _{excipient}	X _{excipient} = 50 % w/w
SS:GA	36	5	8 (4)	0	22 (9)	21 (4)
SS:AA	21	34	63 (2)	46 (5)	92 (2)	87 (4)
SS:PA	22	31	64 (2)	42 (4)	100	99 (1)

For the SDM:diacid co-milled systems, a trend was noted between the rank order of difference of Hildebrand solubility parameter between API and excipient and the degree of crystallinity of API on co-milling. The closer the Hildebrand solubility parameter of the excipient to the API, the greater was the inhibition of API amorphisation on co-milling. The difference in the Hildebrand solubility parameters for SDM and GA is 0.1 MPa^{1/2} and the difference for BUD and GA is 0.1 MPa^{1/2}. In both cases API amorphisation was eliminated on co-milling with 50% w/w excipient, as quantified by DVS. In contrast, the solubility of MAN in amorphous SDM was determined to be just 4%, which was not surprising considering a difference of 12.5 MPa^{1/2} in the Hildebrand solubility parameter for

the individual components. The findings have recently found application by Hu et al. (2013) who examined the effects of milling and co-milling on the solid state transformations of sulphathiazole. They observed that milling sulphathiazole with GA promoted crystallisation of the amorphous drug and linked this to the fact that the difference in the Hildebrand solubility parameter of sulphathiazole with SDM was very small. The difference in Hildebrand solubility parameter between sulphathiazole and GA was therefore, by inference, very small and hence the API and excipient were expected to show good solubility in each other.

Co-melt quenched SDM:GA and SDM:AA, at excipient weight fractions corresponding to Sol_{GA} and Sol_{AA} , had T_g minimum values which differed by only 4°C. Nevertheless it was noted that co-milling SDM with GA was more effective at mitigating amorphisation in the API. Hence it is likely that another variable(s), in addition to solubility and T_g , has an effect on the the degree of crystallinity of API on co-milling. Trasi and Taylor (2012) studied the effect of polymer and small molecule additives on the crystallisation of amorphous flutamide. Crystallisation involves two processes, nucleation and growth, and the authors particularly focused on better understanding the impact of the additives on these events. Interestingly, it was highlighted that changes in mobility as manifested by changes in T_g could not provide an adequate explanation for the observed results. For instance, the T_g s of the API:polymer binary systems were only elevated by a few degrees relative to the amorphous drug alone. While this would impact mobility, the extent of such a change could not be correlated with the difference in crystal growth rates observed. Although nilutamide was the additive which resulted in the most elevated dispersion T_g , it was not the most effective additive at inhibiting crystal growth rates. Hence, while acknowledging that T_g is a factor in understanding the effects of additives on

amorphous phase stability, the authors were particularly interested in correlating specific API:excipient interactions with nucleation growth rates. Crystal growth rates were measured by hot stage microscopy and polymers which formed better hydrogen bonds were most effective at inhibiting crystal growth rates.

When SDM was co-milled with MA ($T_g = -15^\circ\text{C}$), API amorphisation was actually promoted. This was partly attributed to the excipient having the poorest solubility of all the excipients with SDM, as well as the additional hydroxyl group on its alkyl backbone. MA, as discussed in Chapter 5, is a hydroxylated diacid and the extra hydroxyl group on the alkyl backbone offers the possibility for hydrogen bond interactions and thus could potentially act as a crystal growth inhibitor. The usefulness of its low T_g was made redundant by its very poor miscibility with SDM. Trasi and Taylor (2012) measured nucleation behaviour by DSC and noted that polymers which were effective at reducing crystal growth rates had no similar impact on nucleation rates. It therefore appears that the ideal excipient, in the context of this work, would have a low T_g coupled with high solubility in the amorphous API, and which could promote and accelerate the processes of nucleation and crystal growth. The potential then exists that these excipients would not just function as diluents or bulking agents but rather as functional excipients in the formulation, preventing solid state changes in the API during mechanical activation as it progresses through the dosage form production process.

7.5 Comparison of co-spray dried composites and composites produced by mechanical activation

In Chapter 6 SDM was co-spray dried with three of the dicarboxylic acids (GA, AA and SA) and with MAN. The API was amorphous for all co-spray dried systems,

and for excipients which displayed polymorphic behaviour, the metastable form at room temperature was produced. Amorphous composites of SDM:AA and SDM:GA were produced on co-spray drying when the excipient weight fraction was less than its solubility in the amorphous drug. This contrasted with the co-milling results, where these excipients proved effective at mitigating amorphisation of the API. The difficulty when comparing the results by mechanical activation with those of spray drying is that the processes are fundamentally different. Caron et al. (2011) compared, for the first time, spray drying and milling in the production of amorphous dispersions of sulphathiazole and sulfadimidine with PVP. The authors noted that spray drying was a more efficient process at generating amorphous composites over a wider concentration range. They attributed this to the fact that the drug and excipient are already in solution prior to process and are in a 'disordered' state already. In addition, amorphisation of the system simply requires rapid evaporation of the solvent which prevents nucleation and growth of the crystalline components. In contrast, mechanical activation involves breaking the crystalline structures of one or both components through impact and attrition before miscibility at the amorphous state can occur. Milling is a very dynamic process and hence it is possible that an API, when milled for several hours, will experience multiple amorphisation/crystallisation phase transitions. When the APIs in this work become amorphous on milling, the good miscibility of GA and AA with the drugs enabled them to exert a T_g lowering effect which then acted to advance and accelerate the process of crystallisation. This effect is also facilitated by the restoration process associated with a temperature rise during milling (section 1.9 in chapter 1).

Both milling and spray drying have parameters which can be finely tuned which could give rise to materials with very different solid state properties. Table 7.4 below lists some adjustable parameters specific to both techniques.

Table 7.4 List of adjustable parameters for milling and spray drying.

Tehchnique	Adjustable parameter
Milling	Ball to powder ratio Milling intensity Milling duration Temperature of milling (ambient v cryogenic) Type of mill
Spray drying	Solvent concentration Feed composition Inlet temperature Feed rate Spray drier operator mode

In Chapter 6 it was observed that spray drying MAN with SDM resulted in formation of the metastable δ polymorph of the excipient at room temperature. The δ polymorph was not produced when the excipient was spray dried alone. Bianco et al. (2012) noted that either the crystalline or amorphous form of a drug could be produced by spray drying depending on the process parameters selected. Sulphathiazole could be amorphised when spray dried from ethanolic solutions in open mode configuration. In contrast, crystalline sulphathiazole was produced on spray drying the drug from acetonic or ethanolic solutions with the spray drier operating in closed mode. Hence it is not straightforward to compare directly the

results on co-processing by spray drying and mechanical activation. In this thesis it was shown that co-milling SDM with 50% w/w GA completely eliminated amorphisation in the milled drug, with the excipient existing as the stable β form. However co-spray drying at the same API:excipient composition resulted in completely amorphous API by pXRD, with crystallinity of the composite system associated with the metastable α polymorph of GA. For the systems investigated in this thesis, the final solid state form of API on co-processing was dependent on the choice of excipient and to which process the composites were exposed to.

7.6 Main findings

- The solid state properties of amorphous SDM, amorphous SS and amorphous BUD vary depending on the process by which the amorphous form of the drug is generated.
- The applicability and importance of utilising multiple complementary analytical techniques when quantifying amorphous content in a processed drug has been demonstrated.
- An excipient with a low T_g coupled with high solubility in the amorphous API can prevent or reduce the generation of an amorphous phase on co-milling.
- The closer the Hildebrand solubility parameter of the excipient to the API, the greater the inhibition of API amorphisation on co-milling.
- Dry mixing with low T_g dicarboxylic acids resulted in a less disordered API, although the extent of reduction was less pronounced relative to the corresponding co-milled data
- Initial amorphisation of the API is followed by dissolution of the excipient which induces a T_g lowering effect on the resulting composite and induces crystallisation of the drug.

- Co-spray drying SDM with a series of low Tg dicarboxylic acids, as well as a low Tg polyol (MAN), resulted in the API being amorphous across all composite systems.

7.7 Suggestions for future work

- Investigate further budesonide:excipient composite systems by mechanical activation and spray drying. Expand work to include other APIs and low T_g excipients with the focus on developing a predictive model for screening crystalline excipients that can selectively mitigate amorphisation in APIs.
- Computational molecular modeling to predict miscibility/solubility for various drug/excipient combinations.
- Explore the effect of the number of excipient carboxyl groups or different functional groups on the propensity to form co-crystals against the potential for mitigating API amorphisation.
- Investigate the possibility of using selective low T_g excipients to prevent amorphisation by mechanical activation in compression/compaction processes.
- Evaluate the effect of different levels of amorphisation on the flow and compaction properties of both single and multi component systems.

References

REFERENCES

- Aaltonen, J.; Rantanen, J.; Siiria, S.; Karjalainen, M.; Jorgensen, A.; Laitinen, N.; Savolainen, M.; Seitavuopio, P.; Louhi-Kultanen, M.; Yliruusi, J. Polymorph screening using near-infrared spectroscopy. *Anal. Chem.* 2003, 75, 5267-5273.
- Airaksinen, S.; Karjalainen, M.; Shevchenko, A.; Westermarck, S.; Leppanen, E.; Rantanen, J.; Yliruusi, J. Role of water in the physical stability of solid dosage formulations. *J. Pharm. Sci.* 2005, 94, 2147-2165.
- Alleso, M.; Chieng, Norman.; Rehder, S.; Rantanen, J.; Rades, T.; Aaltonen, J. Enhanced dissolution rate and synchronized release of drugs in binary systems through formulation: Amorphous naproxen-cimetidine mixtures prepared by mechanical activation. *J. Controlled Release* 2009, 136, 45-53.
- Amidon, G. L.; Lennernas, H.; Seth, V. P.; Crison, J. R. A theoretical basis for a biopharmaceutics drug classification: the correlation of in vitro drug product dissolution and in vivo bioavailability. *Pharm. Res.* 1995, 12, 413-420.
- Anderton, C. Vibrational spectroscopy in pharmaceutical analysis. In: Lee, D.C. and Webb, M. L.; *Pharmaceutical analysis*, Oxford, Blackwell. 2003 203-239.
- Andronis, V.; Yoshioka, M.; Zografi, G. Effects of sorbed water on the crystallisation of indomethacin from the amorphous state. *J. Pharm. Sci.* 1997, 86, 346-351.
- Angell, C. A.; Sare, E. J. Glass forming composition regions and glass transition temperatures for aqueous electrolyte solutions. *J. Chem. Phys.* 1970, 52, 1058-1068.

- Bai, S. J.; Rani, M.; Suryanarayanan, R.; Carpenter, J. F.; Nayar, R.; Manning, M. C. Quantification of glycine crystallinity by near-infrared spectroscopy. *J. Pharm. Sci.* 2004, 93, 2439-2447.
- Baird, J. A.; Van Eerdenbrugh, B.; Taylor, L. S. A classification system to assess the crystallisation tendency of organic molecules from undercooled melts. *J. Pharm. Sci.* 2010, 99, 3787-3806.
- Balani, P. N.; Ng, W. K.; Tan, R. B. H.; Chan, S. Y. Influence of excipients in comilling on mitigating milling-induced amorphisation or structural disorder of crystalline pharmaceutical actives. *J. Pharm. Sci.* 2010, 99, 2462-2474.
- Balani, P. N.; Wong, S. Y.; Ng, W. K.; Widjaja, E.; Tan, R. B. H.; Chan, S. Y. Influence of polymer content on stabilising milled amorphous salbutamol sulphate. *Int. J. Pharm.* 2010, 391, 125-136.
- Barton, A. F. M. *Handbook of Solubility Parameters and Other Cohesive Parameters*. 1984, Boca Raton, FL, CRC Press Inc.
- Barzegar-Jalali, M.; Valizadeh, H.; Dastmalchi, S.; Shadbad, M. R.; Adibkia, K.; Mohammadi, G.; Farahani, A.; Arash, Z.; Nokhodchi, A. Cogrinding as an approach to enhance dissolution rate of a poorly water-soluble drug (glicazide). *Powder Technol.* 2010, 197, 150-158.
- Bates, S.; Zografí, G.; Engers, D.; Morris, K.; Crowley, K.; Newman, A. Analysis of amorphous and nanocrystalline solids from their X-ray diffraction patterns. *Pharm. Res.* 2006, 23, 2333-2349.

- Bauer, J.; Spanton, S.; Henry, R.; Quick, J.; Dziki, W.; Porter, W.; Morris, J. Ritonavir: an extraordinary example of conformational polymorphism. *Pharm. Res.* 2001, 18, 859-866.
- Bianco, S.; Caron, V.; Tajber, L.; Corrigan, O. I.; Nolan, L.; Hu, Y.; Healy, A. M. Modification of the solid-state nature of sulfathiazole and sulfathiazole sodium by spray drying. *AAPS PharmSciTech.* 2012, 13, 647-660.
- Bikiaris, D. N. Solid dispersions Part I: recent evolutions and future opportunities in manufacturing methods for dissolution rate enhancement of poorly water-soluble drugs. *Expert Opin. Drug Deliv.* 2011, 8, 1501–1519.
- Brodka-Pfeiffer, K.; Langguth, P.; Hausler, H.; Graß, P. Influence of mechanical activation on the physical stability of salbutamol sulphate. *Eur. J. Pharm. Biopharm.* 2003, 56, 392–400.
- Buckton G.; Chidavaenzi, O. C.; Koosha, F. The effect of spray drying feed temperature and subsequent crystallization conditions on the physical form of lactose. *AAPS PharmSciTech.* 2002, 3, Technical Note 1.
- Buckton, G.; Darcy, P.; Mackellar, A. J. The use of isothermal microcalorimetry in the study of small degrees of amorphous content of powders. *Int. J. Pharm.* 1995, 117, 253–256.
- Buckton, G.; Darcy, P. Assessment of disorder in crystalline powders - A review of analytical techniques and their application. *Int. J. Pharm.* 1999, 179, 141–158.
- Burger, A.; Henck, J. O.; Dunser, M. N. On the polymorphism of dicarboxylic acids: Pimelic acid. *Microchim. Acta* 1996, 122, 247-257.

- Burger, A.; Henck, J. O.; Hetz, S.; Rollinger, J. M.; Weissnicht, A. A.; Stottner, H. Energy/temperature diagram and compression behaviour of the polymorphs of D-mannitol. *Eur. J. Pharm. Biopharm.* 2000, 89, 457-468.
- Burnett, D. J.; Thielmann, F.; Sokoloski, T.; Brum, J. Investigating the moisture induced crystallisation kinetics of spray dried lactose. *Int. J. Pharm.* 2006, 313, 23-28.
- Burnett, D. J.; Thielmann, F.; Booth, J. Determining the critical relative humidity for moisture-induced phase transitions. *Int. J. Pharm.* 2004, 287, 123-133.
- Burnett, D.; Malde, N.; Williams, D. Characterising amorphous materials with gravimetric vapour sorption techniques. *Pharm. Tech. Eur.* 2009, 21, 41-45.
- Byard, S. J.; Jackson, S. L.; Smail, A.; Bauer, M.; Apperley, D. C. Studies on the crystallinity of a pharmaceutical development drug substance. *J. Pharm. Sci.* 2005, 94, 1321-1335.
- Caron, V.; Willart, J. F.; Danede, F.; Descamps, M. The implication of the glass transition in the formation of trehalose/mannitol molecular alloys by ball milling. *Solid State Commun.* 2007, 144, 288-292.
- Caron V.; Hu, Y.; Tajber, L.; Erxleben, A.; Corrigan, O. I.; McArdle, P.; Healy, A. M. Amorphous solid dispersions of sulphonamide/soluplus and sulphonamide/PVP prepared by ball milling. *AAPS PharmSciTech.* 2013, 14, 464-474.
- Caron, V.; Tajber, L.; Corrigan, O. I.; Healy, A. M. A comparison of spray drying and milling in the production of amorphous dispersions of sulfathiazole/PVP and sulfadimidine/PVP. *Mol. Pharm.* 2011, 8, 532-542.

- Carpentier, L.; Desprez, S.; Descamps, M. Crystallisation and glass properties of pentitols xylitol, adonitol, arabitols. *J. Therm. Anal. Calorim.* 2003, 73, 577-586.
- Chattoraj, S.; Bhugra, C.; Telang, C.; Zhong, L.; Wang, Z.; Sun, C. C. Origin of two modes of non-isothermal crystallization of glasses produced by milling. *Pharm. Res.* 2012, 29, 1020-1032.
- Chawla, A.; Taylor, K. M. G.; Newton, J. W.; Johnson, M. C. R. Production of spray dried salbutamol sulphate for use on dry aerosol formulation. *Int. J. Pharm.* 1994, 108, 233-240.
- Chieng, N.; Aaltonen, J.; Saville, D.; Rades, T. Physical characterisation and stability of amorphous indomethacin and ranitidine hydrochloride binary systems prepared by mechanical activation. *Eur. J. Pharm. Biopharm.* 2009, 71, 47-54.
- Chikhaliya, V.; Forbes, R. T.; Storey, R. A.; Ticehurst M. The effect of crystal morphology and mill type on milling induced crystal disorder. *Eur. J. Pharm. Sci.* 2006, 27, 19-26.
- Chiou, W. L.; Riegelman, S. Pharmaceutical applications of solid dispersion systems. *J. Pharm. Sci.* 1971, 60, 1281-1302.
- Claes, A.; Zografi, G. The molecular basis of moisture effects on the physical and chemical stability of drugs in the solid state. *Int. J. Pharm.* 1990, 62, 87-95.
- Clas, S. D.; Faizer, R.; O'Connor, R. E.; Vadas, E. B. Quantification of crystallinity in blends of lyophilized and crystalline MK-0591 using X-ray powder diffraction. *Int. J. Pharm.* 1995, 121, 73-79.

- Columbano, A.; Buckton, G.; Wikeley, P. A study of the crystallisation of amorphous salbutamol sulphate using water vapour sorption and near infrared spectroscopy. *Int. J. Pharm.* 2002, 237, 171-178.
- Corrigan, O. I.; Holohan, E. M.; Sabra, K. Amorphous forms of thiazide diuretics prepared by spray drying. *Int. J. Pharm.* 1984, 18, 195-200.
- Corrigan, D. O.; Corrigan, O. I.; Healy, A. M. Predicting the physical state of spray dried composites: salbutamol sulphate/lactose and salbutamol sulphate/polyethylene glycol co-spray dried systems. *Int. J. Pharm.* 2004, 273, 171-182.
- Craig, D. Q. M.; Royall, P. G.; Kett, V. L.; Hopton, M. L. The relevance of the amorphous state to pharmaceutical dosage forms: glassy drugs and freeze dried systems. *Int. J. Pharm.* 1999, 179, 179-207.
- Crowley, K. J.; Zografi, G. The effect of low concentrations of molecularly dispersed poly(vinylpyrrolidone) on indomethacin crystallisation from the amorphous state. *Pharm. Res.* 2003, 20, 1417-1422.
- De Gusseme, A.; Neves, C.; Willart, J. F.; Rameau, A.; Descamps, M. Ordering and disordering of molecular solids upon mechanical milling: the case of fanaserine. *J. Pharm. Sci.* 2008, 97, 5000-5012.
- Descamps, M.; Willart, J. F.; Dudognon, E.; Caron, V. Transformation of pharmaceutical compounds upon milling and co-milling: The role of Tg. *J. Pharm. Sci.* 2007, 96, 1398-1407.
- Desprez, S.; Descamps, M. Transformations of glassy indomethacin induced by ball milling. *J. Non-Cryst. Solids* 2006, 352, 4480-4485.

- Dudognon, E.; Willart, J. F.; Caron, V.; Capet, F.; Larsson, T.; Descamps, M. Formation of budesonide/ α lactose glass solution by ball-milling. *Solid State Commun.* 2006, 138, 68-71.
- Dujardin, N.; Willart, J. F.; Dudognon, E.; Hedoux, A.; Guinet, Y.; Paccou, L.; Chazallon, B.; Descamps, M. Solid state vitrification of crystalline α and β - D - glucose by mechanical milling. *Solid State Commun.* 2008, 148, 78-82.
- Fedors, R.F. A method for estimating both the solubility parameters and molar volumes of liquids. *Poly. Eng. Sci.* 1974, 14, 147-154.
- Feng, T.; Rodolfo, P.; Carvajal, M. T. Process induced disorder in crystalline materials: Differentiating defective crystals from the amorphous form of griseofulvin. *J. Pharm. Sci.* 2008, 97, 3207-3221.
- Fisher, E. S. Milling of active pharmaceutical ingredients. In *Encyclopedia of Pharmaceutical Technology*, 3rd ed, 2006, Swarbrick, J.; Informa Healthcare, 2339-2351.
- Forbes, R. T.; Davis, K. G.; Hindle, M.; Clarke, J. G.; Maas, J. Water vapour sorption studies on the physical stability of a series of spray-dried protein/sugar powders for inhalation. *J. Pharm. Sci.* 1998, 87, 1316-1321.
- Ford, J. L. The current status of solid dispersions. *Pharm. Acta Helv.* 1986, 61, 69-88.
- Ford, J. L. *Pharmaceutical thermal analysis: techniques and applications*, Chichester, Ellis Horwood, 1989.

- Friedrich, H.; Nada, A.; Bodmeier, R. Solid state and dissolution rate characterization of co-ground mixtures of nifedipine and hydrophilic carriers. *Drug Dev. Ind. Pharm.* 2005, 31, 719-728.
- Fukuoka, E.; Makita, M.; Yamamura, S. Glass state of pharmaceuticals III. Thermal properties and stability of glassy pharmaceuticals and their binary glass systems. *Chem. Pharm. Bull.* 1989, 37, 1047-1050.
- Gabbott, P. Principles and applications of thermal analysis. 2008, Blackwell publishing.
- Giron, D.; Mutz, M.; Gamier, S. Solid-state of pharmaceutical compounds impact of the ICH Q6 guideline on industrial development. *J. Therm. Anal. Calorim.* 2004, 77, 709-747.
- Gordon, M.; Taylor, J. S. Ideal copolymers and the second-order transitions of synthetic rubbers. I. Non crystalline copolymers. *J. Appl. Chem.* 1952, 2, 493-500.
- Gramaglia, D.; Conway, B. R.; Kett, V. L.; Malcolm, R. K.; Batchelor, H. K. High speed DSC (hyper-DSC) as a tool to measure the solubility of a drug within a solid or semi-solid matrix. *Int. J. Pharm.* 2005, 301, 1-5.
- Greenhalgh, D. J.; Williams, A. C.; Timmins, P.; York, P. Solubility parameters as predictors of miscibility in solid dispersions. *J. Pharm. Sci.* 1999, 88, 1182-1190.
- Griesdale, L. C.; Jamieson, M. J.; Belton, P. S.; Barker, S. A.; Craig, D. Q. M. Characterization and quantification of amorphous material in milled and spray-dried salbutamol sulfate: A comparison of thermal, spectroscopic, and water vapor sorption approaches. *J. Pharm. Sci.* 2011, 100, 3114-3129.

- Grip, J.; Samuelsen, E. J. A raman study of crystalline glutaric acid. *Eur. J. Phys. Scr.* 1984, 29, 556-560.
- Guinot, S.; Leveiller, F. The use of MTDSC to assess the amorphous content of a micronized drug substance. *Int. J. Pharm.* 1999, 192, 63-75.
- Gunawan, L.; Johari, G. P.; Shanker, R. M. Structural relaxation of acetaminophen glass. *Pharm. Res.* 2006, 23, 967-979.
- Gupta, P.; Thilagavathi, R.; Chakraborti, A. K.; Bansal, A. K. Role of molecular interactions in stability of celecoxib-PVP amorphous systems. *Mol. Pharm.* 2005, 2, 384-391.
- Ha, J. M.; Hamilton, B. D.; Hillmyer, M. A.; Ward, M. D. Phase behaviour and polymorphism of organic crystals confined within nanoscale chambers. *Cryst. Growth Des.* 2009, 9, 4766-4777.
- Haleblian, J.; McCrone, W. Pharmaceutical applications of polymorphism. *J. Pharm. Sci.* 1969, 58, 911-929.
- Hancock, B. C. Amorphous pharmaceutical systems. In *Encyclopaedia of Pharmaceutical Technology*. 2007, Informa Healthcare, USA.
- Hancock, B. C.; Dalton, C. R. Effect of temperature on water vapor sorption by some amorphous pharmaceutical sugars. *Pharm. Dev. Technol.* 1999, 4, 125-131.
- Hancock, B. C.; Parks, M. What is the true solubility advantage for amorphous pharmaceuticals? *Pharm. Res.* 2000, 17, 397-404.

- Hancock, B. C.; Zografi, G. Characteristics and significance of the amorphous state in pharmaceutical systems. *J. Pharm. Sci.* 1997, 86, 1-12.
- Hancock, B. C.; Shamblin, S. L.; Zografi, G. Molecular mobility of amorphous pharmaceutical solids below their glass transition temperatures. *Pharm. Res.* 1995, 12, 799-806.
- Hancock, B. C.; York, P.; Rowe, R. C. The use of solubility parameters in pharmaceutical dosage form design. *Int. J. Pharm.* 1997, 148, 1-21.
- Hancock, B. C.; Shalaev, E. Y.; Shamblin, S. L. Polyamorphism: a pharmaceutical science perspective. *J. Pharm. Pharmacol.* 2002a, 54, 1151-1152.
- Hancock, B. C.; Carlson, G. T.; Ladipo, D. D.; Langdon, B. A.; Mullarney, M. P. Comparison of the mechanical properties of the crystalline and amorphous forms of a drug substance. *Int. J. Pharm.* 2002b, 241, 73-85.
- Haque, M.; Roos, Y. H. Water plasticisation and crystallisation of lactose in spray dried lactose/protein mixtures. *J. Food. Sci.* 2003, 69, 23-29.
- Hatley, R. H. M. Glass fragility and the stability of pharmaceutical preparations – excipients selection. *Pharm. Dev. Technol.* 1997, 2, 257-264.
- Heljo, V. P.; Nordberg, A.; Tenho, M.; Virtanen, T.; Jouppila, K.; Salonen, J.; Maunu, S. L.; Juppo, A. M. The effect of water plasticisation on the molecular mobility and crystallisation tendency of amorphous disaccharides. *Pharm. Res.* 2012, 29, 2684-2697.
- Hildebrand, J.; Scott, R. L. The solubility of non electrolytes. Reinhold, New York, 1950.

- Hildebrand, J.; Scott, R. L. *Regular Solutions*, Prentice-Hall, Englewood Cliffs, New Jersey, 1962.
- Hilden, L. R.; Morris, K. R. Physics of amorphous solids. *J. Pharm. Sci.* 2004, 93, 3-12.
- Hockerfelt, M. H.; Nystrom, C.; Alderborn, G. Dry mixing transformed micro-particles of a drug from a highly crystalline to a highly amorphous state. *Pharm. Dev. Technol.* 2009, 14, 233–239.
- Hogan, S. E.; Buckton, G. The application of near infrared spectroscopy and dynamic vapour sorption to quantify low amorphous contents of crystalline lactose. *Pharm. Res.* 2001, 18, 112-116.
- Horter, D.; Dressman, J. B. Influence of physiochemical properties on dissolution of drugs in the gastrointestinal tract. *Adv. Drug Deliv. Rev.* 2001, 46, 75-87.
- Hu, Y.; Macfionnghalie, P.; Caron, V.; Tajber, L.; Healy, A. M.; Erxleben, A.; McArdle, P. Formation, physical stability, and quantification of process-induced disorder in cryomilled samples of a model polymorphic drug. *J. Pharm. Sci.* 2012, 102, 93-103.
- Hu, Y.; Erxleben, A.; Ryder, A. G.; McArdle, P. Quantitative analysis of sulphathiazole polymorphs in ternary mixtures by attenuated total reflectance infrared, near-infrared and raman spectroscopy. *J. Pharm. Biomed. Anal.* 2010, 53, 412-420.
- Hu, Y.; Erxleben, A.; Hodnett, K. B.; Li, B.; McArdle, P.; Rasmusson, A. C.; Ryder, A. G. Solid-state Transformations of Sulfathiazole Polymorphs: the Effects of Milling and Humidity. *Cryst. Growth Des.* 2013, 13 (8), 3404–3413.

- Hulse, W. L.; Forbes, R. T.; Bonner, M. C.; Getrost, M. The characterisation and comparison of spray-dried mannitol samples. *Drug Dev. Ind. Pharm.* 2009, 35, 712-718.
- Hüttenrauch, R.; Fricke, S.; Zielke, P. Mechanical activation of pharmaceutical systems. *Pharm. Res.* 1985, 2, 302-306.
- Ivanisevic, I. Physical stability studies of miscible amorphous solid dispersions. *J. Pharm. Sci.* 2010, 99, 4005-4012.
- Janssens, S.; Van den Mooter, G. Review: physical chemistry of solid dispersions. *J. Pharm. Pharmacol.* 2009, 61, 1571-1586.
- Kadoya, S.; Izutsu, K.; Yonemochi, E.; Terada, K.; Yomota, C.; Kawanishi, T. Glass-state amorphous salt solids formed by freeze drying of amines and hydroxy carboxylic acids: effect of hydrogen bonding and electrostatic interactions. *Chem. Pharm. Bull.* 2008, 56, 821-826.
- Karmwar, P.; Graeser, K.; Gordan, K. C.; Strachan, C. J.; Rades, T. Investigation of properties and recrystallisation behaviour of amorphous indomethacin samples prepared by different methods. *Int. J. Pharm.* 2011, 417, 94-100.
- Katayama, D. S.; Carpenter, J. F.; Manning, M. C.; Randolph, T. W.; Setlow, P.; Menard, K. P. Characterization of amorphous solids with weak glass transitions using high ramp rate differential scanning calorimetry. *J. Pharm. Sci.* 2008, 97, 1013-1024.
- Kaushal, A. M.; Gupta, P.; Bansal, A. K. Amorphous drug delivery systems: Molecular aspects, design and performance. *Crit. Rev. Ther. Drug Carrier Syst.* 2004, 21, 133-193.

- Kaushal, A. M.; Chakraborti, A. K.; Bansal, A. K. FTIR studies on differential intermolecular association in crystalline and amorphous states of structurally related non-steroidal anti inflammatory drugs. *Mol. Pharm.* 2008, 5, 937-945.
- Kerc, J.; Srcic, S. Thermal analysis of glassy pharmaceuticals. *Thermochim. Acta* 1995, 248, 81-95.
- Khatirkar, R. K.; Murty, B. S. Structural changes in iron powder during ball milling. *Mater. Chem. Phys.* 2010, 123, 247-253.
- Kibbe, A. H. Handbook of pharmaceutical excipients, third ed. 2000, Pharmaceutical press, London, 324 – 328.
- Laitinem, R.; Lobmann, K.; Strachan, C. J.; Grohganz, H.; Rades, T. Emerging trends in the stabilisation of amorphous drugs. *Int. J. Pharm.* 2012, 453, 1, 65-79.
- Lane, R. A.; Buckton, G. The novel combination of dynamic vapour sorption gravimetric analysis and near infra-red spectroscopy as a hyphenated technique. *Int. J. Pharm.* 2000, 207, 49-56.
- Lehto, V. P.; Tenho, M.; Heikkila, K. V.; Harjunen, P.; Paallysaho, M.; Valisaari, J.; Niemela, P.; Jarvinen, K. The comparison of seven different methods to quantify the amorphous content of spray dried lactose. *Powder Technol.* 2006, 167, 85-93
- Lefort, R.; De Gusseme, A.; Willart, J. F.; Danede, F.; Descamps, M. Solid state NMR and DSC methods for quantifying the amorphous content in solid dosage forms: An application to ball milling of trehalose. *Int. J. Pharm.* 2004, 280, 209-219.

- Leuner, C.; Dressman, J. Improving drug solubility for oral delivery using solid dispersions. *Eur. J. Pharm. Biopharm.* 2000, 50, 47–60.
- Lin, S. Y.; Hsu, C. H.; Ke, W. T. Solid-state transformation of different gabapentin polymorphs upon milling and co-milling. *Int. J. Pharm.* 2010, 396, 83–90.
- Lin, Y.; Cogdill, R. P.; Wildfong, P. L. D. Informatic calibration of a materials properties database for predictive assessment of mechanically activated disordering potential for small molecule organic solids. *J. Pharm. Sci.* 2009, 98, 2696-2708.
- Liu, J.; Nagapudi, K.; Kiang, Y. H.; Martinez, E.; Jona, J. Quantification of compaction-induced crystallinity reduction of a pharmaceutical solid using ^{19}F solid-state NMR and powder X-ray diffraction. *Drug Dev. Ind. Pharm.* 2009, 9, 1–7.
- Lobmann, K.; Laitinen, R.; Grohgan, H.; Gordon, K. C.; Strachan, C.; Rades T. Coamorphous drug systems: enhanced physical stability and dissolution rate of indomethacin and naproxen. *Mol. Pharm.* 2011, 8, 1919-1928.
- Loerting, T.; Salzmann, C.; Kohl, I.; Mayer, E.; Hallbrucker, A. A second distinct structural ‘state’ of high-density amorphous ice at 77K and 1 bar. *Phys. Chem. Chem. Phys.* 2001, 3, 5355-5357.
- Long, G. L.; Winefordner, J. D. Limit of detection: A closer look at the IUPAC definition. *Anal. Chem.* 1983, 55, 713-724.
- Louey, M.; Mulvaney, P.; Stewart, P. Characterization of adhesional properties of lactose carriers using atomic force microscopy, *J. Pharm. Biomed. Anal.* 2000, 25, 559–567.

- Luner, P. E.; Majuru, S.; Seyer, J. J.; Kemper, M. S. Quantifying crystalline form composition in binary powder mixtures using near-infrared reflectance spectroscopy. *Pharm. Dev. Technol.* 2000, 5, 231-246.
- Mackin, L.; Sartnurak, S.; Thomas, I.; Moore, S. The impact of low levels of amorphous material (< 5%) on the blending characteristics of a direct compression formulation. *Int. J. Pharm.* 2002a, 231, 213-226.
- Mackin, L.; Zanon, R.; Park, J. M.; Foster, K.; Opalenik, H.; Demonte, M. Quantification of low levels (<10%) of amorphous content in micronized active batches using dynamic vapour sorption and isothermal microcalorimetry. *Int. J. Pharm.* 2002b, 231, 227-236.
- Mahieu, A.; Willart, J. F.; Dudognon, E.; Danede, F.; Descamps, M. A new protocol to determine the solubility of drugs into polymer matrixes. *Mol. Pharm.* 2013, 10, 560-566.
- Malkki, L.; Tammilehto, S. Decomposition of salbutamol in aqueous solutions. I. The effect of pH, temperature and drug concentration. *Int. J. Pharm.* 1990, 63, 17-22.
- Mao, C.; ChamCarthy, S. P.; Byrn, S. R.; Pinal, R. Theoretical and experimental considerations on the enthalpic relaxation of organic glasses using differential scanning calorimetry. *J. Phys. Chem.* 2010, 114, 269-279.
- Marsac, P. J.; Li, T.; Taylor, L. S. Estimation of drug-polymer miscibility and solubility in amorphous solid dispersions using experimentally determined interaction parameters. *Pharm. Res.* 2009, 26, 139-151.

- Marsac, P. J.; Shamblin, S. L.; Taylor, L. S. Theoretical and Practical Approaches for Prediction of Drug-Polymer Miscibility and Solubility. *Pharm. Res.* 2006, 23, 2417–2426.
- Martin, G.; Bellon, P. Driven alloys. *Solid State Phys.* 1997, 50, 189-331.
- Master, K. Spray drying in practice. 2002, SprayDryConsult International ApS. Denmark.
- Matsumoto, T.; Zografi, G. Physical properties of solid molecular dispersions of indomethacin with poly(vinylpyrrolidone) and poly(vinylpyrrolidone-co-vinyl-acetate) in relation to indomethacin crystallisation. *Pharm. Res.* 1999, 16, 1722-1728.
- McNamara, D. P.; Childs, S. L.; Giordano, J.; Iarriccio, A.; Cassidy, J.; Shet, M. S.; Mannion, R.; O'Donnell, E.; Park, A. Use of a glutaric acid cocrystal to improve oral bioavailability of a low solubility API. *Pharm. Res.* 2006, 23, 1888–1897.
- Miyazaki, T.; Yoshioka, S.; Aso, Y.; Kojima, S. Ability of polyvinylpyrrolidone and polyacrylic acid to inhibit the crystallization for amorphous acetaminophen. *J. Pharm. Sci.* 2004, 93, 2710-2717.
- Morris, K. R.; Griesser, U. J.; Eckhardt, C. J.; Stowell, J. G. Theoretical approaches to physical transformations of active pharmaceutical ingredients during manufacturing processes. *Adv. Drug Deliv. Rev.* 2001, 48, 91–114.
- Mosharraf, M.; Nyström C. The effect of dry mixing on the apparent solubility of hydrophobic, sparingly soluble drugs. *Eur. J. Pharm. Sci.* 1999, 9, 145–156.

- Muhammad, S. A.; Langrish, T.; Tang, P.; Adi, H.; Chan, H. K.; Kazarian, S. G.; Dehghani, F. A novel method for the production of crystalline micronised particles. *Int. J. Pharm.* 2010, 388, 114-22.
- Nascimento, M. L. F.; Souza, L. A.; Ferreira, E. B.; Zanotto, E. D. Can glass stability parameters infer glass forming ability. *J. Non-Cryst. Solids* 2005, 351, 3296-3308.
- Nernst, W.; Brunner, E. Theorie der reaktionsgeschwindigkeit in heterogenen systemen. *A. Phys. Chem.* 1904, 47, 56-102.
- Newman, A. W.; Reutzel-Edens, S. M.; Zografis, G. Characterisation of the hygroscopic properties of active pharmaceutical ingredients. *J. Pharm. Sci.* 2008, 97, 1047-1059.
- Ng, W. K.; Kwek, J. W.; Yuen, A.; Tan, C. L.; Tan, R. Effect of milling on DSC thermogram of excipient adipic acid. *AAPS PharmSciTech.* 2010, 11, 159-167.
- Nolan, L. PhD thesis, 2008, Trinity College Dublin.
- Ogain, O. N.; Li, J.; Tajber, L.; Corrigan, O. I.; Healy, A.M. Particle engineering of materials for oral inhalation by dry powder inhalers. Particles of sugar excipients (trehalose and raffinose) for protein delivery. *Int. J. Pharm.* 2011, 405, 23-35.
- Oh, D. M.; Curl, R. L.; Yong, C. S.; Amdidon, G. L. Effect of micronisation on the extent of drug absorption from suspensions in humans. *Arch. Pharm. Res.* 1995, 18, 427-433.
- Okamoto, P. R.; Lam, N. Q.; Rehn, L. E. Physics of crystal to glass transformations. *Solid State Phys.* 1999, 52, 1-135.

Otsuka, M.; Matsumoto, T.; Kaneniwa, N. Effect of environmental temperature on polymorphic solid-state transformation of indomethacin during grinding. *Chem. Pharm. Bull.* 1986, 34, 1784-1793.

Palacio, M. A.; Cuffini, S.; Badini, R.; Karlsson, A.; Palacios, S. M. Solid-state characterization of two polymorphic forms of R-albuterol sulfate. *J. Pharm. Biomed. Anal.* 2007, 43, 1531-1534.

Paluch, K. J.; Tajber, L.; Corrigan, O. I.; Healy, A. M. Impact of process variables on the micromeritic and physicochemical properties of spray-dried porous microparticles. Part 1: introduction of a new morphology classification system. *J. Pharm. Pharmacol.* 2012, 64, 1570-1582.

Parrott, E. Milling of pharmaceutical solids. *J. Pharm. Sci.* 1974, 63, 813-829.

Patterson, J. E.; James, M. B.; Forster, A. H.; Lancaster, R. W.; Butler, J. M.; Rades, T. Preparation of glass solutions of three poorly water soluble drugs by spray drying, melt extrusion and ball milling. *Int. J. Pharm.* 2007, 336, 22-34.

Patterson, J. E.; James, M. B.; Forster, A. H.; Lancaster, R. W.; Butler, J. M.; Rades, T. The influence of thermal and mechanical preparative techniques on the amorphous state of four poorly soluble compounds. *J. Pharm. Sci.* 2005, 94, 1998-2012.

Petrie, S. E. B. Thermal behavior of annealed organic glasses. *J. Polym. Sci. Pt. A-2* 10, 1255.

- Pikal, M.; Lukes, A.; Lang, J.; Gaines, K. Quantitative crystallinity determinations for beta-lactam antibiotics by solution calorimetry : correlations with stability. *J. Pharm. Sci.* 1978, 67, 767-773.
- Pokharkar, V. B.; Mandpe, L. P.; Padamwar, M. N.; Ambike, A. A.; Mahadik, K. R.; Paradkar, A. Development, characterization and stabilization of amorphous form of a low Tg drug. *Powder Technol.* 2006, 167, 20-25.
- Qi, S.; Belton, P.; Nollenberger, K.; Clayden, N.; Reading, M.; Craig, D. Q. M. Characterisation and prediction of phase separation in hot-melt extruded solid dispersions: A thermal, microscopic and NMR relaxometry Study. *Pharm. Res.* 2010, 27, 1869–1883.
- Qian, F.; Huang, J.; Hussain, M. A. F. Drug–polymer solubility and miscibility: stability consideration and practical challenges in amorphous solid dispersion development. *J. Pharm. Sci.* 2010, 99, 2941–2947.
- Rabel, S. R.; Jona, J. A.; Maurin, M. B. Applications of modulated differential scanning calorimetry in preformulation studies. *J. Pharm. Biomed. Anal.* 1999, 21, 339-345.
- Repka, M. A.; Majumdar, S.; Kumar, B. S.; Srirangam, R.; Upadhye, S. B. Applications of hot-melt extrusion for drug delivery. *Expert Opin. Drug Deliv.* 2008, 5, 1357–1376.
- Reutzel-Edens, S. M.; Newman, A. W. The physical characteristics of hygroscopicity in pharmaceutical solids. In: Hilfiker, R. *Polymorphism in the Pharmaceutical Industry*. Chapter 9, Weinheim: Wiley-VCH. 235-238.

- Rodriguez-Sprong, B.; Price, C. P.; Jayasankar, A.; Matzger, A. J.; Rodriguez-Hornedo, N. General principles of pharmaceutical solid polymorphism: A supramolecular perspective. *Adv. Drug Deliv. Rev.* 2004, 56, 241-274.
- Royall, P. G.; Craig, D. Q.; Doherty, C. Characterisation of the glass transition of an amorphous drug using modulated DSC. *Pharm. Res.* 1998, 15, 1117-1121.
- Rumonder, A. C. F.; Ivanisevic, I.; Bates, S.; Alonzo, D. E.; Taylor, L. S. Evaluation of drug-polymer miscibility in amorphous solid dispersion systems. *Pharm. Res.* 2009, 26, 2523-2534.
- Saleki-Gerhardt, A.; Ahlneck, C.; Zografi, G. Assessment of disorder in crystalline solids. *Int. J. Pharm.* 1994, 101, 237-247.
- Samra, R. M.; Buckton, G. The crystallisation of a model hydrophobic drug (terfenadine) following exposure to humidity and organic vapours. *Int. J. Pharm.* 2004, 284, 53-60.
- Sareen, S.; Mathew, G.; Joseph, L. Improvement in solubility of poor water-soluble drugs by solid dispersion. *Int. J. Pharm. Investig.* 2012, 2, 12-17.
- Saunders, M.; Podlun, K.; Shergill, S.; Buckton, G.; Royall, P. The potential of high speed DSC (Hyper-DSC) for the detection and quantification of small amounts of amorphous content in predominantly crystalline samples. *Int. J. Pharm.*, 2004, 274, 35-40.
- Serajuddin, A. T. M. Solid dispersion of poorly water-soluble drugs: early promises and recent breakthroughs. *J. Pharm. Sci.* 1999, 88, 1058-1066.

- Seyer, J. J.; Luner, P. E.; Kemper, M. S. Application of Diffuse Reflectance Near-Infrared Spectroscopy for determination of crystallinity. *J. Pharm. Sci.* 2000, 89, 1305-1316.
- Shah, B.; Kakumanu, V. K.; Bansal, A. K. Analytical techniques for quantification of amorphous/crystalline phases in pharmaceutical solids. *J. Pharm. Sci.* 2006, 95, 1641-1665.
- Shakhtshneider, T. P.; Boldyrev, V. V. Mechanochemical synthesis and mechanical activation of drugs. In: Boldyreva, E.; Boldyrev, V. *Reactivity of molecular solids*. John Wiley & Sons, 1999, 271-312.
- Shakhtshneider, T. P. Phase transformations and stabilisation of metastable states of molecular crystals under mechanical activation. *Solid State Ionics* 1997, 101-103, 851-856.
- Shakhtshneider, T. P.; Vasilchenko, M. A.; Politov, A. A.; Boldyrev, V. V. The mechanochemical preparation of solid disperse systems of ibuprofen-polyethylene glycol. *Int. J. Pharm.* 1996, 130, 25-32.
- Shakhtshneider, T. P.; Danede, F.; Capet, F.; Willart, J. F.; Descamps, M.; Paccou, L.; Myz, S. A.; Boldyreva, E. V.; Boldyrev, V. V. Grinding of drugs with pharmaceutical excipients at cryogenic temperatures. Part 1. Cryogenic grinding of piroxicam-polyvinylpyrrolidone mixtures. *J. Ther. Anal. Chem.* 2007, 89, 699-707.
- Simha, R.; Boyer, R. F. On a general relation involving the glass transition and coefficients of expansion of polymers. *J. Chem. Phys.* 1962, 37, 2622-2629.

- Singhal, D.; Curatolo, W. Drug polymorphism and dosage form design: a practical perspective. *Adv. Drug Deliv. Rev.* 2004, 56, 335-347.
- Smekal, A. Ritzvorgang and molekulare festigkeit. *Naturwissenschaften* 1942, 30, 224.
- Snyder, H. E.; Ballesteros, D. L. Spray drying: Theory and pharmaceutical applications. In *Pharmaceutical Dosage Forms: Tablets*. 3rd ed.; Augsburger, L. L.; Hoag, S. W. Informa Healthcare, London, U.K.; 2008, Vol. 1, 227-261.
- Socrates, G. *Infrared and Raman characteristic group frequencies*. John Wiley & Sons, Chichester, 2001.
- Srinarong, P.; de Waard, H.; Frijlink, H. W.; Hinrichs, W. L. J. Improved dissolution behaviour of lipophilic drugs by solid dispersions: the production process as starting point for formulation considerations. *Expert Opin. Drug Deliv.* 2011, 8, 1–20.
- Stubberud, L.; Forbes, R. T. The use of gravimetry for the study of the effect of additives on the moisture-induced recrystallisation of amorphous lactose. *Int. J. Pharm.* 1998, 163, 145-156.
- Surana, R.; Suryanarayanan, R. Quantitation of crystallinity in substantially amorphous pharmaceuticals and study of crystallisation kinetics by X-ray powder diffractometry. *Powder Diff.* 2000, 15, 2-6.
- Surana, R.; Pyne, A.; Suryanarayanan, R. Effect of aging on the physical properties of amorphous trehalose. *Pharm. Res.* 2004, 21, 867-874.

- Suryanarayana, C. Mechanical alloying and milling. *Prog. Mater. Sci.* 2001, 46, 1-184.
- Tajber, L.; Corrigan, O. I.; Healy, A. M. Physicochemical evaluation of PVP-thiazide diuretic interactions in co-spray dried composites-analysis of glass transition composition relationships. *Eur. J. Pharm. Sci.* 2005, 24, 553-563.
- Tajber, L.; Corrigan, O. I.; Healy, A. M. Spray drying of budesonide, formoterol fumarate and their composites—I. Physicochemical characterization. *Int. J. Pharm.* 2009, 367, 79-85.
- Takeda, K.; Murata, K.; Yamashita S. Thermodynamic study of the glass transition in polyamine-polyalcohol mixtures: Entropy-theoretical interpretation of anomalous glass transition behaviour. *J. Phys. Chem.* 1999, 103B, 3457-3460.
- Tang, X. C.; Pikal, M. J.; Taylor, L. S. A spectroscopic investigation of hydrogen bond patterns in crystalline and amorphous phases in dihydropyridine calcium channel blockers. *Pharm. Res.* 2002, 19, 477-483.
- Tao, J.; Sun, Y.; Zhang, G. G.; Yu, L. Solubility of small molecule crystals in polymers: D-mannitol in PVP, indomethacin in PVP/VA, and nifedipine in PVP/VA. *Pharm. Res.* 2009, 26, 855– 864.
- Taylor, L. S.; Zografi, G. Spectroscopic characterisation of interactions between PVP and indomethacin in amorphous molecular dispersions. *Pharm. Res.* 1997, 14, 1691-1698.
- Telang, C.; Mujumdar, J.; Mathew, M. Improved physical stability of amorphous state through acid base interactions. *J. Pharm. Sci.* 2009, 98, 2149-2159

- Tewes, F.; Tajber, L.; Corrigan O. I.; Ehrhardt, C.; Healy A. M. Development and characterisation of soluble polymeric particles for pulmonary peptide delivery. *Eur. J. Pharm. Sci.* 2010, 41, 337-352.
- Theeuwes, F.; Hussain, A.; Higuchi, T. Quantitative analytical method for determination of drugs dispersed in polymers using differential scanning calorimetry. *J. Pharm. Sci.* 1974, 63, 427-429.
- Threlfall, T. L. Analysis of organic polymorphs. A review. *Analyst*, 1995, 120, 2435-2460.
- Ticehurst, M. D.; Basford, P. A.; Dallman, C. I.; Lukas, T. M.; Marshall, P. V.; Nichols, G.; Smith, D. Characterisation of the influence of micronisation on the crystallinity and physical stability of revatropate hydrobromide. *Int. J. Pharm.* 2000, 193, 247-259.
- Tobyn, M.; Staniforth, J.; Morton, D.; Harmer, Q.; Newton, M. Active and intelligent inhaler device development, *Int. J. Pharm.* 2004, 77, 31-37.
- Trasi, N. S.; Boerrifter, S. X. M.; Byrn, S. R. Investigation of the milling-induced thermal behaviour of crystalline and amorphous griseofulvin. *Pharm. Res.* 2010, 27, 1377-1389.
- Trasi, N. S.; Taylor, L. S. Effect of additives on crystal growth and nucleation of amorphous flutamide. *Cryst. Growth Des.* 2012, 12, 3221-3230.
- Tsukushi, I.; Yamamuro O.; Suga, H. Heat capacities and glass transitions of ground amorphous solid and liquid quenched glass of tri-O-methyl-[α]-cyclodextrin. *J. Non Cryst. Solid.* 1994, 175, 187-194.

- Van Arnum, P. Solubilising the insoluble. *Pharm. Technol.* 2011, 34, 50-56.
- Van den Mooter, G.; Wuyts, M.; Blaton, N.; Busson, R.; Grobet, P.; Augustijns, P.; Kinget, R. Physical stabilisation of amorphous ketoconazole in solid dispersions with polyvinylpyrrolidone K25. *Eur. J. Pharm. Sci.* 2001, 12, 261-269.
- Vasconcelos, T.; Sarmiento, B.; Costa, P. Solid dispersions as strategy to improve oral bioavailability of poor water soluble drugs. *Drug Discov. Today* 2007, 12, 1068-1075.
- Vippagunta, S. R.; Brittain, H. G.; Grant, D. J. W. Crystalline solids. *Adv. Drug Deliv. Rev.* 2001, 48, 23-26.
- Vyazovkin, S.; Dranca, I. Effect of physical ageing on nucleation of amorphous indomethacin. *J. Phys. Chem. B* 2007, 111 (25), 7283-7287.
- Walter-Levy, L. Cristallochimie-sur les varieties cristallines du D-mannitol. 1968, C. R. Acad. Sc. Paris Ser. C. 267, 1779-1782.
- Ward, G. H.; Schultz, R. K. Process induced crystallinity changes in albuterol sulphate and its effects on powder physical stability. *Pharm. Res.* 1995, 12, 773-779.
- Watanabe, T.; Hasegawa, S.; Wakiyama, N.; Kusai, A.; Senna, M. Comparison between polyvinylpyrrolidone and silica nanoparticles as carriers for indomethacin in a solid state dispersion. *Int. J. Pharm.* 2003, 250, 283-286.
- Willart, J. F.; Gusseme, A. D.; Hemon, S.; Odou, G.; Danede, F.; Descamps, M. Direct crystal to glass transformation of trehalose induced by ball milling. *Solid State Commun.* 2001, 119, 501-505.

- Willart, J. F.; Descamps, M. Solid state amorphisation of pharmaceuticals. *Mol. Pharm.* 2008, 5, 905–920.
- Willart, J. F.; Carpentier, L.; Danede, F.; Descamps, M. Solid state vitrification of crystalline griseofulvin by mechanical milling. *J. Pharm. Sci.* 2012, 101, 1570–1577.
- Willart, J. F.; Caron, V.; Descamps, M. Transformation of crystalline sugars upon milling. *J. Therm. Anal. Calorim.* 2007, 90, 125-130.
- Willart, J. F.; Caron, V.; Lefort, R.; Danede, F.; Prevost, D.; Descamps, M. A thermal character of the solid state amorphisation of lactose induced by ball milling. *Solid State Commun.* 2004, 132, 693-696.
- Winkel, K.; Hage, W.; Loerting, T.; Price, S. L.; Mayer, E. Carbonic acid: from polyamorphism to polymorphism. *J. Am. Chem. Soc.* 2007, 129, 13863-13871.
- Yang, X.L.; Liu, J.; Yang, L.; Zhang, X. Y. Synthesis, characterization and susceptibility of bacteria of selenium dioxide complexes with sulfadruugs. *Synth. React. Inorg. Met. Org. Nano-Met. Chem.* 2005, 35, 761-766
- Yoo, S. U.; Krill, S. L.; Wang, Z.; Telang, C. Miscibility/stability consideration in binary solid dispersion systems composed of functional excipients towards the design of multi component amorphous system. *J. Pharm. Sci.* 2009, 98, 4711-4723.
- Yoshinari, T.; Forbes, R. T.; York, P. Kawashima, Y. Moisture induced polymorphic transformation of mannitol and its morphological transformation. *Int. J. Pharm.* 2002, 247, 69-77.

- Yoshioka, M.; Hancock, B. C.; Zografi, G. Crystallization of indomethacin from the amorphous state below and above its glass transition temperature. *J. Pharm. Sci.* 1994, 83, 1700–1705.
- Yu, L. Amorphous pharmaceutical solids: preparation, characterization and stabilisation. *Adv. Drug Deliv. Rev.* 2001, 48, 27–42.
- Zhang, G. G.; Gu, C.; Zell, M. T.; Burkhardt, R. T.; Munson, E. J.; Grant, D. J. Crystallisation and transitions of sulfamerazine polymorphs. *J. Pharm. Sci.* 2002, 91, 1089-1100.
- Zhao, M.; Barker, S. A.; Belton, P. S.; McGregor, C.; Craig, D. Q. M. Development of fully amorphous dispersions of a low T_g drug via co-spray drying with hydrophilic polymers. *Eur. J. Pharm. Biopharm.* 2012, 82, 572-579.
- Zheng, E.; Jain, A.; Papoutsakis, D.; Dannenfelser, R. M.; Panicucci, R.; Garad, S. Selection of oral bioavailability enhancing formulations during drug discovery. *Drug Dev. Ind. Pharm.* 2012, 38, 235-247.
- Zhou, D. L.; Zhang, G. G. Z.; Law, D.; Grant, D. J. W.; Schmitt, E. A. Physical stability of amorphous pharmaceuticals: Importance of configurational thermodynamic quantities and molecular mobility. *J. Pharm. Sci.* 2002, 91, 1863-1872.
- Zimper, U.; Aaltonen, J.; McGoverin, C. M.; Gordon, K. C.; Goellner, K. K.; Rades, T. Quantification of process induced disorder in milled samples using different analytical techniques. *Pharm.* 2010, 2, 30-49.

Appendices

Appendix I

Table 1 Spray drying conditions used for API, excipient and API:excipient systems in this thesis. All systems were spray dried in open mode configuration using compressed air as the drying medium.

System	Solvent (% v/v)	Solid concentration (%w/v)	Inlet temperature (°C)	Outlet temperature (°C)	Pump rate (%)	Gas- flow rate (L/hr)	Aspirator (%)
Sulfadimidine	EtOH:H ₂ O (70:30)	0.4	78	43-50	30	473	100
Salbutamol sulphate	H ₂ O	10	150	77-78	30	473	100
Budesonide	EtOH:H ₂ O (95:5)	1	78	56-57	30	473	100
Glutaric acid	EtOH:H ₂ O (70:30)	0.4	78	42-46	30	473	100
Adipic acid	EtOH:H ₂ O (70:30)	0.4	78	45-46	30	473	100
Succinic acid	EtOH:H ₂ O (70:30)	0.4	78	49-51	30	473	100
Malic acid	EtOH:H ₂ O (70:30)	0.4	78	50-51	30	473	100
Pimelic acid	EtOH:H ₂ O (70:30)	0.4	78	50-51	30	473	100
Mannitol	EtOH:H ₂ O (70:30)	0.4	78	47-48	30	473	100
Sulfadimidine:Adipic acid (80:20 w/w)	EtOH:H ₂ O (70:30)	0.4	78	44-45	30	473	100
Sulfadimidine:Adipic acid (60:40 w/w)	EtOH:H ₂ O (70:30)	0.4	78	46	30	473	100

Appendices

System	Solvent (% v/v)	Solid concentration (%w/v)	Inlet temperature (°C)	Outlet temperature (°C)	Pump rate (%)	Gas- flow rate (L/hr)	Aspirator (%)
Sulfadimidine:Adipic acid (50:50 w/w)	EtOH:H ₂ O (70:30)	0.4	78	45-46	30	473	100
Sulfadimidine:Adipic acid (40:60 w/w)	EtOH:H ₂ O (70:30)	0.4	78	44	30	473	100
Sulfadimidine:Glutaric acid (90:10 w/w)	EtOH:H ₂ O (70:30)	0.4	78	41-43	30	473	100
Sulfadimidine:Glutaric acid (80:20 w/w)	EtOH:H ₂ O (70:30)	0.4	78	42-43	30	473	100
Sulfadimidine:Glutaric acid (70:30 w/w)	EtOH:H ₂ O (70:30)	0.4	78	41	30	473	100
Sulfadimidine:Glutaric acid (70:30 w/w)	EtOH:H ₂ O (70:30)	0.4	90	50	30	473	100
Sulfadimidine:Glutaric acid (70:30 w/w)	EtOH:H ₂ O (90:10)	0.4	78	50	30	473	100
Sulfadimidine:Glutaric acid (60:40 w/w)	EtOH:H ₂ O (70:30)	0.4	78	41-42	30	473	100

Appendices

System	Solvent (% v/v)	Solid concentration (%w/v)	Inlet temperature (°C)	Outlet temperature (°C)	Pump rate (%)	Gas- flow rate (L/hr)	Aspirator (%)
Sulfadimidine:Glutaric acid (50:50 w/w)	EtOH:H ₂ O (70:30)	0.4	78	42-44	30	473	100
Sulfadimidine:Glutaric acid (40:60 w/w)	EtOH:H ₂ O (70:30)	0.4	78	43-45	30	473	100
Sulfadimidine:Succinic acid (50:50 w/w)	EtOH:H ₂ O (70:30)	0.4	78	50-51	30	473	100
Sulfadimidine:Mannitol (96:4 w/w)	EtOH:H ₂ O (70:30)	0.4	78	48	30	473	100
Sulfadimidine:Mannitol (90:10 w/w)	EtOH:H ₂ O (70:30)	0.4	78	47-48	30	473	100
Sulfadimidine:Mannitol (80:20 w/w)	EtOH:H ₂ O (70:30)	0.4	78	47-48	30	473	100
Sulfadimidine:Mannitol (60:40 w/w)	EtOH:H ₂ O (70:30)	0.4	78	48	30	473	100
Sulfadimidine:Mannitol (50:50 w/w)	EtOH:H ₂ O (70:30)	0.4	78	47-48	30	473	100
Sulfadimidine:Mannitol (40:60 w/w)	EtOH:H ₂ O (70:30)	0.4	78	46-48	30	473	100
Sulfadimidine:Mannitol (20:80 w/w)	EtOH:H ₂ O (70:30)	0.4	78	46-47	30	473	100

Appendix II

Table 1 List of systems analysed by DVS using water and/or ethanol as probe vapour.

System	Probe vapour	
	Water	Ethanol
SDM unprocessed	✓	✓
SDM spray dried	✓	✓
SDM milled		✓
SDM:excipient co-milled composites and physical mixtures		✓
SDM:MAN co-spray dried composites	✓	
SDM:GA co-spray dried composites	✓	✓
SDM:AA; SDM:SA co-spray dried composites		✓
SS unprocessed	✓	
SS milled, dry mixed, spray dried	✓	
SS:excipient co-milled composites	✓	
SS:excipient co-mixed composites	✓	
BUD unprocessed		✓
BUD milled	✓	✓
BUD spray dried		✓
BUD:GA co-milled composite		✓

Appendix III

Table 1 Calculation of the Hildebrand solubility parameter for sulfadimidine.

Group (number)	$E_v/\text{kJ mol}^{-1}$	$\Sigma E_v/\text{kJ mol}^{-1}$	$V_m/\text{cm}^3 \text{mol}^{-1}$	$\Sigma V_m/\text{cm}^3 \text{mol}^{-1}$
-NH ₂ (1)	12.55	12.55	19.2	19.2
-SO ₂ - (1)	12.34	12.34	23.7	23.7
-NH- (1)	8.37	8.37	4.5	4.5
-CH= (5)	4.31	21.55	13.5	67.5
-CH ₃ (2)	4.71	9.42	33.5	67
-C= (5)	4.31	21.55	-5.5	-27.5
-N= (2)	11.72	23.44	5.0	10
Double bond (6)	1.67	10.02	-2.2	-13.2
Ring closure (2)	1.05	2.1	16	32
	Total	121.34	Total	183.2

$$\delta = (121340/183.2)^{1/2} = 25.7 \text{ MPa}^{1/2}$$

Table 2 Calculation of the Hildebrand solubility parameter for budesonide.

Group (number)	$E_v/\text{kJ mol}^{-1}$	$\Sigma E_v/\text{kJ mol}^{-1}$	$V_m/\text{cm}^3 \text{mol}^{-1}$	$\Sigma V_m/\text{cm}^3 \text{mol}^{-1}$
-CO (2)	17.36	34.72	10.8	21.6
-OH (2)	29.97	59.94	10	2
-C- (2)	1.46	2.92	-19.2	-38.4
-CH= (3)	4.31	12.93	13.5	40.5
-CH ₃ (1)	4.71	4.71	33.5	33.5
-CH ₂ (7)	4.94	34.58	16.1	112.7
-CH (6)	3.43	20.58	-1.0	-6.0
-O- (2)	3.35	6.7	3.8	7.6
Ring closure (5)	1.05	5.25	16	80
	Total	182.330	Total	271.5

$$\delta = (182330/271.5)^{1/2} = 25.9 \text{ MPa}^{1/2}$$

Table 3 Calculation of the Hildebrand solubility parameter for glutaric acid.

Group (number)	$E_v/\text{kJ mol}^{-1}$	$\Sigma E_v/\text{kJ mol}^{-1}$	$V_m/\text{cm}^3 \text{mol}^{-1}$	$\Sigma V_m/\text{cm}^3 \text{mol}^{-1}$
-COOH (2)	27.61	55.22	28.5	57
CH ₂ (3)	4.94	14.82	16.1	48.3
	Total	70.04	Total	105.3

$$\delta = (70040/105.3)^{1/2} = 25.8 \text{ MPa}^{1/2}$$

Table 4 Calculation of the Hildebrand solubility parameter for adipic acid.

Group (number)	$E_v/\text{kJ mol}^{-1}$	$\Sigma E_v/\text{kJ mol}^{-1}$	$V_m/\text{cm}^3 \text{mol}^{-1}$	$\Sigma V_m/\text{cm}^3 \text{mol}^{-1}$
-COOH (2)	27.61	55.22	28.5	57
CH ₂ (4)	4.94	19.74	16.1	64.4
	Total	74.98	Total	121.4

$$\delta = (74980/121.4)^{1/2} = 24.9 \text{ MPa}^{1/2}$$

Table 5 Calculation of the Hildebrand solubility parameter for succinic acid.

Group (number)	$E_v/\text{kJ mol}^{-1}$	$\Sigma E_v/\text{kJ mol}^{-1}$	$V_m/\text{cm}^3 \text{mol}^{-1}$	$\Sigma V_m/\text{cm}^3 \text{mol}^{-1}$
-COOH (2)	27.61	55.22	28.5	57
CH ₂ (2)	4.94	9.88	16.1	32.2
	Total	65.10	Total	89.2

$$\delta = (65100/89.2)^{1/2} = 27.0 \text{ MPa}^{1/2}$$

Table 6 Calculation of the Hildebrand solubility parameter for malic acid.

Group (number)	$E_v/\text{kJ mol}^{-1}$	$\Sigma E_v/\text{kJ mol}^{-1}$	$V_m/\text{cm}^3 \text{mol}^{-1}$	$\Sigma V_m/\text{cm}^3 \text{mol}^{-1}$
-COOH (2)	27.61	55.22	28.5	57
CH ₂ (1)	4.94	4.94	16.1	16.1
-OH	29.79	29.79	10	10
-CH	3.43	3.43	3.43	3.43
	Total	99.38	Total	82.1

$$\delta = (99380/82.1)^{1/2} = 33.7 \text{ MPa}^{1/2}$$

Table 7 Calculation of the Hildebrand solubility parameter for mannitol.

Group (number)	$E_v/\text{kJ mol}^{-1}$	$\Sigma E_v/\text{kJ mol}^{-1}$	$V_m/\text{cm}^3 \text{mol}^{-1}$	$\Sigma V_m/\text{cm}^3 \text{mol}^{-1}$
-OH (6)	21.84	131.04	13	78
-CH ₂ (2)	4.94	9.88	16.1	32.2
-CH (4)	3.43	13.72	-1	-4
	Total	154.634	Total	88.2

$$\delta = (154634/88.2)^{1/2} = 38.2 \text{ MPa}^{1/2}$$

Table 8 Calculation of the Hildebrand solubility parameter for xylitol.

Group (number)	$E_v/\text{kJ mol}^{-1}$	$\Sigma E_v/\text{kJ mol}^{-1}$	$V_m/\text{cm}^3 \text{mol}^{-1}$	$\Sigma V_m/\text{cm}^3 \text{mol}^{-1}$
-OH (5)	21.84	109.20	13	65
-CH ₂ (2)	4.94	9.88	16.1	32.2
-CH (3)	3.43	10.29	-1	-3
	Total	129.37	Total	94.2

$$\delta = (129370/94.2)^{1/2} = 37.1 \text{ MPa}^{1/2}$$

Appendix IV

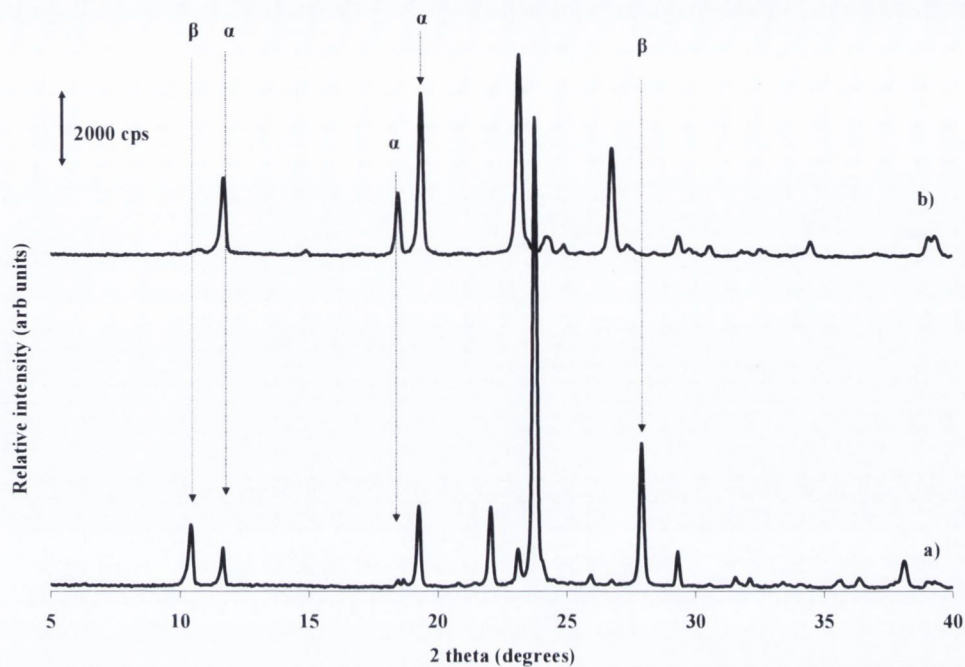


Figure 1 pXPD patterns of a) pimelic acid unprocessed, b) pimelic acid spray dried.

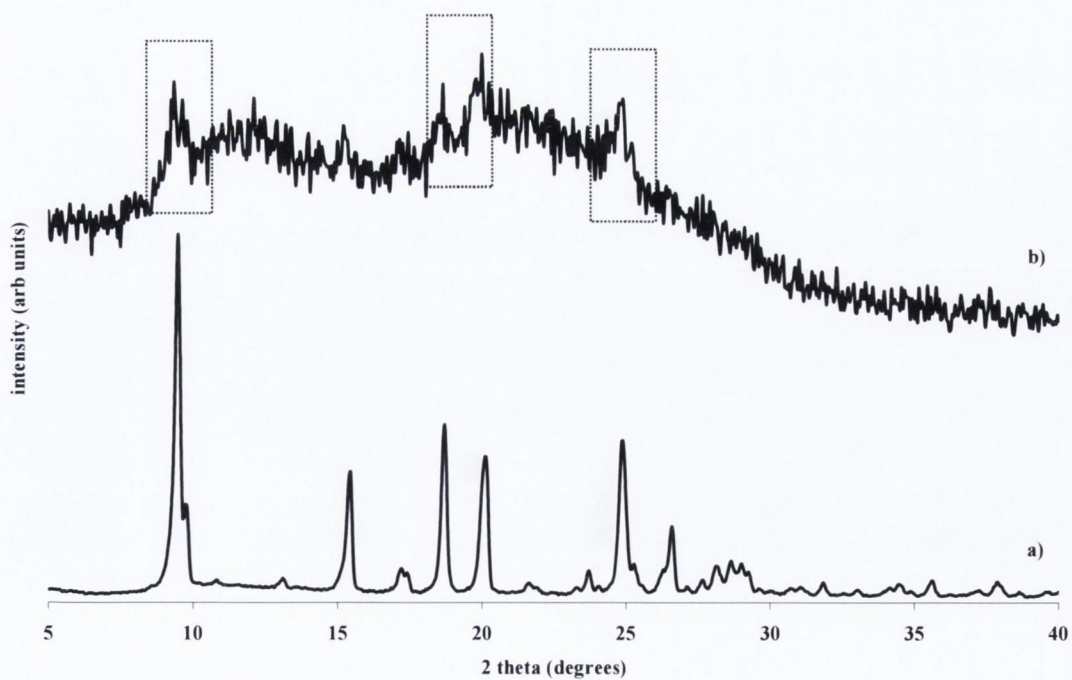


Figure 2 pXRD patterns of a) sulfadimidine unprocessed, b) sulfadimidine milled for 20 hours at room temperature.

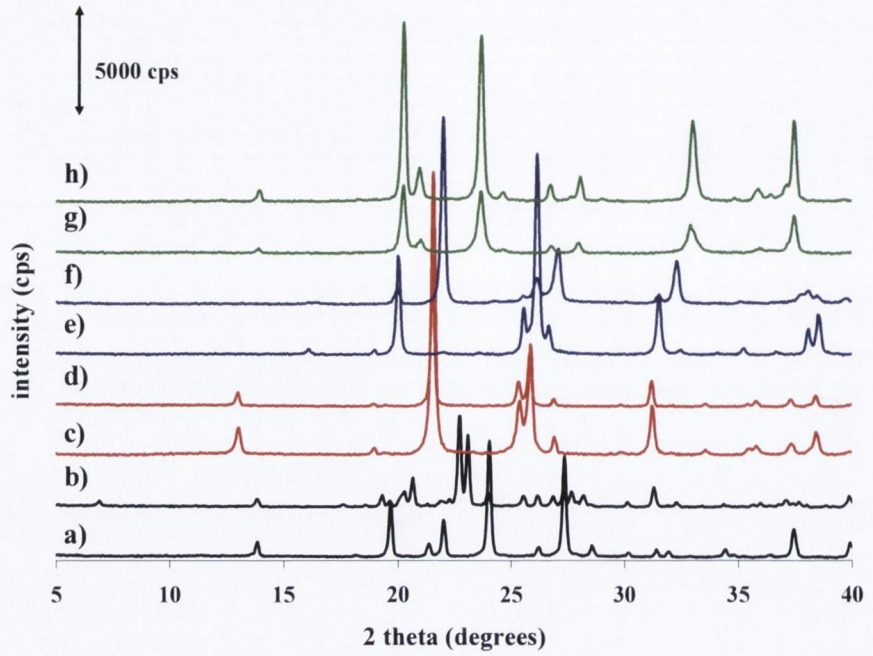


Figure 3 PXRD patterns of a) GA milled; b) GA spray dried; c) AA milled; d) AA spray dried; e) SA milled; f) SA spray dried; g) MA milled; h) MA spray dried. Milling was performed for 10 hours.

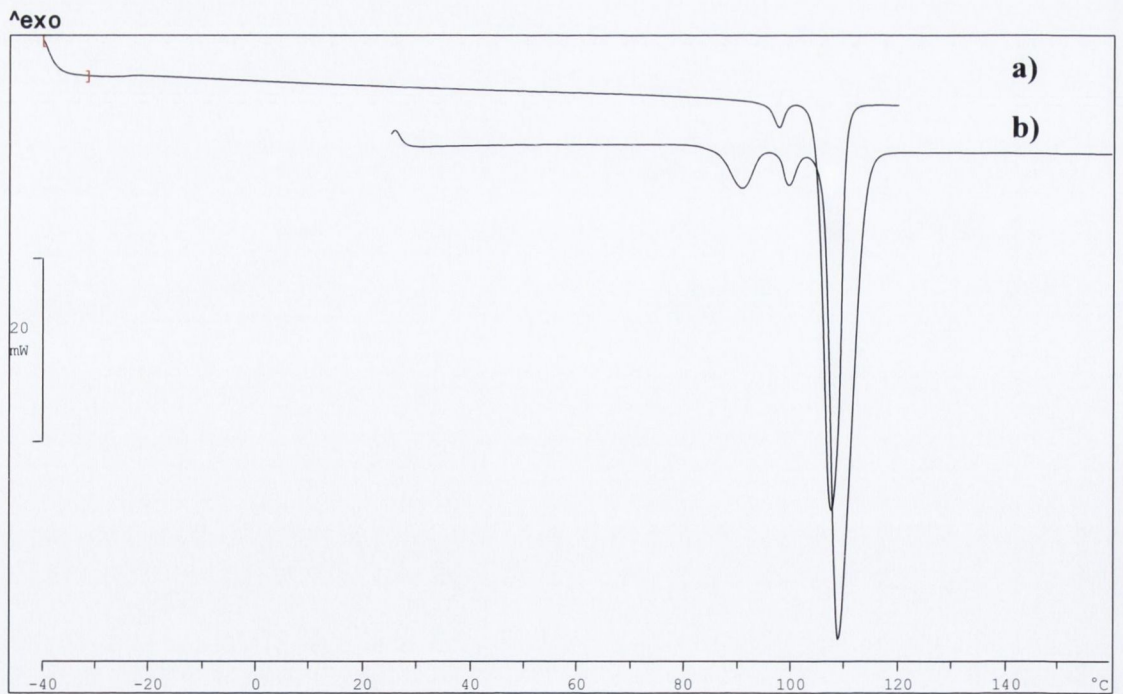


Figure 4 DSC thermograms of a) pimelic acid melt quenched, b) pimelic acid raw.

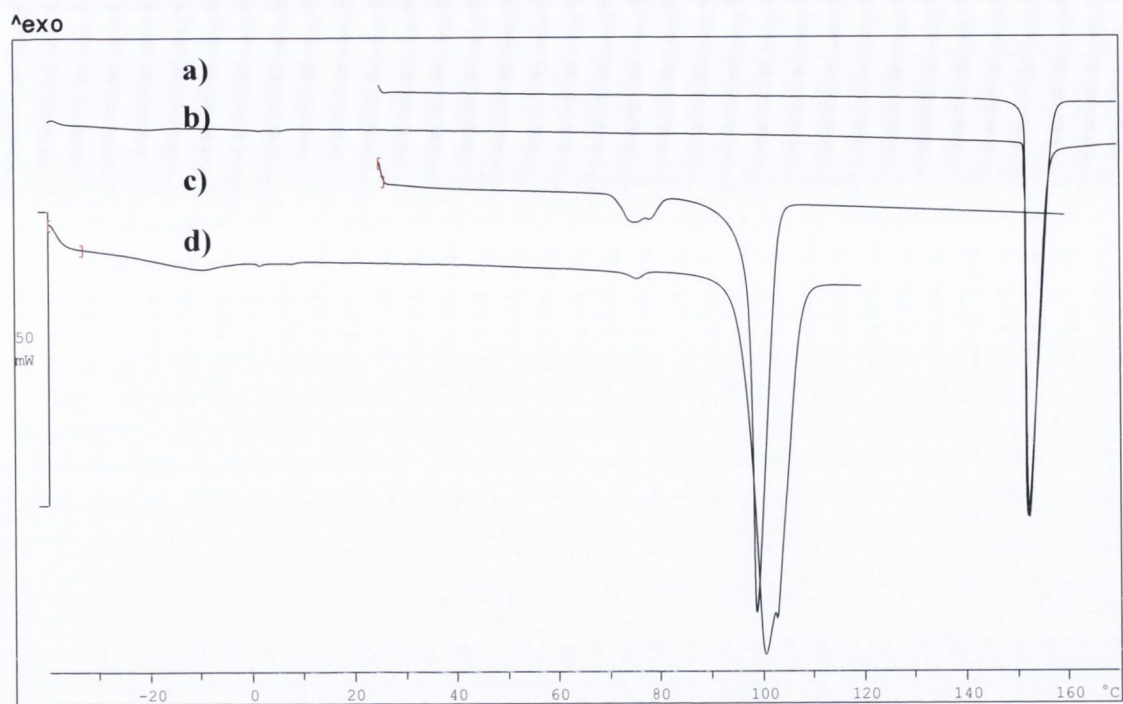


Figure 5 DSC thermograms of a) adipic acid unprocessed, b) adipic acid melt quenched, c) adipic acid unprocessed, d) glutamic acid melt quenched.